Universitat Autònoma de Barcelona

SURVEILLANCE MECHANISMS IN MAMMALIAN MEIOSIS

Marina Marcet Ortega

Universitat Autònoma de Barcelona

SURVEILLANCE MECHANISMS IN MAMMALIAN MEIOSIS

Thesis submitted by

Marina Marcet Ortega

To opt for the title of

Doctor in Cellular Biology

Doctoral thesis directed by

Dr. Ignasi Roig Navarro

Departament de Biologia Cel·lular, Fisiologia i Immunologia

Institut de Biomedicina i Biotecnologia (IBB)

Universitat Autònoma de Barcelona

Director	PhD candidate
Dr. Ignasi Roig Navarro	Marina Marcet Ortega

Bellaterra (Cerdanyola del Vallès), 2016

This work received financial support from:

- Ministerio de Ciencia e innovación grant (BFU2010-18965)
- FPI program fellowship (BES-2011-045381)
- Estancias breves FPI (EEBB-I-13-06647, EEBB-I-14-08517, EEBB-I-15-09556)

A la meva família,

INDEX

ABSTRACT

In order to protect germinal cells from genomic instability, surveillance mechanisms ensure that meiosis occurs properly. In mammals, spermatocytes that display recombination or sex body defects experience an arrest at pachytene stage. Previous studies from our lab described that the MRE11 complex-ATM-CHK2 pathway activates the recombination-dependent arrest in the presence of unrepaired double strand breaks (DSBs). In this work we aimed to identify if p53 family members, which are putative targets of ATM and CHK2, participate in the activation of the recombination-dependent arrest. As a genetic approach, we bred double mutant mice carrying a mutation of a member of the p53 family (p53, TAp63, p73) in a *Trip13* defective background. *Trip13* mutation causes recombination defects, which activate the recombination-dependent arrest in pachytene-stage spermatocytes. Thus, we studied how the absence of p53 family members affected the arrest phenotype of *Trip13*$^{mod/mod}$ spermatocytes. Our data showed that p53 and TAp63 deficiency, but not p73, allowed spermatocytes to progress further into late pachynema, despite accumulating numerous unrepaired DBSs. In addition, lack of p53 or TAp63 resulted in a decrease of apoptotic spermatocytes at early pachytene stage. Therefore, our results indicate that p53 and TAp63 are responsible to activate the recombination-dependent arrest in mouse spermatocytes. Even though, double mutant spermatocytes still arrested at pachytene stage. To study if double mutant spermatocytes were arresting due to the activation of the sex body deficient arrest we analyzed MSCI functionality in *Trip13* mutants. Thus, by bypassing the recombination-dependent arrest has allowed us to elucidate a role for TRIP13 protein in meiotic silencing, which consequently triggers apoptosis in double mutants at late pachytene stage due to sex body impairment. These results infer that the recombination-dependent and the sex-body deficient arrest are activated by two genetically separated mechanisms. From the observation that TRIP13 is required to implement MSCI silencing, we performed an exhaustive analysis of transcription in *Trip13* mutants. Our results suggested that RNA expression in *Trip13* mutants was increased in early meiotic stage spermatocytes, assessed by EU-labeling RNA and phosphorylated(S2)-RNA polymerase II. Moreover, RNA sequencing data highlighted the observation that sex chromosome genes and pre-meiotic genes are overexpressed in *Trip13* mutants, suggesting that TRIP13 is required to maintain the expression of these genes at low levels. Overall, the data presented in this work contributes to the understanding on how surveillance mechanisms control several crucial steps of meiotic prophase progression in mammalian spermatocytes.

ACRONYMS AND ABBREVIATIONS

#: number
µl: microliter
µm: micrometer
AE: Axial Element
APC: Anaphase Promoting Complex
APS: ammonium persulfate
ATM: Ataxia Telangiectasia Mutated
ATR: Ataxia Telangiectasia and Rad-3 related
ATRIP: ATR Interacting Protein
BACs: Bacterial Artificial Chromosome
bp: base pair
BRCA1: Breast Cancer Protein 1
BSA: Bovine Serum Albumin
CDC25: Cell Division Cycle Protein
CDKs: Cycling-Dependent Kinases
cDNA: complementary DNA
CHK1: Checkpoint kinase 1
CHK2: Checkpoint kinase 2
CO: Crossover
DAPI: 4',6-diamidino-2-phenylindole
DDR: DNA Damage Response
dHJ: double Holliday junction
DMC1: DNA meiotic recombinase
DNA: deoxyribonucleic acid
dNTP: desoxinucleotid phosphate
dpp: days post partum
DSBs: Double Strand Breaks
dsDNA: double stranded DNA
EDTA: Ethylenediaminetetraacetic acid
EtOH: Ethanol
EU: 5-Ethynyl Uridine
FBS: Fetal Bovine Serum
FDR: False discovery rate
Fig: Figure
FITC: Fluorescein Isothiocyanate
GBSS: Gey's Balanced Solution
gDNA: genomic DNA
H1t: testicular H1 histone
HCl: Hydrochloride
Hop1: Homolog pairing protein 1
HORMAD: HORMA-domain containing proteins
HRP: Horseradish Peroxidase
kDa: kilodalton
LB: Lysogeny broth
LH: Luteinizing Hormone
MDC1: Mediator of DNA-damage checkpoint 1
Mec1: Mitosis entry checkpoint 1
mg: milligram
$MgCl_2$: Magnesium chloride
ml: milliliter
MLH1: MutL Homolgue protein 1
mm: millimeter
mM: millimolar
MRN: Mre11-Rad50-Nbs1 complex
mRNA: messenger RNA
MSCI: Meiotic Sex Chromosome Inactivation
MSUC: Meiotic Silencing of Unsynapsed Chromatin
N/A: not applicable
NaAc: Sodium Acetate

NaCl: Sodium chloride
NCO: Non-crossover
NHEJ: Non-Homologous End Joining
ºC: Celsius degrees
PAR: Pseudo-Autosomal Region
PAS: Periodic Acid Shiff
PBS: Phosphate Buffered Saline
PBST: PBS-Tween 20
Pch2: pachytene checkpoint gene 2
PCR: Polymerase Chain Reaction
PFA: Paraformaldehyde
PGCs: Primordial Germ Cells
Phospho(S2)-RNApol II: serine 2 phosphorylated RNA polymerase II
PI3K: Phosphoinositide 3-kinase
PTBG: PBS-Tween 20-BSA-Gelatin
qPCR: quantitative real time PCR
RAD51: Radiation Sensitive protein 51
rDNA: ribosomal DNA
RNA: ribonucleic acid
RNA-FISH: RNA Fluorescence *in Situ* Hybridization
RNAseq: RNA sequencing
RPA: Replication Protein A
rpm: revolutions per minute
SAC: Spindle Assembly Checkpoint
SC: Synaptonemal Complex
Scml2: Scm-like 2 X-linked gene
SD: Standard Deviation
SDS: Sodium dodecyl sulfate
SDSA: Synthesis-Dependent Strand Annealing
SPO11: Sporulation Protein 11
SSC: spermatogonial stem cells
ssDNA: single stranded DNA
SUMO-1: Small Ubiquitin-related Modifier 1
SYCP1: Synaptonemal Complex Protein 1
SYCP2: Synaptonemal Complex Protein 2
SYCP3: Synaptonemal Complex Protein 3
Tel1: Telomere maintenance protein 1
TEMED: Tetramethylethylenediamine
TOPBP1: DNA Topoisomerase 2-binding protein 1
TRIP13: Thyroid Hormone Receptor Interacting Protein 13
Tris-HCl: Tris(hydroximethyl) amonimethane hydrochloride
TUNEL: Terminaldeoxynucleotidyl Transferase dUTP Nick End Labelling
Zfx: Zinc finger X-linked gene
Zfy1: Zinc finger Y-linked gene 1
Zfy2: Zinc finger Y-linked gene 2
γH2AX: serine 9 phosphorylated H2AX

INTRODUCTION

1. INTRODUCTION

1.1 Gametogenesis

Sexual reproduction depends on the correct formation of haploid gametes. Germ cells (2n) undergo several steps to ultimately form spermatozoa or eggs (1n). The half chromosome complement will be reconstituted upon egg fertilization to become a diploid zygote (2n) and develop into a new organism with genetic information coming from both parents. Mammalian gametes present an extreme sexual dimorphism (Fig. 1.1).

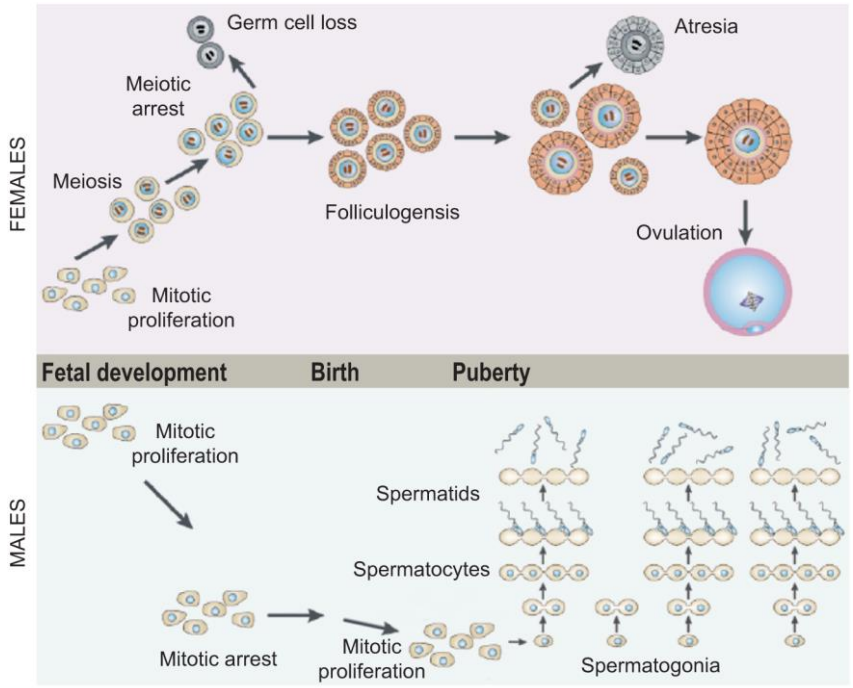

Figure 1.1. Sexually dimorphic gametogenesis in mammals. Representative scheme of gamete production throughout lifespan highlighting the differences between sexes. Prenatally, primordial germ cells from both sexes undergo mitotic divisions to proliferate and migrate to the genital ridges. In fetal females (top section), proliferation of germ cells is followed by entry into meiosis. Oocytes present the peculiarity to arrest prophase I at diplotene stage until ovulation. Around birth time the oocyte pool suffers a heavily reduction by atresia and the surviving oocytes become surrounded by granulosa cells to form primordial follicles. Puberty promotes folliculogenesis progression, which comprises formation of several layers of granulosa cells and oocytes growth, in order to develop into secondary and antral follicles. After extrusion of the first polar body the oocyte is ovulated and remains arrested at metaphase II until fertilization. In contrast, in males (bottom section) mitotic proliferation of primordial germ cells is followed by an extended mitotic arrest. After birth, germ cells resume mitotic divisions to develop into spermatogonia that enter meiosis around 6 dpp to initiate the first meiotic wave. Primary spermatocytes develop into secondary spermatocytes and these to spermatids, which mature to form spermatozoa. Spermatogenesis is then maintained during adulthood. Image adapted from Hassold and Hunt (2001).

For instance, while sperm are motile, eggs are immobile and contribute to most part of the embryonic cytoplasm. Therefore, gamete selection has triggered differential gametogenesis processes in the males and females (White-Cooper and Bausek 2010). During embryonic development primordial germ cells (PGCs) migrate from the epiblast to reach the genital ridge. PGCs associate with somatic cells to form the embryonic gonads (seminiferous cords). At this embryonic point, male PGCs proliferate through several rounds of mitosis and then undergo an arrest at embryonic day 12, which is maintained until birth. Contrarily, female PGCs, proliferate and differentiate into oogonia which enter meiosis and arrest at the end of prophase I while start to form primordial follicles. After birth, around 3 days postpartum (dpp) in male mice, prospermatogonia start to migrate from the center of the seminiferous cord to the basement membrane turning into spermatogonial stem cells (SSCs) around 6 dpp (see Fig. 1.1) (Oatley and Brinster 2012; Griswold and Oatley 2013).

1.1.1 Oogenesis

In mammals, female germ cells start the meiotic program during fetal development. Early stages of prophase I occur before birth, and meiosis blocks after diplonema, at dictyotene stage of meiosis I. Around this time, a large proportion of oocytes is depleted by atresia, possibly regulated by a quality control mechanism (Tingen et al. 2009). The remaining oocytes surround by somatic granulosa cells forming primordial follicles. Metabolic cooperation between oocytes and granulosa cells ensures substrate provision for the growing oocytes and allows exchange of regulatory signals for cell cycle progression and fertilization. Productive folliculogenesis starts after puberty, with primordial follicles recruitment for further development into secondary follicles and antral follicles (granulosa cells proliferate generating several cell layers and the oocyte increases in size). Oocyte and granulosa cell communications influence the oocyte maturation and meiosis progression, which is resumed in response to luteinizing hormone (LH), involving germinal vesicle breakdown (GVBD) and completion of meiosis I. Finally, once the first polar body is extruded the mature follicle is ready to be ovulated (Li and Albertini 2013). At this point, oocytes remain arrested at metaphase II until they become fertilized and completion of meiosis takes place (van den Hurk and Zhao 2005; Li and Albertini 2013).

1.1.2 Spermatogenesis

Spermatogenesis resumes at puberty and continues cyclically through adult's whole life (Cheng and Mruk 2010). Testes epithelium is composed by seminiferous tubules, the structures that support germ cells undergoing spermatogenesis. The generation of spermatozoa is maintained by SSC population that are located at the basement membrane of the seminiferous tubule. Spermatogonia have the capacity to self-renew and to form differentiated spermatogonia. From two populations of stem cells, type A_0 (reserve stem cells) and A_{1-4} (renewing stem cells), the second type divides to form B-type spermatogonia, which continues to develop into transient populations: primary spermatocyte, secondary spermatocyte and spermatid (Dym et al. 2009). Therefore, the transition from spermatogonia into spermatocyte requires exit from the mitotic cell cycle and commitment to meiosis. The differentiation of the first spermatogonias into spermatozoa is known as the first wave of spermatogenesis, which occurs in a semi-synchronic fashion starting around 6 days post-partum (dpp) in mice. DNA replication (S-phase) occurs in B-type spermatogonia and then meiotic prophase initiates (White-Cooper and Bausek 2010). As meiosis progresses, spermatocytes and post-meiotic cells advance from the periphery of the tubules, close to the basal membrane, to the lumen of the tubule (Fig. 1.2). After meiosis is completed, round spermatids (haploid cells) undergo spermiogenesis which consists in drastic morphological changes to become mature motile spermatozoa. Spermiogenesis comprises several processes, like nuclear polarization, condensation and elongation; and assembly of the acrosome and the axoneme (central component of the flagellum) (O'Donnell 2015). These processes are followed by a final compaction of the chromatin, thanks to histone replacement by protamines (Braun 2001). The last activation steps for sperm maturation and storage take place outside of the testis in the epididymis.

In adult mice, different waves of spermatogenesis occur simultaneously, so the seminiferous tubule epithelium contains germ cells at different development stages. According to the different germ cell types each tubule contains, seminiferous tubule cross sections can be classified into XII stages (Ahmed and de Rooij 2009). Somatic Sertoli cells are in contact with the basement membrane of the tubule and intimately associate with the developing germ cells (Fig. 1.2). They represent important contributors for the maintenance of a spermatogonial stem cell niche environment by secreting soluble factors essential for spermatogenesis. Outside the basement membrane, the interstitial tissue mainly contains capillary cells, mesenchymal cells, macrophages, and Leydig cells (testosterone producers) which may also contribute to the micro-environment (White-

Cooper and Bausek 2010; Oatley and Brinster 2012). Male germline cell development also depends on the expression of many testis-specific genes, so transcriptional regulation becomes a key process (White-Cooper and Bausek 2010). For instance, 11% of genes expressed in mouse spermatocytes are testis-specific, which are mainly implicated in fertilization, transcriptional regulation, nuclear integrity and sperm motility/structure (Choi et al. 2007).

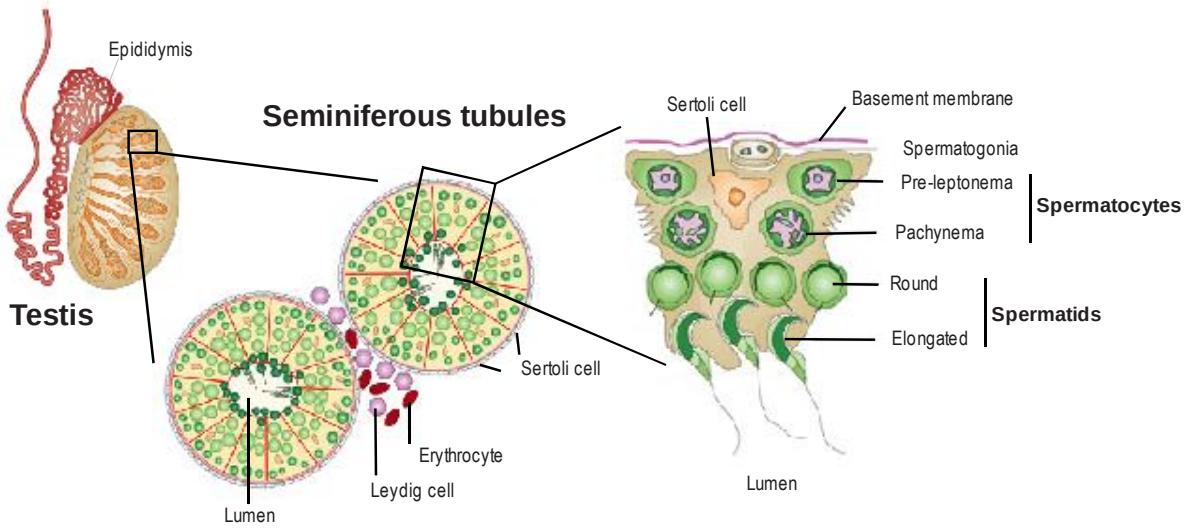

Figure 1.2. Organization of seminiferous tubules in the testis. Testis are organized into seminiferous tubules, the structures that contain spermatogenic cells supported by Sertoli cells. Spermatogonia, adjacent to the basement membrane, enter meiosis and as they differentiate into spermatocytes and spermatids they advance towards the lumen of the tubule. Once meiosis is completed, haploid cells, named spermatids, undergo spermiogenesis to become spermatozoa that are released in the lumen to finally maturate in the epididymis. Image modified from Cooke and Saunders (2002).

1.1.3 Meiosis

Meiosis is a specialized cell division that generates haploid gametes from a diploid cell. Chromosome reduction is achieved through two consecutive chromosome segregation events preceded by a single round of DNA replication (Kleckner 1996). Paternal and maternal homologous chromosomes are separated in the first meiotic division, followed by a second meiotic division that pulls apart sister chromatids of each chromosome (Page and Hawley 2003). Following DNA replication, the first meiotic division starts with an extraordinary prophase, which is subdivided into four consecutive stages: leptonema, zygonema, pachynema and diplonema. These stages can be cytologically distinguished by the configuration of the meiosis-specific proteinaceous scaffold that forms along the chromosomes, the synaptonemal complex (Fig. 1.3) (Handel and Schimenti 2010).

At the onset of prophase, SPO11 protein generates deliberated double strand breaks (DSBs) throughout the genome (Keeney et al. 1997). A characteristic feature of meiosis is that these DSBs start to repair through homologous recombination, which uses the homologous chromosome as a template. This process promotes paring initiation and synapsis of the homologous chromosomes, reaching full synapsis at pachytene stage followed by desynapsis at diplonema. All this chromosomal choreography is tightly coordinated with the recombination process. In mouse, about 10% of the SPO11-generated DSBs will be repaired as crossovers (CO) (Cole et al. 2012). The formation of CO implies genetic exchange between the homologues, which increases genetic diversity, but also provides a physical connection between the homologous chromosomes (called chiasmata). These connections between the homologous chromosomes ensures correct orientation on the spindle and chromosome segregation to eventually produce balanced haploid gametes (Miller et al. 2013). Therefore, defects in CO formation can result in aneuploid gametes, one of the major causes of miscarriages and chromosome abnormality found in humans (Hassold et al. 2007).

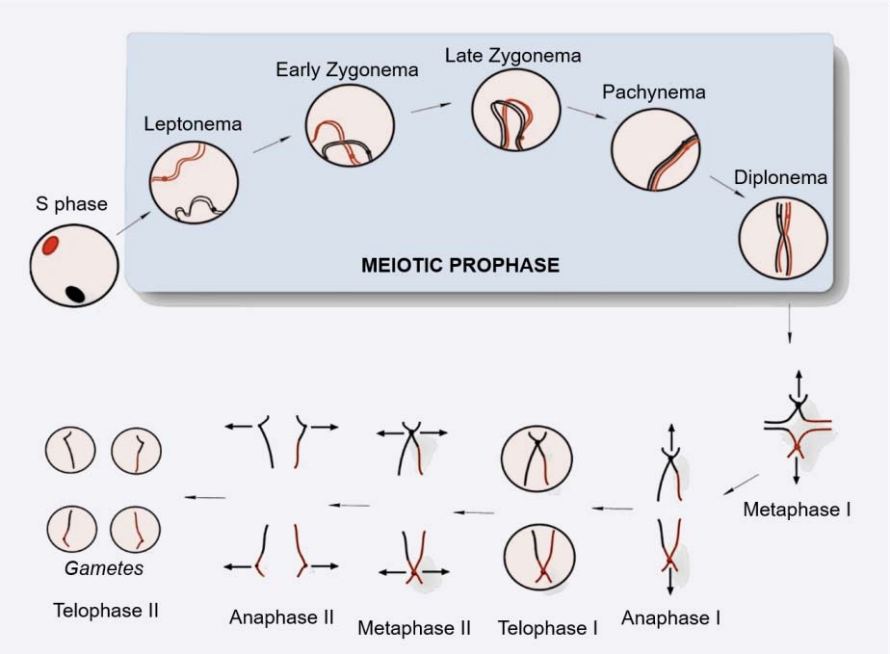

Figure 1.3. Meiosis progression. Meiosis generates haploid gametes (n) from a diploid cell by two consecutive rounds of chromosome segregation preceded by an S-phase. The first meiotic division comprises a special prophase, which consists in four consecutive stages: leptonema, zygonema, pachynema and diplonema. At the onset of prophase, at leptonema, SPO11 protein induces formation of DSBs which initiates homologous recombination. As DSBs repair, homologous chromosomes start to pair and synapse at zygonema. At pachytene stage synapsis is completed and homologous chromosomes recombinate in order to provide physical connections between them (CO formation).Then, homologous chromosomes desynapse at diplonema stage. During Metaphase I and anaphase I, COs ensure segregation of homologous chromosomes into the opposite poles. Soon after, the second meiotic division segregates sister chromatids in order to form haploid cells. Image modified from Roig (2005).

1.1.4 Meiotic recombination

Meiotic recombination initiates at leptotene stage when the evolutionary conserved SPO11 enzyme (Keeney et al. 1997) cleaves DNA via a topoisomerase II-like mechanism generating DSBs. SPO11 catalyzes DSBs with the help of other partner proteins, like TOPO-VIBL, MEI1, MEI4 or REC114 in mice (Lam and Keeney 2015; Robert et al. 2016). SPO11 remains covalently linked at the end of each DNA 5' terminus, until it is released by MRE11-dependent endonucleolytic incisions near the DSBs. Recognition of the DSB sites by MRE11-complex, activates ATM which promotes the first wave of H2AX phosphorylation on ser139 (γH2AX) at leptonema that will marks DSBs until they become repaired (Mahadevaiah et al. 2001; Barchi et al. 2005; Bellani et al. 2005).

At the site of DSBs, Exo1 exonuclease resects DNA ends 5´to 3', producing exposed 3' single stranded DNA (ssDNA) ends (Zakharyevich et al. 2010; Garcia et al. 2011). Then, the RecA homologs RAD51 and the meiosis-specific DMC1 proteins, bind to these ssDNA ends (Plug et al. 1996); enhanced by RPA ssDNA binding protein (Krogh and Symington 2004). RAD51/DMC1 form the nucleoprotein filaments that catalyze the strand invasion into the homologous DNA duplex to search for the homologous repair template and form a joint molecule intermediate (Neale and Keeney 2006; Lam and Keeney 2015). At zygonema, γH2AX and other recombination markers progressively decrease as DSBs become repaired (Moens et al. 1997). During meiosis inter-homolog bias is implemented, forcing the use of the homologous chromosome for DSB repair (instead of using the sister chromatid as it occurs in somatic cells). At pachytene stage, most of the DSBs become repaired preferentially using the homologue; however few unrepaired DSBs remain on the X chromosome of the spermatocytes. In mammalian males, DSBs generated on the asynapsed regions of the sex chromosomes (which lack an homologue) repair later, presumably when the barrier for inter-sister chromatid repair becomes weaker (Lao and Hunter 2010; Inagaki et al. 2010).

DSBs repair by homologous recombination can result as a CO, when genetic exchange occurs between homologous chromosomes, or as a non-crossover (NCO) (Börner et al. 2004). When the ssDNA tail invades the duplex DNA, repair can be processed through double Holliday junction (dHJ) pathway (when strand invasion intermediates are stabilized by the balanced action of the putative E3 SUMO ligase RNF212 and ubiquitin ligase HEI10 (Reynolds et al. 2013; Qiao et al. 2014)). Alternatively, ssDNA tail intermediates are displaced from the homolog and processed by synthesis-dependent strand annealing pathway (SDSA). At the dHJ pathway, the invading strand captures the second end of the DSB forming a dHJ intermediate junction that it resolves forming a CO.

In SDSA, the 3' invading strand is displaced after being extended by DNA synthesis and anneals to the other 3' end of the DSB and becomes a NCO (see Fig. 1.4) (Allers and Lichten 2001; Lam and Keeney 2015).

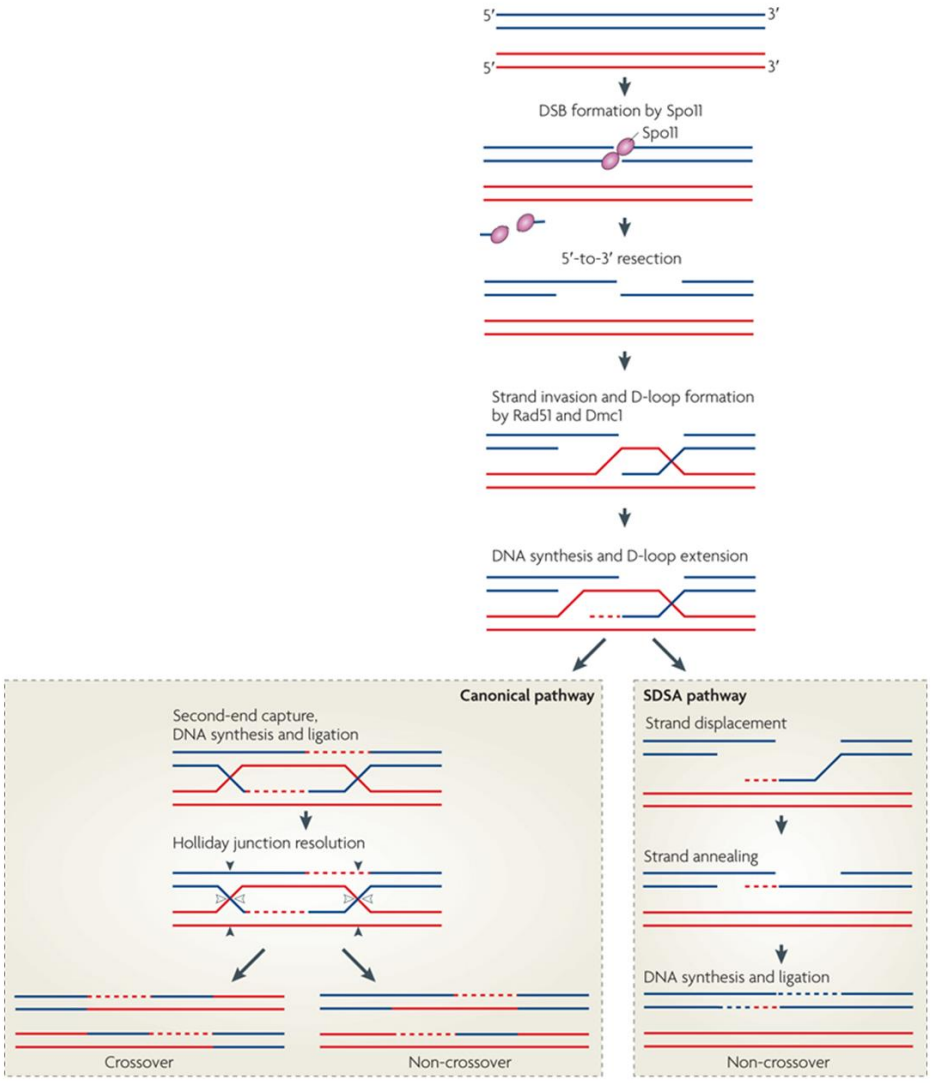

Figure 1.4. Meiotic recombination pathways. Recombination initiates with SPO11 protein (red circle) introducing DSBs throughout the genome. SPO11 remains covalently linked at the DNA, until it is released by the MRE11 complex-dependent endonucleolytic cleavage. DNA ends from the DSB undergo a 5'-to-3' resection that generates exposed 3' ssDNA tails, which are recognized by RPA protein. Then DMC1 and RAD51 proteins bind to these DNA ends and catalyze the strand invasion into the homologous DNA duplex generating a displacement loop (D-loop) intermediate, and then initiate DNA synthesis and D-loop extension. Recombination intermediates can be processed as crossover (CO) or non-crossover (NCO). In the canonical pathway, when strand invasion is stabilized, the capture of the other end and DNA synthesis generates double Holliday junction (dHJ), which can be resolved by cutting the external strands (black arrowheads) or the crossed strands (white arrowheads). Most dHJ will primarily resolve forming a CO product. The other alternative pathway, the synthesis-dependent strand annealing (SDSA), occurs when the D-loop intermediates are displaced from the homologous and the invading strand anneals again with the opposite end of the original DSB, leading to a NCO product. Image adapted from Sasaki et al. (2010).

1.2 Control of meiotic recombination

Several meiotic mechanisms act in conjunction in order to ensure correct formation and placement of the induced DSBs and to ensure the repair of these DSBs resulting in proper COs or NCOs. In mouse, most DSBs occur at preferential recombination sites (recombination hotspots) and seem to be determined by PRDM9, a DNA binding methyltransferase. PRDM9 protein has a PR/SET domain with histone 3 lysine 4 (H3K4me3) methyltransferase activity at the N-terminus. At the C-terminus PRDM9 contains a highly polymorphic multiple-zinc-finger domains that recognize specific DNA sequences. So when PRDM9 recognizes the DNA motif, the SET domain leaves an epigenetic signature (H3K4me3) (Baudat et al. 2010; Parvanov et al. 2010). However, PRDM9 is not required for DSB generation since in *Prdm9*$^{-/-}$ mouse DSBs are form but on a different position than in wild type. In PRDM9 absence DSBs accumulate at promoter regions or at other PRDM9-independent H3K4me-enriched sites, suggesting that besides its methyltransferase activity, PRDM9 protein also recruits the recombination machinery (sequestering the DSB machinery away from promoters) (Brick et al. 2012). Besides PRDM9, it is thought that other high-order chromosome structures may influence DSB locations (Lam and Keeney 2015).

Every chromosome needs to get a minimum number of DSBs in order to get at least one CO, but due to its dangerous nature it is also important to tightly regulate them since high levels of DSBs are deleterious for spermatocytes. For instance, *Atm* mutants present increased levels of SPO11-generated DSBs. ATM-lacking spermatocytes have multiple meiotic abnormalities (like meiotic arrest, unsynapsed chromosomes, failure to form a sex body, fragmented SC, uncompleted meiotic recombination and no CO formation) (Barlow et al. 1998) but interestingly some of these defects become alleviated in Spo11 heterozygosity (e. g. *Spo11*$^{+/-}$*Atm*$^{-/-}$) (Bellani et al. 2005; Barchi et al. 2008). Several regulatory mechanisms have been found to control DSBs formation. Firstly, ATM protein which is directly activated by DSBs early processing, inhibits DSB formation via a negative-feedback control. In ATM deficiency, *Drosophila* and mice meiocytes present an increased abundance of DSBs, assessed by DSBS markers or through augmented SPO11-oligonucleotide complexes respectively (Joyce et al. 2011; Lange et al. 2011). The MRE11 complex, which sense DSBs and activates ATM, also participates in this feedback control of DSBs formation in mice (Pacheco et al. 2015). In *S. cerevisiae*, both ATM^{Tel1} and also ATR^{Mec1} control DSBs levels by down-regulating Spo11 cofactor Rec114 (Carballo et al. 2013). On another side, regulation of DSBs is also controlled by homologous chromosomes engagement through ZMM proteins (factors that control recombination and SC

completion). Yeast cells lacking ZMM proteins (*zip1*, *zip3* or *msh5* mutants) also present increased formation of DSBs. It is suggested that when the two homologues engage, ZMM proteins signal to stop making DSBs through a negative feedback loop (Thacker et al. 2014). Finally, there is an established window for DSBs formation during meiotic prophase which its initiation seems to be controlled through meiosis-specific gene transcription (coordinated after replication) and its termination is regulated by the pachytene-exit Ndt80 transcription factor (Allers and Lichten 2001; Lam and Keeney 2015).

In mouse, about two hundred DSBs are generated at leptonema but only 10% of these will be resolved as COs, but at least one CO per homologue pair is necessary to ensure proper chromosome segregation at anaphase I. Connection between the homologous chromosomes is required in order to provide tension in their centromeres when they are aligned at the metaphase plate helping to pull each homologue to the opposite poles. Not surprisingly, CO formation is highly regulated by three main CO control processes (Wang et al. 2015). Firstly, assurance of the obligatory CO is required, since getting at least one CO for each homologous pair ensures correct segregation. Secondly, CO interference ensures that COs occur widely spaced along the chromosomes (Bishop and Zickler 2004; Hillers 2004). ATM protein is required for the obligate CO between the X and Y chromosome, and its deficiency results in increased number of COs and with reduced CO interference (Barchi et al. 2008). In *S. cerevisiae* ATM^{Tel1}/ATR^{Mec1} dependent phosphorylation of RPA and $RNF212^{Zip3}$ control CO distribution (Bartrand et al. 2006; Serrentino et al. 2013). And finally, CO homeostasis guarantees a sustained number of COs despite a variable initial dosage of DSBs. Recombination initiates with the programmed DSB, but even if the number of the DSBs increases or decreases (due to cell-to-cell variability or induced by mutations), the final number of COs remains similar to avoid aneuploidy (Martini et al. 2006; Cole et al. 2012).

1.2.1 Homologous chromosome synapsis

DSBs formation is also facilitated by higher-order chromosome structures. Sister chromatids organize into loops that anchor into the structural protein axis scaffold: the axial element (AE). The loop-axis structure starts to organize coupled with DNA replication and is completed at leptonema. The two principal proteins of the AEs are SYCP3 and SYCP2, which are recruited to chromosome axes (Borde and de Massy 2013). As homologous chromosomes start to pair at zygotene stage, the two axial elements of

each chromosome assemble into the synaptonemal complex (SC). The SC is a zipper-like structure that consists on the assembly of the two lateral elements (the former AEs), held together by the transverse filaments of the central element, made of SYCP1 among other proteins (de Vries et al. 2005). At pachytene stage homologous chromosomes are fully synapsed giving place to bivalents. The SC complex is therefore important for driving synapsis, recombination and holding the homologous chromosomes together during meiotic prophase (see Fig. 1.5) (Zickler and Kleckner 1999; Page and Hawley 2004; Zickler and Kleckner 2015).

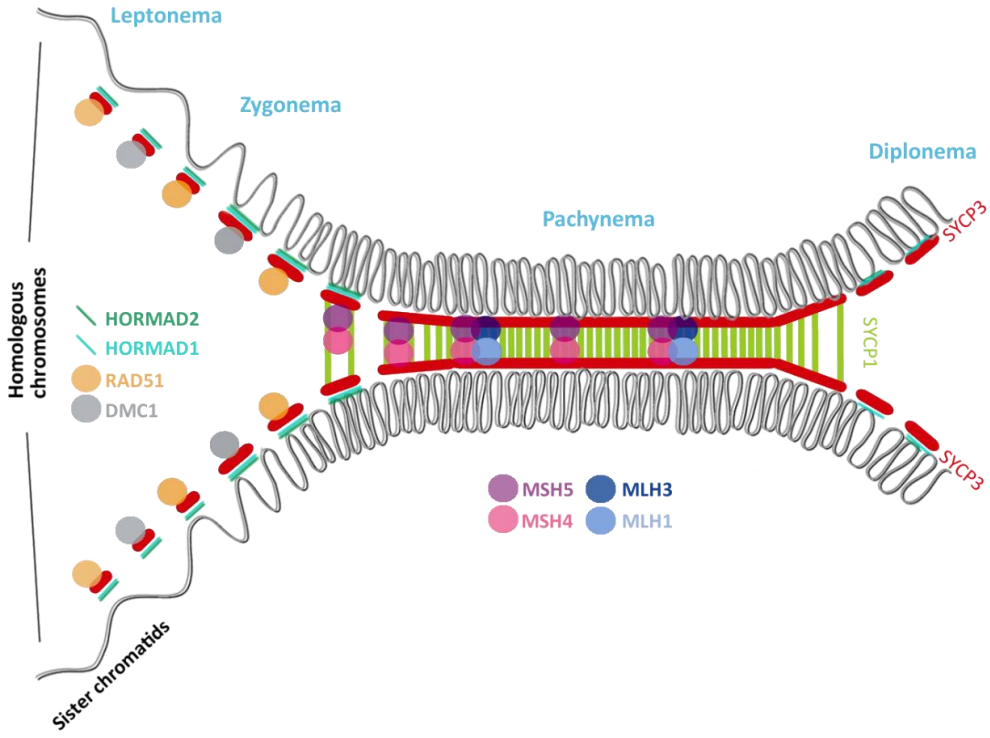

Figure 1.5. **Synaptonemal complex structure and organization.** At the onset of prophase sister chromatids organize into loops that anchor into the chromosome axes that will form the synaptonemal complex (SC) scaffold. The SC is a zipper-like structure formed by the lateral elements (SYCP3 and SYCP2, in red) and the central element (SYCP1, in light green). At leptonema stage SYCP3 and SYCP2 proteins start to localize along the chromosome axes (axial elements). At the same time, repair proteins like DMC1 (grey) and RAD51 (orange) are recruited at the DSBs sites. Additionally, other proteins are located over the asynapsed axes, like HORMAD1 (turquoise line) and HORMAD2 (dark green line), which mediate the asynapsis signaling network. At zygonema, when homologous chromosomes start to synapse SYCP1 and other proteins are recruited between the lateral elements to forms the transverse filaments (central element). As DSB repair progresses mismatch repair MSH4 and MSH5 proteins (pink and purple respectively), localize over the recombination intermediates. At pachytene stage synapsis is completed and MLH1 and MLH3 proteins (light and dark blue respectively) mark crossover sites. Finally, homologous chromosomes start to desynapse at diplonema held together by the CO sites. Image modified from Cohen and Holloway (2010).

Remarkably, meiotic recombination and homologous synapsis need to occur in a coupled manner during meiotic prophase. As a matter of fact, there is a mutual dependency between these processes, and failure of one will probably alter the correct progression of the other (e.g. *Dmc1*$^{-/-}$ (Pittman et al. 1998), *Sycp1*$^{-/-}$ mutants (de Vries et al. 2005) or SC null mutants (Kouznetsova et al. 2011)). This fact, highlights the importance of recombination and synapsis processes being monitored by surveillance mechanisms.

1.2.1.1 Asynapsis and transcriptional silencing

Asynapsis triggers meiotic silencing, which consists in a process where chromatin remodeling inactivates the transcription from genes located at the unsynapsed regions during late meiotic prophase. Some sensor proteins are retained over the axis only in unsynapsed regions like HORMA (Hop1, Rev7 and Mad2) domain proteins HORMAD1 (Daniel et al. 2011) and HORMAD2 proteins (Wojtasz et al. 2012). Both HORMAD1 and HORMAD2 are part of the meiotic chromosome axis. Once homologous chromosomes have synapsed, HORMAD1/2 are depleted from the axes in a TRIP13-dependent manner (Wojtasz et al. 2009; Roig et al. 2010). Thus, in pachytene-stage spermatocytes HORMAD1/2 are only present on the unsynapsed portions of the X and Y chromosomes. Surprisingly, at diplonema HORMADS1/2 are loaded again onto the chromosome axes. Apart from sensing unsynapsed axis, HORMAD1/2 have other functions during meiosis. HORMAD1 promotes efficient formation of DSBs, SC assembly and is necessary for efficient expansion of ATR over the asynapsed chromatin in DSBs absence (Daniel et al. 2011), and HORMAD2 principally ensures recruitment of ATR and cofactors over the unsynapsed axes (Wojtasz et al. 2012). Interestingly, the phosphorylated form of HORMAD1 and HORMAD2 are exclusively located over the unsynapsed axes. The fact that these proteins can experience post-translational modifications suggests that this serves as a signal to promote recruitment of other factors that contribute to promote silencing and the synapsis surveillance system (Fukuda et al. 2012). HORMAD1 and HORMAD2 mediate zygotene asynapsis sensing signaling and promote BRCA1 localization on the asynapsed axes. Then, ATR is recruited to asynapsed axes through a BRCA1-, HORMAD1-, HORMAD2-dependent manner, and facilitates the enrichment of other cofactors to the unsynapsed axes, like ATRIP, TOPBP1 (Refolio et al. 2011) or phosphorylated HORMAD1/2 (Turner et al. 2005; Refolio et al. 2011; Royo et al. 2013; Turner 2015). If asynapsis persists, MDC1 effector cofactor helps ATR to translocate and accumulate over the chromatin loops emanating from the asynapsed axes (Ichijima et al. 2011), catalyzing the second wave of H2AX phosphorylation, the key epigenetic event to promote meiotic silencing of the

unsynapsed chromatin (MSUC) (Perera et al. 2004; Turner 2015; Burgoyne et al. 2009; Mahadevaiah et al. 2001; Royo et al. 2013). This second wave of H2AX phosphorylation is independent of SPO11-induced DSBs, since *Spo11* mutant mice experience silencing of part of their unsynapsed chromosomes (Barchi et al. 2005; Bellani et al. 2005).

In males, the X and Y sex chromosomes only share homology in a short region: at the pseudoautosomal region (PAR). At pachytene stage, while the PAR region is able to synapse, most of the sex chromosomes remain unsynapsed. Sex chromosomes asynapsis triggers formation of the so called sex body, which leads the transcriptional silencing mechanism (reminiscent of the MSUC) known as Meiotic Sex Chromosome Inactivation (MSCI) (see Fig. 1.6) (Turner et al. 2005; Page et al. 2012; Turner et al. 2004; Royo et al. 2013). The silencing of the sex chromosomes has been found to be required for proper spermatocyte progression, since MSCI failure drives apoptosis and pachytene arrest at epithelial stage IV (Burgoyne et al. 2009). Specifically, it was found that aberrant expression of Y genes during pachytene stage becomes deleterious for spermatocytes (Royo et al. 2010).

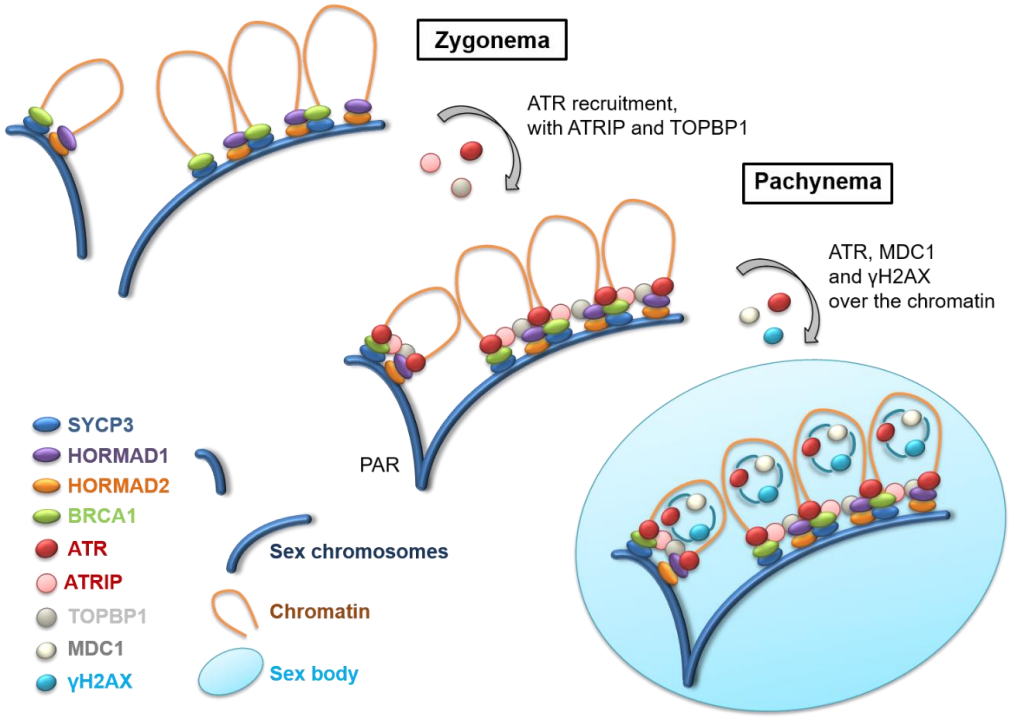

Figure 1.6. Meiotic silencing. Schematic representation of meiotic silencing signaling of the unsynapsed regions, showing in particular the meiotic sex chromosomes inactivation (MSCI). At zygonema, asynapsed regions of the chromosomes axes (labelled with SYCP3, HORMAD1 and HORMAD2) recruit BRCA1 protein. There asynapsis sensing components promote recruitment of ATR and its cofactors ATRIP and TOPBP1 to the unsynapsed chromosome axes at the transition of zygonema-early pachynema stage. Then, since sex chromosomes remain unsynapsed (with the exception of the PAR region) at pachytene stage, MDC1 helps ATR to translocate into the chromatin loops promoting H2AX phosphorylation consequently silencing of the unsynapsed chromatin region (MSCI). Image based on Royo et al. (2013).

A characteristic of first meiotic division is that transcription is suppressed at the onset of prophase, and it essentially restarts again at mid pachynema (Monesi, 1964), when chromosomes are fully synapsed and most DSBs are repaired. In pachytene stage spermatocytes, when autosomes reactivate transcription, sexual chromosomes are subjected to transcriptional repression by the sex-body (Turner et al. 2004); which is crucial to allow correct progression of meiosis (Royo et al. 2010). It is generally believed that the meiotic sex chromosome inactivation (MSCI) is a manifestation of the global meiotic silencing of unsynapsed chromosomes (MSUC) that is detectable at the end of zygotene stage (Burgoyne et al. 2009; Turner et al. 2005). Moreover, it has been hypothesized that MSUC could also be active during all meiotic prophase. Thus, the repression of transcription that occurs at the onset of meiotic prophase could also be a global manifestation of the MSUC mechanism(Page et al. 2012).

1.2.2 Checkpoint mechanisms control meiotic progression

Meiotic prophase comprises the execution of many processes that need to be coordinated successfully in order to obtain viable gametes. For this, meiotic progression, recombination and homologous chromosome synapsis occur concomitantly in a highly regulated manner. For instance, correct repair of the SPO11-induced DSBs becomes a determining process, since errors at this point could contribute to generate genomic instability and introduce germ line mutations. Therefore, it is essential that meiotic prophase is subjected to stringent surveillance mechanisms that can detect deleterious events during prophase, delay cell cycle and, if necessary, promote programmed cell death.

Depending on the organisms, different strategies are adopted. In *S. cerevisiae* for example, persistent DSBs or synapsis defects result in a prolonged prophase that can be followed by DNA damage adaptation and forced meiosis or mitotic growth (Roeder and Bailis 2000; Subramanian and Hochwagen 2014). Remarkably, in many organisms, most known mechanisms that control prophase progression involve the DNA damage response (DDR) proteins ATM and ATR (Roeder and Bailis 2000; MacQueen and Hochwagen 2011; Subramanian and Hochwagen 2014). ATM and ATR are conserved serine/threonine kinases that in meiosis respond to different forms of DNA damage and synapsis errors, and achieve their functions in coordination with other cofactors and through phosphorylation of a large net of substrates. Detection of the DSBs is mainly driven by ATM/ATR, however following downstream signaling differs among organisms.

Cell cycle arrest in *S. cerevisiae* occurs in the presence of recombination and synapsis defects, such as *Dmc1*, *Zip1* or *Hop2* mutants and checkpoint activation requires Mek1 (a meiosis specific CHK2 homolog). *Drosophila* similarly requires Mnk (CHK2) protein to activate the checkpoint that occurs in mutants defective for DSB repair proteins (e.g. *okr*, *spn-B* and *spn-C*) (Roeder and Bailis 2000; MacQueen and Hochwagen 2011). This meiotic checkpoint is also active in *C. elegans syp-1* and *rad-51* mutants; but contrary, checkpoint apoptosis depends on CHK1 presence to promote p53 activation (Jaramillo-Lambert et al. 2010). The downstream targets of the pachytene checkpoint identified in *S. cerevisiae* are Swee1, which phosphorylates and inactivates Cdc28 (Leu and Roeder 1999); and Ndt80, a meiotic transcription factor of genes required to exit pachytene (like *CLB1*) (Chu and Herskowitz 1998).

1.2.2.1 The pachytene arrest in mammals

The pachytene checkpoint ensures that recombination and synapsis are fully completed before progressing to diplonema stage, but in the presence of deleterious events it can promote cell cycle arrest and apoptosis. Mouse surveillance mechanisms act at two different stages: either monitoring recombination or synapsis at pachytene stage, or later at metaphase I controlling bipolar attachment to the spindle (known as the spindle assembly checkpoint, SAC) (Di Giacomo et al. 2005; Barchi et al. 2005; Touati and Wassmann 2016).

In mammalian males, several studies suggest the presence of at least two independent control mechanisms that would monitor meiotic prophase progression and activate the arrest that occurs at pachytene stage in spermatocytes. One is dependent on the correct repair of the induced DSBs (referred as recombination-dependent arrest) (Barchi et al. 2005; Pacheco et al. 2015) and the other depends on the proper meiotic silencing of the sex chromosomes by the sex body (named here as sex body-deficient arrest) (Barchi et al. 2005; Royo et al. 2010). Cytologically, the activation of these two arrest mechanisms can be distinguished using the incorporation of the testis specific histone 1t (H1t) as a marker, which in wild type mouse accumulates on chromatin from mid-pachynema onwards (Drabent et al. 1996; Inselman et al. 2003). It has been described that spermatocytes with persistent unrepaired DSBs (e.g., *Dmc1*$^{-/-}$ (Pittman et al. 1998; Yoshida et al. 1998)), arrest at early pachytene stage before expressing H1t (Barchi et al. 2005; Pacheco et al. 2015). In contrast, mutant spermatocytes that arrest due to a defective sex body (e.g., *Spo11*$^{-/-}$ (Baudat et al. 2000; Romanienko and Camerini-Otero 2000)) reach mid/late pachynema and accumulate H1t (Barchi et al. 2005; Pacheco et al.

2015). This incorporation of H1t has been interpreted as these mutant cells progress further into meiotic prophase (Barchi et al. 2005; Pacheco et al. 2015). However, even though these spermatocytes present differential H1t expression, and arrest their cell cycle at different stages, cells experiencing either the recombination-dependent or the sex body-deficient arrest undergo apoptosis at epithelial stage IV, which corresponds to mid-pachynema stage in wild type mice (see Fig. 1.7) (Inselman et al. 2003; Pacheco et al. 2015).

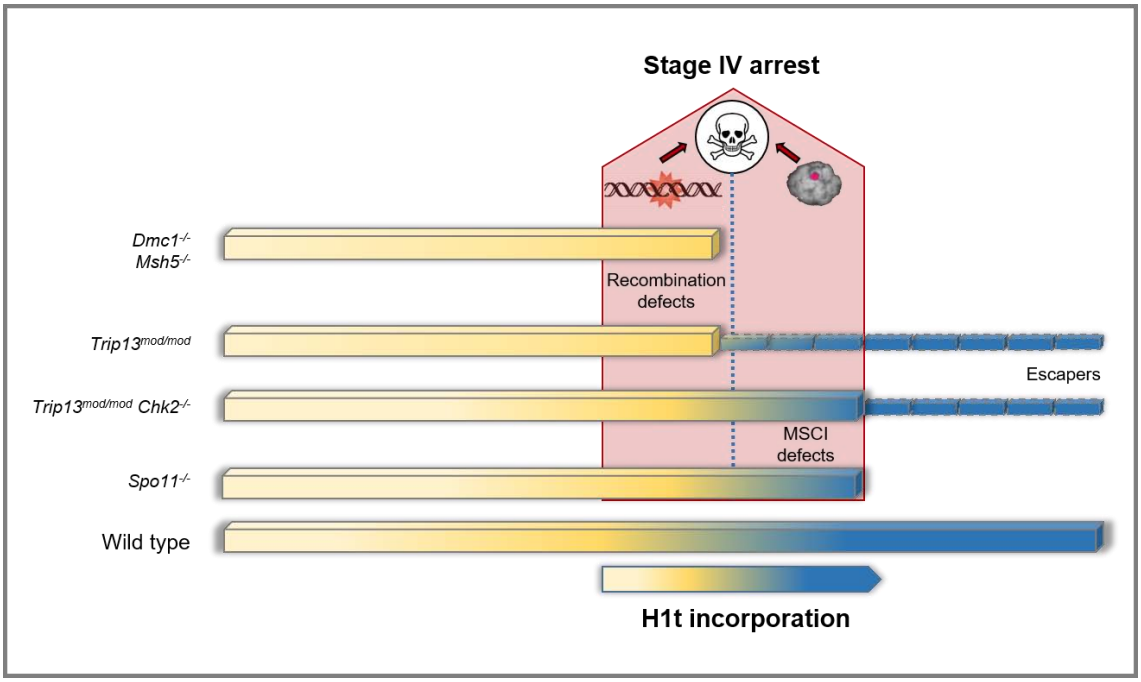

Figure 1.7. **Schematic represtation of pachytene arrest in males.** Both recombination-dependent and sex body-defiecient arrest result in a block of spermatogensis at pachytene stage (epithelial stage IV arrest). However, they are activated by different mechanisms and their spermatocytes apoptose at different timings. While recombination-defective spermatocytes (e.g. *Dmc1*$^{-/-}$, *Msh5*$^{-/-}$) apoptose at early pachynema (before H1t incorporation), spermatocytes that arrest due to synapsis defects (e.g. *Spo11*$^{-/-}$) apoptose at late pachynema (after accumulating H1t, blue bar). Most *Trip13*$^{mod/mod}$ spermatocytes arrest before incorporating H1t, but still some cells manage to escape this arrest, incorporate H1t and complete meiosis. Note that when in *Trip13*$^{mod/mod}$ mice the recombination-dependent arrest is inactivated by *Chk2* mutation (in *Trip13*$^{mod/mod}$ *Chk*$^{-/-}$), most spermatocytes apoptose once they have incorporated H1t into their chromatin. As previously, a subset of cells is able to escape the arrest and complete meiosis.

Mammalian oocytes are also subjected to two control mechanisms that monitor recombination and synapsis progression (Di Giacomo et al. 2005). In females, recombination-dependent response occurs few days after birth when the number of oocytes is greatly reduced. Similarly to what has been found in males, DSB-independent

arrest due to synapsis defects occurs later, and as a result the pool of oocytes is reduced about two weeks after birth (e.g., *Spo11*$^{-/-}$ mutants) (Di Giacomo et al. 2005).

1.2.2.1.1 The recombination dependent arrest

Unrepaired DSBs promote the activation of ATM/ATR kinases triggering a delay in meiotic progression in many organisms, which is called the recombination-dependent checkpoint/arrest. This response gives more time to repair the DSBs before progressing to the next stages, or if cells are unable to repair the DSBs they are eliminated through apoptosis (MacQueen and Hochwagen 2011). In mice, recombination failure triggers pachytene block (e.g. *Dmc1*$^{-/-}$, *Msh4*$^{-/-}$, *Msh5*$^{-/-}$ *or Trip13*$^{mod/mod}$) (Pittman et al. 1998; de Vries et al. 1999; Edelmann et al. 1996, 1999; Yoshida et al. 1998; Kneitz et al. 2000).

Recently, some of the proteins involved in the activation of the recombination-dependent arrest in mouse meiocytes have been reported thanks to the use of *Trip13* mutants (Pacheco et al. 2015; Bolcun-Filas et al. 2014). *Trip13* mutants present recombination defects, triggering the activation of the recombination-dependent arrest, which blocks spermatocyte progression at an early pachytene stage (before H1t incorporation) (Li et al. 2007; Roig et al. 2010; Pacheco et al. 2015). Mutation of MRE11, NBS1, ATM or CHK2 bypassed *Trip13* arrest by increasing the number of H1-positive cells and reducing the number of spermatocytes that apoptose at early pachynema (see *Trip13*$^{mod/mod}$ versus *Trip13*$^{mod/mod}$ *Chk2*$^{-/-}$ in Fig. 1.7). Therefore, the MRE11 complex, ATM and CHK2 signaling pathway implements the recombination-dependent arrest occurring in mouse spermatocytes (Pacheco et al. 2015). Similarly, CHK2 protein through p53 and TAp63 downstream activation, are responsible for eliminating oocytes with persistent unrepaired DSBs; as CHK2 or p53 (and TAp63 in some extent) rescue *Trip13* mutants oocyte loss (Suh et al. 2006; Bolcun-Filas et al. 2014; Kim and Suh 2014).

1.2.2.1.2 The synapsis dependent arrest

In mouse, the asynapsed regions of the chromosomes are detected and silenced by the MSUC mechanism. This meiotic silencing serves as a prophase surveillance mechanism, since impaired synapsis activates this mechanism promoting a meiotic arrest. Mouse meiocytes lacking *Spo11* are not able to properly complete homologous chromosome synapsis driving a DSB-independent apoptosis, which is distinctively activated in males or females due to sexual dimorphism (Baudat et al. 2000; Romanienko and Camerini-Otero 2000; Di Giacomo et al. 2005; Barchi et al. 2005).

In males, the MSUC mechanism detects the asynapsed X and Y chromosomes and promotes the MSCI. This silencing of the X and Y genes is crucial for meiotic progression, since misexpression of sex chromosome genes at pachynema becomes "toxic" for spermatocytes (Royo et al. 2010). Extensive asynapsis of the autosomes in synapsis-defective mutants (e.g. in *Spo11*$^{-/-}$) or associated with persistent DNA damage (e.g. *Dmc1*$^{-/-}$ mutants), is thought to dilute the MSUC silencing cofactors along the asynapsed axes (e.g. HORMAD1/HORMAD2 remain spread over all the autosomes; BRCA1 and ATR remain sequestered at the DSBs sites). Consequently, this alteration of the silencing cofactors mitigates MSUC mechanism, specially attenuating silencing of the XY chromosomes, which results in apoptosis due to sex chromosome genes expression (Mahadevaiah et al. 2008; Royo et al. 2010).

On the other hand, in mouse synapsis-defective females, MSUC detects asynapsed chromosome axes and promotes silencing of these regions. It has been found that oocytes display a less efficient meiotic silencing on asynapsed chromosomes than males, with absence of the epigenetic marker H3K9me (Taketo and Naumova 2013; Cloutier et al. 2015b). Therefore, gene silencing across the γH2AX-coatted unsynapsed chromosome occurs in a stochastic manner, which would possibly affect genes required for post-pachytene oocyte progression and consequently drive a meiotic arrest (Cloutier et al. 2015b). In fact, oocyte loss due to extended asynapsis of *Spo11* mutants can be rescued by deletion of silencing components like *Hormad1*, *Hormad2* or *H2ax* (Daniel et al. 2011; Wojtasz et al. 2012; Cloutier et al. 2015a).

1.3 Pachytene checkpoint 2 protein / TRIP13

Pch2 (Pachytene checkpoint 2 gene) is a widely conserved protein that can be found in *S. cerevisiae*, *A. thaliana*, *D. melanogaster*, *C. elegans* (pch-2) and mammals (called TRIP13). Pch2 belongs to AAA+ ATPases family, a diverse group of enzymes that couple ATP binding and hydrolysis inducing conformational changes on substrates. They participate in multiple cellular processes including protein degradation, transcriptional regulation, DNA replication, protein folding and unfolding and assembly and disassembly of protein complexes (Hanson and Whiteheart 2005; Tucker and Sallai 2007). Like many AAA+ ATPases, Pch2 oligomerizes into hexameric rings with a central pore in the presence of nucleotides (Chen et al. 2013). In yeast, Pch2 is a meiosis specific gene that is transcribed before entering meiosis I and peaks at pachytene stage having multiple functions (San-Segundo and Roeder 1999). Pch2 controls CO outcome, as *pch2* deficiency

results in defective interhomolog bias, reduced CO interference, increased CO levels and defective homeostasis (Zanders and Alani 2009; Joshi et al. 2009; Wu and Burgess 2006; Börner et al. 2008).

Pch2 was first identified in *S. cerevisiae* as a checkpoint protein that bypassed *zip1* arrest (San-Segundo and Roeder 1999). Zip1 protein is a component of the central element of the SC, and its absence drives synapsis defects and accumulation of recombination intermediates, triggering a checkpoint arrest at pachytene stage. The *zip1 pch2* double mutants recover wild type levels of sporulation frequency. Thus, it was rapidly assumed that Pch2 was required to implement the synapsis-dependent checkpoint in yeast. Studies in other model organisms confirmed this was a conserved function, *C. elegans* Pch2 is also required to induce the apoptosis originated by defective homologous synapsis (Bhalla and Dernburg 2005). Nonetheless, Pch2 checkpoint functions are more complex since yeast Pch2 absence also abolishes *zip2* and *dmc1* mutants arrest (San-Segundo and Roeder 1999). Furthermore, Pch2 homologue in *Drosophila* was found to be required for the delay in oocyte selection produced by recombination defects (Joyce and McKim 2009).

In yeast, Pch2 has been reported to interact with DDR proteins in response to unprocessed DSBs. Since Pch2 has been found to interact with Xrs2 (NBS1 homologue from the MRE11 complex) and via Tel1^{ATM} pathway Pch2 facilitates Hop1$^{HORMAD1/2}$ phosphorylation; it has been proposed that Pch2 could help to recruit Hop1 to DSBs sites to facilitate Hop1 roles in DSB formation, interhomolog bias and checkpoint function (Carballo et al. 2008; Ho and Burgess 2011; Panizza et al. 2011). Hop1 is a DNA binding protein that contains a zinc finger domain and a HORMA domain that localizes over the chromosome axes and can be phosphorylated by Mec1^{ATR} and Tel1^{ATM} kinases in response to DNA damage (Hollingsworth et al. 1990; Carballo et al. 2008). *In vitro* Pch2 binds to Hop1$^{HORMAD1/2}$ and can displace it from DNA substrates (Chen et al. 2013), which can be related with Pch2 control over chromosome axis conformation. Pch2 regulates Hop1 localization on the chromosome axes by promoting the Zip1/Hop1 alternating pattern, where Hop1 tends to localize at designated CO sites. Absence of Pch2 results in uniform distribution of Hop1 over the entire Zip1 length (Börner et al. 2008). Therefore, Pch2 is proposed to bind Hop1 *in vivo* and induce a conformational change upon ATP hydrolysis, modulating Hop1 localization at specific sites to regulate interhomolog repair (Joshi et al. 2009; Chen et al. 2013).

Interestingly, in yeast, most Pch2 protein localizes in the nucleolus, the region containing ribosomal DNA (rDNA). Nucleolar Pch2 it is thought to represses DSBs formation and interhomolog recombination in rDNA by excluding Hop1 from the

nucleolus (San-Segundo and Roeder 1999). The rest of Pch2 protein is present forming foci on the synapsed chromosomes co-localizing with Zip1 (San-Segundo and Roeder 1999). Nucleolar Pch2 localization is Sir2-dependent. Sir2 is a chromatin silencing factor (modulates closed chromatin conformation) that also localizes in the nucleolus and controls repression of recombination in the rDNA (Gotta et al. 1997; Gottlieb and Esposito 1989). Indeed, *sir2* mutation also bypassed *zip1* arrest, showing that the nucleolus Pch2 fraction is the one responsible to control the meiotic checkpoint (San-Segundo and Roeder 1999).

1.3.1 Mammalian TRIP13

In mouse, TRIP13 (thyroid hormone receptor interacting protein 13) is the mammalian Pch2 orthologue, which is expressed during development and in many tissues. It is also expressed in testis, where it presents a specific isoform (lacking the Walker B ATPase motif) in spermatocytes and spermatids (Roig et al. 2010). TRIP13 is required for gametogenesis completion of both male and female (Li et al. 2007; Roig et al. 2010). *Trip13* null mutation is incompatible with embryo development (J. Schimenti, personal communication), thus most studies performed in mouse have used hypomorphic mutations that significantly decrease *Trip13* expression. Two *Trip13* mutants where generated from ES cell lines containing a gene-trap disrupted allele either in the second intron (CH0621 cell line) or the third intron (RRB047 cell line), leading to two hypomorphic mutations with distinct penetrance phenotype (Li et al. 2007; Roig et al. 2010). *Trip13*^{RRB047} (or *Trip13*^{Gt} or *Trip13*^{mod}, for *moderate*) testes present lower *Trip13* expression levels than wild type, but these are even more reduced in *Trip13*^{CH0621} (or *Trip13*^{sev}, for *severe*), which is related to a more penetrant effect (Roig et al. 2010). Male *Trip13*$^{mod/mod}$ mutant mice present reduced testes size associated to pachytene arrest. Most spermatocytes from *Trip13*$^{mod/mod}$ present recombination defects: reduced Rad51 foci at leptonema, inefficient recombination completion, reduced CO formation and altered CO interference (Li et al. 2007; Roig et al. 2010). However, most spermatocytes carrying the *moderate Trip13* mutant allele are able to achieve full homologous synapsis despite the presence of abundant recombination intermediates. Importantly, few *Trip13*$^{mod/mod}$ escapers (that probably contain high TRIP13 levels) can complete meiosis reaching round spermatid stage (Li et al. 2007; Roig et al. 2010). Still, since most *Trip13*$^{mod/mod}$ spermatocytes accumulate unrepaired DSBs they activate the recombination-dependent arrest and apoptose at early pachynema (before incorporating H1t), triggering epithelial

stage IV arrest at pachytene stage (Li et al. 2007; Roig et al. 2010; Pacheco et al. 2015). Characterization of the *Trip13 severe* mutant allele revealed that *Trip13*$^{sev/sev}$ spermatocytes are not able to complete synapsis and no spermatocytes progress any further than zygotene stage (no escapers found) (Roig et al. 2010). Regarding females, oogenesis is also defective for both allele mutants. At 21 dpp *Trip13 moderate* mutant females have fewer developing follicles than the wild type, but no primordial follicles are observed. *Trip13 severe* female phenotype is more penetrant, since no oocytes are found at already 21 dpp; such early block of folliculogenesis is associated with recombination failure (Di Giacomo et al. 2005), suggesting that TRIP13 is also required for completing meiotic recombination in oocytes. (Li et al. 2007; Roig et al. 2010).

Similarly to Pch2, mouse TRIP13 also regulates the chromosome axis composition by controlling localization of HORMAD1 and HORMAD2 proteins (yeast Hop1) (Wojtasz et al. 2009; Fukuda et al. 2010). In wild type spermatocytes, HORMAD1 and HORMAD2 proteins become depleted from chromosomal axis once synapsis has occurred (Wojtasz et al. 2009). Instead, in pachytene-stage *Trip13*$^{mod/mod}$ spermatocytes HORMAD proteins are still present on the synapsed axis. Thus, TRIP13 is required to deplete HORMAD1 and HORMAD2 from the synapsed chromosome axis (Wojtasz et al. 2009; Roig et al. 2010). This role on HORMAD1 and HORMAD2 might explain the fact that TRIP13 protein has been recently found to be required to form a functional sex body. In *Trip13*$^{mod/mod}$ spermatocytes HORMAD proteins cover all the axes of the autosomes, which limit the asynapsis signaling over the sex body. Indeed, *Trip13*$^{mod/mod}$ mutant spermatocytes fail to properly load ATR over the sex chromosome axes, which leads to reduced H2AX phosphorylation and SUMO-1 incorporation over the sex body chromatin, resulting in inefficient MSCI (see results in section 4.3.2 and (Pacheco et al. 2015)).

TRIP13 is emerging as a key regulator of chromosomes structure, through controlling several HORMA-domain containing proteins. In somatic cells, TRIP13 has been found to be a kinetochore protein that interacts with several mitotic regulators, among them p31^{comet} and MAD2 (HORMA domain proteins). The Spindle Assembly Checkpoint (SAC, composed by MAD2, BUBR1 and BUB3 proteins) prevents chromosome segregation until all chromosomes are correctly bioriented at the spindle, by inhibiting the Anaphase Promoting Complex (APC). Precisely, TRIP13 biding to p31^{comet} has been found to promote MAD2 release from the SAC and consequently turns off the checkpoint (Tipton et al. 2012; Wang et al. 2014; Eytan et al. 2014). Remarkably, TRIP13 has been found to be overexpressed in multiple cancers, which is suggested to lead malignant transformation, aggressive tumor growth and treatment resistance due to premature mitotic checkpoint

signaling and enhanced DNA repair. Moreover, TRIP13 has been shown to promote DNA repair via NHEJ in human cells; by its interaction with KU70, KU80 and DNA-PKcs (members of the NHEJ repair pathway). (Banerjee et al. 2014).

1.4 DNA damage response in somatic cells

As DNA damage represents a hazardous event for organisms, cells have developed a highly organized network of signaling pathways, named DNA damage response (DDR). The DDR detects the presence of DNA lesions through "sensor" proteins and via "transducers" amplifies the signal (protein kinase cascade) to activate a series of effectors that will trigger DNA repair, cell cycle or apoptosis. Slowing down cell cycle progression allows extra time for DNA repair, and if the DNA damage cannot be repaired programmed cell death is activated in order to avoid genome integrity defects. Two PIKKs (phosphoinositide-3-kinase related proteins) family members are the principal surveillance regulators of this response: the ATM (ataxia-telangiectasia mutated) and ATR (ataxia-telangiectasia and Rad-3 related protein).Both ATM and ATR promote the DDR by phosphorylating a large subset of substrates (Fig. 1.8) (Matsuoka et al. 2007).

Of the various forms of DNA damage, DSB represent the most dangerous form. The two helix strands are broken simultaneously, which makes it more difficult to repair and more prone to inappropriate recombination. When DSBs occur in somatic cells, they are detected by the MRE11 complex (MRE11, RAD50, NBS1) which activates the downstream serine/threonine kinase ATM (Lavin 2007; Paull 2015). By binding to the MRE11 complex, at the DSBs sites, ATM is retained over the chromatin and transduces the downstream signaling pathway (Derheimer and Kastan 2010). ATM spreads the signaling cascade by phosphorylating a large set of target effectors involved in DNA repair, cell cycle progression and apoptosis (Stracker et al. 2013; Paull 2015). In somatic cells, ATM impairment reduces DSBs repair capacity, defective activation of checkpoints and apoptosis. ATM substrates include CHK2 (Chaturvedi et al. 1999; Matsuoka et al. 2000) and p53 proteins among others (Fig. 1.8) (Canman et al. 1998; Khanna et al. 1998; Banin et al. 1998).

Other mechanisms, like the repair of DSBs by homologous recombination or replication stress, may lead to the formation of single stranded DNA (ssDNA), which primarily activates ATR. RPA protein binds to the ssDNA, which promotes ATR recruitment to the ssDNA lesion through the help of ATRIP (ATR-interacting protein)

cofactor (Cortez et al. 2001) and binding of TOPBP1 activator (Acevedo et al. 2016). ATR activation also requires binding of the 9-1-1 complex (RAD9-RAD1-HUS1) to the adjacent ssDNA/dsDNA (Yan and Michael 2009). Once activated, ATR phosphorylates several substrates, among them CHK1 kinase that controls intra-S and G2/M checkpoints (Cimprich and Cortez 2008).

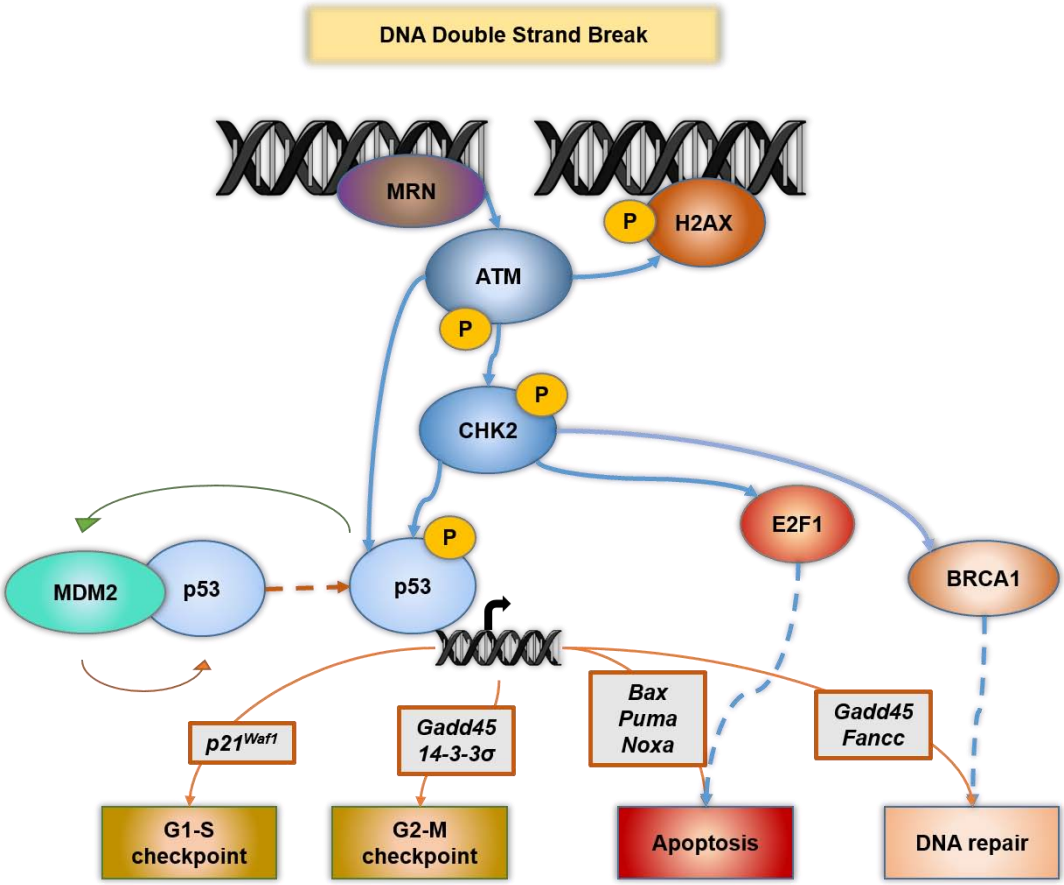

Figure 1.8. DNA damage response by ATM kinase in somatic cells. DSBs are detected by the MRE11 complex (MRE11-RAD50-NBS1) which recruits ATM to the DSBs sites and promotes its auto-phosphorylation. ATM phosphorylates H2AX and a large set of downstream targets to expand the DDR cascade, which promote DNA repair, cell cycle arrest and apoptosis. ATM principal substrates are CHK2 kinase and P53 protein. Both ATM and CHK2 can phosphorylate p53 transcription factor. Upon phosphorylation, p53 unbinds MDM2 (which targets p53 for degradation through the ubiquitin proteolytic pathway) and becomes stabilized being able to perform its function. As a transcription factor, p53 principal functions consist in checkpoint activation, apoptosis and DNA repair. Through $p21^{Waf1}$ activation, p53 arrest cell cycle at G1-S; and G2-M arrest by activating GADD45 and 14-3-3σ. Besides, p53 promotes pro-apoptotic such as PUMA, NOXA or BAX. Moreover, p53 also promotes DNA repair and controls its own levels by a negative feedback loop activating MDM2 expression.

1.4.1.1 Cell cycle control and apoptosis by the DDR

Cell cycle is a complex biological process by which identical diploid chromosome sets are transmitted to two daughter cells. This happens through four sequential phases: G1, S, G2 and M-phase (Lavin and Kozlov 2007). Thus, when DNA damage occurs it is important that the cycle progression of these phases is regulated by checkpoint mechanisms; which allow extra time for repair in order to maintain genomic integrity. If the damage is not repaired, the checkpoint mechanisms activate apoptosis in order to eliminate the damaged cell and thus guarantee genome integrity.

In DNA damaged cells, DSBs activate ATM and ATR which phosphorylates several substrates that control cell cycle progression at G_1/S, S-phase and at G_2/M transition. ATM notably phosphorylates CHK2 a serine/threonine kinase, which has an important role as a signal transducer, and p53 tumor suppressor gene. For G_1/S checkpoint activation, ATM and CHK2 induce p53 tumor suppressor phosphorylation at serine15 (S15) (Banin et al. 1998; Barlow et al. 1997a; Derheimer and Kastan 2010). Once phosphorylated, p53 becomes stabilized and promotes transcription of target genes, delaying G1 to S-phase (Kastan and Lim 2000) and G2/M transition (Taylor and Stark 2001). One of the principal targets of p53 is $p21^{WAF-1}$, which binds and inhibits the S-phase promoting Cdk2-CyclinE complex, and also Cdk4-CyclinD (preventing Rb phosphorylation which promotes S-phase progression) (see other p53 targets in the next section 1.3.2.1 and Fig. 1.8) (Harper et al. 1993; Sancar et al. 2004). Other mediators of cell cycle progression that are included as ATM substrates are MDM2 and MDMX, which influence p53 stabilization (Lavin and Kozlov 2007). Besides, CHK2 also activates the G1/S arrest by phosphorylating CDC25A phosphatase and promoting its degradation (CDC25 phosphatases control cell cycle progression by removing inhibitory residue phosphorylation from cycling-dependent-kinases (CDKs)) (Falck et al. 2001).

Independent of p53, ATM regulates intra S-phase arrest via two pathways. One is the ATM-CHK2-CDC25A-Cdk2. The second requires phosphorylation of SMC1, BRCA1, NBS1 and FANCD2 phosphorylation on multiple sites, which promote the recovery of collapsed replication forks (Kim et al. 2002; Yazdi et al. 2002). Moreover, CHK2 activation regulates G2/M checkpoint through phosphorylation of CDC25 phosphatase, which promotes CDC25 binding to 14-3-3σ protein (becomes degraded) and blocks activation of cyclin B-dependent CDC2 kinase, which is required for initiation of mitosis (Peng et al. 1997).

ATR activates CHK1 kinase, which phosphorylates CDC25 family regulators. Downregulation of CDC25A through phosphorylation promotes p53 stabilization triggering G1/S arrest and inhibits replication origins (Sancar et al. 2004). Phosphorylation of CDC25C on serine-216 creates a binding site for 14-3-3σ protein which inhibits the phosphatase activity (Peng et al. 1997); preventing cell cycle progression by activating the intra-S checkpoint (Sanchez 1997; Feijoo et al. 2001). During S-phase, ATR also promotes phosphorylation of BRCA1 and NBS1 to inhibit replication and promote repair. DNA damage during G2 phase also promotes the ATR-CHK1-CDC25 pathway to activate the G2/M checkpoint (Sancar et al. 2004).

1.4.2 P53 family members

The mammalian p53 family includes: p53 (Lane and Crawford 1979; Linzer and Levine 1979), p63 (Yang et al. 1998) and p73 (Jost et al. 1997); which are transcription factors encoded by three highly conserved genes (Dötsch et al. 2010; Belyi et al. 2010). Each p53 family member has a similar structure with three major domains consisting of an amino-terminal transactivation domain (TA), a DNA binding domain in the center and a carboxy-terminal oligomerization domain. Additionally, only p63 and p73 present a carboxy-terminal sterile α-motif (SAM) involved in protein-protein interaction and a transcription inhibition motif (TI) (see Fig. 1.9) (Dötsch et al. 2010; Allocati et al. 2012). Because of the presence of two alternative promoters at the amino-terminus different isoforms are transcribed in p53, p63 and p73. For instance, p53 has at least six different isoforms which are transcribed in a tissue-dependent manner (Bourdon et al. 2005). For p63 and p73 these promoters also generate several transcript variants, and among these, two major isoforms are: the transactivating isoform (containing the TA domain) and the ΔN isoforms produced by the second promoter (lacking the TA) (Yang et al. 2002; Allocati et al. 2012). Generally, the TA isoforms tend to have tumor suppressor activities, while the ΔN isoforms exert dominant-negative effects, since these variants can bind DNA but do not promote transcription. However the ΔN isoforms have also been seen to activate some targets (Dötsch et al. 2010; Allocati et al. 2012; Yang et al. 2002; Bourdon et al. 2005). Additional splicing of the carboxy terminus and posttranslational cleavage generates several other isoforms resulting in more complexity (Dötsch et al. 2010; Bourdon et al. 2005; Yang et al. 2002; Levine et al. 2011). Because of structural differences and biological functions, each member activates a specific transcriptional network, however there is a common set of shared gens, specially DDR responsive genes (Lin et al. 2009). For instance,

both p53 and TAp63 can promote transcription of the same genes (Yang et al. 1998), and can associate with each other through direct interaction (Gaiddon et al. 2001)). Although tetramerization of p53 with the other family member is less clear, p63 and p73 have been found to form heterotetramers (Joerger et al. 2009). The interplay between the family members, multiple isoforms, their differential tissue expression and ability to oligomerize yields in high complexity and diverse biological functions including prominent roles in the DDR (Candi et al. 2014; Joerger et al. 2009; Murray-Zmijewski et al. 2006).

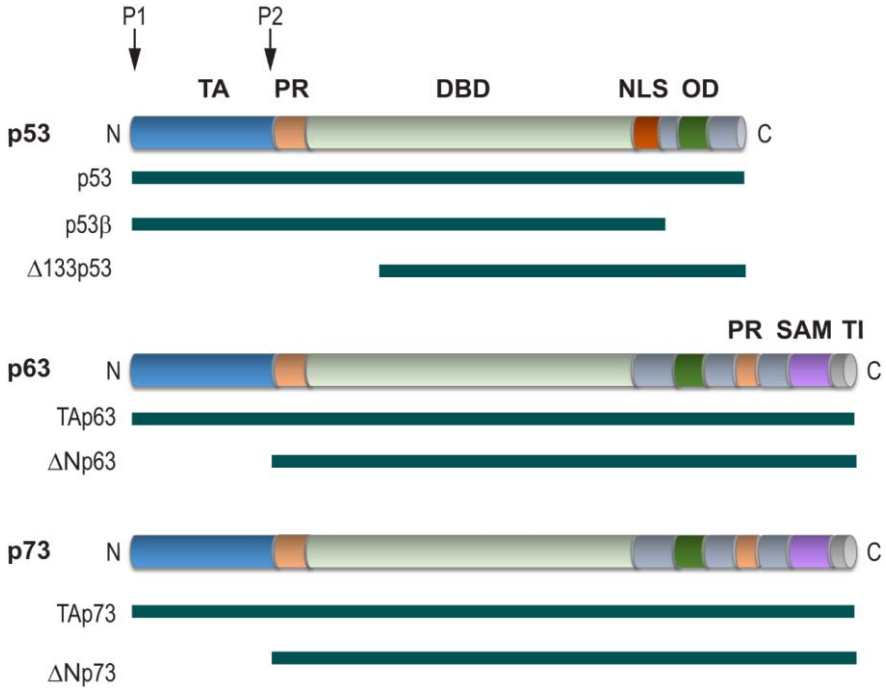

Figure 1.9. P53 family members gene structure. The genes encoding p53 family members: *Trp53*, *Trp63* and *Trp73* are highly conserved and maintain a similar structure. The three members present a trans-activating domain (TA) at the amino-terminus (N), a very similar DNA-binding domain (DBD) and an oligomerization domain (OD) at the carboxyl-terminus. The (PR) correspond to Pro-domains, and p53 contains a nuclear localization signal (NLS). Only p63 and p73 have a sterile α-motif domain (SAM) and a transcription inhibitory domain (TI) at the C-terminal end (C). The presence of two alternate promoters (P1 and P2), 3'-splicing events and posttranslational cleavage generates several distinct isoforms for all the three members. Both p63 and p73 present two principal isoforms: one that contains the TA domain (TAp63 and TAp73), the other is transcribed by P2 amino-truncated (ΔNp63 or ΔNp73) lacking the TA (and principally act as dominant-negative effectors). All this complexity, added to the fact that p53 family member can heteroligomerize, emphasizes the importance of balancing the various members and their isoforms. Image based on Levine et al. (2011).

Although p63 and p73 are able to regulate p53 target genes (Lin et al. 2009), and, like p53, induce cell cycle arrest and apoptosis, studies from knockout mice have demonstrated that each member has distinct functions. The p53 knockout mice are viable and present a normal development, with higher predisposition to tumor malignancy (Donehower et al. 1992; Jacks et al. 1994). Contrarily, p63 knockout mice show several

developmental defects, including limbs development failure and epithelial morphogenesis defects (attributed to ΔN isoforms); and do not survive beyond a few days after birth (Mills et al. 1999). Differently, p73 knockout mice suffer neurodevelopmental hippocampal dysgenesis, pheromone sensory pathway alteration and immunological defects such as chronic infections and inflammation (Yang et al. 2000). However, both p63 and p73 mutants also present development of spontaneous tumors (Flores et al. 2005).

1.4.2.1 p53

The principal role of p53 is to stop proliferation of stressed cells by inhibiting cell cycle progression or promoting apoptosis, in response to diverse stresses such as DNA damage, in order to guarantee genome integrity. Importantly, p53 protein stands out for being a tumor suppressor gene, which explains why is mutated in 50% of human cancers (Petitjean et al. 2007). One of the principal stresses that cells may suffer is DNA damage. Indeed, generation of DSBs promotes an increase of p53 levels. In response to stress, p53 is displaced from its negative regulator MDM2, by independent pathways that activate the p53 network. The main pathway responds to DNA damage, where activation of ATM at the DSBs sites phosphorylates CHK2 kinase, which subsequently phosphorylates p53 at the amino terminus. This phosphorylation on p53 affects its ability to bind MDM2 and consequently avoids its degradation (Fig. 1.8) (Vogelstein et al. 2000). Degradation of p53 requires ubiquitin labelling by the MDM2 protein, which works as a negative feedback loop since MDM2 expression is also regulated by p53 (Momand et al. 2000). A second pathway is activated by aberrant hyperproliferation signals, resulting from oncogenes Ras or MYC signaling, where p53 activation depends on $p14^{ARF}$. Stabilization of ARF promotes its binding to MDM2, which inhibits MDM2 activity and sequesters it into the nucleolus (Sherr and Weber 2000; Lin and Lowe 2001). Besides these two main classical pathways, p53 is also activated in response to replicative stress, hypoxia, oxidative stress, ribonucleotide depletion, nutrient starvation and telomere attrition (Fig. 1.10) (Bieging et al. 2014).

These pathways inhibit degradation of p53, leading to its stabilization and increased levels, promoting p53 to bind DNA and consequent transcription. Through the tetramerization domain, p53 monomers form active tetramers that recognize p53 target binding sites (Friedman et al. 1993). Historically two main subsets of p53 target genes were identified: negative regulators of cell cycle progression and apoptosis inducers. However, the number of p53 target genes is very extensive, including genes involved in

DNA repair, senescence, metabolism, autophagy, stem cells biology, tumor invasion and tumor microenvironment (Fig. 1.10) (Bieging et al. 2014).

Regarding cell cycle regulation, p53 promotes transcription of the cyclin dependent kinase (cdk) *p21* which inhibits Cyclin-E/CDK2 complex, causing an arrest of cell cycle progression from G1 to S-phase (el-Deiry et al. 1994; Kastan and Lim 2000). Moreover, p53 seems to maintain the G2/M checkpoint in part by up-regulating other DNA-damage genes GADD45, BTG, 14-3-3σ or by signaling retinoblastoma protein (Lavin and Kozlov 2007; Derheimer and Kastan 2010; Jin et al. 2000). If DNA damage persists, p53 levels increase and induce transcription of pro-apoptotic genes like *Puma*, *Noxa* or the Bcl-2 associated *Bax*, which activate caspases and programmed cell death (Fig. 1.8 and 1.10) (Roos and Kaina 2006; Oren 1994; Reinhardt and Schumacher 2012). Moreover, p53 has also been found to eliminate damaged cells through the innate immune system and to participate in tissue degenerating and aging (Reinhardt and Schumacher 2012).

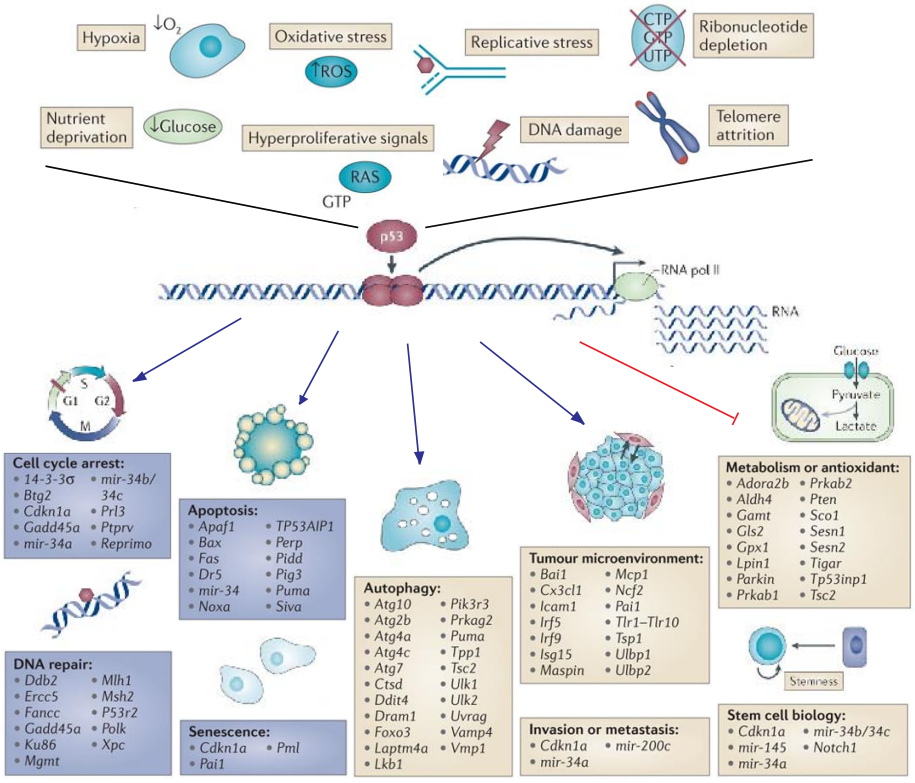

Figure 1.10

The p53 network: activating signals and responses in somatic cells. p53 protein is activated upon stresses coming from different sources: hypoxia, oxidative stress, replicative stress, ribosomal nucleotide depletion, nutrient deprivation, hyperproliferative signals, DNA damage and telomere attrition. Once p53 is activated and stabilized it promotes transcription of several genes which principally lead towards tumor suppression. Among several responses, the classical ones include cell cycle arrest, apoptosis, promote DNA repair and senescence. Other responses are related with activation of autophagy, regulation of the microenvironment and tumor invasion; as well as inhibiting tumor metabolism and stem-cell renewal. Image adapted from Bieging et al. (2014).

1.4.2.2 p63 and p73

Both p63 and p73 can control cell cycle progression and apoptosis through similar mechanisms attributed to p53. However, the mechanisms remain less clear than in p53 due to redundant properties and balance complexity. For instance, p53-dependent apoptosis upon DNA damage in mouse embryonic fibroblasts requires the presence of at least either p63 or p73 (Flores et al. 2002). Expression of p73 during cell cycle peaks at the S-phase and during mitosis p73 is phosphorylated by $p34^{cdc2}$-CyclinB complex (Fulco et al. 2003). G1/S checkpoint arrest can be induced by TAp73, but also by TAp63, through transcriptional up regulation of p21 (Jost et al. 1997; Zhu et al. 1998; Osada et al. 1998; Dohn et al. 2001). Another target of p73 is $p57/^{Kip2}$ (a cyclin-dependent kinase inhibitor), which coordinates mitotic exit and transition to G1 (Merlo et al. 2005); but is the ΔNp63α isoform that induces $p57/^{Kip2}$ activation (Beretta et al. 2005; Pateras et al. 2009). Surprisingly, ΔN isoforms (although lacking the transactivation domain) can induce transcription of some gens at low levels (Dohn et al. 2001; Allocati et al. 2012). However, in general ΔN isoforms usually repress promoters by acting as dominant negative forms and thus allowing cell cycle progression. Moreover, in the absence of p53, p73 has been shown to regulate cyclin-Cdks: cyclin E-Cdk2 and cyclin A-Cdk2 and cyclin B-Cdk1 in G1 phase (Talos et al. 2007). Like p53, TAp73 also contributes to G2/M checkpoint by upregulating 14-3-3σ (Zhu et al. 1998) and by repressing the expression of other regulators like CDC25B, CDC25C, *cdk1, Cyclin B1*, Cyclin B2, cdc2 (Jung et al. 2001; Allocati et al. 2012). Interestingly, p63 and ΔNp63 have similar repressive activity over Cyclin B2, CDC25C and CDC2 (Allocati et al. 2012; Lau et al. 2013) but also activate induction of GADD45 to regulate G2/M checkpoint (Dohn et al. 2001). Additionally, TAp73 has been found to participate in the SAC checkpoint, which prevents anaphase progression by negatively regulating CDC20, restricting anaphase promoting complex (APC) polyubiquitination activity. TAp73 interacts and cooperates with spindle assembly checkpoints BUB1, BUB3 and BUBR1 proteins. Thus, p73 deficient expression results in an increased aneuploidy (Vernole et al. 2009; Tomasini et al. 2009).

Finally, TAp63 and TAp73 can also induce apoptosis through several mechanisms in response to DNA damage (Talos et al. 2007; Toh et al. 2010). Both p53 family members can control upregulation of the pro-apoptotic Bcl-2 family member BAX, furthermore, p73 promotes expression of other pro-apoptotic genes, like PUMA and NOXA among others (Jost et al. 1997; Melino et al. 2004; Levine et al. 2011; Yoon et al. 2015).

1.4.2.3 P53 family members in mammalian reproduction

The p53 family genes are conserved from invertebrates to mammals. The fact that p53 family members are present in organisms with short life spans, like *Drosophila* or *C. elegans*, suggests that p53 tumor suppression role may not be the original function of the family. Accordingly, recent findings shed light to the p53 family participation in development and fecundity (Hu 2009).

Importantly, p53 family members have been found to participate into surveillance mechanisms during meiosis in non-mammalian species. p53-like proteins in *Drosophila* (Dmp53) and *C. elegans* (CEP-1) are highly expressed in the germ cells. Dmp53 plays an important function in regulating DNA damage-induced apoptosis of primordial germ cells and participates in the ovary development (Brodsky et al. 2000; Sogame et al. 2003). Furthermore, Dmp53 is activated in oocytes in response to SPO11-generated DSBs, and such activation is conserved in mouse spermatocytes (Lu et al. 2010). Similarly, CEP-1 eliminates defective germ cells after irradiation through DNA damaged-induced apoptosis (Derry et al. 2001).

Regarding mammals, p53 is highly expressed during spermatogenesis, and its activation is enhanced after irradiation in spermatocytes and spermatogonia, suggesting a role in DNA damage response (Sjöblom and Lähdetie 1996; Almon et al. 1993; Schwartz et al. 1993; Beumer et al. 1998). In addition, *p53* defective mice present degenerative giant-cells attributed to spermatocytes being unable to repair DSBs (Rotter et al. 1993), and p53-dependent apoptosis is observed on *Arf* mutant spermatocytes, which display increased levels of γH2AX at pachynema (Churchman et al. 2011). In females, as mentioned before, p53 and TAp63 participate in the activation of the recombination-dependent arrest in mouse oocytes (Bolcun-Filas et al. 2014). Also, p53 is important for implantation of the fertilized eggs into the uterus. Indeed, *p53*$^{-/-}$ females give birth to smaller litters, which seems to be a consequence of p53 transcriptional regulation of its target gene leukemia inhibitory factor (LIF), which is required for implantation of the blastocyst (Hu et al. 2007).

The role of p63 in protecting female germ line integrity has been extensively studied. Especially the TAp63 isoforms, but also the ΔNp63 isoforms, are highly expressed in mouse ovaries and testis (Hu 2009). However, in the absence of p63, meiocytes appear to progress normally (Kurita et al. 2005). Nevertheless, p63 was found to be necessary to eliminate irradiated dictyotene-arrested oocytes, protecting them from genomic instability (Suh et al. 2006; Livera et al. 2008). The phosphorylation of TAp63α isoform by

ABL1 is important for stabilizing TAp63 and executing DNA-damage control mechanism. These findings opened potential medical implications, since inhibition of p63 or its activators could help to preserve oocyte reserve during chemotherapy (Gonfloni et al. 2009).

p73$^{-/-}$ mice do not show reproduction defects, however TAp73 null mutants present female infertility and impaired spermatogenesis. Male mouse presented impaired spermatogonial proliferation with increased DNA damage and apoptosis on the seminiferous tubules, resulting in a reduction of spermatocytes and spermatids (Tomasini et al. 2008; Inoue et al. 2014). TAp73 is highly expressed in oocytes, and has been found to regulate several oocyte processes. Indeed, TAp73 deficient females presented more oocytes with spindle abnormalities and exhibited altered folliculogenesis. Moreover, their embryos presented multiple defects like multinucleated blastomeres, leading to embryonic preimplantation failure (Tomasini et al. 2008). Therefore, it has been proposed that the TAp73 isoform participates in the oocyte SAC checkpoint, preventing anaphase progression until chromosomes are properly oriented and attached to the spindle.

Altogether, all these evidences highlight the important role of p53 family members in protecting the germ line from DNA damage and maintaining genomic stability, ensuring successful sexual reproduction.

OBJECTIVES

2. OBJECTIVES

The aim of this work was to better characterize the surveillance mechanisms that exist in mouse meiotic prophase, which contribute to the critical role of maintaining genome integrity of the species. The DNA damage signaling pathway has been associated with the activation of meiotic checkpoint mechanisms in several organisms. Previous work from our group highlighted the role of the MRE11complex-ATM-CHK2 pathway in activating the recombination-dependent arrest in mouse spermatocytes. Therefore, we aimed to identify other proteins involved in the recombination-dependent arrest. Since in somatic cells it is well established that ATM and CHK2 induce p53 phosphorylation to promote cell cycle checkpoint activation, we decided to focus our work in studying the role of the p53 family members in this arrest mechanism. To do so, we used *Trip13* mutants as a model of spermatocytes that arrest at pachytene stage due to the presence of unrepaired DSBs (Li et al. 2007; Roig et al. 2010). Our data from analyzing recombination-dependent arrest in *Trip13* mutants prompt us to investigate TRIP13 role in meiotic silencing of the unsynapsed chromatin (MSUC) and in particular in the sex chromosomes (MSCI).

We established the following objectives in order to accomplish our purposes:

I. **Identify the components that mediate the recombination-dependent arrest.** For this, we analyzed activation of several candidate proteins in recombination and/or synapsis defective mutants.

II. **Study p53 role in male mouse meiosis**. To achieve this objective we characterized in detail synapsis, recombination and prophase progression in *p53* mutant spermatocytes.

III. **Evaluate the participation of p53 family members in the recombination-dependent arrest.** To address this objective we studied the phenotype of double mutants that carried *p53*, *TAp63* or *p73* mutation in combination with a hypomorphic mutation of the *Trip13* gene.

IV. **Analyze TRIP13 role in meiotic silencing of unsynapsed chromosomes.** We studied the transcriptional silencing occurring on unsynapsed chromosomes of Trip13 mutant spermatocytes.

V. **Analyze the role of TRIP13 in the transcriptional regulation during meiotic prophase.** We studied the global RNA expression levels and transcription profile in *Trip13* mutants to investigate TRIP13 involvement in the regulation of gene expression during meiosis.

MATERIALS AND METHODS

3. MATERIALS AND METHODS

3.1 BIOLOGICAL MATERIAL

3.1.1 Experimental mutant mice

Mice carrying *Trip13*, *p53*, *TAp63*, *p73, Spo11* and *Dmc1* mutations were previously generated and described elsewhere (Roig et al. 2010; Jacks et al. 1994; Su et al. 2009; Yang et al. 2000; Baudat et al. 2000; Pittman et al. 1998). These lines were maintained in a C57Bl/6-129/Sv mixed background. All experiments were performed using at least two animals (unless mentioned in the text) and compared with control littermates when possible, or from animals of closely related parents.

Experiments performed in this study comply with US and EU regulations and were approved by the Ethics Committee of the UAB and Catalan Government and by the MSKCC Institutional Animal Care and Use Committee.

3.2 MOLECULAR BIOLOGY

3.2.1 Genomic DNA extraction

Tail-extracted genomic DNA was used for genotyping, in order to detect the newborn mice carrying the described mutations.

Protocol:

- Place 0.5 mm of mouse tail into a 1.5 ml tube.
- Add 490 µl of Lysis buffer (0.1 M Tris-HCl pH= 8.5-9, 0.2 M NaCl, 0.2% SDS and 5 mM EDTA in Milli-Q water) + 0.4 µg/µl of Proteinase K (10 µl of 20 mg/ml stock, Roche Diagnostics).
- Incubate tubes overnight at 56ºC and 350 rpm in a thermomixer.
- Centrifuge tubes at 13200 rpm for 15 minutes. Transfer the supernatant into a new tube containing 0.5 ml of isopropanol. Shake vigorously until DNA precipitates.
- Centrifuge tubes at 13200 rpm for 3 minutes. Discard supernatant (without disturbing the pellet formed at the bottom).
- Add 0.5 of ice-cold 70% ethanol to wash the pellet. Shake the tube.

- Centrifuge tubes at 13200 rpm for 3 minutes. Discard supernatant and air dry the pellet at room temperature.
- Add 100 µl of Milli-Q water and dissolve the pellet placing the tubes at 60ºC for 10 minutes. Keep the extracted DNA at -20ºC.

3.2.2 Genotyping

Genomic DNA was amplified by the Polymerase Chain Reaction (PCR) in order to genotype the mice. Previously designed primers for every gene were used to amplify the wild type or the mutated allele, which were distinguished based on the corresponding length of the amplified products.

Table 3.1 *p53* primers

Primer name	Allele specificity	Sequence	Amplified product
p53x6-5 R	+/-	5' – ACAGCGTGGTGGTACCTTAT – 3'	
neop53	-	5' – TCCTCGTGCTTTACGGTATC – 3'	525 bp
p53x7 F	+	5' – TATACTCAGAGCCGGCCT – 3'	375 bp

Table 3.2 *TAp63* primers

Primer name	Allele specificity	Sequence	Amplified product
WT-R	+/-	5' – ACTGAGCATATAGGCCTAGCAC – 3'	
TAp63-KO-F	-	5' – CCACATAGCCATATCTGCC – 3'	700 bp
WT-F	+	5' – ACTGGTGAGCTTGTAGAATCGG – 3'	300 bp

Table 3.3 *p73* primers

Primer name	Allele specificity	Sequence	Amplified product
ex1-188-13	+/-	5' – GGGCCATGCCTGTCTACAAGAA – 3'	
p73neo	-	5' – GAAAGCGAAGGAGCAAAGCTG – 3'	400 bp
ex5-188-19	+	5' – CCTTCTACACGGATGAGGTG – 3'	600 bp

Table 3.4 *Spo11* primers

Primer name	Allele specificity	Sequence	Amplified product
SP16R	+/-	5' – ATGTTAAAAAACATAGGTTTGTAAGTT – 3'	
Forward PRSF2	-	5' – CTGAGCCCAGAAAGCGAAGGAA – 3'	600 bp
Forward SP1F	+	5' – CTACCTAGATTCTGGTCTAAGC – 3'	1024 bp

Table 3.5 *Trip13 moderate* primers

Primer name	Allele specificity	Sequence	Amplified product
RRB047 R	+/-	5' – ACCCACCTTTGACCATTTAGTTT – 3'	
RRB047 MUT F	-	5' – CCACGCTCACCGGCTCCAGA – 3'	855 bp
RRB047 WT F	+	5' – GGGAGGGAGGCGTGGCAGAG – 3'	387 bp

Table 3.6 *Trip13 moderate* primers

Primer name	Allele specificity	Sequence	Amplified product
TRIP13GENO R5	+/-	5' – CTATAGTGCCCTTAGGCTCAGG – 3'	
TRIP13GENO F4	-	5' – CGGGCCCTATCTTTTCAGTTCC – 3'	1150
RRB047 End F2	+	5' – TAACCCACTCGTGCACCCAACT – 3'	1050

Table 3.7 *Trip13 severe* primers

Primer name	Allele specificity	Sequence	Amplified product
SIGTR 621 R2	+/-	5' – CCAGGGCACATCAGTAGGAAGC – 3'	
RRB047END-F4	-	5' – GCGGTTAGCTCCTTCGGTCCTC – 3'	642 bp
SIGTR 621 F2	+	5' – CTCAGAGAAGACCCAAAGCACAGT – 3'	319 bp

Table 3.8 *Dmc1* primers

Primer name	Allele specificity	Sequence	Amplified product
DmcFor2	-	5' – CCACTGCCCGGCCAGATTACAT – 3'	
pGKR	-	5' – GACTAGGGGAGGAGTAGAAGGT – 3'	280 bp
DP2	+	5' – GAAGTCAGAGGACAACTTGCC – 3'	
DP18	+	5' – CTGTCTGGGGTTGAATTCTGTC – 3'	165 bp

Protocol:

- Add 1 µl of genomic DNA or 1 µl of MilliQ-water for the negative control into a 0.2 µl PCR tube.
- Prepare the PCR Mix following manufacturer Canvax mix Horse-Power Taq DNA Polymerase recombinant Kit, and add the corresponding volume to the 0.2 µl PCR tube.

Table 3.9 PCR Mix reaction

PCR Mix	Volume (for a 20 µl reaction)
10x PCR buffer	2 µl
$MgCl_2$ 25 mM	1.36 µl
dNTPs 8 mM	2 µl
Primer Forward 10 µM	1 µl
WT Primer Reverse 10 µM	1 µl
Mutant Primer Reverse 10 µM	1 µl*
Template Genomic DNA	1 µl
Horse-Power-Taq DNA polymerase (5 U/µL)	0.5 µl
MilliQ-water	to 20 µl

* 2 µl for neop53 primer, separate reactions for the wild type and mutant bands of *Trip13* moderate (RRB047 R, RRB047 MUT F, RRB047 WT F) and add a fourth primer for *Dmc1*.

- Place PCR tubes in the thermal cycler and perform the corresponding cycling program for each genotyping reaction.

Table 3.10 *p53* cycling program

p53		
Predenaturation	94ºC for 2 minutes	
Denaturation	94ºC for 45 seconds	x 25 cycles
Annealing	60ºC for 1 minute	
Extension	72ºC for 21 minute1	
Hold	4ºC	

Table 3.11 TAp63 cycling program

TAp63		
Predenaturation	94ºC for 3 minutes	
Denaturation	94ºC for 1 minute	x 30 cycles
Annealing	60ºC for 1.5 minutes	
Extension	72ºC for 2 minutes	
Final extension	72ºC for 5 minutes	
Hold	4ºC	

Table 3.12 *p73* cycling program

p73		
Predenaturation	95ºC for 5 minutes	
Denaturation	95ºC for 30 seconds	x 40 cycles
Annealing	60ºC for 30 seconds	
Extension	72ºC for 1.5 minutes	
Final extension	72ºC for 7 minutes	
Hold	4ºC	

Table 3.13 *Spo11* cycling program

Spo11	
Predenaturation	94ºC for 4 minutes
Denaturation	94ºC for 20 seconds
Annealing	59ºC for 45 seconds
Extension	72ºC for 35 seconds
Final extension	72ºC for 7 minutes
Hold	4ºC

x 35 cycles

Table 3.14 *Trip13 moderate* cycling program

Trip13 moderate	
Predenaturation	94ºC for 2 minutes
Denaturation	94ºC for 20 seconds
Annealing	59ºC for 30 seconds
Extension	72ºC for 35 seconds
Hold	4ºC

x 34 cycles

Table 3.15 *Trip13 moderate* and *severe* cycling program

Trip13 moderate and severe	
Predenaturation	94ºC for 2 minutes
Denaturation	94ºC for 20 seconds
Annealing	59ºC for 30 seconds (-0.1C/cycle)
Extension	72ºC for 35 seconds (+00:01/cycle)
Hold	4ºC

x 34 cycles

Table 3.16 *Dmc1* cycling program

Dmc1		
Predenaturation	94ºC for 2 minutes	
Denaturation	94ºC for 20 seconds	x 39 cycles
Annealing	62ºC for 30 seconds	
	(-0.1ºC/cycle)	
Extension	72ºC for 25 seconds	
	(+ 1 second/cycle)	
Hold	4ºC	

- Run the amplification products in a 1% agarose gel with 1% of Ethidium bromide, together with a weight molecular marker.
- Read the gel with GelDoc XR+ system (Bio-Rad) and determine the size of the amplified bands.

3.2.3 RNA extraction

RNA was extracted from whole testis using the RNeasy Plus mini kit from Qiagen, in order to perform Real time PCR or RNA sequencing.

Protocol:

- Cut a piece of frozen testis, a quarter of an adult wild type testis or use a whole testis for mutant or juvenile mice (about 30 mg or less).
- Disaggregate the tissue in a 1.5 µl tube with a pestle.
- Add 600 µl of RLT buffer + 10 µl β-mercaptoethanol and homogenize the lysate with a 20-gauge needle and a syringe (pass the lysate five times).
- Centrifuge three minutes at maximum speed.
- Transfer the supernatant into a gDNA Eliminator spin column paced in a 2ml collection tube.
- Centrifuge for 30 seconds at 10000 rpm. Discard column.
- Add 600 µl of 70% ethanol to the eluted liquid and mix with the pipette.

- Transfer 700 µl to the RNeasy spin column.
- Centrifuge for 15 seconds at 10000 rpm. Discard eluted liquid, repeat previous step and discard liquid.
- Add 700 µl of RWI buffer to the column to wash the column membrane.
- Centrifuge for 15 seconds at 10000 rpm and eliminate eluted liquid.
- Add 500 µl of RPE buffer to wash the column membrane.
- Centrifuge for 2 minutes at 10000 rpm and eliminate eluted liquid.
- Place column to a new 1.5 ml tube and add 30 µl of RNase-free water to the column.
- Centrifuge for 1 minute at 10000 rpm to obtain the extracted RNA diluted in the eluted water.
- Quantify the extracted RNA with Nanodrop (Thermo scientific) and its quality with the Bioanalyzer (Agilent 2100).

3.2.4 RNA sequencing

For RNA sequencing 2 µg of RNA, with a RNA Integrity Number (RIN) > 8, were sequenced at Centre Nacional d'Anàlisi Genòmica (CNAG). RNA samples were quantified again with qubit-RNA Fluorometer. In order to generate the cDNA sequencing library poly-A tails primers were used. From this "Stranded mRNA" library it was performed the mRNA-Sequencing for a paired-end 75 pb read length with sequencing depth of >55 M of reads for each sample (Illumina).

The 75x2 pair-end reads were mapped with the software GEM-Spit-RNA-Mapper (to map the reads to the mouse genome reference annotation GRCm38) (Marco-Sola et al. 2012). To quantify the transcripts that maps to each gene Flux Capacitator software was used (Montgomery et al. 2010). Then, to study the differential expression, and to normalize: number of reads per gene/total of mapped reads, between the wild type and mutant mice the R EdgeR software was used (Robinson et al. 2010). This algorithm normalizes the data with the TMM method (Robinson and Oshlack 2010) considering different library sizes and different RNA composition between the samples.

3.2.5 Real-time PCR

RNA sequencing was validated with quantitative PCR gene expression analysis.

Protocol:

- 2µg of total RNA were used for cDNA synthesis with iScript Advanced cDNA Synthesis (Bio-rad), which uses oligo(dT) and random primers, according to manufacturer's instructions:

Table 3.17 Reverse transcription mix

Mix	20 µl reaction
Reaction mix	4 µl
Reverse Transcriptase	1 µl
RNA	2 µg
MilliQ-water	Up to 20 µl

- Tubes were first incubated for 30 minutes at 42ºC and then 5 minutes at 85ºC.
- All samples used in the experiment were reverse transcribed at the same time and diluted into a concentration of 15 ng/µl with nuclease-free water.
- For Real Time-PCR (qPCR) amplification intro-spanning PrimePCR primers (Bio-Rad) and iTaq Universal SYBR Green Supermix (Bio-Rad) were used.

Table 3.18 PrimePCR primers used

Gene	UniqueAssayID
Atp8b3	qMmuCID0022076
Hmbs	qMmuCID0022816
Qrich2	qMmuCID0017034
Tktl1	qMmuCID0021812
Trip13	qMmuCID0019092
Xaf1	qMmuCID0009205
Zfy2	qMmuCID0021345

- 96-well plate were designed and each well contained (Table 3.19):

Table 3.19 Real time PCR reaction mix

Mix	10 µl reaction
PrimePCR primers	0.5 µl
SYBR green	5 µl
cDNA	1 µl (15ng)
MilliQ-water	3.5 µl

- The protocol program consisted in an initial denaturation step at 95ºC for 3 minutes, followed by 40 cycles of denaturation at 95ºC for 10 seconds, primer annealing and extension at 60ºC for 30 seconds. After the extension cycles, a step at 95ºC for 5 seconds and a melting curve 65ºC to 95º (at an increment of 0.5ºC every 5 seconds) was applied.
- RT-PCR was performed in a CFX96™ Real-Time PCR Detection System thermocycler (Bio-Rad) and analyzed with Bio-Rad CFX Manager 3.1 software.
- Housekeeping Hmbs gene was used as a control to normalize expression.
- All samples were run in triplicate and non-template controls were included.

3.2.6 Protein extraction and quantification

Protocol:

- Dissect testis and decapsulate or use frozen testis.
- Resuspend the tissue in 500 µl of RIPA buffer (50 mM Tris pH=8, 1% Triton X-100, 0.1% SD, 150 mM NaCl, 1 mM EDTA, 0.5 % Sodyum Deoxycholate and supplement with 1x Proteases inhibitor cocktail (PI, Roche Dianostics) and 10 mM NaF) for wild type testis in a 1.5 ml tube (or 200 µl of RIPA buffer for juveniles or mutant mice testis).
- Disaggregate the tissue using a plastic pestle.
- Place the tubes in the thermomixer for 10 minutes at 95ºC.
- Disaggregate again the tissue with the pestle.

- Centrifuge at 13200 rpm for 10 minutes at 4ºC.
- Keep the supernatant and transfer it into a new 1.5 ml tube. Take an aliquot for protein quantification and freeze the remaining protein extract at -80ºC.
- Quantify total protein levels in the extract using Pierce BCA protein Assay Kit (Thermo scientific), based on colorimetric detection. Following manufacturer instructions, prepare BSA solutions ranging from 0 to 2000 µg/ml in order to obtain a standard curve. Add working reagent to the BSA dilutions and unknown samples. Incubate the tubes for 30 minutes at 37ºC in the thermomixer and then cooled on ice. Read protein concentration with the spectrophotometer (Cary 400 Bio) at 562 nm absorbance.

3.2.7 Western Blot

Western Blot technique was used in order to detect the levels of specific proteins in mutant and wild type mice. A total protein extract was prepared from whole testis and quantified with colorimetric detection. Running the samples into an electrophoresis gel separates the specific proteins according to their specific molecular weight (kDa) and when transferred into a membrane the protein bands of interest are detected with specific primary antibodies.

Protocol:

Gel Electrophoresis

- Take 30-40 µg of proteins for each sample, and equilibrate them with Laemmli buffer. If final volumes are very different, adjust with RIPA buffer.
- Boil for 5 minutes at the thermoblock to denature the proteins and spin down. Cool samples at 4ºC.
- Make a 7-15% SDS Acrylamide gel (1.5 M Tris-HCl pH= 8.8, 20% SDS, 10% APS, TEMED for the running gel solution, and 1 M Tris-HCl pH= 6.8, 20% SDS, 10% APS, TEMED) using the Mini-Protean cell casting module 1mm (Bio-Rad).
- Introduce the gel into the electrophoretic chamber and add running buffer (250 mM Tris base, 14.4% Glycine, 1% SDS in Milli-Q water).
- Load the 30-40 µg of proteins with Laemmli buffer (optionally adjusted with RIPA buffer) into the wells of the gel and add Dual Color marker (Bio-Rad).
- Run at 80-100 volts for 1.5 hours approximately.

Semi-dry transfer

- Transfer the gel into a PVDF membrane using Trans-Blot Turbo system (Bio-Rad) with the 7 minutes transfer program.

Antibody Incubation

- Block the membrane with blocking solution: 5% fat-free milk, 0.1% Tween-20 in PBS.
- Block for 30 minutes at room temperature in agitation.
- Incubate with primary antibody of interest diluted with blocking solution, overnight at 4ºC in agitation.
- Wash the membrane three times with PBST (0.1% Tween-20 in PBS) for 5 minutes in agitation.
- Incubate with secondary antibody conjugated with horseradish peroxidase (HRP) diluted in PBST for 1 hour at room temperature in agitation.
- Wash three times with PBST for 5 minutes in agitation.
- Develop with Luminata Forte Western HRP Substrate (Millipore) for Chemiluminescent detection using the VersaDoc (Bio-Rad).

Table 3.20 List of primary antibodies used for Western blot

Antigen	Host	Company	Dilution
β-ACTIN	Mouse	Abcam	1:10000
CHK2	Mouse	Abcam	1:1000
PUMA	Rabbit	Sigma	1:1000
BAX	Rabbit	Abcam	1:1500
E2F1	Rabbit	Santa Cruz	1:3000

Table 3.21 List of secondary antibodies used for Western blot

Target	Host	Company	Dilution
Anti-mouse-HRP	Goat	Bio-Rad	1:3000
Anti-rabbit-HRP	Goat	Bio-Rad	1:3000

Stripping

If it was necessary to reincubate the membrane with another primary antibody, stripping was performed to eliminate the previous antibody signal.

- Wash the membrane for 15 minutes with stripping buffer (15% Glycine, 1% SDS and 0.1% Tween-20).

3.3 HISTOLOGY TECHNIQUES

3.3.1 Fixation, embedding and sectioning

Testis from 2 to 6 months old adult mice were collected and processed for histology. Testes were fixed either with Bouin's solution or 4% paraformaldehyde, embedded in paraffin and sectioned. For histological staging analysis (Russell et al. 1993), testes sections fixed with *Bouin's* solution were stained with Periodic Acid-Shiff (PAS) and Hematoxilyn. Testes sections fixed with paraformaldehyde were used for TUNEL or Immunofluorescence analysis.

Protocol:

Bouin's fixation

- Prepare fresh fixative *Bouin's* solution (70% of Saturated Picric acid, 25 % Formaldehyde, 35% and 5 % Acetic acid) and keep it at 4ºC.
- Remove testis from mice.
- Punctuate the tunica albuginea of the testis with forceps to perfuse.
- Place freshly dissected tissue into a 50 ml tube with 5-8 ml of *Bouin's* solution.
- Keep it overnight at 4ºC.

Paraformaldehyde fixation

- Prepare fresh fixative 4% paraformaldehyde solution made in PBS (pH=7.4) and keep it at 4ºC.
- Remove testis from mice.
- Punctuate the tunica albuginea of the testis with forceps to perfuse.
- Place freshly dissected tissue into a 50 ml tube with 5-8 ml of the 4% paraformaldehyde Solution.
- Keep it overnight at 4ºC.

Dehydration washes and deparaffinization

- Submerge the sample two times in cold PBS for 30 minutes.
- Submerge the sample in cold 50% ethanol for 30 minutes.
- Submerge the sample in cold 70% ethanol for 30 minutes (or keep it at this step for 2-4 months).
- Submerge the sample in 85% ethanol for 30 minutes.
- Submerge the sample in with 96% ethanol for 30 minutes.
- Submerge the sample two times in 100% ethanol for 30 minutes.
- Submerge the sample three times in Histo-Clear (National Diagnostics) ethanol for 30 minutes.
- Place the tissue into a cassette.
- Submerge the cassette in 1:1 Histo-Clear/Paraffin for 45 minutes at 56ºC.
- Submerge the cassette in 100% paraffin at 56°C overnight to allow proper paraffin infiltration.

Embedding testis in Paraffin blocks

- Turn on the heat block of the paraffin station and introduce the metal mold in the 60ºC melted paraffin bath.
- Open the cassette, transfer the tissue over the mold and place it on the cold plate. Using the forceps orient the testis to a vertical position.
- Add hot paraffin to cover the tissue and let the block form over the cold platform for two hours.
- Keep the blocks overnight at room temperature. Store at 4ºC.

Sectioning

- Section the paraffin blocks at a thickness of 6 µm using the microtome (which is the thickness of a cell), and let the sections float onto a hot water bath.
- Transfer the sections onto poli-lysine treated slides and dry them into an incubator overnight at 37ºC.

Deparaffinization and re-hydration washes

- Deparaffinize the slides with three washes for 5 minutes in xylene.
- Rehydrate the tissue with a gradient of ethanol washes:
    - Submerge two times with 100% ethanol for 3 minutes.

- Submerge two times with 96% ethanol for 2 minutes.
- Submerge two times with 70% ethanol for 2 minutes.
- Submerge with distilled water for 2 minutes.

3.3.2 PAS-Hematoxylin staining

The Periodic Acid Schiff method is used to stain the mucopolysaccharid and glycogen structures in the tissue. Hematoxylin stains acidic compounds, such as DNA or RNA into dark blue.

Protocol:

- Immerse the slides in a 1% Periodic Acid solution for 15 minutes at room temperature.
- Wash two times in distilled water for 3 minutes.
- Incubate the slides in Schiff's reagent for 30 minutes, at room temperature and darkness.
- Wash two times in sulphurous water (10% Potassium metabisulfite, 0.1 M HCl in Milli-Q water) for 3 minutes.
- Wash two times in distilled water for 3 minutes.
- Stain with Mayer's Hematoxylin for 1 minute at room temperature.
- Rinse with running tap water to eliminate Hematoxylin excess.

Dehydration and mounting

Use a gradient of ethanol series to dehydrate the tissue:

- Submerge two times with 70% ethanol for 2 minutes.
- Submerge two times with 96% ethanol for 2 minutes.
- Submerge two times with 100% ethanol for 3 minutes.

- Submerge two times in xylene for 5 minutes.
- Place several drops of DPX mounting medium over each section and add a coverslip. Let air dry the slides.
- Analyze with an Optical microscope.
- Images were captured in a Zeiss Axioskop microscope with a ProgRes C10 camera using the ProgRes Pro 2.7.7 software. Images were then processed with Photoshop.

3.3.3 TUNEL test: In situ cell death detection over tissue sections

In order to detect apoptotic cells in the sectioned tissue the In situ Cell Death Detection kit (Roche Diagnostics) was used. With this TdT-mediated dUTP-X nick end

labeling (TUNEL method), the DNA damage (single and double strand breaks) are labelled. The terminal deoxynucleotidyl transferase (TdT) catalyzes the incorporation of modified nucleotides –which contain a fluorescein- at the free 3'-OH DNA ends so that the apoptotic cells can be visualized under a fluorescence microscope.

Protocol:

- Deparaffinize and rehydrate the sectioned tissue.
- Wash the slides with PBS for 2 minutes at room temperature.
- Permeabilize with 0.5% Triton X-100 in PBS for 15 minutes.
- Wash two times with PBS for 2 minutes.
- Add 100 µl of Dako solution (to reduce background) on each slide, cover with parafilm and incubate in a humid chamber for 15 minutes at room temperature.
- Rinse the slides in PBS for 2 minutes.
- Add 6-10 µl of TUNEL reaction mix (10% TdT enzyme solution in buffer solution) over each section. Incubate in a humid chamber for 1 hour at 37ºC.
- Wash the slides three times in PBS for 5 minutes.
- Add 20 µl of Vectashield mounting medium (Vector) containing DAPI at a concentration of 0.1 µg/ml and cover with a coverslip.
- Analyze with the fluorescence microscope or store at -20ºC.
- Images were captured in a Zeiss Axioskop microscope with a ProgRes C10 camera using ProgRes Pro 2.7.7. Images were then processed with Photoshop.

3.4 CELL BIOLOGY AND CYTOLOGY TECHNIQUES

3.4.1 Spermatocyte nuclei spreads from fresh testis

Spermatocyte preparations can be made from fresh mouse testis. Since the nuclear membrane is still functional in these cells, a hypotonic sucrose buffer can be used in order to expand the cell. With this technique, we can study the nuclear proteins of a specific cell by immunofluorescence.

Protocol:

- Remove the testis from the mouse and rinse them on a petri dish with cold PBS.
- Decapsulate the testis with forceps to release the seminiferous tubules into 200 µl PBS and mince the tubules with the scalpel.
- Transfer the cell suspension into a 15 ml tube containing 10 ml of PBS and pipette back and forth to homogenize. Let large pieces settle to the bottom of the 15 ml tube.

- Transfer 1 ml of cell suspension into ten 1.5 ml tubes.
- Centrifuge the 1.5 ml tubes at 1500 rpm for 5 minutes.
- Discard supernatant and remove the remaining PBS with a pipette.
- Add 40 µl of 0.1 M sucrose solution at 37ºC and resuspend the pellet.
- Prepare Superfrost slides on a humid chamber and distribute 65 µl of cold fixative solution (1% paraformaldehyde, 0.1% Triton X-100 and 1x protease inhibitor cocktail (Roche Diagnostics) in MilliQ-water, pH= 9.2).
- Add 20 µl of cell suspension onto each slide.
- Close the humid chamber and let cells fix for 2 hours at room temperature.
- Open the chamber and let slides air dry for 30-60 minutes.
- Rinse slides with 0.4% Photo-Flo solution (Kodak) for 2 minutes.
- Air dry the slides completely and store them at -80ºC.

3.4.2 Spermatocytes nuclei spreads from frozen testis

Nuclear surface spreads were also prepared from frozen testis samples, which can be preserved and stored at -80ºC for many months. This method has also the advantage that only a very little piece of tissue is needed. The principal difference between frozen and fresh testis spreading techniques is that once the testis are frozen, the cell membrane breaks, so in this case a detergent (Lipsol) is used in order to help to expand the volume of the spermatocytes.

Protocol:

- Keep all solutions cold and add fresh Protease inhibitor cocktail (Complete EDTA-free Protease Inhibitor Cocktail Tablets, Roche Diagnostics).
- Cut a small portion of mouse frozen testis with a scalpel over a glass slide (placed on ice platform).
- Add up to 60 µl of cold PBS and mince the sample with the scalpel.
- Transfer the cellular suspension into 1.5 µl tube and pipette few times to homogenize. Let large pieces settle down to the bottom.
- Place 20 µl of the cellular suspension on each slide.

- Add 80 µl of 1% Lipsol (detergent solution) and leave for 10-15 minutes (12 minutes usually enough).
- Fix the cells by adding 150 µl of fixative solution (1% paraformaldehyde, 0.15% Triton X-100 and MilliQ water; pH= 9.2-9.4) and let the slides fix for 2 hours in a humid chamber at room temperature.
- Open the humid chamber and let slides air-dry at room temperature.
- Wash slides four times for 2 minutes with 0.4% Photo-Flo (Kodak) solution.
- Slides can be used for immunofluorescence, or air dried and stored at -80ºC.

3.4.3 Spermatocytes squashed preparation

Squashed spermatocyte preparations –which preserve nuclear chromosome structure- were performed as previously described (Page et al. 1998).

Protocol:

- Prepare the slides to use by rinsing them in chloroform/ethanol (1:1) for 2 minutes and air dry them.
- Cut a small portion of frozen testis tissue.
- Disaggregate the tissue in 30 µl of fixing solution (2% paraformaldehyde, 0.05% Triton X-100 in PBS; pH= 7.4) for 10 minutes at room temperature.
- Add 6 µl of the cellular suspension to each slide. Place a coverslip over the slide and apply pressure to squash the cells.
- Submerge the slide in liquid nitrogen and keep it in dry ice.
- Proceed to perform immunofluorescence or store slides at -80ºC.

3.4.4 Immunofluorescence

Spermatocyte preparations were stained for immunofluorescence in order to visualize the proteins of interest. Immunofluorescence is a technique based on fluorescent-labeled antibodies, were a primary antibody targets a specific antigen, and then a secondary antibody –which is labeled with a fluorophore-, binds specifically to the primary antibody.

Protocol:

- Block slides with PTBG (0.2% BSA, 0.2% gelatin, 0.05% Tween-20 in PBS) for 10 minutes in agitation.
- Prepare the primary antibody dilution in PTBG and add 100 µl to each slide (cover with parafilm). Incubate at 4ºC in a humidified chamber overnight.
- Wash four times for 3 minutes in agitation with PTBG.
- Prepare the secondary antibody dilution in PTBG and add 100 µl to each slide (cover with parafilm). Incubate at 37ºC in a humidified chamber for 1 hour.
- Wash four times for 3 minutes with PTBG in agitation. Drain the slide.
- Add 20 µl of Vectashield mounting medium (Vector) containing DAPI at a concentration of 0.1 µg/ml and cover with a coverslip.
- Observe under the fluorescence microscope or store at-20º C (or 4º C for short periods).
- Images were captured in a Zeiss Axioskop microscope with a ProgRes C10 camera using ProgRes Pro 2.7.7. Images were then processed with Photoshop.

Table 3.22 List of the primary antibodies used for immunofluorescence

Antigen	Host	Source	Dilution
SYCP3	Mouse	Abcam	1:200-1:400
SYCP3	Rabbit	Abcam	1:200-1:400
SYCP3	Rabbit	Santa Cruz	1:200-1:400
SYCP3	Goat	Santa Cruz	1:50-1:100
γH2AX (ser 139)	Mouse	Millipore	1:100-1:400
γH2AX (ser 139)	Rabbit	Santa Cruz	1:100
H1T	Guinea pig	Dr. M.A. Handel	1:500
ATR	Rabbit	Calbiochem	1:100
SUMO-1	Mouse	Invitrogen	1:100
MLH1 (G168-15)	Mouse	BD Biosciences	1:50
TOPBP1	Rabbit	Abcam	1:10-1:50
Phospho(S2)-RNA pol II	Mouse	Abcam	1:100

Table 3.23 List of the secondary antibodies used for immunofluorescence

Dye	Antigen	Host	Company	Dilution
FITC	Mouse	Goat	Jackson Immunoresearch	1:200
FITC	Rabbit	Goat	Jackson Immunoresearch	1:200
Cy3	Mouse	Goat	Jackson Immunoresearch	1:200
Cy3	Rabbit	Goat	Jackson Immunoresearch	1:200
Cy3	Guinea Pig	Goat	Jackson Immunoresearch	1:200
Cy5	Mouse	Goat	Jackson Immunoresearch	1:100
Alexa 488	Mouse	Donkey	Life Technologies	1:200-1:400
Alexa 594	Goat	Donkey	Molecular Probes	1:200
Alexa 594	Mouse	Goat	Molecular Probes	1:200
Alexa 594	Rabbit	Chicken	Molecular Probes	1:50-1:400
Alexa 647	Rabbit	Donkey	Molecular Probes	1:100-1:200

3.4.5 TUNEL staining over IF-stained slides

The In Situ Cell Death Detection kit (Roche Diagnostics) was used to detect apoptotic spermatocytes in immunostained slides.

Protocol:

- Wash three times immunostained-slides for 5 minutes with 0.5% Triton X-100 in PBS.
- Wash slides three times for 1 minute with PBS.
- Add 50 µl of TdT reaction mixture (45 µl of solution 2 + 5 µl solution 1 enzyme, according to manufacturer's protocol) and cover with parafilm.
- Incubate at 37ºC in a humid chamber for 1 hour.
- Wash three times for 5 minutes with PBS.

3.4.6 RNA FISH and Immunofluorescence on spermatocytes

RNA fluorescence in situ hybridization (RNA-FISH) technique permits to detect gene transcription at the cellular level, which allows to directly observing gene expression at a specific locus in every meiotic phase. The technique consists in applying a digoxigenin-labeled probe to a permeabilized and fixed nuclei, followed by stringency washing and to observe the probe-transcript by fluorescence microscopy (Mahadevaiah et al. 2008; Mahadevaiah et al. 2009). BAC DNA probes used for this study were: *Scml2*, RP24-204O18 (CHORI BACPAC library) and *Zfx,* bMQ-372M23 (Mouse bMQ BAC library). BAC-containing bacteria (BACs) were grown in LB-chloramphenicol culture overnight at 37ºC. A standard miniprep method was used to isolate BAC DNA.

Protocol:

BAC DNA extraction and probe preparation

BACs culture: (keep sterility)

- Set up 25 ml of LB medium (with Cloramphenicol 10µg/ml) into a 50 ml falcon.
- Add 5 µl of BAC glycerol stock.
- -Incubate at 37ºC overnight in agitation.

DNA extraction:

- Keep the BACs culture at 4ºC until proceeding.
- Prepare miniprep solutions (in Milli-Q water):

  P1: 15 mM Tris pH= 8, 10Mm EDTA, 100 µg/ml RNAse A.

  P2: 0.2 M NaOH, 1% SDS, made fresh.

  P3: 3 mM KOAc; pH= 5.5 (set pH with Acetic acid).

- Centrifuge at 4500 rpm the 25 ml BACs culture at 4ºC for 15 minutes. Remove the supernatant.
- Re-suspend the pellet in 1.7 ml of P1 by vortexing (no more vortex after this point).
- Add 1.7 ml of P2 and invert twenty times to mix. Incubate for 5 minutes at room temperature. BACs will lyse and become viscous.
- Add 1.7 ml of P3 and invert twenty times to mix. Incubate 5 minutes on ice. Genomic DNA and proteins denature (observe a white precipitate).

- Aliquot 1 ml into five 1.5 ml tubes. Centrifuge at 13000 rpm at room temperature for 10 minutes.
- Take 900 µl of the supernatant into five new 1.5 ml tubes.
- Add 540 µl of isopropanol and invert to mix. Immediately centrifuge at 14000 rpm at room temperature for 15 minutes. BAC DNA will precipitate.
- Remove isopropanol by decanting and finish the process with the pipette.
- Wash with 500 µl of cold 75% ethanol and centrifuge at 12000 rpm for 5 minutes. Discard liquid and spin again. Remove all liquid with the pipette.
- Air dry the pellets (for approximately 12 minutes).
- Add 120 µl of water to each 1.5 ml tube to dissolve the DNA. Mix and combine the DNA solution from all the tubes.
- Add 2 µl of RNase A and 33 µl of buffer H (500 mM Tris-HCl, pH 7.5 100 mM $MgCl_2$ 10 mM Dithiothreitol (DTT) 1000 mM NaCl).
- Mix and incubate at 37ºC on a water bath overnight.

Phenol:Chloroform DNA extraction:

- Add 440 µl of saturated Phenol (kept at 4ºC). Mix by inverting twenty times (Perform in fume hood).
- Centrifuge at 12000 rpm for 5 minutes. Slowly remove 430 µl from the top layer (which contains the DNA) to a new 1.5 ml tube.
- Add 430 µl of Phenol:Chloroform:Isoamyl Alcohol (PCI). Mix up and down vigorously, until it becomes white.
- Centrifuge at 12000 rpm for 5 minutes. Slowly remove 420 µl from the top layer to a new 1.5 ml tube.
- Add 420 µl of Chloroform:Isoamyl Alcohol (CI). Mix up and down vigorously.
- Centrifuge at 12000 rpm for 5 minutes. Slowly remove 410 µl from the top layer to a new 1.5 ml tube.
- To precipitate DNA: Add 40 µl of 3M Sodium acetate (NaAc) (pH 5.2) and 1000 µl of 100% ethanol. Shake vigorously.
- Centrifuge at 13000 rpm for 15 minutes. Decant and remove liquid with the pipet.

- Wash with 400 µl of 75% ethanol. Centrifuge at 13000 rpm for 5 minutes. Decant and spin again. Remove remaining liquid with the pipet.
- Let the pellet air dry (for approximately 12 min).
- Dissolve in 20 µl of MilliQ-water for each 1.5 ml tube and leave it at room temperature overnight or for 10 min at 37ºC to dissolve DNA. Combine the four 1.5 ml tubes with BAC DNA in one tube.

Probe labelling:

- Into a 1.5 ml round tap tube add: 16 µl of BAC DNA (approximately 2µg) and 4 µl of the DIGMIX (DIG-Nick Translation Mix, Roche). Incubate at 15ºC for 50 minutes in a water bath (made with ice and water).
- Run in a 2% agarose gel with 6.25% Ethidium Bromide.
- Run 2 µl of Nick translation reaction DNA + 8 µl of loading buffer at 90 volts for 30 minutes.
- A smear should be around 500 bp (until 100 bp would stil be fine). In case the DNA needs to be cut more, put the probes for an extra 2-3 minutes at 37ºC.
- Precipitate the entire probe which will be used for nine reactions, mix in a 1.5 µl tube:
  - 18 µl of probe.
  - 27 µl of Cot-1 DNA (Invitrogene).
  - 9 µl salmon sperm DNA (Stratagene).
  - 160 µl 100% ethanol.
- Centrifuge at 13000 rpm at 4ºC for 10-15 minutes. Discard liquid.
- Add 200 µl of 75% ethanol.
- Centrifuge at 13000 rpm at 4ºC for 5 minutes. Remove liquid and spin. Remove the rest of the remaining liquid.
- Let the pellet air dry for approximately 12-15 minutes.
- Add 135 µl of formamide to the probe stock tube. For each slide, 15 µl of this stock will be used.
- Keep at 37ºC for 10 minutes in order to dissolve. Store at -20ºC.

RNA FISH slides preparation

Probe hybridization:

- Prepare 4% paraformaldehyde in PBS pH= 7.4 (dissolve at 65ºC in a water bath and filter).
- Prepare CSK buffer: 100 mM NaCl, 300 mM sucrose, 3mM $MgCl_2$, 10 mM PIPES, 0.5% Triton X-100 and 2 mM vanadyl ribonucleoside (New England Biolabs).
- Boil Superfrost slides for 10 minutes and let them air dry.
- Mince frozen testis samples with the scalpel and add three drops of RPMI medium. Tilt the disaggregated material and add more drops according to the number of slides.
- Mix with Pasteur pipette.
- Add one drop of cells suspension in the middle of the slide (let it settle for 2 minutes).
- Add 4 drops of CSK buffer for 10 minutes to permeabilize.
- Add 6 drops of 4% paraformaldehyde for 10 minutes to fix.
- Meanwhile, denature the probe: Place 15 µl of probe at 80ºC for 10 minutes. Spin and add 15 µl of 2x hybridization buffer (4x SSC, 50% dextran sulphate, 2 mg/ml BSA and 2 mM Vanadyl ribonucleoside) and place at 37ºC for 20 minutes (to pre-hybridize).
- Decant liquid from the slides (with absorbing paper).
- Rinse slides in cold PBS (each genotype with different PBS).
- Dehydrate slides with cold ethanol series washes:
  - Wash two times with 70% ethanol for 3 minutes.
  - Wash with 80% ethanol for 3 minutes.
  - Wash with 95% ethanol for 3 minutes.
  - Wash with 100% ethanol for 3 minutes.
  - Air dry the slides vertically.
- Spin and add 30 µl of the probe to the slides and cover with a 50 mm coverslip.
- Incubate in a humid chamber (filled with Formamide) at 37ºC overnight.

Stringency washes and probe detection:

- Prepare solution A: 50% Formamide in SSC, pH= 7.2-7.4.

- Prepare solution B: 2x SCC pH= 7-7.2.
- Prepare solution C: 4x SCC, 0.1% Tween-20, pH= 7-7.2.
- Prepare blocking buffer: 4x SCC, 4 mg/ml BSA and 0.1% Tween-20.
- Prepare detection buffer: 4x SCC, 1 mg/ml BSA and 0.1% Tween-20.
- Place a mixer and a water bath at 45ºC in the fume-hood. Keep solution A and solution B at 42ºC.
- Wash three times with solution A for 5 minutes (remove coverslip after the first wash).
- Wash three times with solution B for 5 minutes.
- Rinse with solution C.
- Add 100 µl of blocking buffer and place a 60 mm coverslip. Incubate at 37ºC in a humid chamber for 30 minutes.
- Prepare the antibodies with detection buffer or solution C and centrifuge them at 13000 rpm at room temperature for 5 minutes:
    - Anti-digoxigenin-FITC (Millipore) (1:10).
    - Primary antibodies (see Table 3.11).
    - Secondary antibodies (see Table 3.12).
- Add the anti-digoxigenin-FITC 50 µl for slide and incubate at 37ºC for 1 hour.
- Wash three times with solution C for 2 minutes.
- Add the primary antibodies: 50 µl for slide and incubate at room temperature for 30 minutes.
- Wash three times with solution C for 2 minutes.
- Add secondary antibodies: 50 µl for slide and incubate at room temperature for 30 minutes.
- Wash three times with solution C for 2 minutes.
- Mount in Vectashield mounting medium with DAPI (at a concentration of 1.5 µg/ml).
- Keep slides for 15-30 minutes at 4ºC, and then store them at -20ºC.
- Analyze slides on a fluorescence microscope.
- Images were captured with Olympus IX70 inverted microscope and computer-assisted (DeltaVision) CCD camera (Photometrics) and processed with ImageJ and Photoshop.

3.4.7 EU Imaging on spermatocytes

To analyze global RNA expression in meiotic cells, we have used the EU Click-it Imaging technique (Click-iT® RNA Alexa Fluor® 488 Imaging Kit, Life Technologies) to cytologically detect newly synthesized RNA. We obtained a cell suspension from fresh testis and then incubated these cells in the presence of a Uridine analogue (5-Ethynyl Uridine (EU), Life Technologies), which is specifically incorporated to nascent RNA. From this cell suspension slides are prepared using a protocol similar to the RNA-FISH (Mahadevaiah et al. 2009), in order to preserve the nuclei structure and keep cellular volume. Then, modified RNA was labeled with a dye (Alexa Fluor 488) through a chemoselective ligation or "click" reaction between an azide-containing dye and an alkyne, which allows the visualization of the RNA by fluorescence microscopy. With this technique we can cytologically evaluate the RNA expression of cells at different stages of prophase.

Protocol:

Enzymatic testis dissociation

- Isolate the two testes from the mouse and decapsulate.
- Transfer the testis (one for the wild type, and two for the mutant mice) to a 50 ml tube containing 10 ml Gey's Balanced Solution (GBSS, Sigma) + 0.5 mg/ml Collagenase (Sigma, freshly made).
- Incubate at 33ºC and 350 rpm for 15 minutes in the thermomixer, shaking vigorously every 5 minutes to disassociate the tubules.
- Let the seminiferous tubules settle down to the bottom for 4 minutes at room temperature. Discard supernatant.
- Wash two times with 10 ml GBSS, centrifuge at 2400 rpm at room temperature for 3 minutes.
- Resuspend tubules in 10 ml GBSS containing 0.5 mg/ml Trypsin (Sigma) and 2 µg/ml DNase I.
- Incubate at 33ºC and 350 rpm for 15 minutes (for the last 3 minutes mix up and down gently with a Pasteur pipette, so that spermatocytes become suspended and homogeneous).

- Stop Trypsin reaction by adding 0.5 ml of Fetal Bovine Serum (5% FBS, Gibco Life Technologies) and mix.
- Filter the cell suspension through a 70 µm strain to a new 50 ml tube (to remove clumps). Centrifuge at 2400 rpm at room temperature for 3 minutes. Discard supernatant.
- Wash two times with 4 ml GBSS + 5% FBS + 2 µg/ml DNase I.
- Centrifuge at 2400 rpm at room temperature for 3 minutes. Discard supernatant.

EU incubation and spreads preparation

- Resuspend pellet in 500 µl of 5 mM EU in of RPMI medium (with 10% FCS and 1x penicillin/spretomycin/fungizone) in a 50 ml tube (and incubate control with 500 µl RPMI without EU).
- Incubate at 33ºC and 350 rpm for 2.5 hours at the thermomixer.
- Prepare 4% paraformaldehyde in PBS, pH= 7.4.
- Prepare CSK buffer: 100 mM NaCl, 300mM sucrose, 3 mM MgCl2, 10 mM PIPES, and add freshly 0.5% Triton X-100 and 2 mM Vanadyl ribonucleoside (New England Biolabs).
- Place 60 µl of cell suspension per slide (Superfrost) over a cold platform, al let it settle down for 10 minutes.
- Add four drops of CSK buffer for 13 minutes.
- Add six drops of 4% paraformaldehyde in PBS for 30 minutes.
- Tilt cold platform to eliminate liquid excess from the slides.
- Rinse slides in cold PBS.
- Air dry slides.
- Store at -80ºC or proceed to Click-iT reaction.

Click-iT EU staining reaction and IF

- Wash two times with cold PBS at 4ºC for 3 minutes.
- Wash with cold 0.5% Triton-PBS at 4ºC for 30 minutes (to permeabilize cells).

- Wash with cold PBS at 4ºC for 3 minutes.
- Prepare Click-iT Reaction master mix according manufacturer (Click-iT® RNA Alexa Fluor® 488 Imaging Kit, Life Technologies): 428 µl compound C + 20 µl compound D + 1.8 µl Biotin Azide (Life Technolgies) + 50 µl working solution + 5 µl Vanadyl ribonucleoside.
- Add 100 µl of the Mix to each slide and cover with parafilm.
- Incubate in a humid chamber at room temperature for 30 minutes.
- Add 100 µl of Rinse buffer to each slide, cover with parafilm and let it rest for 5 minutes.
- Rinse slides with cold PBS.
- Block slides with cold PTBG (0.2% BSA, 0.2% gelatin, 0.05% Tween-20 in PBS) for 10 minutes.
- Add primary antibodies in PTBG with 2 mM Vanadyl ribonucleoside: Streptavidin Alexa Fluor 488 (1:100, Life Technologies), mouse anti-SYCP3 at 1:100 (Santa Cruz) and rabbit anti-γH2AX (1:100, Millipore).
- Incubate primary antibodies in a humid chamber at 37ºC for 1 hour.
- Wash three times with PBS for 5 minutes.
- Add secondary antibodies in PTBG with 2 mM Vanadyl ribonucleoside: anti-mouse Alexa Fluor 594 (1:200) and anti-rabbit Alexa Fluor 647 (1:200).
- Incubate secondary antibodies in a humid chamber at room temperature for 1 hour.
- Wash three times with PBS for 5 minutes.
- Mount slides with Vectashield mounting medium with DAPI at a concentration of 1.5 µg/ml (Vector) and a coverslip.
- Visualize slides under a fluorescence microscope (Axio2 microscope, Zeiss) and capture images with a CCD camera and process them with Slidebook software package (Intelligent Imaging Innovations). Capture 0.5 µm stacks from the top to the bottom of the cells. From these stacks create a sum projection image.
- Measure fluorescence intensity with ImageJ 1.49g software (National Institutes of Health, USA; http://imagej.nih.gov/ij/). Quantify EU intensity signal taking into account the nuclei area identified with DAPI, and obtain background signal from the surrounding areas. Use the ImageJ parameter Integrated density to plot the graphics

(which is the sum of the values of the pixels in that selection, equivalent to the product of the Area and the Mean Gray Value –fluorescence intensity values-).

- Quantification of phosphorylated RNA polymerase II was performed over slides obtained following this protocol but cultivated without EU. IF was performed as in 3.4.4 . Images were obtained and processed as in EU quantification.

3.4.8 Cell Sorting

The Fluorescence activated cell sorting (FACS) of live cells technique is used to separate the cellular heterogeneity present in the testis into meiotic sub-populations. This technique uses flow cytometry to separate the cells according to their fluorescent labeling with Hoechst 33342 and Propidium Iodide. Hoechst 33342 dye diffuses through plasma membrane and bind to DNA poly(dAT) sequences, helping to detect DNA content and chromatin structure. Meiotic cells are classified according to the blue fluorescence (which depends on the DNA content); and the red fluorescence they emit (which corresponds to chromatin complexity). Propidium iodide fluorochrome staining penetrates through impaired plasma membranes, allowing to discriminate dead cells (for an example see Fig. 3.1) (Bastos et al. 2005; Cole et al. 2014).

Protocol:

Enzymatic testis dissociation

- Isolate the two testes from the mouse and decapsulate them.
- Transfer the testis (one for the wild type, and two for the mutant mice) to a 50 ml tube containing 10 ml GBSS containing 0.5 mg/ml Collagenase (Sigma).
- Incubate at 33ºC and 350 rpm for 15 minutes in the thermomixer, shaking vigorously every 5 minutes to disassociate the tubules.
- Let the seminiferous tubules settle down to the bottom for 4 minutes at room temperature. Discard supernatant.
- Wash two times with 10 ml GBSS, centrifuge at 2400 rpm at room temperature for 3 minutes.
- Resuspend tubules in 10 ml GBSS containing 0.5 mg/ml Trypsin (Sigma) and 2 µg/ml DNase I.

- Incubate at 33ºC and 350 rpm for 15 minutes (for the last 3 minutes mix up and down gently with a Pasteur pipette, so that spermatocytes become suspended and homogeneous).
- Stop Trypsin reaction by adding 5% of Fetal Bovine Serum (FBS, Gibco Life Technologies) and mix.
- In order to individualize cells filter the cell suspension through a 70 µm strain (BD Falcon) to a new 50 ml tube. Centrifuge at 2400 rpm at room temperature for 3 minutes. Discard supernatant.
- Wash two times with 4 ml GBSS containing 5% FBS and 2 µg/ml DNase I. If processing several samples keep them on ice.
- Centrifuge at 2400 rpm at room temperature for 3 minutes to spin the pellet and discard supernatant.
- Stain the cells with Hoechst 33342 by adding 4 ml of GBSS containing 10 µg/ml Hoechst 33342, 5% FBS (Life Technologies) and 2 µg/ml DNase I and incubate in the thermomixer at 33ºC for 45 minutes at 350 rpm.
- Centrifuge at 2400 rpm at room temperature for 3 minutes to spin the pellet and remove supernatant.
- Just before fluorescent-activated cell sorting stain with Propidium Iodide by adding 0.2 µg/ml of Propidium Iodide in 1 ml GBSS containing 5% FBS and 2 µg/ml DNase I to resuspend the cells. Mix gently.
- Filter the cell suspension through a 40 µm strainer of the FACS tube. Leave cell suspension on ice until proceeding to sorter.
- Take FACS tubes for collecting the sorted cells (according to number of populations collected) with 300 µl of GBSS containing 5% FBS in each tube.
- Sort cells in the FACS core facility using FCCF-MoFlo1 (Dako) flow cytometer with a 350-nm argon laser.
- Proceed to prepare spermatocytes spreads with the sorted cells. Place the cell suspension (all the volume, or divide into fractions if cells are needed for other purposes) into a new eppendorf. Centrifuge for 3 minutes at room temperature at 2400 rpm. Remove supernatant.
- Add 100 µl of 0.1 M sucrose to each eppendorf and keep it for 8-10 minutes.
- Add 65 µl of 1% paraformaldehyde with 0.1% Triton X-100 to each slide.

- Add all the cell suspension to each slide, and keep it for 2 hours into a humid chamber at room temperature. Then, open the chamber and let the slides completely air dry.
- Wash two times with 0.4 % Photo-Flo solution for 1 minute.
- Wash slides one time with Milli-Q water.
- Block slide with PTBG for 10 minutes in agitation.
- Proceed to stain SYCP3 and γH2AX for immunofluorescence in order to classify meiotic sub stages as in 3.4.4.

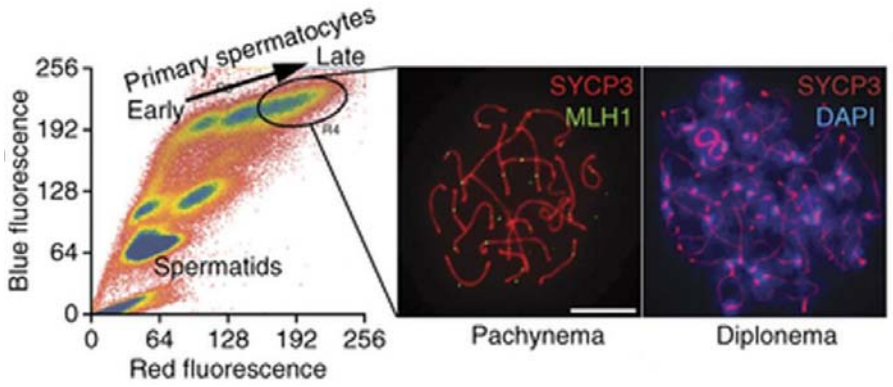

Figure 3.1. Example of published cell sorting to obtain spermatocytes population. In this work, single cell suspension stained with Hoechst 33342 and Propidium iodide was sorted in a MoFlo cytometer. The plot shows different cell type populations separated according blue and red fluorescence. Examples of gated cells (98% MLH1-positive pachynema and diplonema spermatocytes (stained with MLH1 (green), SYCP3 (red) and DAPI (blue)) are shown as representative images. Image taken from Cole et al. (2014)

RESULTS

4. RESULTS

4.1 Study the pachytene arrest in male mammalian meiosis

4.1.1 Determine other members of the signaling pathway that activates the pachytene arrest in mouse spermatocytes

Several studies have involved DDR proteins in meiotic checkpoints in several organisms (MacQueen and Hochwagen 2011). For our work, we wanted to study if we could use biochemical tools to detect the activation of the DDR pathway in recombination-deficient mutants in mouse meiosis. As a first approach, we performed Western blot against several proteins of the DDR pathway from adult whole testis protein extracts. We used *Trip13*$^{mod/mod}$ mutants, as mice that present recombination impairment (Roig et al. 2010; Li et al. 2007) and *Arf*$^{-/-}$ mutants, which present a p53-dependent apoptosis due to accumulation of γH2AX (Churchman et al. 2011). We also examined whole testis extracts from wild type mice as controls, and *Spo11*$^{-/-}$ mutants as negative control (since their spermatocytes do not present SPO11-generated DSBs (Baudat et al. 2000)).

Specifically, since our group reported that the MRE11 complex-ATM-CHK2 pathway participated in the activation of the recombination-dependent arrest (Pacheco et al. 2015), first we wanted to see if we could observe this activation by Western blot and screen for other known factors of this signaling pathway. We focused our investigations on the following proteins: CHK2, PUMA, BAX and E2F1. CHK2 is the checkpoint effector kinase activated by ATM in response to DSBs (Chaturvedi et al. 1999). In somatic cells, both ATM and CHK2 signal downstream to p53, which induces transcriptional activation of multiple genes, including the pro-apoptotic factors PUMA and BAX (Roos and Kaina 2006). The transcription factor E2F1 is phosphorylated and activated by CHK2 in response to DNA damage, resulting in apoptosis entry (Stevens et al. 2003).

AS regards CHK2, we observed an increased signal in *Trip13*$^{mod/mod}$ mutant samples compared to the wild type, and also the appearance of a lower mobility band, presumably the phosphorylated form of CHK2 (Fig. 4.1A). However, we also observed a similar intensity band and a phospho-CHK2 band in *Spo11*$^{-/-}$ mutant. The CHK2 band on *Arf*$^{-/-}$ mutant presented an intermediate intensity, higher than the wild type but less intense than the ones observed in either *Trip13*$^{mod/mod}$ or *Spo11*$^{-/-}$ mutants, and no lower mobility

band could be observed in this case (Fig. 4.1A). These results show that CHK2 protein is more activated in *Trip13*$^{mod/mod}$ mutant than in the wild type. However since we observe a similar band and phosphorylation on *Spo11*$^{-/-}$ mutant, we cannot conclude that this is specific of the activation of the recombination-dependent arrest. Also, we expected to find more CHK2 protein in the *Arf*$^{-/-}$ mutant, which we know they do experience a p53-dependent recombination-dependent arrest.

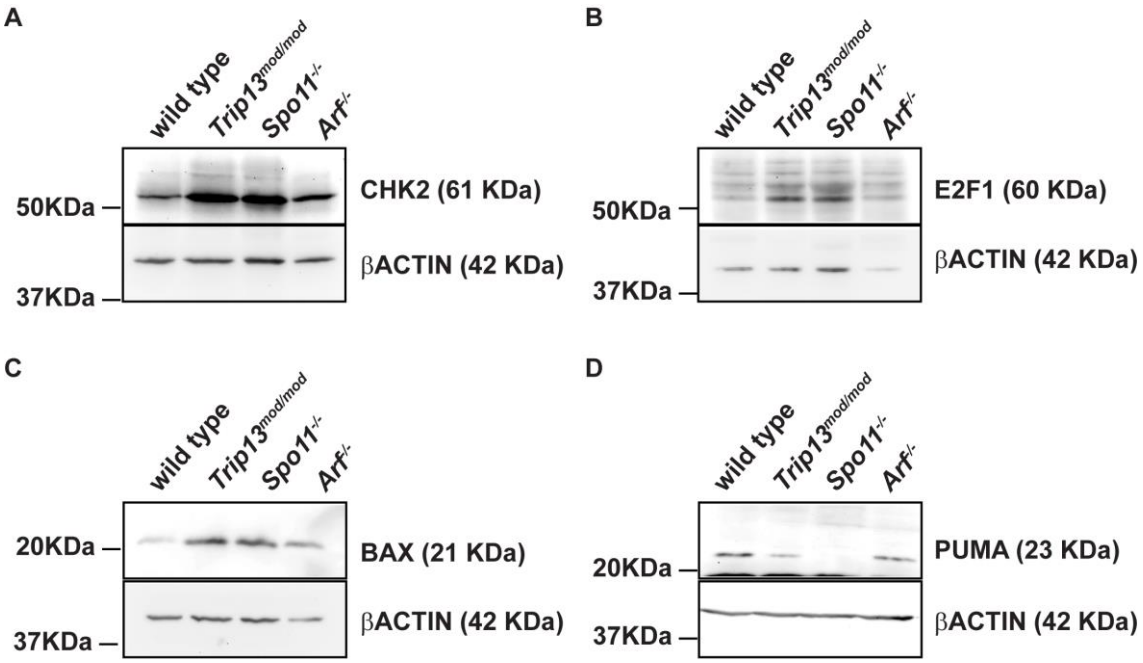

Figure 4.1. Activation of DDR proteins in pachytene-stage arrested mutant testes. Western blot analysis of (A) CHK2, (B) E2F1, (C) BAX and (D) PUMA of the indicated genotypes from adult mice testes. Below each panel, β-ACTIN serves as a loading control.

For E2F1 protein, we observed that the bands present in *Trip13*$^{mod/mod}$ and *Spo11*$^{-/-}$ lanes were more intense than those found in the wild type. However, for *Arf*$^{-/-}$ mutant, E2F1 band was similar to the wild type (Fig. 4.1B). These results are similar to what we observed for CHK2 protein, where there is a stronger band on *Trip13*$^{mod/mod}$ that could suggest that E2F1 is activated when a recombination-dependent arrest occurs, but we cannot conclude that since we find a similar band on *Spo11*$^{-/-}$ mutant which has no DSBs. And again, for the other recombination-defective mutant we analyzed, *Arf*$^{-/-}$, we don't see an increased presence of either E2F1 or any of its post-translationally modified versions as compared to wild type samples, suggesting the contradictory result that E2F1 does not participate in recombination-defective arrest occurring in *Arf* mutants.

We also examined the pro-apoptotic BAX and PUMA proteins. For BAX protein, we observed an increased presence in *Trip13*$^{mod/mod}$ and *Spo11*$^{-/-}$ mutants, and a slighter increase in *Arf*$^{-/-}$ mutants, in comparison with the wild type (Fig. 4.1C). These results would suggest that BAX protein is in some extent activated when a pachytene block occurs, independently from being recombination-dependent or sex-body deficient related. Surprisingly, PUMA protein levels where decreased in *Trip13*$^{mod/mod}$ and *Arf*$^{-/-}$ mutants compared to the wild type, and almost absent in *Spo11*$^{-/-}$ mutants (Fig. 4.1D). These results would suggest that the apoptosis occurring at pachytene-stage is independent of PUMA.

Globally, results from CHK2, E2F1 and BAX suggest that proteins from the DDR pathway might be activated under recombination-dependent arrest conditions in *Trip13*$^{mod/mod}$ mutants. But inconclusively, this activation seemed to not occur in *Arf*$^{-/-}$ mutants, suggesting that their apoptosis is independent of the DDR proteins analyzed here. However, since we also see increased levels of CHK2, E2F1 and BAX proteins in *Spo11*$^{-/-}$ mutants, we cannot conclude if these results are due to the recombination-dependent arrest activation or as a consequence of a pachytene block itself. Nevertheless, we need to take into account that when comparing adult mutant testis arrested at pachytene stage with wild type mice, the percentage of the different kinds of spermatogenic cells between them is considerably different. Furthermore, the different proteins analyzed are present in all testis cell types, therefore we cannot conclude that the amount of protein we observe comes specifically from the spermatocytes. Thus, since results obtained from the Western blot analysis are inconclusive and contradictory, we had to address our question through other different approaches that allowed us to obtain highly enriched spermatocyte samples.

4.1.2 Evaluate the possibility of separating prophase stages through cell sorting technique

As a first attempt, we sought to classify spermatocytes into every prophase stage with the purpose to perform specific cell type Western blot analysis, or other techniques like RNA sequencing. For that purpose, we set up a technique to purify different testis cell type populations by FACS-sorting and gated them accordingly to previously published reports, where cells separate according to its DNA content (blue fluorescence) and chromatin complexity (red fluorescence) (see section 3.4.8) (Bastos et al. 2005; Getun et al. 2011; Cole et al. 2014). We performed cell sorter technique in adult mice testis and prepared spermatocyte spreads from the gated cells in order to classify the collected cells.

To cytologically classify prophase stages, we applied immunofluorescence against SYCP3 (a component of the axial element of the synaptonemal complex (Lammers et al. 1994)) and γH2AX. We were able to get plots with separated populations that looked similar to the previously reported ones (Bastos et al. 2005; Getun et al. 2011; Cole et al. 2014). However, our plots often varied from each other, which made it difficult to keep the same exact gates between different experiments, and we were not able to gate cells into highly enriched cell type population in any experiment. Usually, leptonema and zygonema populations were mixed in our R8 gated cells, which should mostly correspond to zygotene cells (according to previously published plots). The corresponding pachynema gate, R5, also collected some zygonema and diplonema cells, and pachytene-stage cells did not even represent half of the total number of cells. For R4 gate, which should correspond to diplonema spermatocytes, we collected a majority of diplonema spermatocytes and few pachytene cells (see two plots examples and corresponding tables with quantifications in Fig. 4.2A,B).

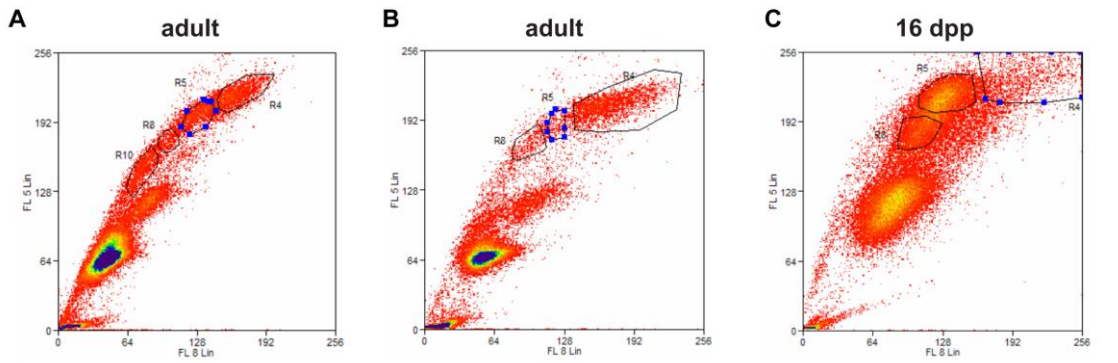

	R8	R5	R4
No SYCP3	5.0	5.6	0.0
Leptonema	35.0	0.9	0.0
Zygonema	55.0	4.6	0.0
Pachynema	5.0	50.0	14.0
Diplonema	0.0	38.9	86.0

	R8	R5	R4
No SYCP3	10.0	3.0	0.0
Leptonema	38.0	20.0	0.0
Zygonema	46.0	31.0	0.0
Pachynema	6.0	15.0	5.0
Diplonema	0.0	31.0	95.0

	R8	R5	R4
No SYCP3	86.6	3.0	5.0
Leptonema	13.3	46.5	38.0
Zygonema	0.0	39.6	39.0
Pachynema	0.0	5.9	14.0
Diplonema	0.0	5.0	4.0

Figure 4.2. Sorting of adult and juvenile mouse spermatocytes. (A-B) Representative FACS plots of two independent experiments from adult mice and (C) from 16 dpp juvenile mice testis. Single-cell suspensions from whole testis were stained with Hoechst 33342 and propidium iodide are plotted. Cells are classified on the Y axis according to the blue fluorescence (which depends on the DNA content); and the red fluorescence on the X axis (which corresponds to chromatin complexity). Sorted cells were obtained from the indicated gates: R8, R5 and R4. Below the plots, tables show the percentage of spermatocytes collected from each gate.

Besides, we also sought to use juvenile mice since they present a first synchronic meiotic wave. We performed the same technique in juvenile mice between 10 and 16 dpp,

and found the same inconvenient that we still collected cells at different stages in the gates analyzed. Although the first meiotic wave is very synchronous, when some spermatocytes reached zygonema, there were other spermatocytes still at leptonema stage that sorted in the same gate, and pachynema spermatocytes were also mixed with zygotene cells (see an example of a 16 dpp plot in Fig. 4.2C). Therefore, as we were not able to perform reproducible and reliable plots to obtain highly enriched cell-type populations, we discarded the use of this technique for Western blot analysis or either RNA sequencing analysis (see below).

4.1.3 Analysis of p53 role in an unperturbed mouse meiosis and possible implications in the pachytene arrest

Recent studies have suggested that p53 may have a role in mouse meiosis. For instance, p53 is activated in response to SPO11-generated DSBs (Lu et al. 2010). Also, p53 mediates apoptosis of *Arf* mutant spermatocytes, that accumulated γH2AX foci at pachynema (Churchman et al. 2011). First studies that analyzed *p53* null mice phenotype reported normal development and proper fertility (Donehower et al. 1992; Jacks et al. 1994). Nonetheless, others described that partial impairment of p53 expression was associated with the presence of testicular multinucleated "giant-cells", suggesting that p53 was expressed at pachytene stage to allow proper DNA repair (Rotter et al. 1993). Indeed, it was only recently found that p53 participates in the elimination of oocytes with persistent unrepaired DSBs (Bolcun-Filas et al. 2014). However, since genetic evidences of p53 role in male pachytene quality control remained incomplete, we decided to perform an exhaustive analysis of *p53* mutants meiotic phenotype.

4.1.3.1 Analysis of p53 mutant mice spermatogenesis

Testicular size is a good indicator of spermatogenesis progression, as most of the mutations that compromise meiosis result in a reduction of testis weight. Therefore, first of all we analyzed testis size relative to the body weight. *p53*$^{-/-}$ mouse testis weight (Mean±SV= 0.96±0.15) was comparable to their wild type littermates (0.92±0.18, P=0.51 T-test; Fig. 4.3A). This was an expected result, as it was previously described that mice carrying p53 mutation are fully fertile (Jacks et al. 1994).

To have a better understanding of how meiosis proceeds in the absence of p53, we examined histological sections of *p53* mutant mouse testis. Germ cells going through

spermatogenesis develop within the seminiferous tubules which are arranged in circular layers. Pre-meiotic cells (spermatogonia) are located at the periphery of the tubule and as they progress through meiosis (spermatocytes) they advance towards the lumen until becoming post-meiotic cells (spermatids) (Russell et al. 1993). Histological cross sections from *p53*$^{-/-}$ testis showed that as in the wild type mice (Fig. 4.3B), all spermatogenic cell types were present in seminiferous tubules of *p53* mutant mice (Fig. 4.3C). We did not found any "giant cells" in our mutants. This is consistent with the fact that this degenerative phenotype depends on the genetic background of the mice and is not present in C57BL/6 and 129/Sv mixed background mice (Rotter et al. 1993), like the one we have in our colony.

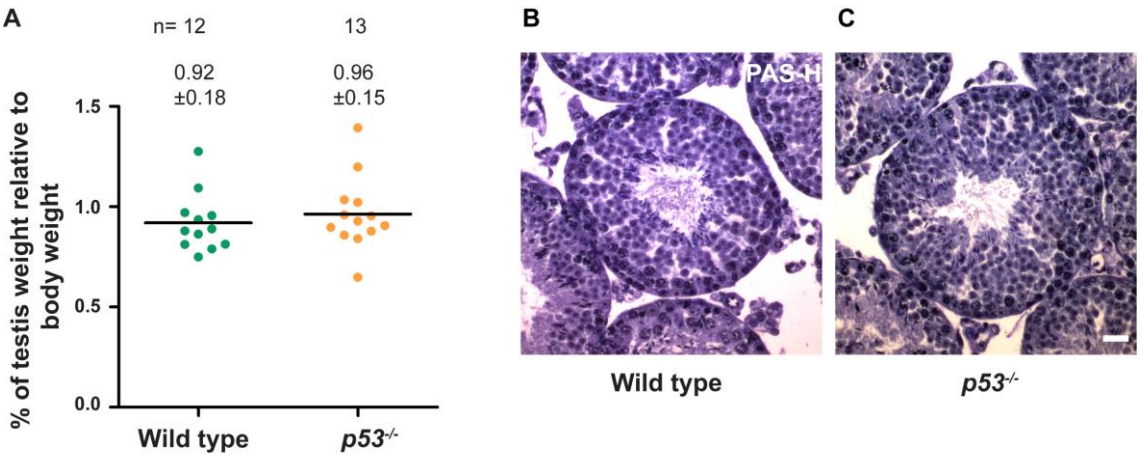

Figure 4.3. Absence of p53 does not alter spermatogenesis. (A) Graph shows normalized testis weight (testis weight divided by body weight) of wild type and *p53*$^{-/-}$ testis. Horizontal lines represent means. Means (± SD) are indicated above the graph. (B-C) Representative tubule sections from adult testes of the indicated genotypes stained with PAS-Hematoxylin. Wild type and *p53*$^{-/-}$ seminiferous tubules contain spermatogonia, spermatocytes and spermatids. Scale bar in C represents 20 μm and applies to all panels.

Increased apoptosis in seminiferous tubules can also be an indicator of impaired meiosis. Therefore, we performed TUNEL test assay on histological sections to determine if apoptosis levels are altered in *p53* mutants (Fig. 4.4). We observed a minor but statistically significant increase in the number of apoptotic cells per tubule in *p53*$^{-/-}$ testis sections (Mean±SV=0.38±1.01) compared to the wild type (0.29±0.92, P=0.009, T-test, Fig. 4.4A). Even though it was statistically significant, as we only found one more TUNEL-positive cell in every ten tubules, we reasoned that this difference may not be biologically relevant. Altogether, results from testis size and histological analysis showed that spermatogenesis is not compromised in the absence of p53.

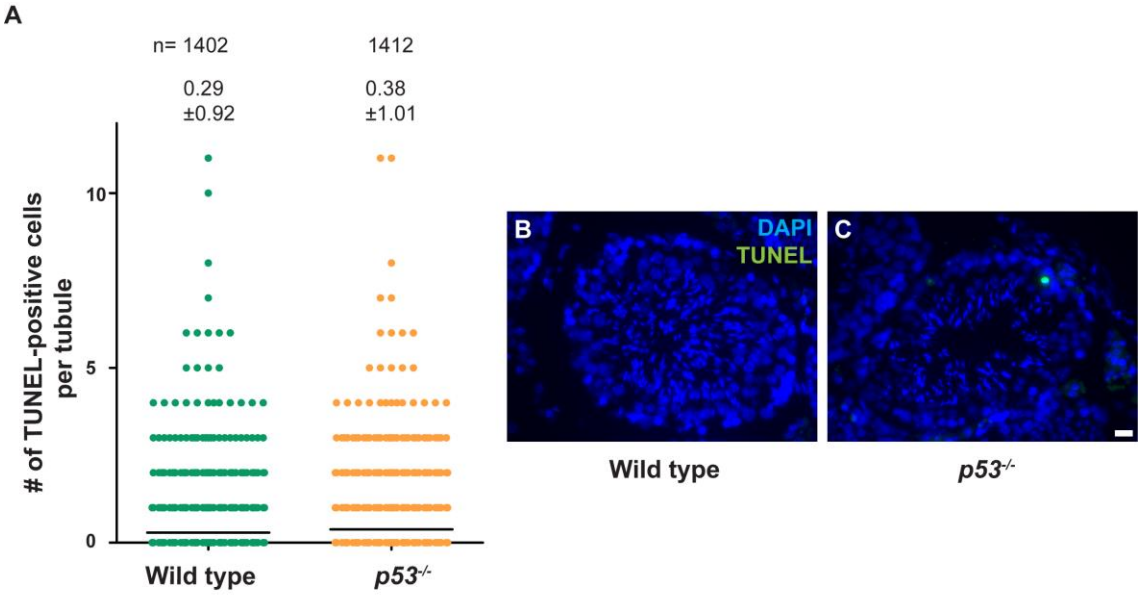

Figure 4.4 Absence of p53 slightly increases apoptosis at the seminiferous tubules. (A) Quantification of the number of TUNEL-positive cells per tubule of the indicated genotypes. Apoptotic levels of *p53*$^{-/-}$ are slightly significantly higher than wild type. Horizontal lines represent the mean, which is indicated over the graph (mean ± SD). N shows the number of tubules counted per genotype. (B-C) Representative tubules are shown from testis sections of a wild type and *p53*$^{-/-}$ testis stained with TUNEL to detect apoptotic spermatocytes (green) and DAPI (blue). Scale bar in C represents 20 µm and applies to all panels.

4.1.3.2 Study of p53 role in synapsis and prophase progression in mouse spermatocytes

Because p53 is implicated in cell cycle control as a checkpoint protein in somatic cells (Vogelstein et al. 2000) and in females it was found that its absence accelerated the initiation of prophase stages (Ghafari et al. 2009), we exhaustively studied meiotic progression in *p53*$^{-/-}$ spermatocytes.

As mentioned above, the first wave of spermatogenesis is semisynchronous and begins around 6 days post-partum (dpp). Pachytene stage appears approximately at 12-14 dpp and afterwards, the first spermatocytes that initiate diplotene stage appear around 17-18 dpp. After this first meiotic wave, in adult males meiosis becomes asynchronous and thus, all kind of spermatocytes can be found in any given testis sample.

In order to evaluate if p53 monitors meiotic progression, and for example is able to delay cell cycle -which would increase the available time to repair DSBs-, we studied the chronology of the first wave of meiosis in juvenile mice. For this, we performed immunofluorescence over 17 dpp spermatocyte spreads and stained the axial element of

the synaptonemal complex (SYCP3) to follow synapsis progression and γH2AX to observe DSBs and sex body formation. Globally, we observed a similar prophase progression pattern for control and for *p53* mutant mice. We observed proper synapsis of the homologous chromosomes and prophase progression in adult *p53*$^{-/-}$ mice. Interestingly, when we compared the percentage of spermatocytes that started to reach diplotene stage at 17 dpp we found a significant increase in the percentage of cells at diplonema in *p53*$^{-/-}$ mice (2.75%) in comparison with control heterozygotes (1.00%, P=0.015 Fisher's exact Test; Fig. 4.5A). Therefore, these results suggest that in the absence of p53 the meiotic prophase accelerates, possibly because p53 controls meiotic prophase progression.

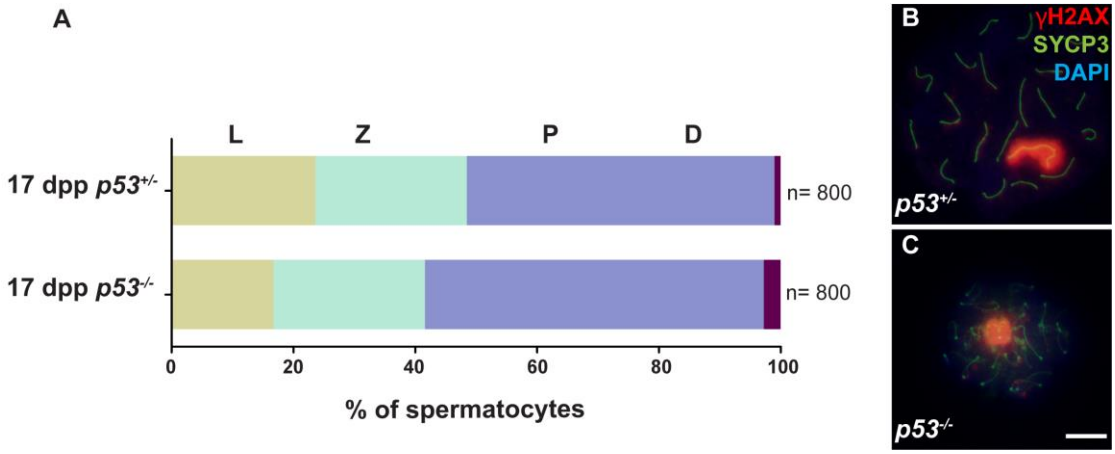

Figure 4.5. Absence of p53 accelerates meiotic prophase progression at the first wave of spermatogenesis. (A) Quantification of the percentage of spermatocytes at each prophase stage (leptonema (L), zygonema (Z), pachynema (P) and diplonema (D) at 17 dpp in *p53*$^{-/-}$ and *p53*$^{+/-}$ mice. N shows the number of spermatocytes counted per each genotype. (B) Representative *p53*$^{+/-}$ pachytene spermatocyte and (C) *p53*$^{-/-}$ diplotene spermatocyte stained against the axial element protein SYCP3 (green), γH2AX (red) and DAPI (blue). Scale bar in C represents 10 μm and applies to all panels.

In adult wild type mice, the meiotic waves become asynchronous and we can observe all prophase stages in the mouse testis in different proportions. We corroborated that *p53* mutants synapsis progression behaved as the wild type (Fig. 4.6A-H). At the onset of prophase, at leptotene stage, the axial elements begun to form in each homologue and γH2AX signal covered most chromatin marking the recently formed DSBs. As these DSBs got repaired at zygotene stage, the γH2AX signal decreased and the homologous chromosomes started to progressively pair and synapse. At pachytene stage we observed full synapsis of the homologous chromosomes and γH2AX was mostly confined to the sex body. At diplonema, homologous chromosomes desynapse and decondense and the signal at the sex body became fainter. We also analyzed the proportion of spermatocytes at each prophase stage and we observed that they were significantly altered between the *p53*

mutant and control mice (P=0.00047, G Test). Distinctively, there was a statistically significant increase in the number of zygotene stage spermatocytes in *p53*$^{-/-}$ mice (24.42%) compared with the wild type (15.23) (P=0.0027, Fisher's exact test; Fig. 4.6J). Additionally, the percentage of diplonema spermatocytes presented a significant reduction in *p53* mutant mice (24.96%) in comparison with the wild type (33.13%) (P=0.0393, Fisher's exact test; Fig. 4.6I). The percentage of leptonema cells in *p53*$^{-/-}$ (6.60%) and wild type (5.18%) was not significantly different (P=0.4404, Fisher's exact test) and neither the percentage of pachynema spermatocytes in *p53*$^{-/-}$ (44.03%) and wild type (46.46%) (P=0.6237, Fisher's exact test). This alteration of percentage stage pattern suggests that p53 absence might have some effect on spermatocyte meiotic progression.

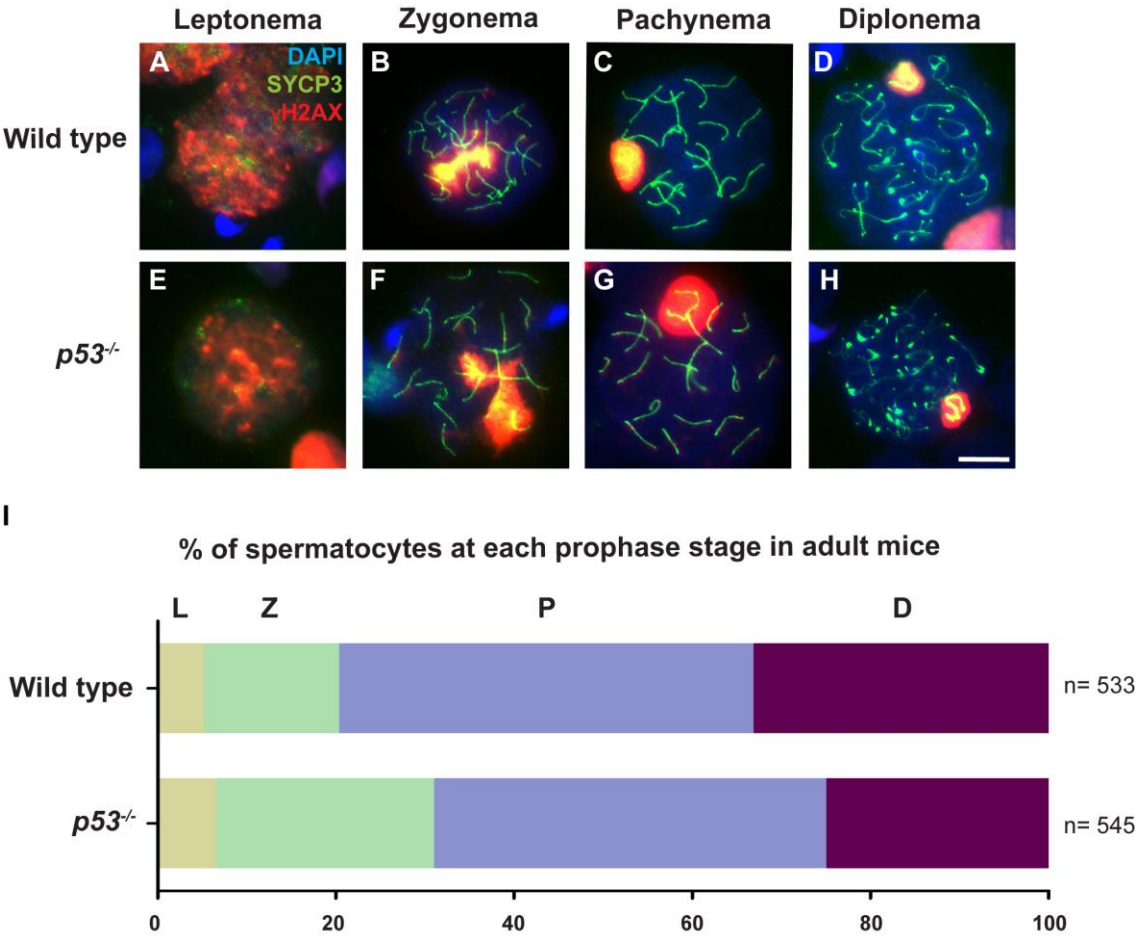

Figure 4.6. Meiotic progression in adult *p53* mutants. (A-J) Spread chromosomes from representative spermatocytes of *p53*$^{-/-}$ and wild type mice from leptonema to diplonema stage, stained against the axial element protein SYCP3 (green), γH2AX (red) and DAPI (blue). Scale bar in H represents 10 μm and applies to all panels. (K) Quantification of the percentage of spermatocytes at each prophase stage (leptonema (L), zygonema (Z), pachynema (P) and diplonema (D)) in *p53*$^{-/-}$ and wild type adult mice. (n) shows the number of spermatocytes counted per each genotype.

Altogether, these results indicate that although p53 could have some control over cell cycle progression, it is dispensable to correctly complete meiotic prophase. This is an expected observation for a presumably checkpoint protein, where in normal conditions we might not observe any drastic phenotype in its absence.

4.1.3.3 Analysis of p53 participation in meiotic recombination

One of the first signs of the activation of the DNA damage response is the phosphorylation of the histone H2AX (γH2AX) around the DSBs sites, where it persists until these are repaired. In order to study meiotic recombination in the absence of p53, we used γH2AX as a DSBs marker. We examined the number of γH2AX foci (determined as every faint signal over the synaptonemal complex) at pachynema and diplonema stages. At early pachynema, we found similar numbers of γH2AX foci between *p53* mutant (Mean±SD= 22.54±12.78) and wild type cells (Fig. 4.7A) (24.21±12.54, P=0.49, T test).

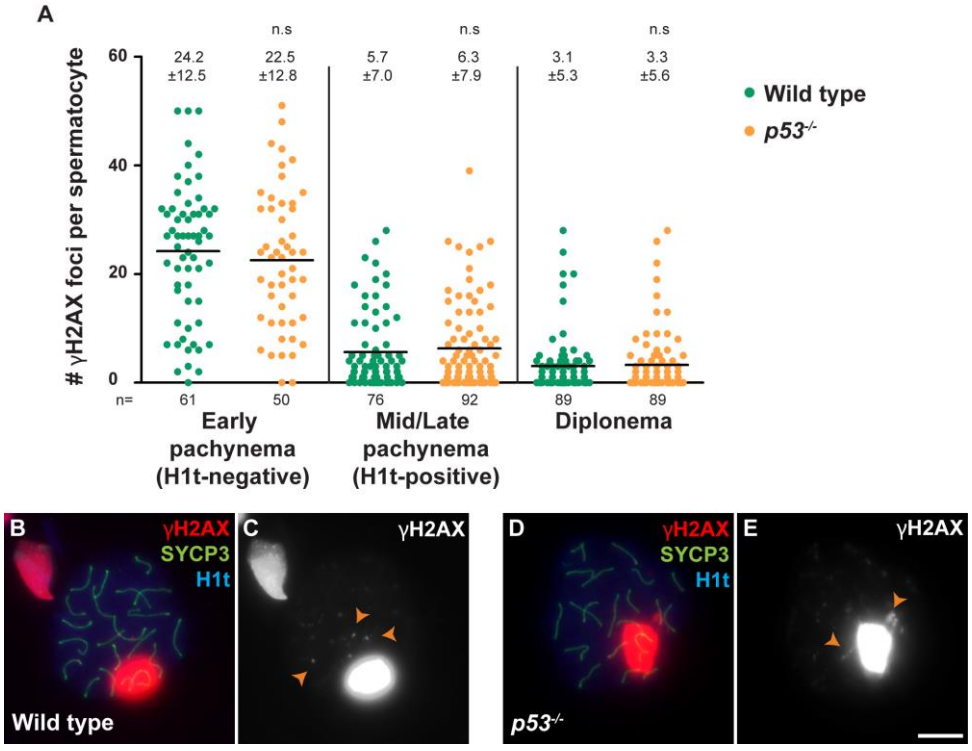

Figure 4.7. Absence of p53 does not affect DSBs repair. (A) Quantification of the number of γH2AX foci per spermatocyte at each indicated stage in wild type and *p53*$^{-/-}$ mice. The large, bright blobs of γH2AX staining are the sex bodies and the smaller γH2AX foci reflect unrepaired DSBs (orange arrowheads) Horizontal lines represent means. Means (± SD) are indicated above the graph, (n.s.) indicates not significant compared to the wild type. The number of cells counted (n) is indicated below the graph. (B-E) Representative pachytene spermatocytes are shown from wild type and *p53*$^{-/-}$ mice, stained against γH2AX (red), SYCP3 (green) and H1t (blue). Scale bar in E represents 10 μm and applies to all panels.

We used H1t protein as a marker of mid/late pachynema cells. The number of γH2AX foci at mid/late pachynema presented no significant differences between *p53*$^{-/-}$ (6.29±7.87) and control spermatocytes (Fig. 4.7A-E) (5.65±6.96, P=0.56, T test). Similarly, we obtained an equivalent number of γH2AX foci in *p53* mutant (3.28±5.55) and wild type spermatocytes (3.05±5.29, P=0.77, T test) at diplonema (Fig. 4.7A). Therefore, these results suggest that *p53* absence does not grossly alter DSB repair during prophase.

We also characterized CO formation in the absence of *p53*. In mouse, about two hundred DSBs are generated at leptonema by SPO11 protein, but only 10% of these recombination sites become COs. COs provide a physical linkage between the homologous chromosomes which ensures accurate segregation during the first meiotic division. CO formation is tightly regulated and each pair of homologous chromosomes gets at least one CO, therefore preventing genomic instability. To study CO formation, we used MLH1, which is a mismatch repair protein that localizes at CO sites at pachynema (Fig. 4.8B,C). We analyzed MLH1 foci number in *p53*$^{-/-}$ spermatocytes, and observed a slight significant increase of MLH1 foci in *p53*$^{-/-}$ spermatocytes (Mean±SD, 24.10±1.92), compared to wild type (23.30±2.04, P=0.036, Mann-Whitney test; Fig. 4.8A).

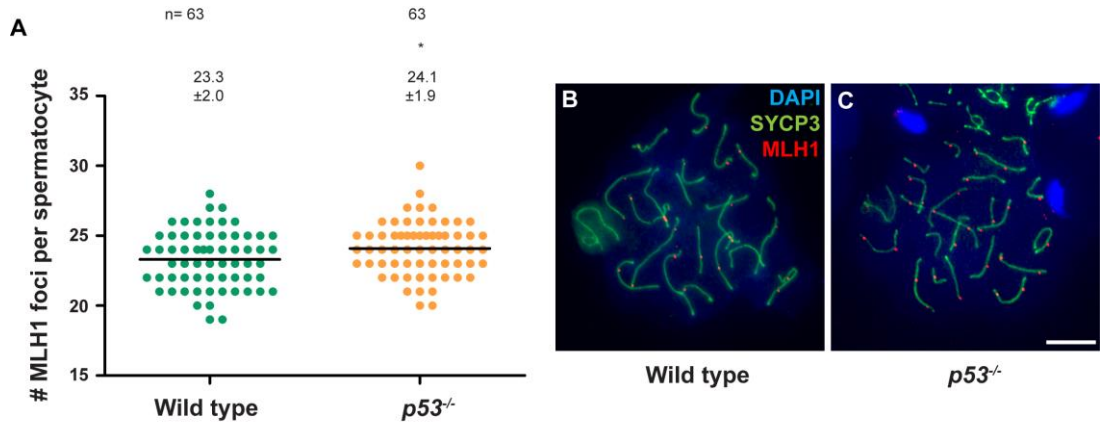

Figure 4.8. Absence of p53 slightly alters CO formation. (A) Quantification of the number of MLH1 foci per spermatocyte at pachytene stage. Horizontal lines represent means. Means (± SD) are indicated above the plot, (*) indicates statistically significant compared to the wild type. The number of cells counted per each genotype (n) is also indicated. (B-C) Representative pachytene spermatocytes are shown from wild type and *p53*$^{-/-}$ mice, stained against MLH1 (red), SYCP3 (green) and DAPI (blue). Scale bar in C represents 10 μm and applies to all panels.

However, although significant, the increase of COs accounts for only one more CO per *p53*$^{-/-}$ spermatocyte. These results suggest that p53 might be involved in controlling meiotic recombination in a very subtle manner, maybe affecting CO interference, or the alteration of the cell cycle progression occurring in the absence of *p53* could have some minor effect on CO formation. All together these results indicate that p53 is not required for properly executing meiotic recombination, although it might have some slight effect.

4.2 Study p53 family participation in the pachytene recombination-dependent arrest mechanism

Our group has described that the DDR proteins MRE11, NBS1, ATM and CHK2, promote the activation of the recombination-dependent arrest of *Trip13*$^{mod/mod}$ mutant spermatocytes at pachynema (Pacheco et al. 2015). Therefore, based on these results, we asked if p53 family might be involved in the activation of this arrest, since p53 family members are activated downstream of ATM and CHK2 in somatic DDR.

To determine if p53 family members participate in the activation of the recombination-dependent arrest, and analyzed if their absence could rescue *Trip13* mutant arrest, we bred double mutant mice combining *p53* family members with *Trip13* mutation as follow: *Trip13*$^{mod/mod}$ *p53*$^{-/-}$, *Trip13*$^{mod/mod}$ *TAp63*$^{-/-}$ and *Trip13*$^{mod/mod}$ *p73*$^{-/-}$ (also referred from now on as double mutants), and subsequently analyzed their phenotype.

4.2.1 Evaluate p53 family members role in the activation of the Recombination-dependent arrest in mouse spermatocytes

4.2.1.1 Study the ability of bypassing the recombination-dependent arrest

As mentioned earlier, the pachytene checkpoint in male mouse meiosis is a control mechanism that can be activated by two main arrest pathways. One responds to defective repair of DSBs (referred to as recombination-dependent arrest) (Barchi et al. 2005; Di Giacomo et al. 2005), and the other responds to failure in transcriptional silencing of the non-homologous portions of the sex chromosomes (sex body-deficient arrest) (Royo et al. 2010; Turner et al. 2005). These arrest mechanisms can be distinguished cytologically using the incorporation of the testis-specific histone variant H1t (Barchi et al. 2005), which in wild type mice accumulates on chromatin from mid-pachynema onwards (Fig. 4.9A) (Inselman et al. 2003). Mutant spermatocytes that fail to complete meiotic recombination (e.g., *Dmc1*$^{-/-}$ or *Trip13*$^{mod/mod}$), arrest meiosis before incorporating H1t; whereas mutants that fail to complete MSCI (e.g., *Spo11*$^{-/-}$), present H1t-positive spermatocytes (Barchi et al. 2005; Pacheco et al. 2015). According to this, when the recombination-dependent arrest is inactivated (e.g., *Trip13*$^{mod/mod}$ *Chk2*$^{-/-}$), spermatocytes

progress further and accumulate H1t –despite having multiple unrepaired DSBs (Pacheco et al. 2015).

First of all, as we previously demonstrated for *Trip13*$^{mod/mod}$ *Chk2*$^{-/-}$ mutants (Pacheco et al. 2015), if the recombination-dependent arrest is deactivated in the double mutants, we would expect an increased number of cells expressing H1t compared to the single *Trip13*$^{mod/mod}$ mutant. Thus, we stained squashed spermatocytes against SYCP3 and H1t. In wild-type mice, 53.0% of spermatocytes were H1t-positive, whereas in *Trip13*$^{mod/mod}$ mutants we only found a 21.3% of H1t-positive spermatocytes. All these H1t-positive cells have been attributed to be previously reported escapers that complete meiosis (Pacheco et al. 2015; Li et al. 2007; Roig et al. 2010). However, interestingly, we observed that a 47.5% of *Trip13*$^{mod/mod}$ *p53*$^{-/-}$ and a 51.3% of *Trip13*$^{mod/mod}$ *TAp63*$^{-/-}$ spermatocytes were H1t-positive (Fig. 4.9B). Therefore, we found a significant increase of H1t-positive cells in the p53 and TAp63 double mutants compared to the single *Trip13*$^{mod/mod}$ mutant (respectively P=0.0006 and P=0.0034, T test).

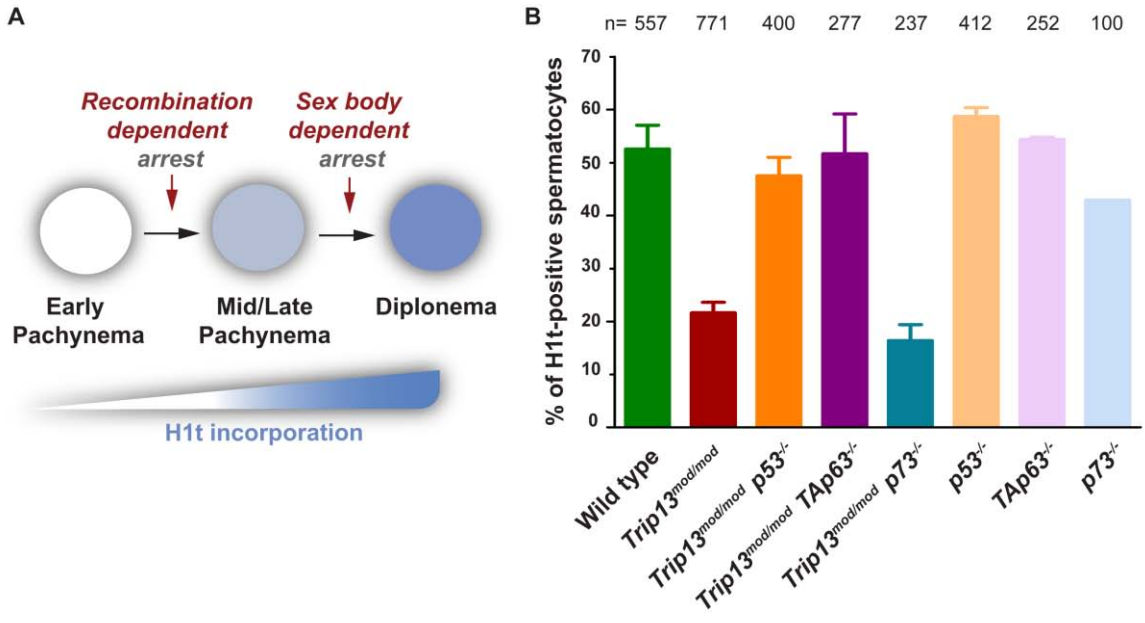

Figure 4.9. Absence of p53 or TAp63, but not p73, allows TRIP13-deficient spermatocytes to accumulate H1t. (A) Schematic representation of arrest events and H1t incorporation from early pachynema to diplonema. (B) Bars graph showing the average percentage of spermatocytes that have incorporated H1t for each genotype. The total number of cells analyzed is shown above each bar (n) and error bars represent standard deviation (SD).

In contrast, *Trip13*$^{mod/mod}$ *p73*$^{-/-}$ showed 16.5% of H1t-positive spermatocytes, which resembles what we found in the single *Trip13*$^{mod/mod}$ (P=0.0898, T test; Fig. 4.9B). These results suggest that in the absence of p53 or TAp63, but not p73, *Trip13* mutant spermatocytes are able to progress further into meiotic prophase and thus to bypass the recombination-dependent arrest.

4.2.1.2 Determine the presence of unrepaired DSBs after bypassing the recombination-dependent arrest

As a consequence of escaping the recombination-dependent arrest, we would expect that double mutant H1t-positive spermatocytes accumulate more unrepaired DSBs than H1t-positive *Trip13* single mutant cells. Thus, we quantified γH2AX patches in single and double mutant spermatocytes.

Before the activation of the recombination-dependent arrest, thus, in H1t-negative cells, numbers of unrepaired DSBs in the single *Trip13*$^{mod/mod}$ mutant and p53 and p73 double mutants were similar (P=0.36 and P=0.086, T-test, respectively) or slightly decreased for *Trip13*$^{mod/mod}$ *TAp63*$^{-/-}$ (P=0.0005, T-test, Fig. 4.10Q). Interestingly, *Trip13*$^{mod/mod}$ *p53*$^{-/-}$ and *Trip13*$^{mod/mod}$ *TAp63*$^{-/-}$ H1t-positive cells presented a significant increase in the number of unrepaired DSBs compared to the single *Trip13* mutant (*Trip13*$^{mod/mod}$ vs. *Trip13*$^{mod/mod}$ *p53*$^{-/-}$ P≤0.0001, and vs. *Trip13*$^{mod/mod}$ *TAp63*$^{-/-}$ P≤0.0001, T-test; Fig. 4.10E-F,I-J,Q). In contrast, *Trip13 p73* double mutant H1t-positive cells displayed similar number of γH2AX patches as *Trip13*$^{mod/mod}$ (P=0.488, T-test; Fig. 4.10M-N,Q), which agrees with previous results suggesting that *p73* does not participate in the recombination-dependent arrest.

To further corroborate that cells progressing to late meiotic prophase in *Trip13 p53* and *Trip13 TAp63* double mutants accumulated more unrepaired DSBs, we analyzed presence of unrepaired DSBs at diplonema cells from single and double mutants. Both p53 and TAp63 double mutants presented an increased number of unrepaired DSBs when compared to *Trip13* single mutant (*Trip13*$^{mod/mod}$ vs. *Trip13*$^{mod/mod}$ *p53*$^{-/-}$ P=0.00003, and vs. *Trip13*$^{mod/mod}$ *TAp63*$^{-/-}$ P=0.00025, negative binomial regression, Fig. 4.10G-H,K-L,Q), whereas *p73* double mutant showed no significant difference with *Trip13*$^{mod/mod}$ mutant (P=0.648, negative binomial regression test; Fig. 4.10O-P,Q).

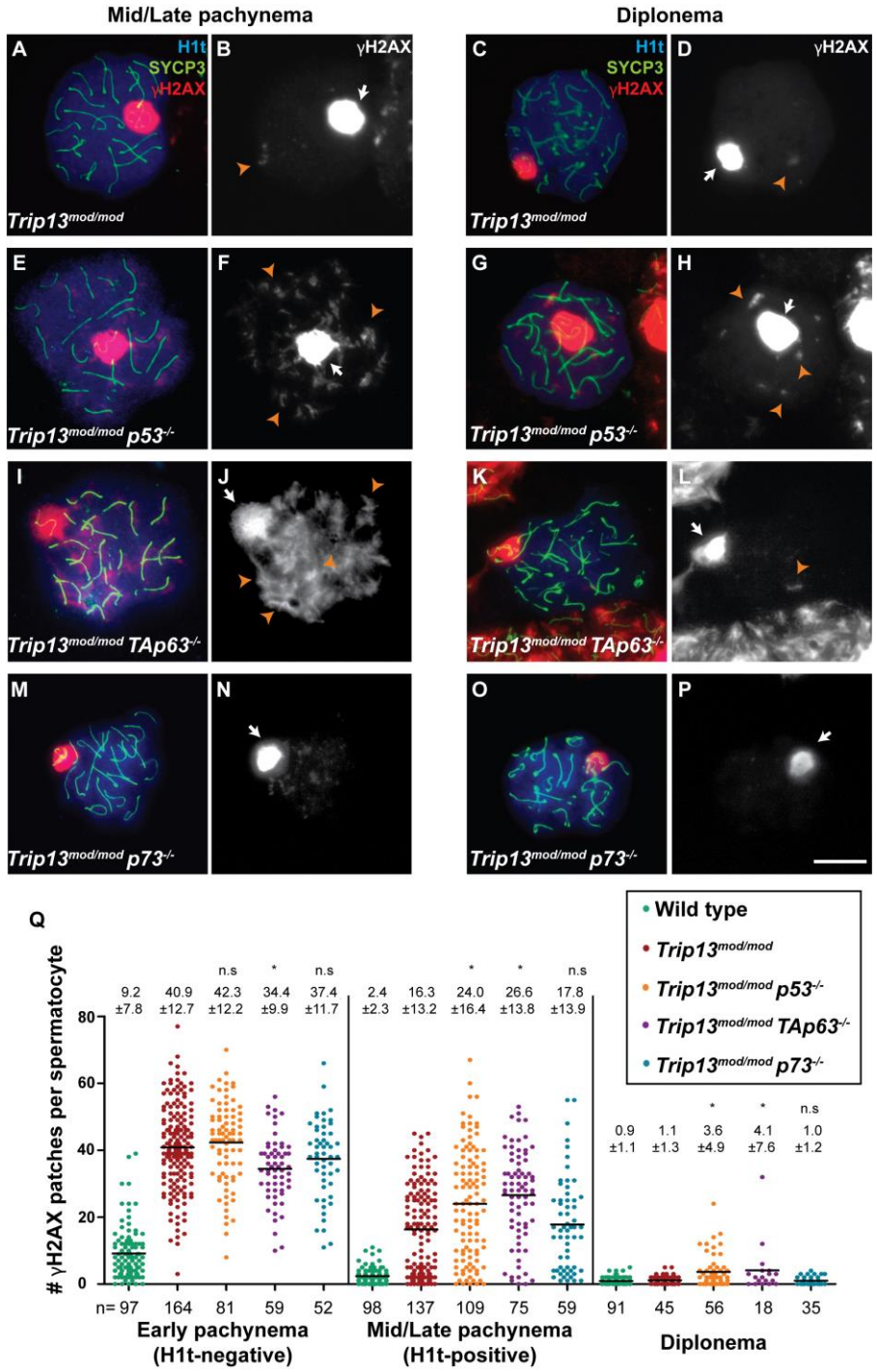

Figure 4.10. H1t-positive spermatocytes of *Trip13*$^{mod/mod}$ *p53*$^{-/-}$ and *Trip13*$^{mod/mod}$ *TAp63*$^{-/-}$ accumulate more unrepaired DSBs than H1t-positive *Trip13*$^{mod/mod}$ spermatocytes. (A-P) Spread chromosomes from representative spermatocytes of the indicated genotypes at mid/late pachynema (first column) or diplonema (second column) stained against the axial element protein SYCP3 (green), H1t (blue), and γH2AX (red). Large bright blobs of γH2AX staining are the sex bodies (arrows); the smaller γH2AX patches reflect unrepaired DSBs (orange arrowheads). Notice the presence of multiple unrepaired DSBs in *Trip13*$^{mod/mod}$ *p53*$^{-/-}$ and *Trip13*$^{mod/mod}$ *TAp63*$^{-/-}$, but not in *Trip13*$^{mod/mod}$ *p73*$^{-/-}$. Scale bar in P represents 10 μm and applies to all panels. (Q) Quantification of the number of γH2AX patches per spermatocyte. Horizontal lines represent means. Means (± SD) are indicated above the graph, and the number of cells counted (n) is indicated below. Above, (n.s.) indicates not significant and (*) indicates significantly different relative to *Trip13*$^{mod/mod}$ (T-test for pachynema stages; negative binomial regression for diplonema stage).

4.2.1.3 *Study of the influence of the p53 family members in the apoptotic profile of Trip13 mutants*

Finally to corroborate the involvement of p53 and TAp63 in the activation of the recombination-dependent arrest, we tested another prediction from our model. If *Trip13*$^{mod/mod}$ *p53*$^{-/-}$ and *Trip13*$^{mod/mod}$ *TAp63*$^{-/-}$ are able to escape the recombination-dependent arrest; they would present less H1t-negative apoptotic spermatocytes than the single *Trip13*$^{mod/mod}$. Therefore, we investigated the apoptotic profile of double mutants performing TUNEL staining on IF-stained slides. As expected, most *Trip13*$^{mod/mod}$ TUNEL-positive spermatocytes were H1t-negative (80.1%), similarly to what we observed in *Trip13*$^{mod/mod}$ *p73*$^{-/-}$ (73.3%, 1 mouse analyzed, P=0.2127, Fisher's exact test; Fig. 4.11). In contrast, the percentage of apoptotic H1t-negative spermatocytes in *Trip13*$^{mod/mod}$ *p53*$^{-/-}$ and *Trip13*$^{mod/mod}$ *TAp63*$^{-/-}$ was significantly lower (26.8%, P=0.002; and 7%, P=0.0007, T test, respectively; Fig. 4.11).

All together, these results suggest that p53 and TAp63, but not p73, are required to hold spermatocytes with numerous unrepaired DSBs at early pachynema stage (H1t-negative). Therefore, p53 and TAp63 control progression of male meiotic prophase, so that when recombination is impaired, they mediate the arrest of meiotic progression.

4.2.2 *Trip13* double mutants still present stage IV arrest

We previously reported that *Trip13*$^{mod/mod}$ *Chk2*$^{-/-}$ spermatocytes, although escaping the recombination-dependent arrest, still present a block in spermatogenesis progression at epithelial stage IV due to sex body-deficient arrest activation. Thus, we analyzed the histological phenotype of the double mutants *Trip13*$^{mod/mod}$ *p53*$^{-/-}$ and *Trip13*$^{mod/mod}$ *TAp63*$^{-/-}$. Both p53 and TAp63 double mutants, and also p73 double mutant, showed an arrest at epithelial stage IV (Fig. 4.12C-E). Since mutants that arrest at epithelial stage IV present an increase in the number of spermatocytes undergoing apoptosis (Yoshida et al. 1998; Baudat et al. 2000), we performed TUNEL staining on histological sections and analyzed the number of apoptotic cells present in *Trip13 p53* and *Trip13 TAp63* double mutants (Fig. 4.13A-C). TUNEL staining on histological sections demonstrated that the occurrence of apoptosis in the p53 and TAp63 double mutants was similar to the *Trip13*$^{mod/mod}$ single mutant (Fig. 4.13D). Taken together, these data show that *Trip13 p53* and *Trip13 TAp63* double mutants still presented an arrest epithelial stage IV, which suggests that these mutants might present sex body defects that activate the sex body-deficient arrest.

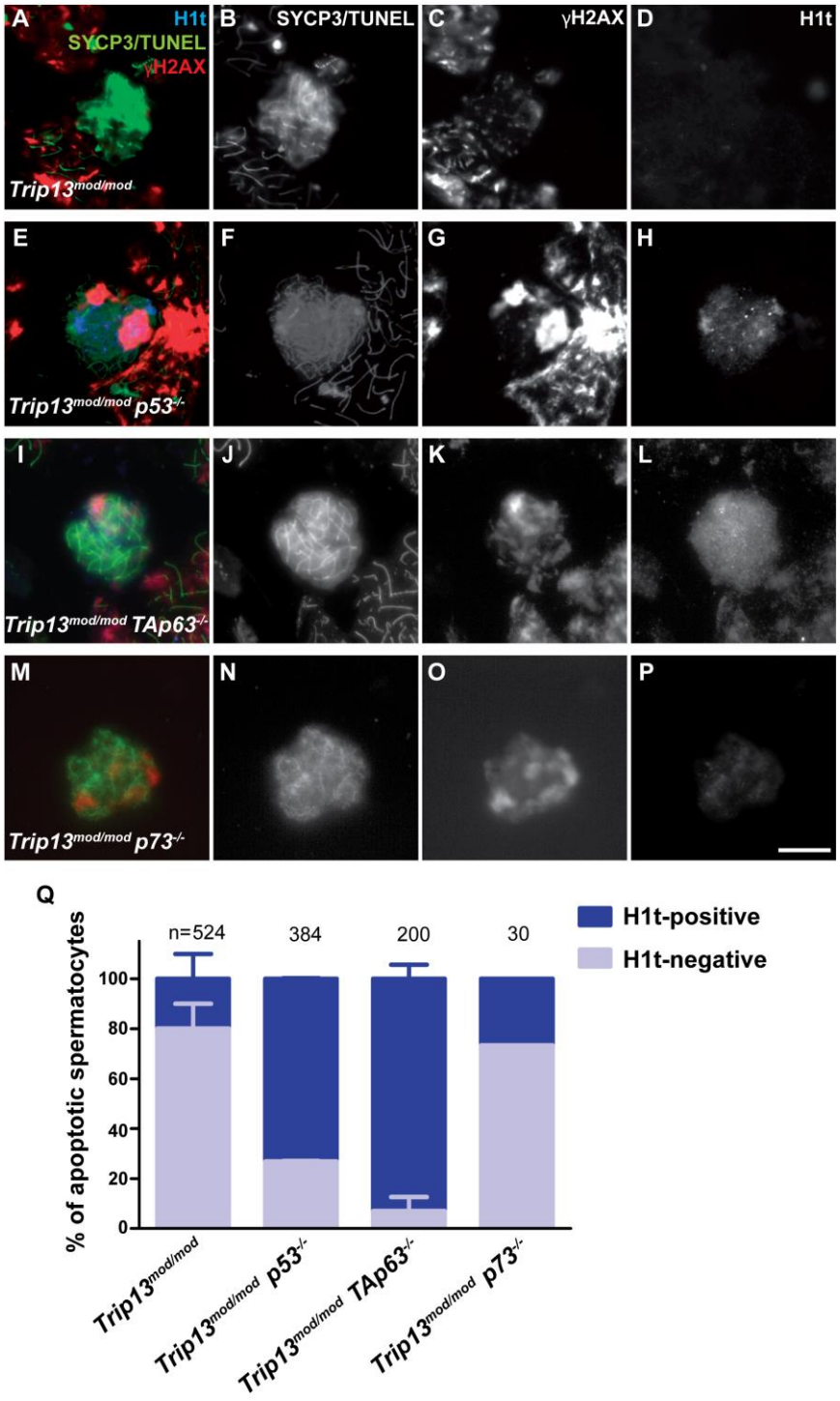

Figure 4.11. Apoptosis tends to occur at a later (H1t-positive) stage in TRIP13-deficient spermatocytes lacking p53 or TAp63, but not p73. (A-P) Representative apoptotic (TUNEL-positive) pachytene-stage spermatocytes stained for SYCP3 and TUNEL (green), H1t (blue) and γH2AX (red). Note the presence of multiple γH2AX patches and abnormal sex body in the apoptotic, H1t-positive spermatocytes from the *Trip13*$^{mod/mod}$ *p53*$^{-/-}$ and *Trip13*$^{mod/mod}$ TA*p63*$^{-/-}$ mutants. Scale bar in P represents 10 μm and applies to all panels. (Q) Percentage of apoptotic spermatocytes that are H1t-negative or H1t-positive. The total number of cells analyzed is shown (n) and error bars represent SD (one *Trip13*$^{mod/mod}$ *p73*$^{-/-}$ mouse analyzed).

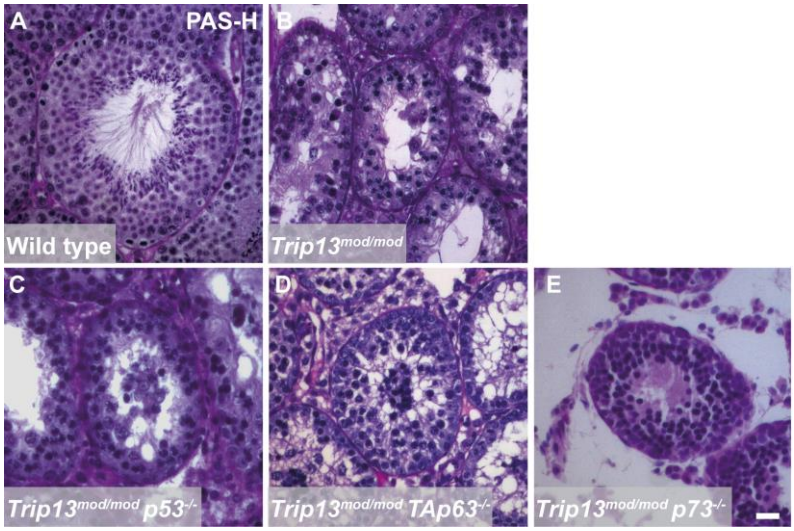

Figure 4.12. Absence of p53 family members does not alleviate the epithelial stage IV arrest in TRIP13-deficient mice. (A-E) Representative tubule sections from adult testes stained with PAS-H. Scale bar in E represents 20 µm and applies to all panels. (A) Wild type seminiferous tubule containing spermatogonia, spermatocytes and spermatids. (B-E) *Trip13*$^{mod/mod}$ single mutant and p53 family member double mutant sections showing condensed (apoptotic) spermatocytes in stage IV tubules, with only few escapers observed.

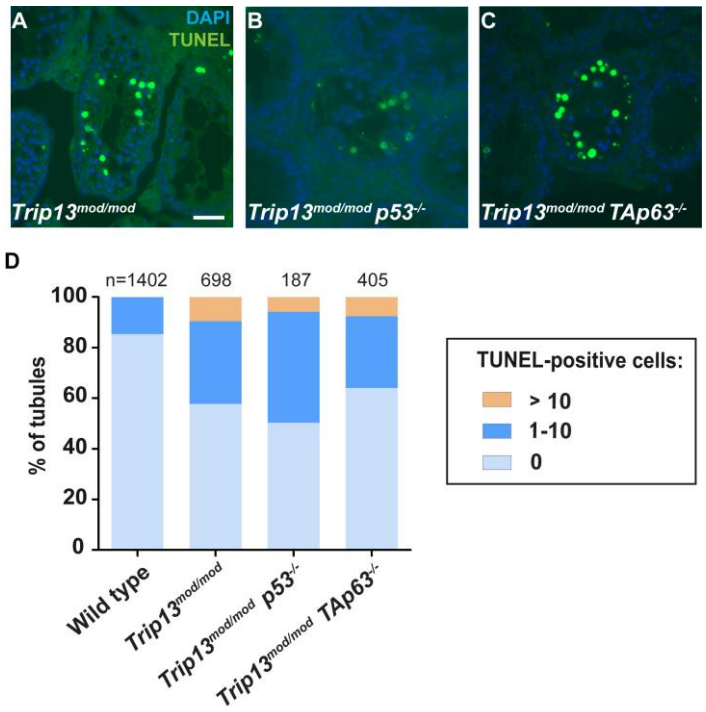

Figure 4.13. Absence of p53 family members does not alleviate spermatocyte apoptosis at epithelial stage IV in TRIP13-deficient mice. (A-C) Representative tubules are shown from testis sections of the indicated genotypes stained by TUNEL to detect apoptotic spermatocytes (green). Scale bar in A represents 40 µm and applies to panels A-C. (D) Quantification of the percentage of tubules with TUNEL-positive cells grouped in 0, 1 to 10 or more than 10 TUNEL-positive cells per tubule. The number of cells analyzed (n) is shown above each bar (one *Trip13*$^{mod/mod}$ *p53*$^{-/-}$ and one *Trip13*$^{mod/mod}$ *TAp63*$^{-/-}$ mouse analyzed).

4.2.3 TRIP13 involvement in the formation of the sex body

4.2.3.1 Qualitative analysis of sex body formation in Trip13 mutants

To determine if *Trip13*$^{mod/mod}$ *p53*$^{-/-}$ and *Trip13*$^{mod/mod}$ *TAp63*$^{-/-}$ epithelial stage IV arrest was due to MSCI failure, like in *Trip13*$^{mod/mod}$ *Chk2*$^{-/-}$ mutants (Pacheco et al. 2015), we analyzed the morphology and functionality of the sex body in *Trip13 p53* and *Trip13 TAp63* double mutants. We previously showed that *Trip13*$^{mod/mod}$ mutants present MSCI defects. If MSCI fails, expression of sex chromosome genes at pachytene stage becomes deleterious and sufficient to cause an arrest and ultimately apoptosis of spermatocytes (Royo et al. 2010). In order to qualitatively study the morphology of the sex body at pachytene stage, we stained several sex body markers in spermatocyte spreads: γH2AX, ATR (the kinase responsible for H2AX phosphorylation in the sex body (Royo et al. 2013)), and SUMO-1 (which accumulates on the X and Y chromatin at pachynema in an ATR dependent manner (Royo et al. 2013)) (see Fig. 4.14A-L for representative images and Table 4.1 for quantification).

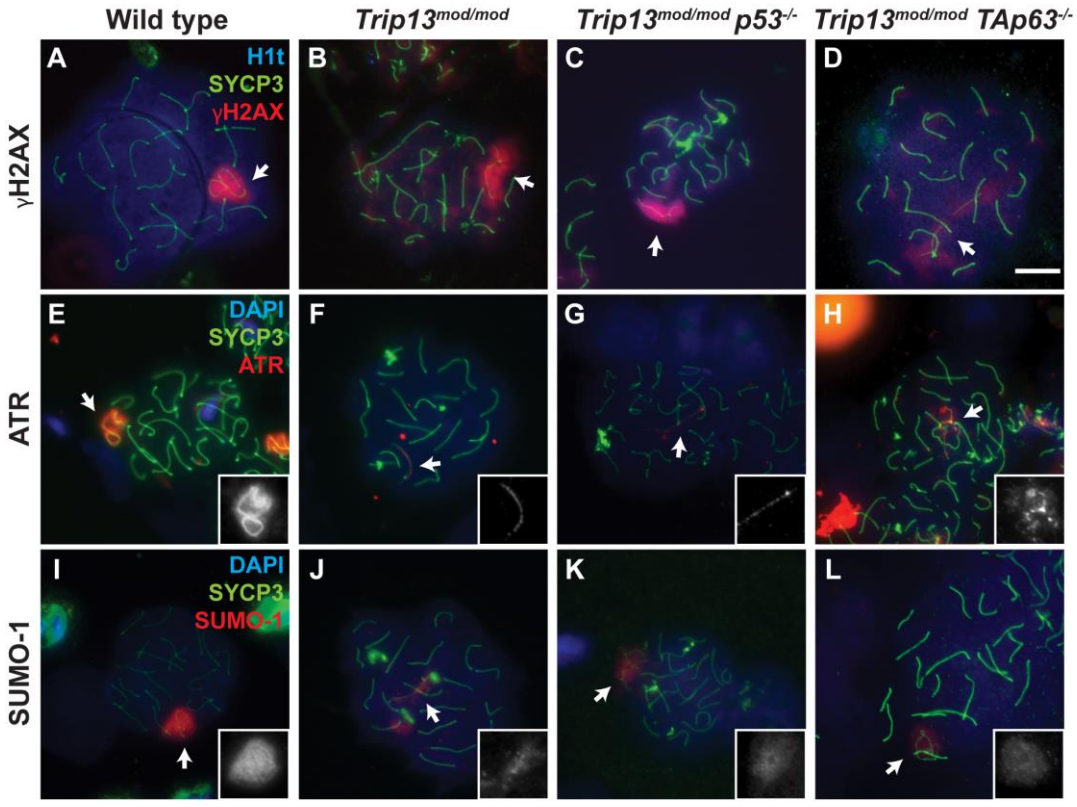

Figure 4.14. **Sex body defects in TRIP13-deficient cells lacking p53, TAp63 or p73.** (A-D) Representative H1t-positive pachytene spermatocytes of the indicated genotypes stained for SYCP3 (green), γH2AX (red) and H1t (blue). (E-L) Representative pachytene spermatocytes of the indicated genotypes stained against SYCP3 (green), either ATR (D-F) or SUMO-1 (G-I) (red) and DAPI (blue). Scale bar in D represents 10 μm and applies to all panels. White arrows indicate sex bodies.

For each marker, the p53 and TAp63 double mutants displayed sex body abnormalities that were qualitatively and quantitatively indistinguishable from the *Trip13*$^{mod/mod}$ single mutant. Specifically, by observing γH2AX staining we found abnormally elongated sex bodies in approximately two thirds of pachytene-stage spermatocytes corresponding to double mutants *Trip13*$^{mod/mod}$ *p53*$^{-/-}$ (70%) and *Trip13*$^{mod/mod}$ *TAp63*$^{-/-}$ (70%), similar to what we found in *Trip13*$^{mod/mod}$ mutants (67.5%, P=0.6662 for both comparisons, Fisher's exact test) (Fig. 4.14B-D and Table 4.1). In contrast, only a minority of wild-type pachytene-stage spermatocytes presented a stretched sex body (20%, vs. *Trip13*$^{mod/mod}$ P≤0.0001, Fisher's exact test), while most of them displayed a round sex body structure (see intensely stained sex body in Fig. 4.14A and Table 4.1 for quantifications).

Table 4.1 *Trip13* mutants present defects in sex body formation.

	Wild type	*Trip13*$^{mod/mod}$	*Trip13*$^{mod/mod}$ *p53*$^{-/-}$	*Trip13*$^{mod/mod}$ *TAp63*$^{-/-}$
γH2AX				
Elongated sex body	20 %	67.5 %	70 %	70 %
Round sex body	80 %	32.5 %	30 %	30 %
(N)	40	40	40	40
ATR				
No staining	0 %	4.25 %	4 %	8.5 %
Discontinuous XY axis	6.8 %	51.3 %	59.5 %	51 %
Complete XY axis	24 %	29 %	27.5 %	25 %
Chromatin staining	69.3 %	15.5 %	9 %	15.5 %
(N)	400	400	200	200
SUMO-1				
No staining	1.5 %	49.8 %	18.5 %	50.5 %
Faint staining	13.8 %	36.3 %	56.5 %	38.5 %
Strong staining	84.8 %	14 %	25 %	11 %
(N)	400	400	200	200

ATR is the kinase responsible for H2AX phosphorylation in the sex body; it loads on the unsynapsed sex chromosomes, and expands into the chromatin triggering H2AX phosphorylation (Royo et al. 2010; Barchi et al. 2008; Baart et al. 2000). Whereas ATR in wild type pachynema usually covered the unsynapsed X and Y chromosome axes and expanded over their chromatin (69.3%) (Fig. 4.14E), less than a 20% of pachytene cells from double mutants or *Trip13*$^{mod/mod}$ single mutant displayed this chromatin-expanded pattern (15.5% in single *Trip13*$^{mod/mod}$, P=0.0001, Fisher's exact test). Instead most double

mutants or *Trip13*$^{mod/mod}$ cells showed a discontinued localization of ATR along the X and Y axes (Fig. 4.14F-H and see Table 4.1 for quantification).

Finally, we also examined SUMO-1 protein, which accumulates on the X and Y chromatin at pachynema in an ATR-dependent manner (Royo et al. 2013). SUMO-1 staining was also altered in all *Trip13* single and double mutants, most mutant pachynema cells displayed only modest SUMO-1 staining (Fig. 4.14J-L and see Table 4.1 for quantification). While the majority (84.8%) of wild type pachytene spermatocytes displayed an intense SUMO-1 signal over the sex body, this was only observed in 14.8% of *Trip13*$^{mod/mod}$ pachytene cells (P≤0.0001 Fisher's exact test). The percentages of strong SUMO-1 staining in *Trip13 p53* and *Trip13 TAp63* double mutants where similar to *Trip13* single mutants and significantly different from the wild type: 25% in *Trip13*$^{mod/mod}$ *p53*$^{-/-}$ (P≤0.0001 Fisher's exact test) and 11% in *Trip13*$^{mod/mod}$ *TAp63*$^{-/-}$ (P≤0.0001 Fisher's exact test; see Fig. 4.14K,L and Table 4.1 for quantifications). These results confirm that *Trip13* mutants have defects in sex body formation, consistent with our previous observations (Pacheco et al. 2015), and demonstrate that these defects are not ameliorated by absence of either p53 or TAp63.

4.2.3.2 Functional analysis of the meiotic sex chromosome inactivation (MSCI) in Trip13 mutants

To test whether the defects found in sex body formation affected its functionality, we performed RNA fluorescence *in situ* hybridization (RNA-FISH) analysis to assess MSCI. RNA-FISH technique allows the detection of a specific transcript in a particular meiotic cell type (Mahadevaiah et al. 2009). For our study, we carried out RNA-FISH for the X-linked genes *Scml2* (located next to the PAR region) and *Zfx* (more interstitially located), which should be silenced throughout pachynema by the MSCI. Slides were immunostained against TOPBP1 (DNA topoisomerase 2 binding-protein 1, which loads to the unsynapsed sex chromosomes at pachynema (Refolio et al. 2011)), in order to detect early pachytene-stage cells.

We found that the percentage of early pachytene cells expressing X-linked genes was significantly higher in *Trip13*$^{mod/mod}$ (27.5% for *Scml2* and 27.2% for *Zfx*) relative to wild-type cells (17.1% for *Scml2,* P<0.05, and 10.9% for *Zfx,* P<0.05, one-way ANOVA, Fig. 15E,F). As we expected from our previous results, we observed that in *Trip13*$^{mod/mod}$ *p53*$^{-/-}$ and *Trip13*$^{mod/mod}$ *TAp63*$^{-/-}$ early pachytene-stage spermatocytes expression for both X-linked genes was similar to the *Trip13*$^{mod/mod}$ mutant. *Scml2* was expressed in 28.8% of

Trip13$^{mod/mod}$ *p53*$^{-/-}$ early pachytene cells (1 mouse, P=0.0330 vs. wild type, Fisher's exact test; Fig. 4.15A,E), and 34.4% of cells in *Trip13*$^{mod/mod}$ *TAp63*$^{-/-}$ mutants (P<0.05, vs. wild type, one-way ANOVA, Fig. 4.15B,E and see Table 4.2).

Frequencies for *Zfx* expression were 33.8% for *Trip13*$^{mod/mod}$ *p53*$^{-/-}$ (vs. wild-type, P≤0.0001, Fisher's exact test; Fig. 4.15C,F and Table 4.2) and 30.6% for *Trip13*$^{mod/mod}$ *TAp63*$^{-/-}$ early pachytene spermatocytes (vs. wild-type, P≤0.0001, Fisher's exact test or P<0.05 one-way ANOVA; Fig. 4.15D,F and Table 4.2). These results support what we previously observed for *Trip13*$^{mod/mod}$ *Chk2*$^{-/-}$ mutants, where although these spermatocytes escape the recombination-dependent arrest, *Trip13*$^{mod/mod}$ *p53*$^{-/-}$ and *Trip13*$^{mod/mod}$ *TAp63*$^{-/-}$ mutants still apoptose at pachytene stage due to MSCI failure. Therefore, p53 and TAp63 absence does not disturb the activation of the sex body-dependent arrest.

Table 4.2 Expression of *Scml2* and *Zfx* on early pachytene cells from wild type and mutant mice.

	Wild type	*Trip13*$^{mod/mod}$	*Trip13*$^{mod/mod}$ *p53*$^{-/-}$	*Trip13*$^{mod/mod}$ *TAp63*$^{-/-}$
% of pachynema cells expressing *Scml2* (mean±SD)	17.1 ±1.9	27.5 ±0.0*	28.8**	34.4 ±4.4*
(N)	200	160	80 [a]	160
% of pachynema cells expressing *Zfx* (mean±SD)	10.9 ±3.0	27.2 ±3.2*	33.8**	30.6 ±0.9*
(N)	225	158	80 [a]	160

* Significantly different from wild type, P < 0.05 one-way ANOVA and Tukey's multiple comparison test.

** Significantly different from wild type, P < 0.05 Fisher's exact test.

[a] One mouse analyzed.

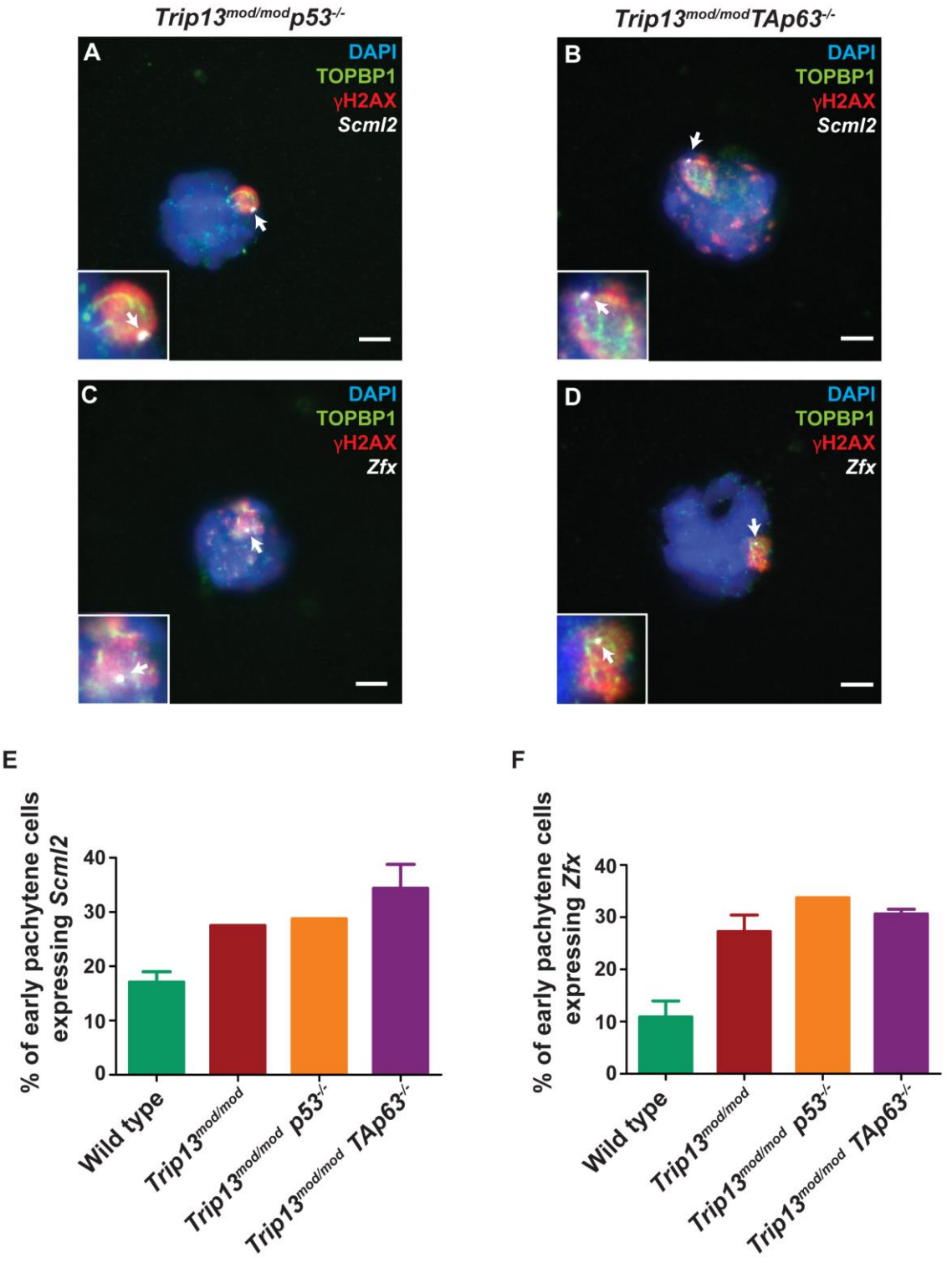

Figure 4.15. **MSCI failure in TRIP13-deficient cells lacking p53 or TAp63.** (A-F) RNA-FISH performed on *Trip13*$^{mod/mod}$ *p53*$^{-/-}$ spermatocytes. Images display *Scml2* or *Zfx* RNA-FISH signal (white arrows), DAPI (blue), and immunostaining for TOPBP1 (green) and γH2AX (red). Insets show zoomed images of the sex bodies. Scale bars represent 10 μm. (G,H) Graphics showing mean percentage of early pachytene spermatocytes expressing *Scml2* (L) or *Zfx* (M). Error bars represent SD (see Table 4.2 for mean±SD and (n) number cells analyzed).

4.2.4 p53 and TAp63 do not activate the sex body-deficient arrest

However, although we observed that *p53* or *TAp63* double mutants could not rescue *Trip13*$^{mod/mod}$ stage IV apoptosis, we wanted to test directly if p53 family members could rescue MSCI failure arrest in other mutants. With this purpose, we used *Spo11*$^{-/-}$ mutants, whose spermatocytes present synapsis defects due to the lack of DSBs and only form a pseudo-sex body (Baudat et al. 2000; Romanienko and Camerini-Otero 2000; Burgoyne et al. 2009). This pseudo-sex body normally does not include the X and Y chromosomes, thus allowing sex chromosome expression leading to the activation of the sex body-defective arrest. We generated *Spo11*$^{-/-}$ *TAp63*$^{-/-}$ and *Spo11*$^{-/-}$ *p53*$^{-/-}$ double mutants; in order to analyze if p53 or TAp63 absence could revert the arrest occurring in *Spo11*$^{-/-}$ mutants.

To account for the possible rescue of the arrested meiotic prophase, first we analyzed the normalized testis weight since, as we mentioned above, mutants with arrested meiosis present significantly smaller testis. The normalized testis weight was obtained dividing the weight of the two testes by the mouse weight in order to account for possible body size variation among different mouse mutants. Normalized testis size can also distinguish between the stages where the arrest occurs during meiosis. While those animals experiencing meiotic prophase arrest (also known as stage IV arrest, e.g. *Spo11*$^{-/-}$ or *Dmc1*$^{-/-}$) present testis that are approximately one third the size of a wild type ($P \leq 0.0001$, T test), mutants that arrest at the metaphase stage of the first meiotic division (stage XII arrest, e.g., *Spo11*$^{+/-}$ *Atm*$^{-/-}$ or *Spo11*$^{-/-}$ *tgβ*$^{+/+}$) have testis which are only 50% the size of a wild type ($P \leq 0.0001$, T test; see Fig. 16A).

The normalized testis size of *Spo11*$^{-/-}$ *TAp63*$^{-/-}$ double mutants (Mean±SD=0.19±0.3) was comparable to those of *Spo11*$^{-/-}$ single mutant (0.21±0.02, P=0.2219, T test; Fig. 4.17A). Also *Spo11*$^{-/-}$ *p53*$^{-/-}$ double mutants had testis size equivalents to *Spo11*$^{-/-}$ single mutants (0.25) (Fig. 4.16A). To confirm these data, we performed an histological analysis of the *Spo11*$^{-/-}$ *p53*$^{-/-}$ testis and observed stage IV arrest as in *Spo11*$^{-/-}$ (Fig 4.16B,C). Therefore, these results indicate that p53 and TAp63 are dispensable to activate programmed cell death in response of the sex body-deficient arrest in mouse spermatocytes. Furthermore, our results show that the recombination-dependent arrest and the sex body-deficient arrest are two genetically separable mechanisms.

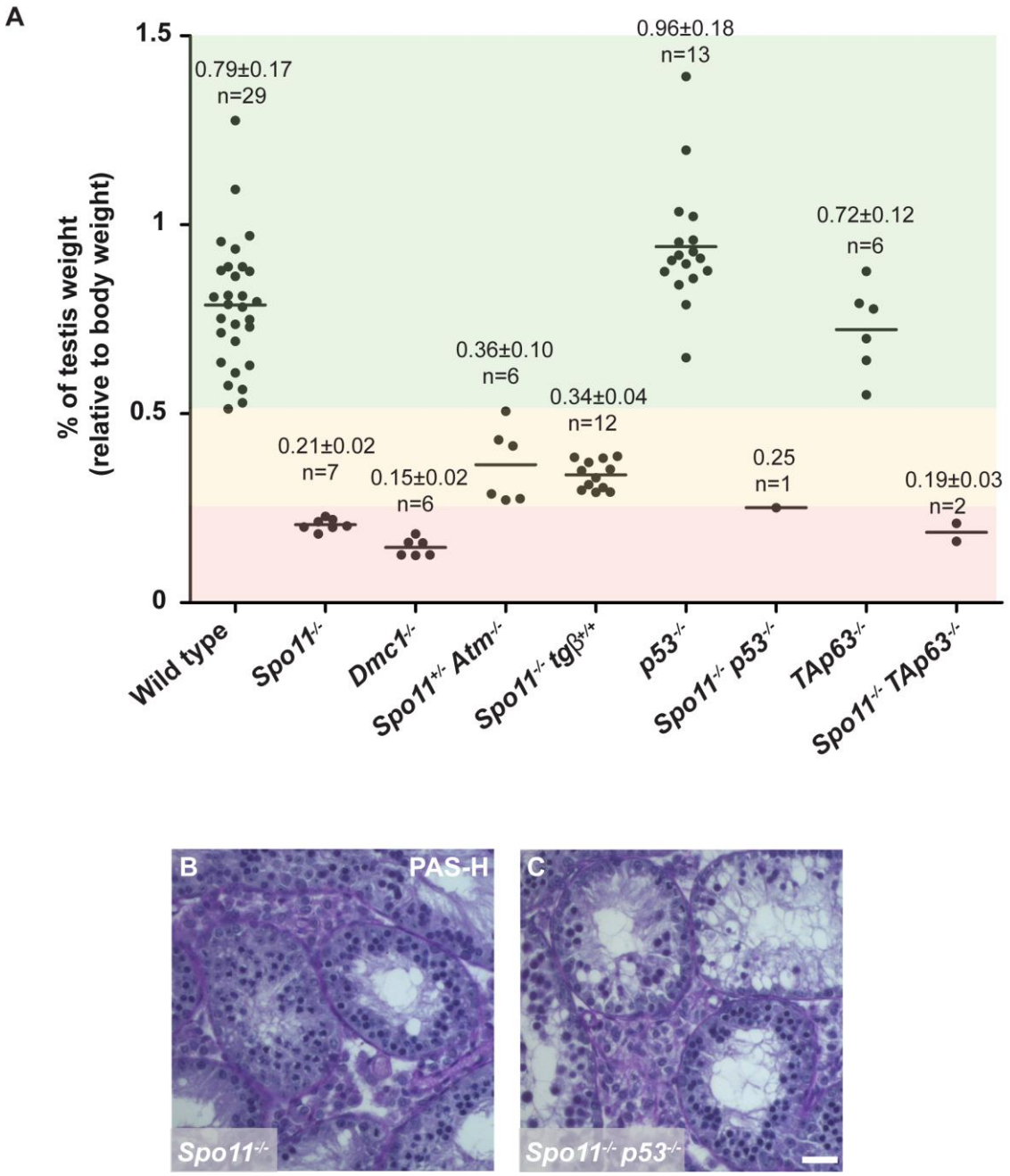

Figure 4.16. **Mutation of *p53* or *TAp63* does not rescue *Spo11*$^{-/-}$ stage IV arrest.** (A) Graph shows normalized testis weight of the indicated genotypes. Green rectangle includes wild type and mutants that complete meiosis. Yellow rectangle accounts for mutant mice that experience an arrest at metaphase stage XII of first meiotic division (*Spo11*$^{+/-}$ *Atm*$^{-/-}$ and *Spo11*$^{-/-}$ *tgβ*$^{+/+}$). Pink rectangle shows mutants that present a stage IV pachytene arrest (*Spo11*$^{-/-}$ or *Dmc1*$^{-/-}$). Data from *Spo11*$^{+/-}$ *Atm*$^{-/-}$ was previously published (Pacheco et al. 2015). Black horizontal lines represent the mean, which is also indicated above the corresponding genotype (Mean±SD). n shows the number of animals analyzed for each genotype (one *Spo11*$^{-/-}$ *p53*$^{-/-}$mouse analyzed). (B) *Spo11*$^{-/-}$ and (C) *Spo11*$^{-/-}$*p53*$^{-/-}$ representative tubule sections from adult testes stained with PAS-H. Scale bar in C represents 20 µm and applies to all panels. Both sections show condensed (apoptotic) spermatocytes in stage IV arrested tubules.

4.3 Analysis of TRIP13 role in meiotic transcription

During the first meiotic division, transcription is suppressed at the onset of prophase, and it only restarts again at mid pachynema (Monesi, 1964), when chromosomes are fully synapsed and DSBs are repaired. In pachytene-stage spermatocytes, when autosomes reactivate transcription, the sex chromosomes are silenced by the sex body (MSCI) (Turner et al. 2004); which is crucial to allow correct progression of meiosis (Royo et al. 2010) and it is proposed to be a manifestation of the global meiotic silencing of unsynapsed chromosomes (MSUC) during zygonema (Burgoyne et al. 2009). Since we identified that TRIP13 is required for the correct silencing of the sex chromosomes at pachytene stage (Pacheco et al. 2015) and it has been hypothesized that the MSUC is a manifestation of the global transcription suppression that occurs at the entry of prophase (Page et al. 2012), we wondered if TRIP13 may also participate in the transcription regulation that occurs at the initiation of meiosis. To test this, we analyzed transcription levels at early stages of meiotic prophase in control and *Trip13* mutant spermatocytes.

4.3.1 Transcription levels in *Trip13* mutants

4.3.1.1 Analyze global RNA expression levels in Trip13 mutants with EU

To analyze global gene expression in meiotic cells, we used the *EU Click-it Imaging technique* (Click-iT® RNA Alexa Fluor® 488 Imaging Kit, Life Technologies) to cytologically detect newly synthesized RNA. Briefly, we obtained a cell suspension from fresh testis and then incubated these cells in the presence of a uridine analogue (EU, 5-Ethynyl Uridine), which is specifically incorporated to nascent RNA. From this cell suspension, slides were prepared using a protocol that preserves the nuclei structure and keeps cellular volume. Then, EU-tagged RNA was labeled with a dye (Alexa Fluor 488) through a chemoselective ligation or "click-it" reaction between an azide-containing dye and an alkyne, which allows the visualization of the RNA in a fluorescence microscope. Slides were also IF-stained against SYCP3 and γH2AX, in order to classify meiotic prophase stages. Images were captured from cells at different stages to quantify the intensity of the RNA signal. In order to get the maximum information of each cell, we obtained stacks of images every 0.5 μm, then we displayed the sum projection and measured the intensity of the EU labelled RNA signal with ImageJ software. With this technique we can cytologically

evaluate total RNA expression of wild type and mutant spermatocytes at different prophase stages.

Firstly, we confirmed that this technique allows detecting how RNA expression profile is low at the onset of prophase and increases at mid pachynema in wild type cells, as previously described (see wild type RNA intensity levels along prophase Fig. 4.17A and representative image in Fig. 4.17B-E) (Monesi 1964). Then, we proceeded to perform this experimental procedure on *Trip13*$^{mod/mod}$ mutants and wild type (littermate pairs from 30-60 dpp). Interestingly, *Trip13*$^{mod/mod}$ mutant spermatocytes presented significantly higher levels of EU signal compared to the wild type at zygonema and pachynema (P<0.0001, T test for zygonema, early pachynema and mid/late pachynema; Fig. 4.17A).

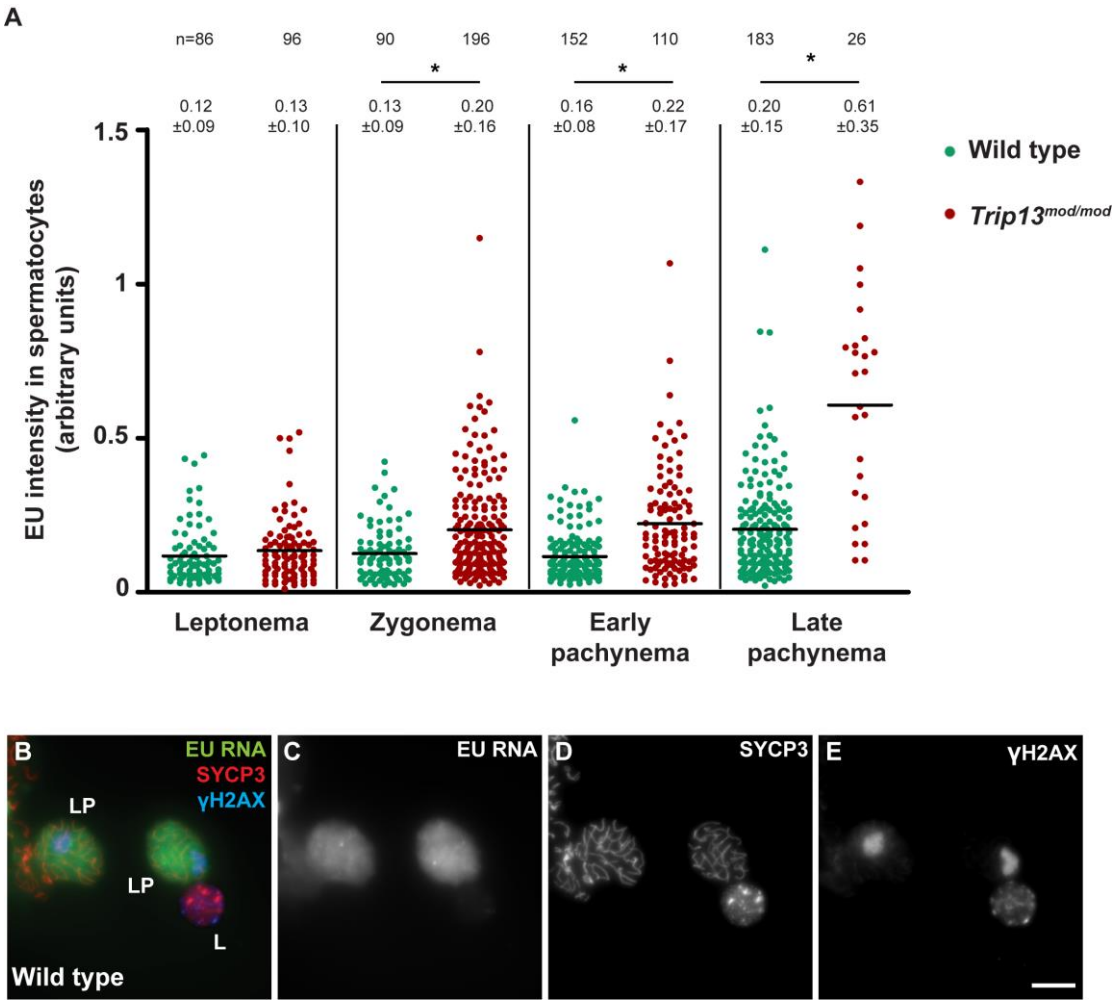

Figure 4.17. Global RNA intensity in *Trip13*$^{mod/mod}$ mutants. (A) Quantification of the EU intensity in *Trip13*$^{mod/mod}$ and wild type mice of spermatocytes at the indicated prophase stages. Horizontal lines represent means. Means±SD and the number of cells counted (n) are indicated above the graph. (*) indicates significantly different relative to the wild type. (B-D) Representative image of EU treated wild type late pachytene (LP) and leptotene (L) spermatocytes. Sum projection of stack images showing EU-RNA (green), SYCP3 (red) and γH2AX (blue). Scale bar in E represents 10 μm and applies to all panels.

To complete our study, we also analyzed RNA levels in other mutants, and in order to compare the results obtained between different mutant mice of different backgrounds we represented the relative values, by dividing the intensity of each mutant cell with the average intensity for its corresponding wild type. For *Trip13 severe (Trip13$^{sev/sev}$)* mutants, which present a more penetrant TRIP13 defective phenotype (Roig et al. 2010), we also observed an increase of EU signal compared to wild type spermatocytes at leptonema and zygonema (P=0.0023 and P=0.0408 respectively, T test; Fig. 4.18A,B).

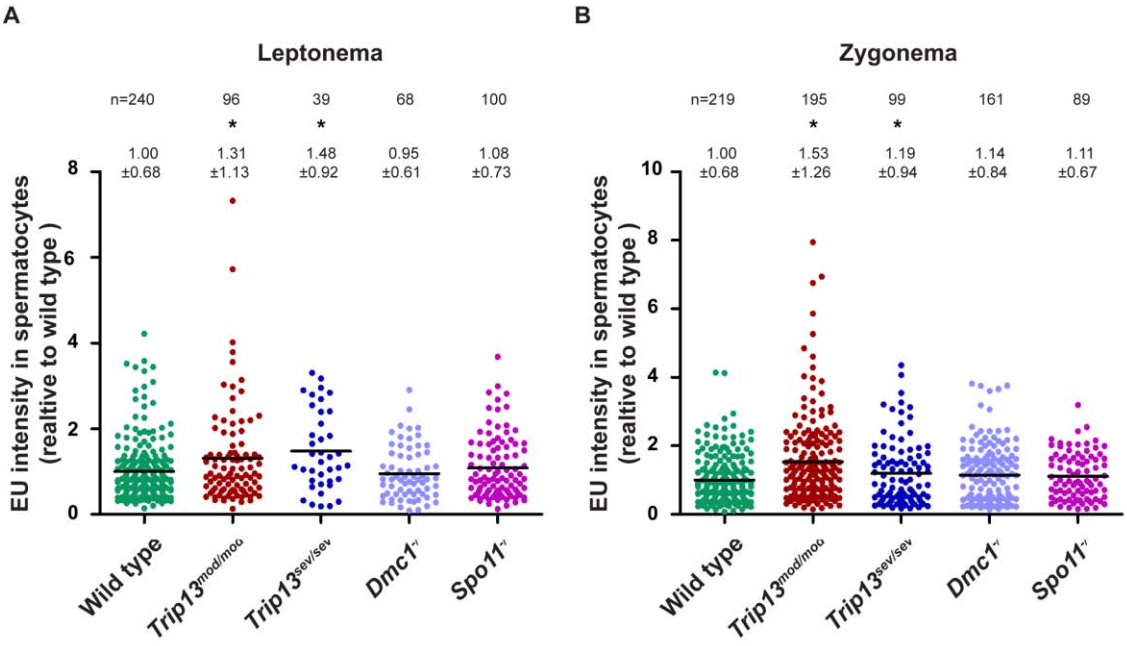

Figure 4.18. Compared global RNA intensity in *Trip13*$^{mod/mod}$, *Trip13*$^{sev/sev}$, *Dmc1*$^{-/-}$ and *Spo11*$^{-/-}$ mutants. (A) Quantification of the EU intensity in leptotene spermatocytes of the indicated genotypes relative to the wild type. (B) Quantification of the EU intensity in zygotene spermatocytes of the indicated genotypes relative to the wild type. Horizontal lines represent means. Means±SD and the number of counted cells (n) are indicated above the graph. Above, (*) indicates significantly different relative to the wild type.

Besides, we also evaluated transcription levels in other mutant mice that present a block at pachytene stage like *Dmc1* and *Spo11* mutants, in order to understand if the increase of RNA expression is due to the *Trip13* mutation or as a consequence of the pachytene arrest. For instance, analysis of *Dmc1* mutants would determine if the higher expression observed in *Trip13* mutants is indeed an effect of *Trip13* absence, or if it caused by the activation of the recombination-dependent arrest. Moreover, analyzing the expression profile of *Spo11* mutants spermatocytes would allow us to figure out if the down-regulation of transcription when meiosis starts is dependent on DSB formation or if it is controlled by the activation of a "meiotic program". Analysis of early prophase stages

in both *Dmc1*$^{-/-}$ and *Spo11*$^{-/-}$ mutants, revealed that they presented similar EU expression levels than the control mice (for leptonema: P=0.5773 and P=0.3334 respectively, T test; for zygonema: P=0.0655 and P=0.2190 respectively, T test; Fig. 4.18A,B). Analysis of pachytene stage was not performed because neither *Dmc1*$^{-/-}$ or *Spo11*$^{-/-}$ mutants are able to properly synapse their homologous chromosomes. Altogether these results suggest that *Trip13* mutant cells present increased global transcription levels at zygonema and pachynema suggesting that TRIP13 protein is necessary to control global transcription levels at early prophase stages.

4.3.1.2 Study transcription levels in Trip13 mutants with phospho-RNA polymerase II

In order to corroborate our previous findings about the transcriptional activity in *Trip13* mutants, we examined the phosphorylated Serine2 RNA polymerase II (phophso(S2)-RNApol II), which corresponds to the active form of the protein (Fig. 19).

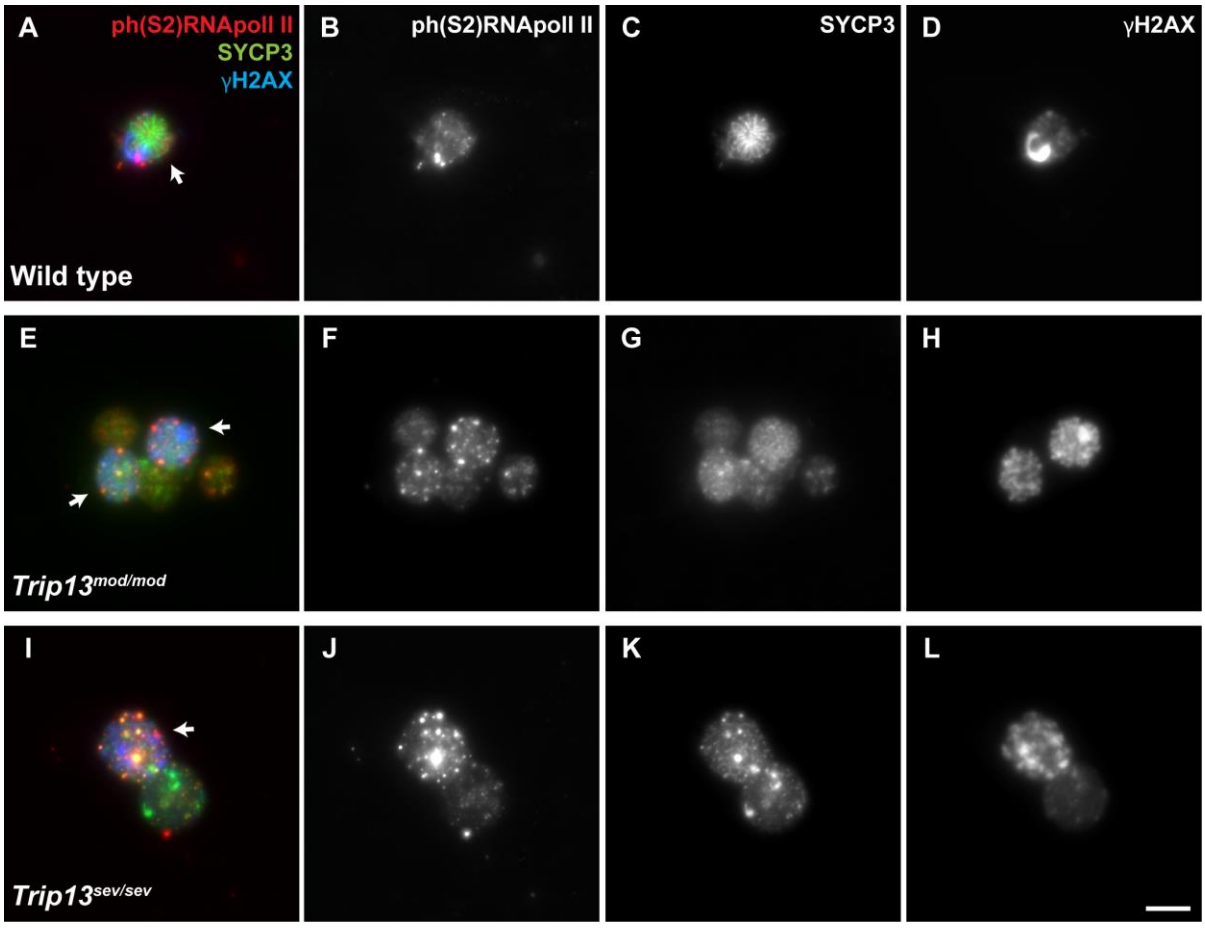

Figure 4.19. Phosphorylated(S2)-RNA polymerase II in TRIP13-deficient zygotene spermatocytes. Representative zygotene spermatocytes (arrows) from (A-D) wild type mice, (E-H) *Trip13*$^{mod/mod}$ and (I-L) *Trip13*$^{sev/sev}$ stained against phosphorylated (S2) RNA polymerase II (red), SYCP3 (green) and γH2AX (blue). Sum projection of stack images is shown. Scale bar in L represents 10 μm and applies to all panels.

The RNApol II, together with other factors, forms a functional holoenzyme required for transcription (Myer and Young 1998). The largest RNApol II subunit contains a carboxy-terminal repeat domain (CTD) with the consensus domain sequence YSPTSPS. The phosphorylation of the CDT determines which factors are assembled and controls the progression of transcription. Phosphorylation occurs principally on Serine2 and Serine5 of the repeats (Phatnani and Greenleaf 2006). After initiation, phosphorylation of Serine2 promotes elongation and at termination phosphatases allow RNApol II to be recruited to another initiation complex (Moorhead et al. 2007).

We observed that in *Trip13* mutants phospho(S2)-RNApol II staining formed bigger clumps than in wild type spermatocytes, which was more evident in zygotene stage (see Fig. 4.19F,J). Quantification of the phospho(S2)-RNA pol II intensity revealed that there was a significant increase of the signal in *Trip13*$^{mod/mod}$ mutants versus the wild type at leptonema stage (P=0.0201, T test; Fig. 4.20A). Remarkably, as it occurred in the EU analysis, this increase was more evident at zygotene stage, where we found a significant increase in *Trip13*$^{mod/mod}$ and *Trip13*$^{sev/sev}$ in comparison with the wild type (P=0.0435 and P=0.0042 respectively, T test; Fig. 4.20B). Therefore, these results suggest that transcriptional activity is increased in early prophase stages of *Trip13* mutants.

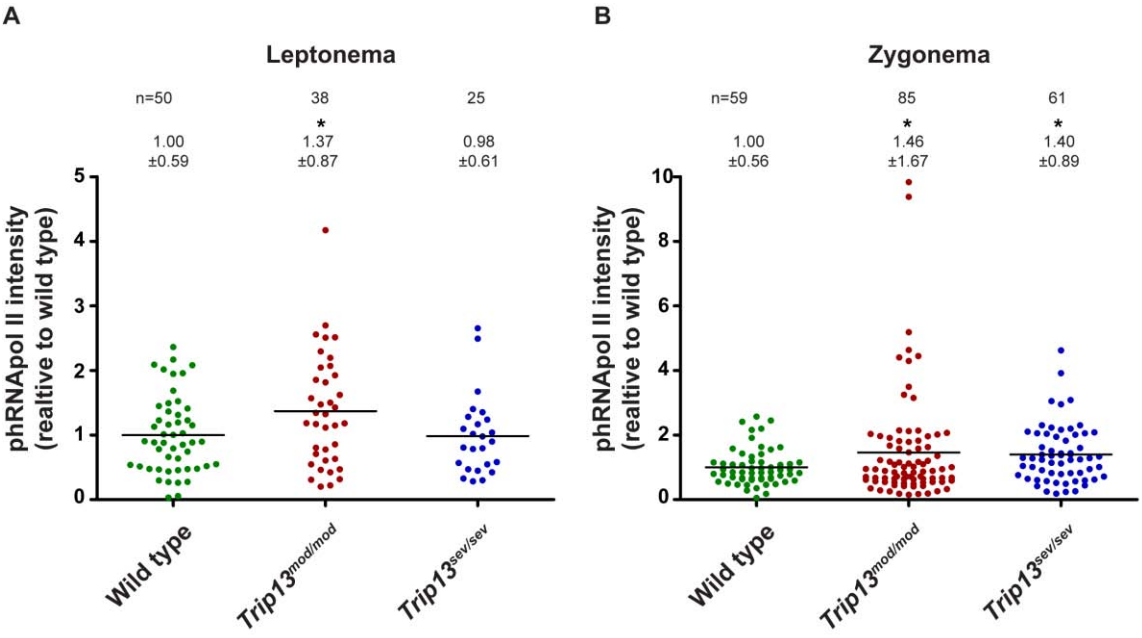

Figure 4.20. Phospho (S2)-RNA polymerase II intensity quantification in *Trip13* mutants. (A-B) Quantification of (phospho S2) RNA polymerase II intensity in leptotene-stage (A) and zygotene-stage (B) spermatocytes of the indicated genotypes relative to the wild type. Horizontal lines represent means. Means±SD and the number of counted cells (n) are indicated above the graph. Above, (*) indicates significantly different relative to the wild type.

4.3.2 Specific RNA expression analysis in *Trip13* mutants: RNA sequencing

Based on our preceding results, we aimed to compare global gene expression in wild type and *Trip13* mutant spermatocytes. Since our previous attempts at purifying spermatocytes by FACS-sorting technique had failed (see section 4.1.2), we decided to use whole testis from juvenile control and *Trip13*$^{mod/mod}$ mice. The advantage of using juvenile mice relies in the fact that they present a first synchronous meiotic wave and that the proportion of somatic and germ cell population remains equivalent between mutants and control samples. For this study we used 14dpp mice in order to compare the most equivalent samples so that *Trip13*$^{mod/mod}$ mutants were analyzed before they experienced the activation of the recombination-dependent arrest. The proportion of cell types remained similar, since 13.1% of wild type cells and 14.3% of *Trip13* mutants cells in the testis were spermatocytes. We corroborated by TUNEL analysis that between 13 and 16 dpp *Trip13*$^{mod/mod}$ mutants present the same apoptosis levels as wild type littermates (at 16 dpp starts to appear a slight significant increase of apoptotic cells in mutants, P=0.0497, T test; Fig. 4.21), suggesting that the recombination-dependent arrest is not yet implemented.

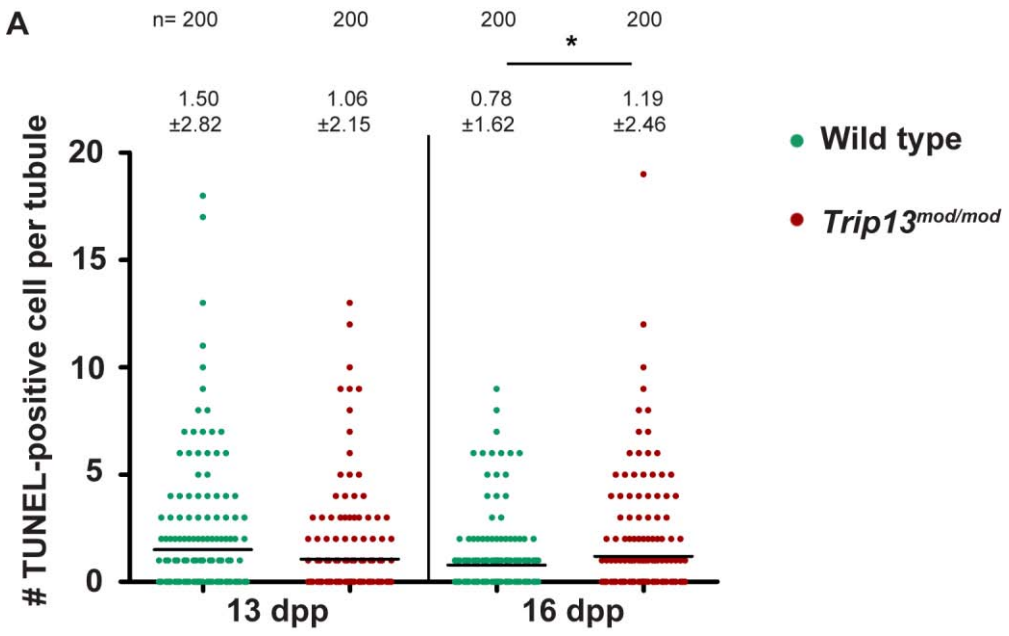

Figure 4.21. Apoptosis in juvenile *Trip13*$^{mod/mod}$ testes. (A) Quantification of the number of TUNEL-positive cells per tubule of juvenile *Trip13*$^{mod/mod}$ and wild type mouse testes at 13 dpp and 16 dpp. Horizontal lines represent the mean, which is indicated over the plot (Mean±SD). N shows the number of tubules counted per genotype. (*) indicates significantly different relative to the wild type.

RNA samples were sequenced at CNAG facility and we obtained list of differential expressed genes between the *Trip13*$^{mod/mod}$ mutants and the wild type. From these genes, we only selected the most significant ones that presented at least a FDR of 0.05 (table in Annex section). The FDR value (false discovery rate) of a test is the expected proportion of false positives among the set of the declared significant results, therefore FDR value of 0.05 implies that we accept that 5% of the results that were found to be statistically significant will be false positives.

We found 221 genes that were overexpressed in *Trip13* mutant and 462 genes that were overexpressed in the wild type. In order to validate the RNA sequencing results we performed quantitative Real-time PCR analysis for three genes overexpressed in *Trip13* mutant (*Xaf1*, *Tktl1* and *Zfy2*, Fig. 4.22A) and three genes overexpressed in wild type samples (*Atp8b3*, *Qrich2* and *Trip13*, Fig. 4.22B). The expression levels profile obtained for the six genes corroborated the results previously observed by RNA sequencing.

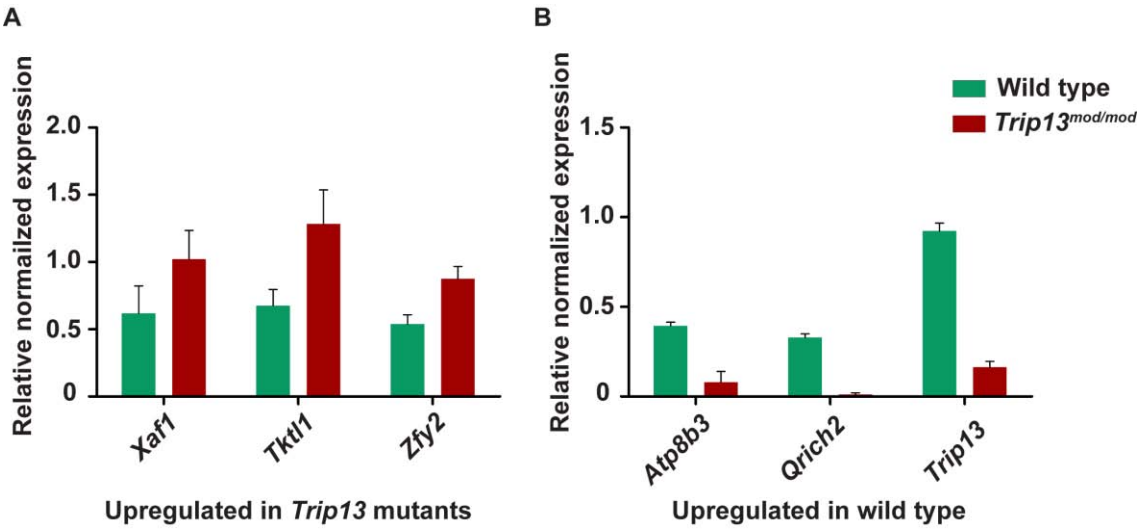

Figure 4.22. RNA-sequencing validation by Real-time PCR. (A) Graph bar represents the relative normalized expression (to housekeeping gene *Hmbs*) in the wild type (green) and *Trip13*$^{mod/mod}$ (red) of (A) *Xaf1*, *Tktl1* and *Zfy2* (overexpressed genes in *Trip13* mutants) and (B) *Atp8b3*, *Qrich2* and *Trip13* (overexpressed genes in the wild type). Error bars represent SD.

The overexpressed genes were similarly distributed among the autosomes in both *Trip13* mutant and wild type, indicating that there is a general deregulation. However, we interestingly found that 64.3% of the overexpressed genes in *Trip13* mutant corresponded to genes located at the sex chromosomes (135 X-linked genes and 7 Y-linked genes), while none of the overexpressed genes in the wild type belonged to the sex chromosomes (Fig. 4.23). These results would corroborate our findings that TRIP13 is required to correctly silence the sexual chromosomes by MSCI.

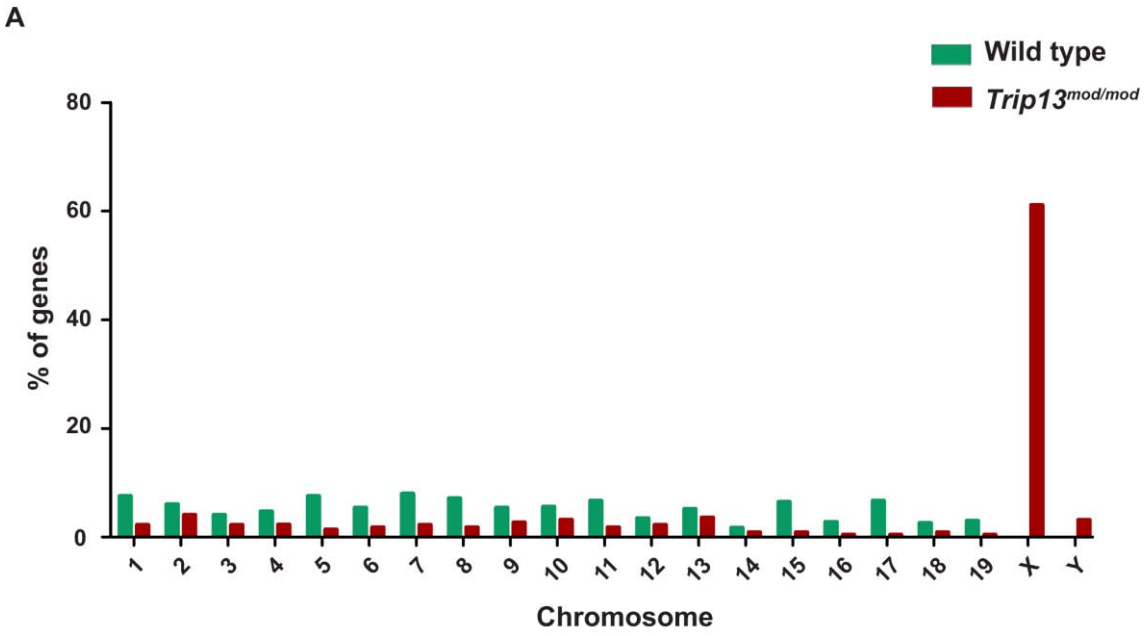

Figure 4.23. Differentially expressed genes for each chromosome. (A) Graph bar represents the percentage of overexpressed genes in the wild type (green) and *Trip13*$^{mod/mod}$ (red) for each chromosome. Note that most overexpressed genes in *Trip13*$^{mod/mod}$ testes correspond to chromosome X, while no sex chromosomes are overexpressed in the wild type.

In order to gain more information about what kind of genes were misregulated in *Trip13* mutants, we used Margolin et al. classification where they subdivided all genes expressed during spermatogenesis into five clusters accordingly to which stage they were expressed. Cluster A: primitive type A spermatogonia and somatic cells (Sertoli, Leydig, myoid cells); B: type A and B spermatogonia, pre-leptotene and leptotene stage spermatocytes; C: zygotene stage spermatocytes; D: spermatocytes at pachynema and E: secondary spermatocytes, round and condensing spermatids (Margolin et al. 2014). We matched our genes according to this cluster classification and analyzed the percentage of the misregulated genes that belonged to each cluster (note that 31.0% of all genes did not enter to the cluster classification). For the genes that were overexpressed in *Trip13* mutant samples, 21.0% were in cluster A, 54.8% belonged to cluster B, 9.7% to cluster C, 4.0% in cluster D and 10.5% were from cluster E (97 genes were not matched into any cluster) (Fig. 4.24A). Therefore, we observed that the majority of the overexpressed genes belonged to cluster B, which mainly corresponds to spermatogonia A and B types, pre-leptotene and leptotene expressed genes. These results could infer that either these "pre-meiotic and early meiotic genes are more expressed in early prophase stages of *Trip13* mutant spermatocytes or it could also be an effect of having a different percentage of spermatocytes at every stage compared with the wild type.

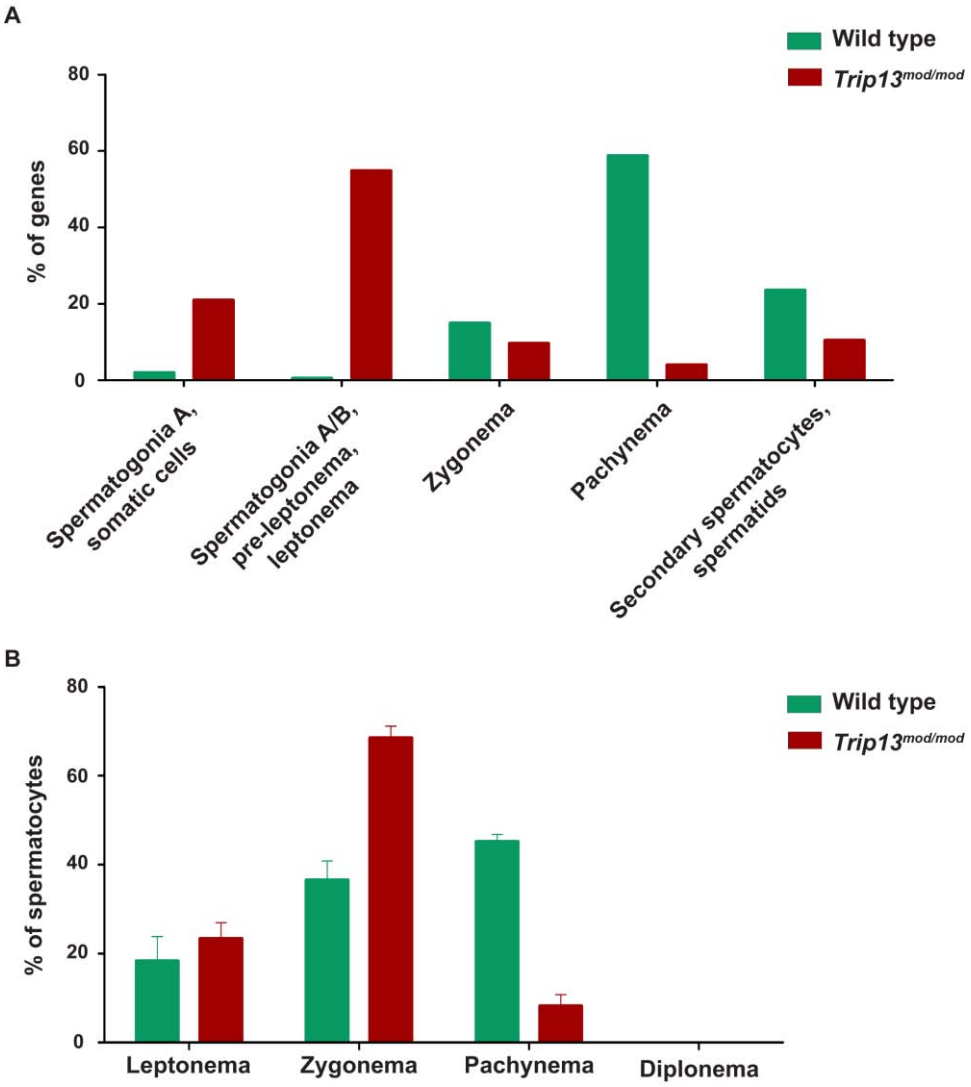

Figure 4.24. Differentially expressed genes classified according to the clusters defined in Margolin et al. (2014). (A) Graph bar represents the percentage of wild type (green) and *Trip13*$^{mod/mod}$ (red) overexpressed genes corresponding to each cluster (correlated to specific cell type). Note that most overexpressed genes from *Trip13*$^{mod/mod}$ correspond to genes normally expressed in spermatogonia, pre-leptonema and leptonema cell type. (B) Graph bar showing the percentage of cells corresponding to each stage found in spermatocyte spreads from the samples used for obtaining the RNAseq data. Error bars represent SD.

In fact, we observed that *Trip13*$^{mod/mod}$ spermatocytes progressed slower through meiosis than wild type littermates. Whereas 14 dpp wild type mice presented 45.2% of spermatocytes at early pachynema, *Trip13* mutants presented only 8.2% of pachytene-stage spermatocytes (P<0.0001, T test) but they had significantly more zygotene–stage spermatocytes (68.5% vs. 36.5% in the wild type, P=0.0004, T test). However, the percentage of leptotene-stage cells was not significantly different between *Trip13* mutants (23.33%) and the wild type (18.33%, P=0.2579, T test) (Fig. 4.24B). Therefore, if we take into account the similar percentage of leptotene-stage cells and spermatocytes (with no apparent reduction of spermatogonial cells), our results taken together show that *Trip13*

mutant spermatocytes express more "pre-meiotic/leptonema cluster genes". Thus, despite the limitations of RNA-sequencing technique and using whole juvenile mice testis, these results imply that *Trip13* mutant testes presented a higher expression of genes expressed in spermatogonia, pre-leptotene and leptotene stages, than the wild type, suggesting that TRIP13 protein is required to properly turn off the expression of this genes at the onset of meiosis.

Regarding overexpressed genes in the wild type samples that matched into a cluster, they classified as follow: 2.02% in cluster A, only 0.58% belonged to cluster B, 14.99% were from cluster C, the 58.79% corresponded to cluster D and 23.63% to cluster E (there were 115 unmatched genes) (Fig. 4.24A). Therefore, the majority of the overexpressed genes in wild type samples belonged to cluster D (which corresponds to pachytene spermatocytes) and some fewer to cluster E (accounting for secondary spermatocytes, round and condensing spermatids). Then, the overexpressed genes observed in wild type spermatocytes that by majority belong to cluster D (pachytene genes) might be a consequence of the four times higher number of pachytene-stage cells present in wild type testes as compared to *Trip13* mutant testes.

To obtain more information, we searched the gene ontology information corresponding to the overexpressed deregulated genes in *Trip13* mutant and wild type testis. Overexpressed genes in both wild type and *Trip13* mutant testes where associated with similar Gene Ontology terms, like development, metabolism, cell cycle, gametogenesis and meiosis; suggesting they had similar functions. Interestingly, overexpressed genes in *Trip13* mutant samples, but not those of the wild type samples, also associated with functions related with transcription and RNA metabolism (see Table 4.3).

In particular, the genes that highlighted transcription and RNA gene ontology were: regulation of transcription (*Nkap*, *Foxa2*, *Scml2*, *Irx2*, *Taf9b*, *Rhox2d*, *Hoxd13*, *Dmrta2*, *Rhox2f*, *Rhox2g*, *Taf7l*, *Zfy2*, *Zfy1*, *Tsc22d3*, *Gata3*, *Foxd2*, *Fgf2*, *Alx3*, *Nkrf*, *Mbtps2*, *Pcbd1*, *Rhox1*, *Tbx4*, *Zfx*, *Suv39h1*, *Esx1*, *Abcg4*, *Cdkn1c*, *Ebf3*, *Rhox13*, *Pbx3*) and for RNA transport and localization (*Fmr1*, *Nxf2*, *Nxt2* genes). Most of the genes involved in transcription act as transcription activators (e.g. *Nkap*, *Irx2*, *Taf9b, Rhox2d/f/g, Hoxd13*, *Dmrta2*, *Zfy1, Zfy2*, *Gata3*, *Foxd2*, *Fgf2, Alx3*, *Pcbd1*, *Rhox1*, *Tbx4*, *Zfx*, *Ebf3, Rhox13, Pbx3*). Some participate in both activation and repression (e.g. *Taf7l*) and only a few act as transcriptional repressors (e.g. *Scml2*, *Tsc22d3*, *Nkrf, Esx1).* Regarding genes involved in RNA transport and localization (e.g. *Fmr1, Nxf2* and *Nxt2*), they are principally involved in nuclear RNA export to the cytoplasm (Table 4.4). Therefore, our results obtained from

RNA sequencing show that *Trip13* mutants overexpressed genes related with transcription and RNA metabolism, which goes along with our hypothesis of TRIP13 being required to switch off transcription at the onset of meiotic prophase.

Table 4.3 Go terms list for differential expressed genes

GO terms for overexpressed genes in *Trip13*$^{mod/mod}$	GO terms for overexpressed genes in Wild type
RNA, transcription, proteins	**Gametogenesis**
regulation of transcription, DNA-dependent	spermatogenesis
regulation of RNA metabolic process	male gamete generation
regulation of transcription	sexual reproduction
RNA localization	gamete generation
establishment of RNA localization	multicellular organism reproduction
mRNA transport	reproductive process in a multicellular organism
RNA transport	reproductive cellular process
nucleic acid transport	germ cell development
	spermatid development
Gametogenesis, meiosis and cell division	spermatid differentiation
sexual reproduction	
Spermatogenesis	**Meiosis and cell division**
male gamete generation	meiosis
reciprocal meiotic recombination	female meiosis I
response to X-ray	M phase of meiotic cell cycle
cell cycle process	M phase
M phase	meiotic cell cycle
	cell cycle
Development	cell cycle process
regulation of cell development	cell cycle phase
regulation of nervous system development	response to tumor cell
regulation of neuron differentiation	anti-apoptosis
regulation of neurogenesis	cell recognition
embryonic morphogenesis	
embryonic limb morphogenesis	**Development**
embryonic appendage morphogenesis	reproductive developmental process
appendage morphogenesis	
appendage development	**Metabolism**
epithelium development	glycolysis
vasculature development	hexose catabolic process
blood vessel development	glucose catabolic process
neuron differentiation	monosaccharide catabolic process
neuron development	cellular carbohydrate catabolic process
reproductive developmental process	glucose metabolic process
development of primary sexual characteristics	alcohol catabolic process
male sex differentiation	generation of precursor metabolites and energy
sex differentiation	

respiratory system development reproductive structure development lung development respiratory tube development limb morphogenesis limb development **Metabolism** catecholamine metabolic process catechol metabolic process phenol metabolic process diol metabolic process regulation of cholesterol biosynthetic process oxidation reduction nitrogen compound biosynthetic process **Proteins** protein homotetramerization	prostanoid metabolic process prostaglandin metabolic process hexose metabolic process carbohydrate catabolic process monosaccharide metabolic process glutathione metabolic process immunoglobulin mediated immune response organophosphate metabolic process piRNA metabolic process lymphocyte mediated immunity icosanoid metabolic process fatty acid metabolic process unsaturated fatty acid metabolic process peptide metabolic process cellular amino acid derivative metabolic process coenzyme metabolic process glycerol-3-phosphate metabolic process **Immune system** B cell mediated immunity tumor necrosis factor-mediated signaling pathway adaptive immune response based on somatic recombination of immune receptors built from immunoglobulin superfamily domains adaptive immune response leukocyte mediated immunity **Proteins** protein folding proteolysis

Table 4.4 Gene function of transcriptional related genes

GENE	FUNCTION
Abcg4	ATP-binding cassette transporter, transport molecules across membranes
Alx3	homeobox DNA-binding that participates in transcriptional regulation in differentiation and development
Cdkn1c	encodes $p57^{Kip2}$ protein, which inhibits several G1 cyclin/Cdk complexes ((cyclin E-CDK2, cyclin D2-CDK4, and cyclin A-CDK2) and also the mitotic cyclin B-CDC2, negatively regulating cell cycle progression
Dmrta2	transcription factor probably involved in sexual development
Ebf3	transcription factor that activates genes involved in cell cycle arrest and apoptosis

GENE	FUNCTION
Esx1	dual protein ESXR1-N acts as a repressor, ESXR1-C inhibits cyclin turnover; during spermatogenesis probably coordinates cell cycle and transcription, it inhibits degradation of ubiquitinated cyclin A and cyclin B1 (to arrest M-phase)
Fgf2	fibroblast growth factor implicated in diverse biological processes with important roles in cell division, cell survival, differentiation and migration
Fmr1	binds to RNA and is associated with polysomes, component of a translational repression, probably involved in mRNA traffic from the nucleus to the cytoplasm
Foxa2	transcriptional activator for metabolism regulators
Foxd2	transcription factor involved in embryogenesis
Gata3	GATA-binding transcription factor important for endothelial and T-cell development
Hoxd13	transcription factor of homeobox family that participates in morphogenesis
Irx2	transcription factor that is important for pattern formation in embryos
Mbtps2	encodes a metalloprotease essential for development
Nkap	participates in the activation of NF-kappa B transcription factor
Nkrf	mediates transcriptional repression of NF-kappa B genes
Nxf2	protein involved in nuclear RNA export from the nucleus to the cytoplasm
Nxt2	nuclear transport factor, with a role in nuclear mRNA export
Pbx3	is a transcriptional activator
Pcbd1	regulates dimerization of HNF1A homeodomain protein and enhances its activity
Rhox1	contains an homeodomain, transcriptional regulation of developmental processes
Rhox13	transcription factor probably involved in reproduction roles
Rhox2d/f/g	DNA binding protein, transcriptional regulation of developmental processes
Suv39h1	encodes for a histone methyltransferase that tri-methylates lysine 9 of histone H3, resulting in transcriptional signaling
Taf9b	participates in basal transcription as coactivator and facilitating RNA polymerase II assembly for transcription initiation
Tbx4	transcription factor involved in developmental and differentiation processes
Tsc22d3	inhibits FOXOA3A to downregulate pro-apoptotic factors
Zfx	probable transcriptional activator, important for stem cell self-renewal
Zfy1/Zfy2	zinc finger transcription factors important for spermatogenesis

DISCUSSION

5. DISCUSSION

Meiotic prophase progression requires coordination of several processes, such as recombination, synapsis and chromosome segregation. Germ cells undergo dramatic reorganizations, starting with induced programmed DSBs throughout the genome. These SPO11-generated DSBs are repaired through homologous recombination, which promote proper homologous pairing, synapsis and eventually gives rise to CO formation (the physical linkage that ensures correct chromosome segregation). In the presence of deleterious events, such as unrepaired DSBs or asynapsis, meiotic surveillance mechanisms control prophase progression and if necessary eliminate defective meiocytes by activating programmed cell death. By avoiding genomic instability, surveillance mechanisms guarantee successful genomic transmission to the progeny. In the recent years, several studies have highlighted the role of the DNA damage response pathway in the meiotic checkpoint network in several organisms (MacQueen and Hochwagen 2011). With this work we aimed to contribute to the understanding of the meiotic surveillance mechanism existent in mouse meiosis.

5.1 Study the components that activate the pachytene arrest occurring in mammalian spermatocytes

One of the first objectives of this work was to determine if we could detect by the use of biochemical tools the activation of the proteins that we had find out to participate in the activation of the recombination-dependent pachytene arrest thanks to a genetic approach. Our first attempt consisted in analyzing the activation of several candidates from the DDR pathway in mutant samples by using Western blot approach from adult mice whole testis extracts. If we could have observed the activation of CHK2 protein (Pacheco et al. 2015) by Western blot and specifically in recombination-defective mutants, it would have validated this technique in order discover new proteins involved in the process. Unfortunately, we did not obtain conclusive results, possibly due to the intrinsic limitations of comparing adult wild type testis with arrested testis, where the percentages of the different germ cell populations extremely differ. For instance, for three of the proteins analyzed (CHK2, E2F1 and BAX), we observed increased protein levels in both *Trip13* and *Spo11* mutants. These findings are against the current knowledge which establishes that independent mechanisms activate the recombination-dependent or the

sex body-deficient arrest (Pacheco et al. 2015). The activation of the DDR and pro-apoptotic proteins that we observed even in wild type and *Spo11* mutants, probably comes from of other cell types than spermatocytes. Adult testis contain heterogeneous cell type populations that also activate the DDR. For instance, spermatogonial cells replicate their DNA, which implies they are subjected to replicative stress and also activates the DDR. Besides, it is known that the number of spermatogonial cells in the testis is auto-regulated, in part, by apoptosis (de Rooij and Grootegoed 1998).

Next, to overcome the limitations derived from working with whole testis samples, we decided to obtain highly enriched spermatocyte populations by using cell sorting techniques, in order to perform Western blot or sequencing. However, by using standardized protocols based on fluorescent labeling with Hoechst 33342 and Propidium Iodide (Bastos et al. 2005; Getun et al. 2011), we were not able to establish defined gates that could provide highly enriched cell type populations from either adult or juvenile testis consistently. Our principal interest was to analyze pachytene-stage spermatocytes, however using gates similar to the previously published ones (Bastos et al. 2005; Getun et al. 2011; Cole et al. 2014), we obtained populations of spermatocyte with very variable proportions of pachytene-stage cells, ranging from 15 to 50% of the cells. We also tried to sort the first wave of meiosis in juvenile mice, but we encountered the same problem of gating mixed cell type populations.

5.2 P53 role in meiosis

Due to the technical limitation reported above, we decided to use the classical genetic approach and study the pachytene arrest by using mutant mice and analyzing their meiotic phenotypes. Since it has been recently seen that the DDR pathway participates in meiotic checkpoints, and that the MRE11 complex-ATM-CHK2 pathway participates in the recombination dependent arrest on mouse spermatocytes, we focused on the study of p53 family as a possible downstream effector of this pachytene block. Other previous reports support p53 role in mouse meiosis, as p53 is activated in response to SPO11-induced DSBs (Lu et al. 2010) and $Arf^{-/-}$ spermatocytes experience a p53-dependent apoptosis (Churchman et al. 2011). However, although some studies have tried to evaluate a possible role of p53 in spermatogenesis, a clear role of p53 in mouse meiosis remained ambiguous. Thus, first of all we performed a detailed analysis of *p53* mutant meiotic phenotype.

p53 mutant mice are viable and develop normally, nevertheless they are highly prone to develop tumor malignancy already at the age of six months (Donehower et al. 1992; Jacks et al. 1994). *p53* null mice are reported to be fertile, but present reduced litter size due to embryonic lethally of a fraction of *p53* null embryos. These embryos are mostly females and display neural tube closure defects and exencephaly (Sah et al. 1995; Armstrong et al. 1995; Gersten and Kemp 1997). We corroborated this observation, as we only obtained very few p53 null females in our colony. Apart from the previously mentioned results, the interest of analyzing p53 role during meiotic prophase also came from the observation that p53 mRNA and protein are present in primary spermatocytes and the highest levels are observed at pachynema (Sjöblom and Lähdetie 1996; Almon et al. 1993; Schwartz et al. 1993). Additionally, p53 expression was seen to be enhanced after irradiation in spermatocytes and spermatogonia, suggesting a role in DNA damage response (Sjöblom and Lähdetie 1996; Beumer et al. 1998). Moreover, multinucleated degenerative giant-cells were detected in testis histology, presumably caused by impaired meiotic divisions. These giant cells were only observed in some mouse strains, like in *p53* null mouse 129/Sv strain; but they were not observed on C57BL/6 x 129/Sv mixed genetic background (Rotter et al. 1993). Our results are consistent with this observation, since we do not observe any multinucleated cells in our samples (also coming from a mixed background) and report normal appearance of *p53* mutant seminiferous tubules.

Since some reports have tried to specifically answer if p53 participates in DNA repair or recombination in mouse spermatogenesis, but results were not conclusive, we decided to perform a more exhaustive analysis. For instance, in one study they found increased number of γH2AX foci in *p53*$^{-/-}$ pachytene spermatocytes and absence of sex body in some pachynema cells (in a CBA background). They also reported that Caspase-3 apoptosis was slightly increased in *p53*$^{-/-}$ mouse seminiferous tubules, accounting for spermatogonia or secondary spermatocytes at stage XII (Paul et al. 2007). In another work, recombination frequency analysis using four polymorphic microsatellites markers revealed no significant difference between p53 mutants or wild type offspring (Gersten and Kemp 1997).

In our *p53* mutants we also observed a slight increase in apoptotic cells, and we similarly observed that the TUNEL-positive cells we detected were mainly somatic cells. These results suggest that p53 might be involved in DSB repair of testis somatic cells, and that the observed apoptosis is p53-independent. We did not observe any synapsis defects in *p53* mutants, and no sex body defects were detected. Regarding meiotic prophase progression, we could only observe that in absence of *p53*, there was an acceleration of

prophase progression in the first meiotic wave, suggesting a role for p53 in checkpoint activation. Interestingly, similar results were found for *p53* mutant oocytes, which presented faster meiotic progression (Ghafari et al. 2009). Regarding meiotic recombination, analysis of DSB repair using γH2AX foci as recombination markers did not reveal any difference between the wild type and mutants, in the analyzed stages (early pachynema, mid/late pachynema and diplonema). We suggest that the fact that we obtained different results than the previously reported (Paul et al. 2007) might be a consequence of using H1t to differentiate early from late pachynema in our case, or may account for the usage of different mouse genetic backgrounds. We also analyzed the number of COs, assed by MLH1 marker, and in this case we observed a slight but significant increase in CO formation in *p53*$^{-/-}$ spermatocytes. This result suggests that p53 may be participating in meiotic recombination in some subtle manner, possibly by affecting CO interference. However, since the increase only represents one extra CO per spermatocyte, we speculate that this difference might not have a relevant biological effect in *p53*$^{-/-}$ recombination frequency, as reported before and corroborated by the fact that *p53* mutants are fertile (Gersten and Kemp 1997). Yet interestingly, studies of p53 mutation in other organisms also suggested a possible role of p53 in CO control. *C. elegans* CEP-1 (p53 homologue) was found to be necessary for proper X chromosome segregation during meiosis (Derry et al. 2001), and female flies lacking *p53* although being fertile they presented a reduced crossover rate (Lu et al. 2010). More recently, it has been proposed that CEP-1, in collaboration with Him-5, participates in the DSB repair pathway choice (Mateo et al. 2016). Thus, the fact that there seems to be a conserved role of p53 in modulating the recombination outcome supports our results. Overall, the observed participation of p53 in regulating meiotic progression and recombination suggests a possible role of p53 in coordinating these events.

As mentioned before, p53 expression was seen to be enhanced after irradiation in spermatocytes suggesting a role in DNA damage response (Sjöblom and Lähdetie 1996; Beumer et al. 1998). Moreover, the physiological activation of p53 in prophase spermatocytes was found to be SPO11-dependent (Lu et al. 2010). Similar results have been observed in other organisms, suggesting a conserved role of p53 in responding to DNA damage in the germinal line. For instance, *Drosophila* transgenic GFP-p53 expression was observed in female oocytes in a Spo11-dependent manner (*Drosophila* males do not present meiotic recombination) (Lu et al. 2010). *C. elegans* CEP-1 was found to be required to activate irradiation -induced apoptosis of germ cells (although not in somatic cells), but did not activate cell cycle arrest (Derry et al. 2001). This observation was similar to what it

was found is *Drosophila* cells, where p53 homolog activates DNA-damaged induced apoptosis, but not cell cycle arrest (Ollmann et al. 2000). The reason why CEP-1/p53 only induces germ cell apoptosis can be explained as *C. elegans* somatic cells have a determinate number of possible cell divisions and cannot be replaced. Therefore, while somatic apoptosis would be extremely deleterious for the animal itself; damaged germ cells that were not eliminated by apoptosis would give rise to defective offspring. This logic supports the first role of p53 as a germline protector, and later evolving as a tumor suppressor in somatic cells (Derry et al. 2001).

5.3 P53 family members p53 and TAp63 participate in the recombination-dependent arrest

From all these evidences suggesting a role of p53 in detecting DNA damage in germ cells, in this study we provide new insights about the functionality of p53 family members in mouse meiotic surveillance mechanisms. One of the main goals of this thesis was to determine if p53, or any member of the p53 family, participated in the activation of the recombination-dependent arrest. Deficient recombination and/or sex body formation drives mammalian spermatocytes to arrest at pachynema, which triggers programmed cell death resulting in infertility. We previously reported that the MRE11 complex-ATM-CHK2 signaling pathway participates in the activation of the recombination-dependent arrest in mouse spermatocytes (Pacheco et al. 2015). Moreover, others described that in females, the activation of CHK2, p53 and TAp63 is required to eliminate mammalian oocytes with persistent unrepaired DSBs (Bolcun-Filas et al. 2014).

In order to study the recombination-dependent arrest, we used a hypomorphic mutation of *Trip13* gene as our recombination-defective model (Li et al. 2007; Roig et al. 2010). The main interest we had in using *Trip13* mutants was that although accumulating unrepaired DSBs at pachynema, *Trip13*$^{mod/mod}$ spermatocytes are able to complete homologous chromosome synapsis, something very unusual. Due to the strong connection between meiotic recombination and homologous chromosome synapsis (see Introduction for more details), most recombination defective mutants, such as *Dmc1*$^{-/-}$ or *Msh4*$^{-/-}$, do not reach full synapsis of their autosomes. Then, failure to complete homologous chromosome synapsis impairs MSCI (Burgoyne et al. 2009), which activates the sex body-deficient arrest. Therefore, most recombination defective mutants present defects that activate the recombination-defective and the sex body-deficient arrest. The fact that *Trip13* mutants

completed synapsis and presented what looked like a normal sex body (Li et al. 2007; Roig et al. 2010), made the *Trip13*$^{mod/mod}$ mice the perfect model to study the recombination-dependent arrest. Therefore, in order to determine if any of the p53 family members participate in the activation of the recombination-dependent arrest, we breed p53 family members mutation in combination of *Trip13* mutation, with the aim of detecting if p53, TAp63 or p73 mutations could rescue the pachytene arrest observed in *Trip13* mutants. If we had deactivated the recombination dependent-arrest (where spermatocytes apoptose at early pachynema), we expected to have more spermatocytes reaching late pachytene stage (accumulating histone H1t). Moreover, the spermatocytes that bypassed the arrest should present a higher number of unrepaired DSBs. Firstly, by analyzing the percentage of spermatocytes that accumulated H1t we observed that while *Trip13*$^{mod/mod}$ presents a reduction of H1t-positive cells than controls, *Trip13*$^{mod/mod}$ *p53*$^{-/-}$ and *Trip13*$^{mod/mod}$ *TAp63*$^{-/-}$ presented a similar proportion of H1t-positive cells than wild type testes. Similar results were obtained in *Trip13* mutants also defective for either *Chk2*, *Atm*, Mre11 or NBS1 (Pacheco et al. 2015), which suggests that p53 and TAp63 might be downstream effectors of CHK2. Besides, we observed that before the activation of the arrest, at early pachynema, we observed similar, or even lower, numbers of unrepaired DSBs in double mutants and in *Trip13*$^{mod/mod}$ spermatocytes. Whereas in late pachynema, *Trip13*$^{mod/mod}$ *p53*$^{-/-}$ and *Trip13*$^{mod/mod}$ *TAp63*$^{-/-}$ spermatocytes presented increased accumulation of γH2AX foci compared to single *Trip13* mutant. Furthermore, this increase was still observable at diplonema, so that the influence of bypassing the recombination arrest can be observed at later stages. Contrary to these observations, *Trip13*$^{mod/mod}$ *p73*$^{-/-}$ phenotype was identical to the single *Trip13*$^{mod/mod}$ mutant one, indicating that p73 has no role on the recombination-dependent arrest.

On another side, we analyzed the apoptotic profile of double mutants; since spermatocytes that present recombination failure apoptose at early pachynema (Barchi et al. 2005; Pacheco et al. 2015), bypassing the arrest should reduce the number of cells apoptosing at this stage (before they accumulate H1t). Accordingly to our model, while in p73 double mutant the proportion of apoptotic H1t-negative cells was very high, similar to *Trip13* mutants, the number of H1t-negative apoptotic spermatocytes in p53 and TAp63 double mutants was greatly reduced compared to the single *Trip13* mutant. Therefore, similarly to what was observed in oocytes (Bolcun-Filas et al. 2014), results obtained in this work highlight that p53 and TAp63 also participate in the activation of the recombination-dependent arrest in mouse spermatocytes (see Fig. 5.1 and 5.2). These new findings further support the idea that the recombination-dependent arrest at pachynema

resembles the G2/M checkpoint of somatic cells, using ATM-CHK2-p53/p63 signaling pathway (Burgoyne et al. 2007; Taylor and Stark 2001). Apart, we discarded p73 participation in this arrest. Furthermore, the resemblance in the phenotype between *Trip13* mutants and *Trip13 p73* double mutants, emphasizes the participation of p53 and TAp63 in the activation of the recombination-dependent arrest.

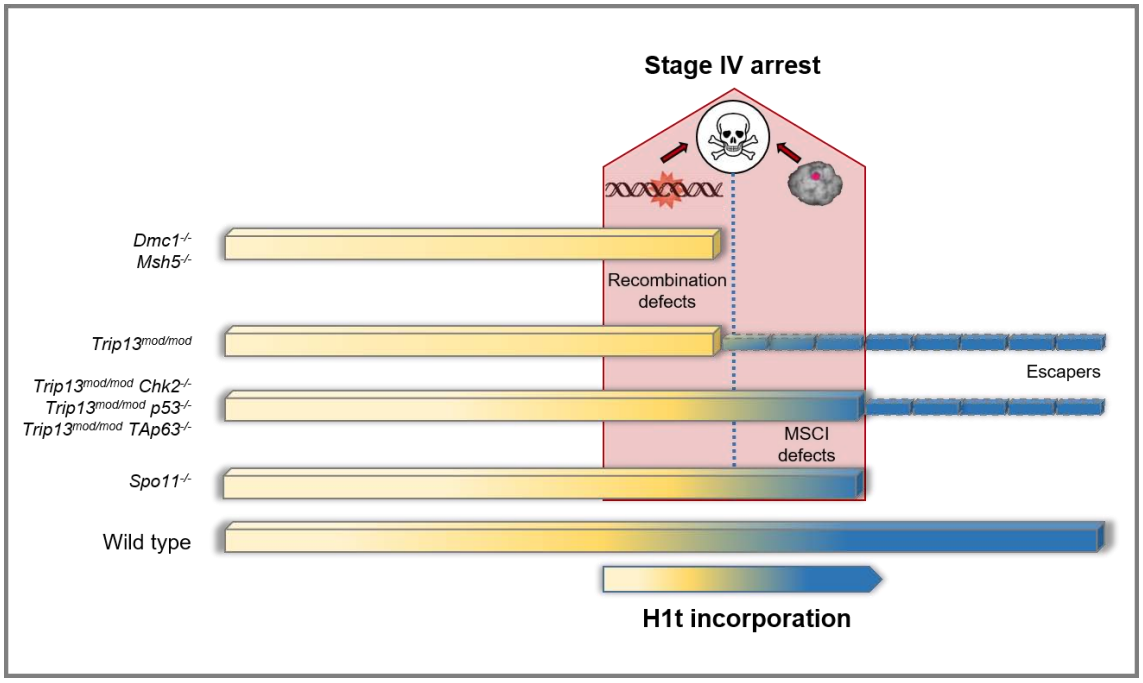

Figure 5.1. Schematic represtation of *Trip13*$^{mod/mod}$ recombination-depednent arrest bypassed by p53 and TAp63 mutation in spermatocytes. Both recombination-dependent and sex body-defiecient arrest result in a block of spermatogensis at pachytene stage (epithelial stage IV arrest). However, they are activated by different mechanisms and their spermatocytes apoptose at different timings. While recombination-defective spermatocytes (e.g. *Dmc1*$^{-/-}$, *Msh5*$^{-/-}$) apoptose at early pachynema (before H1t incorporation), spermatocytes that arrest due to synapsis defects (e.g. *Spo11*$^{-/-}$) apoptose at late pachynema (after accumulating H1t, blue bar). Most *Trip13*$^{mod/mod}$ spermatocytes arrest before incorporating H1t, but still some cells manage to escape this arrest, incorporate H1t and complete meiosis. Note that when in *Trip13*$^{mod/mod}$ mice the recombination-dependent arrest is inactivated mutating *Chk2, p53 or TAp63* (in *Trip13*$^{mod/mod}$ double mutants), most spermatocytes apoptose once they have incorporated H1t into their chromatin. As previously, a subset of cells is able to escape the arrest and complete meiosis.

With these data we shed light on the importance of the p53 family in the pachytene arrest in male mouse meiosis -since previous reports presented contradictory results. A first study observed that deletion of p53 partially rescued the phenotype of mutant spermatocytes that failed to repair DSBs, suggesting the involvement of p53 in the recombination dependent pachytene stage arrest (Barlow et al. 1997b). Nevertheless, two subsequent studies denied these finding. Firstly, another group analyzed the same mutants and could not find any signs of rescue (Ashley et al. 2004). And secondly,

another study reported that p53 ablation had no impact on the meiotic progression of *Sycp3*$^{-/-}$ spermatocytes, that fail to form proper chromosome axes and also accumulate unrepaired DSBs (Yuan et al. 2001). Thus, both studies dismissed the implication of p53 in the so called "pachytene checkpoint". Technical reasons may explain these differences, for instance while the first study used H1t as a marker of meiosis progression (as we have done in this study), the following ones did not. Furthermore, at the time these studies were conducted the existence of two genetically independent mechanisms that trigger pachytene arrest in male mouse was not known (Barchi et al. 2005). This is important since ablation of the recombination-dependent arrest has no impact on the sex body formation surveillance mechanism (Pacheco et al. 2015). Consequently, cytological markers, like H1t, have to be used to accurately account for the time of the arrest.

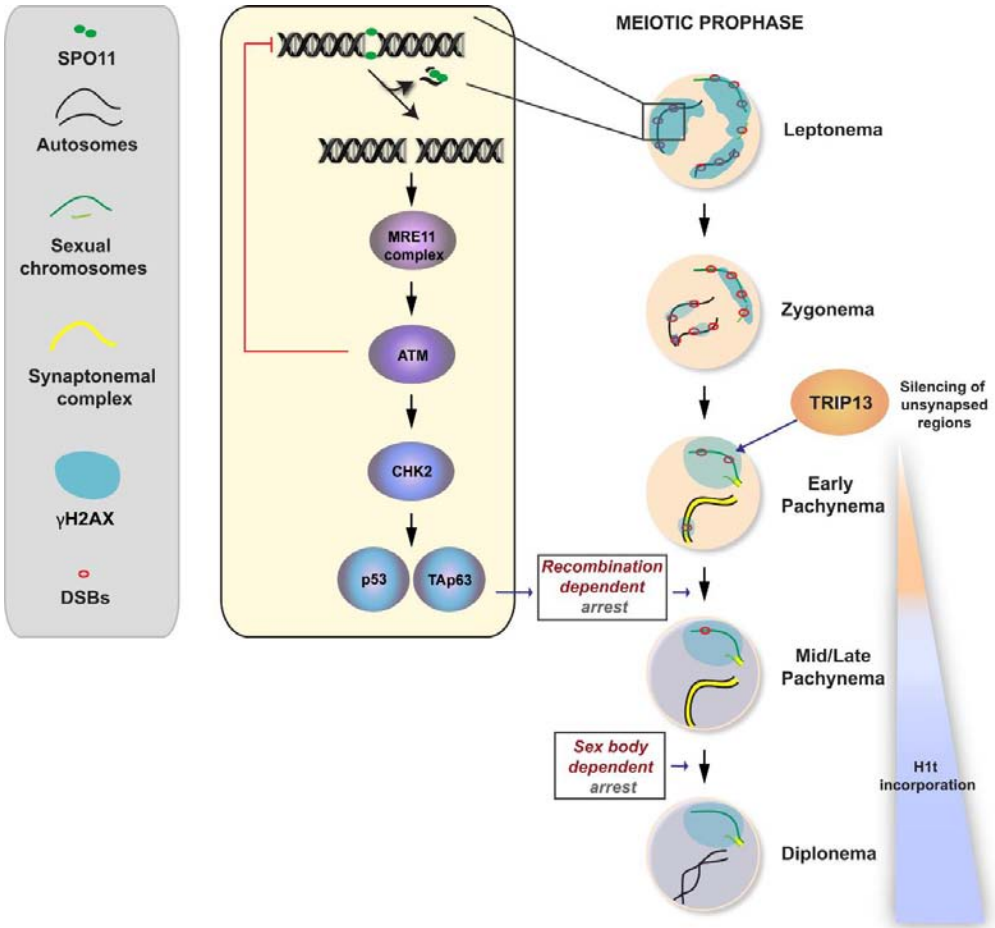

Figure 5.2. Meiotic prophase surveillance mechanisms model in mouse spermatocytes. SPO11-induced DSBs are sensed by MRE11-complex, which activates ATM. ATM participates in a negative feedback loop by inhibiting further DSBs formation. Besides, ATM activates CHK2 kinase and via downstream effectors p53 and TAp63 they control cell cycle by promoting the recombination-dependent arrest. Recombination is coupled with synapsis and sex body formation in spermatocytes. TRIP13 protein necessary for synapsis and recombination progression, but importantly, is also required for silencing the asynapsed sex chromosomes and MSCI implementation, which is essential for post-pachytene progression (sex body-deficient arrest).

Therefore, our data supports that the mammalian meiotic surveillance mechanism uses p53 and TAp63 to activate the recombination-dependent arrest at pachytene stage, participating in the surveillance control of mouse spermatocytes (Fig. 5.2). Both p53 and TAp63 are required to activate the recombination-dependent arrest in the presence of unrepaired deleterious DSBs. Our data seconds the notion that, from an evolutionary point of view, protecting the germ line from DNA damage might be the ancestral function of p53 family, evolving later as tumor suppression guardian.

The fact that *p53* and *TAp63* double mutant spermatocytes phenotype resembles *Trip13*$^{mod/mod}$ *Chk2*$^{-/-}$ (Pacheco et al. 2015), makes us infer that p53 and TAp63 act downstream of CHK2 and that they do not present redundancy in the activation of the recombination-dependent arrest. Furthermore, the observation of a similar phenotype between *p53* and *TAp63* double mutants (with equivalent percentage of cells incorporating H1t and similar number of unrepaired DSBs at mid/late pachynema and diplonema), makes us suggest that p53 and TAp63 are both necessary to properly activate the recombination-dependent arrest. Since both p53 and TAp63 are intimately connected (they can promote transcription of the same genes (Yang et al. 1998) and can associate with each other through direct interaction (Gaiddon et al. 2001)) such complexity could explain why availability of one member can affect the ability of the other to implement an effective arrest. We therefore define that both, p53 and TAp63, protein levels are important to guarantee the proper activation of the recombination-dependent arrest in spermatocytes. This point contrasts with what has been observed in females, where p53 and TAp63 act redundantly. For instance, while *Chk2* mutation completely rescued infertility in *Trip13* mutants, deletion of *p53* only increased mildly the number of oocytes found in *Trip13* mutant. Also, absence of *TAp63* required *p53* heterozygosity in order to mildly revert the arrest observed in *Trip13* mutant oocytes (Bolcun-Filas et al. 2014). All these observations lead to infer that the meiotic recombination-arrest is more robust in females than males, whereas females require alteration of both *p53* and *TAp63* in *Trip13* mutants in order to resemble the stronger rescue phenotype observed in *Trip13*$^{mod/mod}$ *Chk2*$^{-/-}$; in males abolition of either *p53* or *TAp63* is sufficient to bypass the recombination-dependent arrest.

These gender differences may be attributable to the sex dimorphism occurring in mammalian gametogenesis. Mammalian female meiosis differs from male meiosis in several aspects. One of them is that while in the testis, meiosis is a continuous event that starts with sexual maturity and lasts most adulthood, in the ovaries, meiosis starts during fetal development and oocytes arrest at the end of meiotic prophase (around 2 days post-

partum in mouse). These oocytes will not resume meiosis until adulthood. These resting oocytes are also sensitive to DNA damage caused by ionizing radiation (Bolcun-Filas et al. 2014). Importantly, it has been proposed that the same checkpoint mechanism that controls meiotic DSB-repair progression in fetal oocytes could control DNA integrity in the resting oocytes (Bolcun-Filas et al. 2014). Thus, the fact that the recombination-dependent arrest machinery has to control genome integrity for a longer period in resting oocytes may have implemented a stronger female-specific role for p53 and TAp63 in the mechanism that senses DNA damage during meiotic prophase. These findings support the importance of p53 family members in the control of mammalian reproduction (Levine et al. 2011); monitoring the quality and survival of mouse oocytes and spermatocytes.

A remaining question would be to investigate the components activated downstream of p53 and TAp63 in recombination compromised spermatocytes. In somatic cells, after the induction of DNA damage, p53 exerts its function through the transcriptional induction of *p21* (el-Deiry et al. 1994) and pro-apoptotic genes like: *Bax* (Miyashita and Reed 1995), *Puma* (Nakano and Vousden 2001) or *Noxa* (Oda et al. 2000). Remarkably, irradiated oocytes require TAp63 to induce expression of *Puma* and *Noxa*; and irradiated *Puma*$^{-/-}$ and *Puma*$^{-/-}$ *Noxa*$^{-/-}$ mice were protected from oocyte lost (Kerr et al. 2012).Therefore, future studies could be directed to determine if this role of PUMA and NOXA, or other p53 family targets, is also conserved in DNA repair compromised mouse spermatocytes.

Furthermore, we corroborated here that p53 family members are not involved in the activation of the sex body-deficient dependent arrest. Since *Trip13* $^{mod/mod}$ *p53*$^{-/-}$, *Trip13* $^{mod/mod}$ *TAp63*$^{-/-}$, *Trip13*$^{mod/mod}$ *p73*$^{-/-}$ *and Spo11*$^{-/-}$ *TAp63*$^{-/-}$ double mutants still present arrest at epithelial stage IV, these results show that p53 family members are dispensable for the activation of the sex body-deficient arrest. Moreover, these findings confirm our previous results showing that the recombination-dependent and the sex body-deficient arrest are two genetically separable mechanisms that respond to different offenses and are implemented by different protein pathways (Pacheco et al. 2015).

5.4 TRIP13's new role in meiotic silencing

5.4.1 TRIP13 is required to implement the meiotic sex chromosomes inactivation

Although deactivating the recombination-dependent arrest in the *Trip13*$^{mod/mod}$ *p53*$^{-/-}$, *Trip13*$^{mod/mod}$ *TAp63*$^{-/-}$ and *Trip13*$^{mod/mod}$ *Chk2*$^{-/-}$ (Pacheco et al. 2015), we found that seminiferous tubules still arrest at epithelial stage IV, corresponding to pachytene stage. Since most of the double mutant spermatocytes apoptosed after accumulating H1t, we speculated that the arrest could be consequence of a defective sex body formation. In order to study the sex body in p53 and TAp63 double mutants, firstly we analyzed the formation of the sex body and then performed RNA-FISH of two X-linked genes (*Scml2* and *Zfy2*) to study its functionally. RNA-FISH technique presents the advantage to visualize the transcription of a specific transcript at a cellular level. We used TOPBP1 to identify pachynema cells, since TOPBP1 specifically binds to the unsynapsed X and Y chromosomes at early pachytene stage. We reported here that *Trip13 p53* and *Trip13 TAp63* double mutants presented increased expression of sex-linked genes at early pachynema. Therefore, our findings establish sex body defects in *Trip13* and double mutants, resulting in inefficient MSCI and subsequent pachytene arrest; corroborating that TRIP13 participates in the formation of the sex body (Pacheco et al. 2015).

From our results we propose a model where TRIP13 is required to properly load ATR onto unsynapsed X and Y axes and extend its signal to the chromatin, allowing proper H2AX phosphorylation and SUMO-1 loading over the sex body chromatin (Fig. 5.2). TRIP13 protein is required to remove HORMAD1 and HORMAD2 proteins from the chromosomes axes once synapsis has occurred. In wild type spermatocytes at pachynema, HORMAD1 and HORMAD2 only accumulate on the asynapsed portions of the X and Y chromosomes, signaling for the attraction of the silencing machinery to the sex chromosomes. However, in *Trip13* mutant pachytene-stage spermatocytes, HORMAD1 and HORMAD2 remain retained in all synapsed autosomes, which disturbs the silencing signaling and MSCI is not properly implemented. Indeed, correct loading of ATR along the X and Y axes and the sex body chromatin is HORMAD1 and HORMAD2-dependent (Wojtasz et al. 2012). Moreover, *Trip13* mutant spermatocytes present a similar misexpression level of X-linked chromosome genes than *Hormad2* mutants (Wojtasz et al. 2012), which could suggest that TRIP13 and HORMAD2 act in conjunction to implement MSCI. Altogether, with these observations we propose that TRIP13 regulation of HORMAD1/2 unloading from the chromosome axis is required for proper loading of ATR

on asynapsed axes and following activation of the silencing machinery over the sex chromosomes.

5.4.2 TRIP13 mediates transcriptional silencing of the unsynapsed regions at early meiotic stages

5.4.2.1 Global EU-RNA levels analysis in Trip13 mutants

The ability to separate the recombination-dependent arrest from the sex body-deficient arrest allowed us to find out that TRIP13 was necessary for the correct silencing of the sexual chromosomes. Since the MSCI is a manifestation of the global transcription repression that occurs over unsynapsed chromatin (MSUC), which has been hypothesized to promote the transcriptional silencing that is implemented at the entry of meiotic prophase (Page et al. 2012), this lead us to hypothesize that TRIP13 could also participate in transcriptional inactivation that occurs at early prophase stages. To investigate if TRIP13 participates in the suppression of transcription that arises when meiosis initiates, we analyzed global RNA transcription levels and detailed profile expression at early stages of meiotic prophase in control and *Trip13* mutant spermatocytes. To study global RNA synthesis levels we performed two different approaches: one by using EU Click-iT method and the other using the phosphorylated Serine2 RNA polymerase II staining as an indirect marker.

The EU Click-It technique was first used in 2008 to label endogenous RNA in mammalian cells ligation (Jao and Salic 2008). EU is incorporated to nascent RNA in living cells and then EU-labelled RNA can be detected by a reaction based on a chemoselective copper-catalyzed. This methodology has been used for RT-qPCR studies (Ideue et al. 2012) and also for monitoring global RNA synthesis at a single cell level through microscopy quantification in mammalian cells (Kalveram et al. 2013; Biddlestone et al. 2014). To our knowledge, the work presented here is the first attempt to use EU Click-iT technique to measure RNA expression in mouse spermatocytes. We adapted the conventional protocols on cultured cells to fresh spermatocyte cell suspension, which we kept in continuous agitation. Besides, cytological preparations were prepared in order to maintain cell volume. When setting up the protocol, we established the EU incubation time at 2.5 hours, since it was the minimum time where we could clearly observe higher intensity levels of labelled-EU at pachytene stage (when transcription is very active); and used a low concentration of 5mM which is described as non-toxic (Tani et al. 2012). Furthermore, in

order to determine EU-labeled RNA levels as precisely as possible, we took stack images every 0.5 µm and quantified the sum projection obtained. Although we were already quantifying the integrated density that takes into account the area of the cell, we thought this way was the best approach, since we observed that *Trip13* mutant spermatocytes were slightly larger that wild type cells (P<0.001, T test; Fig 5.3).

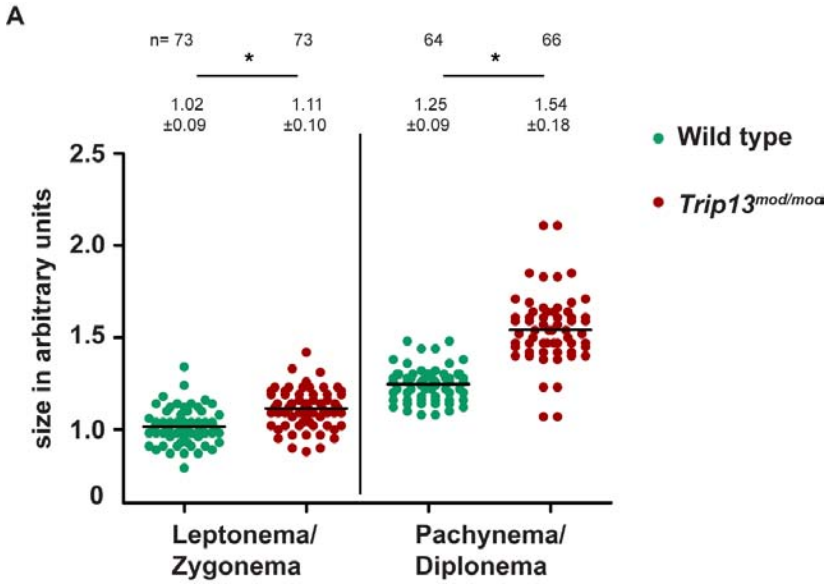

Figure 5.3. *Trip13*$^{mod/mod}$ spermatocytes are larger than wild type cells. (A) Quantification of cells size in wild type (green) and *Trip13*$^{mod/mod}$ mutant (red) mice. Horizontal lines represent the mean, which is indicated over the plot (Mean±SD). N shows the cells counted per genotype. (*) indicates significantly different relative to the wild type.

Since our transcriptional analysis using EU-labelled RNA showed that in wild type cells transcription was repressed at early prophase stages and then resumed at pachytene-stage, similarly to what was previously observed (Monesi 1964), we inferred that these results validated our approach to study global gene expression in *Trip13* mutant spermatocytes. Single cell RNA quantification shows that leptonema and zygonema cells have low expression levels and these start to increase at mid pachynema, corresponding to the stage where transcription is restored. The first study that described transcriptional activity in mouse spermatocytes, used radioactively labeled RNA detected with autoradiography and consequently presented several disadvantages (like using radioactive isotopes for detecting RNA) (Monesi 1964). Therefore, we show here that EU Click-iT method is a useful tool to monitor RNA synthesis in mouse meiosis.

Analysis from EU incubated spermatocytes showed that *Trip13* mutant early prophase stages presented higher EU-labeled RNA intensity levels that the wild type. The differences were more significant at zygotene stage, when most of the autosomes are still

unsynapsed. Moreover, we found that this increase in expression is specific of *Trip13* impairment, since other mutants that similarly arrest a pachynema, like *Dmc1* or *Spo11* mutants, presented any differences regarding the wild type. Therefore, since *Dmc1* mutants present normal expression levels, the increase of RNA intensity observed in *Trip13* mutants is independent of recombination impairment. Interestingly, *Spo11* mutant results indicate that the meiotic silencing at the onset of prophase follows a meiotic program that is independent on the formation of the DSBs. The results obtained with the EU-labeled RNA imaging were further corroborated with phosphorylated (S2) RNA polymerase II staining. Other studies have previously analyzed expression in mouse spermatocytes by following the active form of the RNA polymerase II in immunofluorescence (Turner 2002; Page et al. 2012). It is clearly observable that phospho-RNA polymerase II levels increase at pachytene stage nuclei, with the exception of the small area that corresponds to the sex body (which is more evident at diplonema stage). From our results, we also observed a significant increase of phosphoS2-RNA polymerase II levels in *Trip13* mutant zygotene-stage spermatocytes. Finding the same trend either by directly measuring nascent RNA levels or by indirectly detecting the active form of RNA polymerase corroborates that TRIP13 is required for controlling transcription levels at the early stages of meiotic prophase.

Nonetheless, we noticed a big variability among cells from the same stage and genotype (as observed in figures 3.17-18 and 3.20). Importantly, other studies using EU-labeling technique observed similar differential expressions among cells from the same monolayer of cultured cells (Biddlestone et al. 2014). In our view, this can be explained by an intrinsic characteristic of cells, or a technique limitation due to the time that cells remain in culture before being fixed. We discard a limitation of EU penetrance to the cells, since we observe the same phenotype by marking a post-transcriptional modification of the RNA polymerase II. In addition, if we analyzed a high number of cells we observed a clear trend on wild type cells to increase transcription as meiotic prophase progresses and unsynapsed regions diminish. Furthermore, since all samples were treated in parallel with their control, and we afterwards normalized the expression levels of the mutant cells to their specific controls, we consider that differences between the mutants and wild type may reflect a biological phenotype.

5.4.2.2 Specific gene expression analysis of Trip13 mutants

The analysis of EU-labeled RNA and phosphorylated (S2) RNA polymerase II suggested that transcription activity was increased in *Trip13* mutant early prophase

stages. However since this data only offers information about global RNA expression, we wondered which genes were overexpressed in *Trip13* mutants. We speculated about different scenarios that could originate the increased transcription observed in *Trip13* mutant spermatocytes. One possibility was that the meiotic resumption at pachytene stage was happening earlier in *Trip13* mutants. In such case, we would expect to observe expression of pachytene-related genes already in zygonema spermatocytes. A second alternative could be that *Trip13* mutants are not able to properly apply the transcription repression implemented at the onset of prophase. Such circumstance would result in a higher expression of pre-meiotic related genes. The best strategy to address this issue would have been to sequence RNA samples from highly enriched meiotic prophase stages spermatocytes. Since we could not set up the technique to do this (see above), another strategy to address this question would have been to sequence whole testis RNA from different time points of the first spermatogenic wave in which we would have obtained highly enriched leptotene-stage, zygotene-stage and early pachytene-stage spermatocyte samples. However, due to budget limitations we were not able to use this expensive approach. Thus, in order to be able to distinguish these two possibilities, we took advantage of a recent publication where they characterized gene expression from 6 to 38 dpp in wild type spermatocytes by RNA sequencing. Using a computational approach, they estimated cell-type specific clusters of genes in somatic, pre-meiotic, spermatocytes and spermatid cells (Margolin et al. 2014). Thus, we decided to sequence whole testis RNA from control and mutant juvenile mice and classified it using the clusters defined by Margolin et al (2014).

We decided to analyze 14 dpp mice, when they have already progressed to zygotene stage and before the pachytene block takes place. From our RNA sequencing results we obtained a list of 683 genes that were significantly differentially expressed in *Trip13 mutants* compared to their wild type littermates. From these, 221 genes were upregulated in *Trip13* mutants, and 462 were overexpressed in the wild type. Most of the upregulated genes (~65%) in *Trip13* mutant mapped to the X chromosome. These results agrees with our observations of TRIP13 being required to silence the sex chromosome genes. Therefore, we can confirm that TRIP13 is required to silence the unsynapsed regions of the X and Y chromosome. The fact that the other 35% of upregulated genes map in the autosomes, suggests that expression of autosomal genes could also contribute to the higher expression levels observed in *Trip13* mutants. These increased expression levels could be a consequence of synapsis failing to silence or of a lack of repression at the entry of meiosis. The first scenario seems to be less feasible, as if it was a synapsis defect over

the autosomes this occurs in a stochastic manner all over the genome, so the probability to detect expression of these genes by RNAseq is small (taking into account that every cell would overexpress a different set of genes)., The other possibility, would be that these overexpressed genes are normally repressed at the onset of meiosis in wild type, but in the *Trip13* mutant they are not. Therefore, we also analyzed to which cell-type corresponded the overexpressed genes (Margolin et al. 2014). Remarkably, most *Trip13* overexpressed genes (including autosomic and sex-linked genes) belong to spermatogonia/pre-leptonema/leptonema cluster, where X chromosome genes are the main contributors of this cluster. Still, about 60% of the autosomic overexpressed genes in *Trip13* mutant corresponded to somatic/pre-meiotic and spermatogonia/leptonema cluster. This contrasts with the fact that from cytological quantification most of the spermatocytes at 14 dpp were at zygotene stage. Moreover, since 14 dpp *Trip13* mutants presented the same percentage of spermatocytes (regarding the total number of cells in the testis) as the wild type, we discard the possibility that *Trip13* mutants overexpress pre-meiotic genes because of the presence of more somatic or pre-meiotic cells. Thus, altogether these results could be interpreted as TRIP13 being required to retain the expression of pre-meiotic and early meiotic genes at low levels during meiotic prophase.

Regarding overexpressed genes in the wild type, these corresponded to all autosomes in a similar extend (no sex-linked genes were overexpressed). In addition, most of the overexpressed genes belonged to pachynema cell-type expressed genes. This correlates with cytological observations, where most of the spermatocytes had already reached pachynema stage. Our results seem to discard the possibility that reactivation of transcription is occurring earlier in *Trip13* mutants, since we did not see a major overexpression of pachytene cell-type genes in these 14dpp *Trip13* mutant testis samples. Nevertheless, we need to take into account the limitations of our analysis relating overexpressed genes with specific cell-types, since it is only based on the clusters previously defined by Margolin et al. (Margolin et al. 2014). So for example, we observed some overexpressed genes that correlated with secondary spermatocytes and spermatids cluster. However, since our samples were form 14 dpp juvenile mice, they did not contain any post-pachytene stage cells. This observation is probably a consequence of how genes were classified by Margolin et al. (2014). In that study, genes were found to be expressed in various cell types, but they were classified into the cluster that showed the highest expression. Thus, we are probably observing genes that are classified as “spermatid related-genes” but that are also expressed in earlier stages.

Overall, RNA sequencing analysis corroborated that TRIP13 is required to silence gene expression from unsynapsed regions of the sex chromosomes and to regulate expression of early meiotic genes. At the onset of prophase a global transcription repression occurs, and our data suggest that TRIP13 is required to implement the repression in the transcription of these genes.

Recent studies are increasing the evidence that TRIP13^{Pch2} is a key modulator of several chromosomal processes (Vader 2015). Our results suggesting a new role for TRIP13 in transcription/silencing control, do not seem to be evolutionary conserved. During meiosis, Pch2 has been principally found to participate in chromosome axis conformation, DSB formation, recombination and asynapsis checkpoint response. What seems to be highly conserved is that HORMAD1/2^{Hop1} protein is one of TRIP13^{Pch2} principal cofactors. In mammals, TRIP13 regulates chromosomal configuration by coupling synapsis completion with removing HORMAD1/2^{Hop1} localization from the axes, where HORMAD proteins are key regulators of the silencing network (Wojtasz et al. 2009; Roig et al. 2010). We propose that TRIP13 role on transcription, by coupling asynapsis and silencing, could be a reminiscence of the synapsis checkpoint role observed for Pch2 in other organisms. At least in females, altered transcription has been found to cause the synapsis-dependent arrest. It has been proposed that mutants that fail to complete synapsis lose their oocytes due to the activation of MSUC mechanisms that represses essential genes required for oogenesis (Cloutier et al. 2015a). Therefore, since we have uncovered that TRIP13 is required to implement proper MSUC mechanisms in mouse spermatocytes, it is conceivable that it should have similar functions in the oocytes. Thus, our findings suggest that TRIP13 may have a conserved role in the surveillance mechanism controlling chromosome synapsis during meiotic prophase. Nonetheless, further experiments need to be performed to confirm this hypothesis: the model predicts that if TRIP13 is required to silence unsynapsed regions of the genome and this leads to oocyte arrest and apoptosis, removing TRIP13 from synaptic deficient oocytes would rescue the arrest and apoptosis of these mutants. The lab is currently testing this hypothesis using the proposed genetic approach.

Studies in yeast do not directly correlate TRIP13^{Pch2} with transcription, however Pch2 is found to be highly enriched over the nucleolus where seems to execute important roles. The nucleolus is a transcriptional silenced structure that assembles repetitive ribosomal DNA (rDNA) into a Sir2-dependent closed chromatin conformation, that presumably prevents access of transcriptional and recombination factors. Pch2 nucleolar localization requires Sir2 and Orc1 (origin recognition complex subunit) proteins, and has

been found to be necessary to avoid DSBs formation at the edges of the rDNA (borders between heterochromatin and euchromatin are potential regions for DSB formation); and to repress interhomolog recombination in the rDNA by avoiding Hop1 nucleolar localization (San-Segundo and Roeder 1999; Vader et al. 2011).

Besides, our work provides new data suggesting that TRIP13 could be regulating chromatin configuration in order to keep expression of sex-linked genes and early meiotic genes at low levels. It would be interesting to determinate if TRIP13 also requires HORMAD proteins to perform this function at the onset of meiosis. Moreover, several studies in yeast revealed that Pch2 interacts with other proteins than those containing HORMA domain. For instance, Pch2 interacts with Xrs2 (component of the Mre11 complex) and Orc1 to regulate meiotic recombination (Ho and Burgess 2011; Vader et al. 2011). Also, interactomic studies, using yeast two hybrids, predicts that human TRIP13 interacts with over 100 different proteins (Rual et al. 2005; Rolland et al. 2014), opening the door to more complexity and other interactors that might be involved in TRIP13^{Pch2} diverse functions.

CONCLUSIONS

6. CONCLUSIONS

1. Western blot analysis from adult whole testes extracts is not a valid methodology for studying activation of DDR proteins involved in the recombination-dependent arrest. More precisely, activation of proteins known to be involved in this arrest also appear in wild type and Spo11 mutant samples.

2. Cell sorting technique is not reliable or reproducible enough between different experiments. Using the already described protocols does not allow obtaining enriched fractions of exclusively leptonema, zygonema or pachynema cells. However, it is a good technique for collecting highly enriched diplonema cell population.

3. Mutant mice lacking p53 in C57BL/6 and 129/Sv genetic background are viable and fertile. Spermatogenesis progression is apparently normal, with no presence of multinucleated giant-cells as previously described in other genetic backgrounds.

4. In the absence of p53, synapsis occurs normally. However, meiotic prophase at the first meiotic wave is slightly accelerated, probably associated with a role of p53 in checkpoint activation.

5. Regarding homologous recombination, mutation of p53 does not affect DNA repair in spermatocytes evaluated as γH2AX foci. However p53 seems to have a conserved role in regulating CO formation in mammals.

6. P53 and TAp63 are required to activate the recombination-dependent arrest in the presence of unrepaired deleterious DSBs in mouse spermatocytes. In contrast, p73 does not participate in the activation of these arrest.

7. P53 and TAp63 are dispensable for the activation of the sex body-deficient arrest, which determinates that the recombination-dependent and the sex body-deficient arrest are activated by independent mechanism.

8. Our observations from bypassing the recombination-dependent arrest allowed us to elucidate a role for TRIP13 protein in meiotic silencing. TRIP13 is required for the formation of a functional sex body and MSCI implementation at pachytene stage spermatocytes.

9. TRIP13 regulates global transcription at the onset of meiotic prophase, preferentially repressing the expression of pre-meiotic genes at the initiation of meiosis.

BIBLIOGRAPHY

7. BIBLIOGRAPHY

Acevedo J, Yan S, Michael WM. 2016. Direct Binding to RPA-Coated ssDNA Allows Recruitment of the ATR Activator TopBP1 to Sites of DNA Damage. *J Biol Chem*.

Ahmed EA, de Rooij DG. 2009. Staging of mouse seminiferous tubule cross-sections. *Methods Mol Biol* **558**: 263–77.

Allers T, Lichten M. 2001. Intermediates of yeast meiotic recombination contain heteroduplex DNA. *Mol Cell* **8**: 225–231.

Allocati N, Di Ilio C, De Laurenzi V. 2012. p63/p73 in the control of cell cycle and cell death. *Exp Cell Res* **318**: 1285–90.

Almon E, Goldfinger N, Kapon A, Schwartz D, Levine AJ, Rotter V. 1993. Testicular Tissue-Specific Expression of the p53 Suppressor Gene. *Dev Biol* **156**: 107–116.

Armstrong JF, Kaufman MH, Harrison DJ, Clarke AR. 1995. High-frequency developmental abnormalities in p53-deficient mice. *Curr Biol* **5**: 931–6.

Ashley T, Westphal C, Plug-de Maggio A, de Rooij DG. 2004. The mammalian mid-pachytene checkpoint: meiotic arrest in spermatocytes with a mutation in Atm alone or in combination with a Trp53 (p53) or Cdkn1a (p21/cip1) mutation. *Cytogenet Genome Res* **107**: 256–62.

Baart EB, de Rooij DG, Keegan KS, de Boer P. 2000. Distribution of Atr protein in primary spermatocytes of a mouse chromosomal mutant: a comparison of preparation techniques. *Chromosoma* **109**: 139–47.

Banerjee R, Russo N, Liu M, Basrur V, Bellile E, Palanisamy N, Scanlon CS, van Tubergen E, Inglehart RC, Metwally T, et al. 2014. TRIP13 promotes error-prone nonhomologous end joining and induces chemoresistance in head and neck cancer. *Nat Commun* **5**: 4527.

Banin S, Moyal L, Shieh S, Taya Y, Anderson CW, Chessa L, Smorodinsky NI, Prives C, Reiss Y, Shiloh Y, et al. 1998. Enhanced phosphorylation of p53 by ATM in response to DNA damage. *Science* **281**: 1674–7.

Barchi M, Mahadevaiah S, Di Giacomo M, Baudat F, de Rooij DG, Burgoyne PS, Jasin M, Keeney S. 2005. Surveillance of different recombination defects in mouse spermatocytes yields distinct responses despite elimination at an identical developmental stage. *Mol Cell Biol* **25**: 7203–15.

Barchi M, Roig I, Di Giacomo M, De Rooij DG, Keeney S, Jasin M. 2008. ATM promotes the obligate XY crossover and both crossover control and chromosome axis integrity on autosomes. *PLoS Genet* **4**: e1000076.

Barlow C, Brown KD, Deng CX, Tagle DA, Wynshaw-Boris A. 1997a. Atm selectively regulates distinct p53-dependent cell-cycle checkpoint and apoptotic pathways. *Nat Genet* **17**: 453–6.

Barlow C, Liyanage M, Moens PB, Deng CX, Ried T, Wynshaw-Boris A. 1997b. Partial rescue of the prophase I defects of Atm-deficient mice by p53 and p21 null alleles. *Nat Genet* **17**: 462–6.

Barlow C, Liyanage M, Moens PB, Tarsounas M, Nagashima K, Brown K, Rottinghaus S, Jackson SP, Tagle D, Ried T, et al. 1998. Atm deficiency results in severe meiotic disruption as early as leptonema of prophase I. *Development* **125**: 4007–17.

Bartrand AJ, Iyasu D, Marinco SM, Brush GS. 2006. Evidence of meiotic crossover control in Saccharomyces cerevisiae through Mec1-mediated phosphorylation of replication protein A. *Genetics* **172**: 27–39.

Bastos H, Lassalle B, Chicheportiche A, Riou L, Testart J, Allemand I, Fouchet P. 2005. Flow cytometric characterization of viable meiotic and postmeiotic cells by Hoechst 33342 in mouse spermatogenesis. *Cytometry A* **65**: 40–9.

Baudat F, Buard J, Grey C, Fledel-Alon A, Ober C, Przeworski M, Coop G, de Massy B. 2010. PRDM9 is a major determinant of meiotic recombination hotspots in humans and mice. *Science* **327**: 836–40.

Baudat F, Manova K, Yuen JP, Jasin M, Keeney S. 2000. Chromosome Synapsis Defects and Sexually Dimorphic Meiotic Progression in Mice Lacking Spo11. *Mol Cell* **6**: 989–998.

Bellani MA, Romanienko PJ, Cairatti DA, Camerini-Otero RD. 2005. SPO11 is required for sex-body formation, and Spo11 heterozygosity rescues the prophase arrest of Atm-/- spermatocytes. *J Cell Sci* **118**: 3233–45.

Belyi VA, Ak P, Markert E, Wang H, Hu W, Puzio-Kuter A, Levine AJ. 2010. The origins and evolution of the p53 family of genes. *Cold Spring Harb Perspect Biol* **2**: a001198.

Beretta C, Chiarelli A, Testoni B, Mantovani R, Guerrini L. 2005. Regulation of the cyclin-dependent kinase inhibitor p57Kip2 expression by p63. *Cell Cycle* **4**: 1625–31.

Beumer TL, Roepers-Gajadien HL, Gademan IS, van Buul PP, Gil-Gomez G, Rutgers DH, de Rooij DG. 1998. The role of the tumor suppressor p53 in spermatogenesis. *Cell Death Differ* **5**: 669–77.

Bhalla N, Dernburg AF. 2005. A conserved checkpoint monitors meiotic chromosome synapsis in Caenorhabditis elegans. *Science* **310**: 1683–6.

Biddlestone J, Druker J, Shmakova A, Ferguson G, Swedlow JR, Rocha S. 2014. Analysis of global RNA synthesis at the single cell level following hypoxia. *J Vis Exp* e51420.

Bieging KT, Mello SS, Attardi LD. 2014. Unravelling mechanisms of p53-mediated tumour suppression. *Nat Rev Cancer* **14**: 359–70.

Bishop DK, Zickler D. 2004. Early decision; meiotic crossover interference prior to stable strand exchange and synapsis. *Cell* **117**: 9–15.

Bolcun-Filas E, Rinaldi VD, White ME, Schimenti JC. 2014. Reversal of female infertility by Chk2

ablation reveals the oocyte DNA damage checkpoint pathway. *Science* **343**: 533–6.

Borde V, de Massy B. 2013. Programmed induction of DNA double strand breaks during meiosis: setting up communication between DNA and the chromosome structure. *Curr Opin Genet Dev* **23**: 147–55.

Börner GV, Barot A, Kleckner N. 2008. Yeast Pch2 promotes domainal axis organization, timely recombination progression, and arrest of defective recombinosomes during meiosis. *Proc Natl Acad Sci U S A* **105**: 3327–32.

Börner GV, Kleckner N, Hunter N. 2004. Crossover/noncrossover differentiation, synaptonemal complex formation, and regulatory surveillance at the leptotene/zygotene transition of meiosis. *Cell* **117**: 29–45.

Bourdon J-C, Fernandes K, Murray-Zmijewski F, Liu G, Diot A, Xirodimas DP, Saville MK, Lane DP. 2005. p53 isoforms can regulate p53 transcriptional activity. *Genes Dev* **19**: 2122–37.

Braun RE. 2001. Packaging paternal chromosomes with protamine. *Nat Genet* **28**: 10–2.

Brick K, Smagulova F, Khil P, Camerini-Otero RD, Petukhova G V. 2012. Genetic recombination is directed away from functional genomic elements in mice. *Nature* **485**: 642–5.

Brodsky MH, Nordstrom W, Tsang G, Kwan E, Rubin GM, Abrams JM. 2000. Drosophila p53 binds a damage response element at the reaper locus. *Cell* **101**: 103–13.

Burgoyne PS, Mahadevaiah SK, Turner JMA. 2009. The consequences of asynapsis for mammalian meiosis. *Nat Rev Genet* **10**: 207–16.

Burgoyne PS, Mahadevaiah SK, Turner JMA. 2007. The management of DNA double-strand breaks in mitotic G2, and in mammalian meiosis viewed from a mitotic G2 perspective. *Bioessays* **29**: 974–86.

Candi E, Agostini M, Melino G, Bernassola F. 2014. How the TP53 Family Proteins TP63 and TP73 Contribute to Tumorigenesis: Regulators and Effectors. *Hum Mutat* **35**: 702–714.

Canman CE, Lim DS, Cimprich KA, Taya Y, Tamai K, Sakaguchi K, Appella E, Kastan MB, Siliciano JD. 1998. Activation of the ATM kinase by ionizing radiation and phosphorylation of p53. *Science* **281**: 1677–9.

Carballo JA, Johnson AL, Sedgwick SG, Cha RS. 2008. Phosphorylation of the axial element protein Hop1 by Mec1/Tel1 ensures meiotic interhomolog recombination. *Cell* **132**: 758–70.

Carballo JA, Panizza S, Serrentino ME, Johnson AL, Geymonat M, Borde V, Klein F, Cha RS. 2013. Budding yeast ATM/ATR control meiotic double-strand break (DSB) levels by down-regulating Rec114, an essential component of the DSB-machinery. *PLoS Genet* **9**: e1003545.

Chaturvedi P, Eng WK, Zhu Y, Mattern MR, Mishra R, Hurle MR, Zhang X, Annan RS, Lu Q, Faucette LF, et al. 1999. Mammalian Chk2 is a downstream effector of the ATM-dependent DNA

damage checkpoint pathway. *Oncogene* **18**: 4047–54.

Chen C, Jomaa A, Ortega J, Alani EE. 2013. Pch2 is a hexameric ring ATPase that remodels the chromosome axis protein Hop1. *Proc Natl Acad Sci* **111**: E44–E53.

Cheng CY, Mruk DD. 2010. The biology of spermatogenesis: the past, present and future. *Philos Trans R Soc Lond B Biol Sci* **365**: 1459–63.

Choi E, Lee J, Oh J, Park I, Han C, Yi C, Kim DH, Cho B-N, Eddy EM, Cho C. 2007. Integrative characterization of germ cell-specific genes from mouse spermatocyte UniGene library. *BMC Genomics* **8**: 256.

Chu S, Herskowitz I. 1998. Gametogenesis in yeast is regulated by a transcriptional cascade dependent on Ndt80. *Mol Cell* **1**: 685–96.

Churchman ML, Roig I, Jasin M, Keeney S, Sherr CJ. 2011. Expression of Arf tumor suppressor in spermatogonia facilitates meiotic progression in male germ cells. *PLoS Genet* **7**: e1002157.

Cimprich KA, Cortez D. 2008. ATR: an essential regulator of genome integrity. *Nat Rev Mol Cell Biol* **9**: 616–27.

Cloutier JM, Mahadevaiah SK, ElInati E, Nussenzweig A, Tóth A, Turner JMA. 2015a. Histone H2AFX Links Meiotic Chromosome Asynapsis to Prophase I Oocyte Loss in Mammals. *PLoS Genet* **11**: e1005462.

Cloutier JM, Mahadevaiah SK, ElInati E, Tóth A, Turner J. 2015b. Mammalian meiotic silencing exhibits sexually dimorphic features. *Chromosoma*.

Cole F, Baudat F, Grey C, Keeney S, de Massy B, Jasin M. 2014. Mouse tetrad analysis provides insights into recombination mechanisms and hotspot evolutionary dynamics. *Nat Genet* **46**: 1072–80.

Cole F, Kauppi L, Lange J, Roig I. 2012. Homeostatic control of recombination is implemented progressively in mouse meiosis. *Nat cell …* **14**: 424–430.

Cortez D, Guntuku S, Qin J, Elledge SJ. 2001. ATR and ATRIP: partners in checkpoint signaling. *Science* **294**: 1713–6.

Daniel K, Lange J, Hached K, Fu J, Anastassiadis K, Roig I, Cooke HJ, Stewart AF, Wassmann K, Jasin M, et al. 2011. Meiotic homologue alignment and its quality surveillance are controlled by mouse HORMAD1. *Nat Cell Biol* **13**: 599–610.

de Rooij DG, Grootegoed JA. 1998. Spermatogonial stem cells. *Curr Opin Cell Biol* **10**: 694–701.

de Vries FAT, de Boer E, van den Bosch M, Baarends WM, Ooms M, Yuan L, Liu J-G, van Zeeland AA, Heyting C, Pastink A. 2005. Mouse Sycp1 functions in synaptonemal complex assembly, meiotic recombination, and XY body formation. *Genes Dev* **19**: 1376–89.

de Vries SS, Baart EB, Dekker M, Siezen A, de Rooij DG, de Boer P, te Riele H. 1999. Mouse MutS-like

protein Msh5 is required for proper chromosome synapsis in male and female meiosis. *Genes Dev* **13**: 523–31.

Derheimer FA, Kastan MB. 2010. Multiple roles of ATM in monitoring and maintaining DNA integrity. *FEBS Lett* **584**: 3675–81.

Derry WB, Putzke AP, Rothman JH. 2001. Caenorhabditis elegans p53: role in apoptosis, meiosis, and stress resistance. *Science* **294**: 591–5.

Di Giacomo M, Barchi M, Baudat F, Edelmann W, Keeney S, Jasin M. 2005. Distinct DNA-damage-dependent and -independent responses drive the loss of oocytes in recombination-defective mouse mutants. *Proc Natl Acad Sci U S A* **102**: 737–42.

Dohn M, Zhang S, Chen X. 2001. p63alpha and DeltaNp63alpha can induce cell cycle arrest and apoptosis and differentially regulate p53 target genes. *Oncogene* **20**: 3193–205.

Donehower LA, Harvey M, Slagle BL, McArthur MJ, Montgomery CA, Butel JS, Bradley A. 1992. Mice deficient for p53 are developmentally normal but susceptible to spontaneous tumours. *Nature* **356**: 215–21.

Dötsch V, Bernassola F, Coutandin D, Candi E, Melino G. 2010. p63 and p73, the ancestors of p53. *Cold Spring Harb Perspect Biol* **2**: a004887.

Drabent B, Bode C, Bramlage B, Doenecke D. 1996. Expression of the mouse testicular histone gene H1t during spermatogenesis. *Histochem Cell Biol* **106**: 247–51.

Dym M, Kokkinaki M, He Z. 2009. Spermatogonial stem cells: mouse and human comparisons. *Birth Defects Res C Embryo Today* **87**: 27–34.

Edelmann W, Cohen PE, Kane M, Lau K, Morrow B, Bennett S, Umar A, Kunkel T, Cattoretti G, Chaganti R, et al. 1996. Meiotic pachytene arrest in MLH1-deficient mice. *Cell* **85**: 1125–34.

Edelmann W, Cohen PE, Kneitz B, Winand N, Lia M, Heyer J, Kolodner R, Pollard JW, Kucherlapati R. 1999. Mammalian MutS homologue 5 is required for chromosome pairing in meiosis. *Nat Genet* **21**: 123–7.

el-Deiry WS, Harper JW, O'Connor PM, Velculescu VE, Canman CE, Jackman J, Pietenpol JA, Burrell M, Hill DE, Wang Y. 1994. WAF1/CIP1 is induced in p53-mediated G1 arrest and apoptosis. *Cancer Res* **54**: 1169–74.

Eytan E, Wang K, Miniowitz-Shemtov S, Sitry-Shevah D, Kaisari S, Yen TJ, Liu S-T, Hershko A. 2014. Disassembly of mitotic checkpoint complexes by the joint action of the AAA-ATPase TRIP13 and p31(comet). *Proc Natl Acad Sci U S A* **111**: 12019–24.

Falck J, Mailand N, Syljuåsen RG, Bartek J, Lukas J. 2001. The ATM-Chk2-Cdc25A checkpoint pathway guards against radioresistant DNA synthesis. *Nature* **410**: 842–7.

Feijoo C, Hall-Jackson C, Wu R, Jenkins D, Leitch J, Gilbert DM, Smythe C. 2001. Activation of

mammalian Chk1 during DNA replication arrest: a role for Chk1 in the intra-S phase checkpoint monitoring replication origin firing. *J Cell Biol* **154**: 913–23.

Flores ER, Sengupta S, Miller JB, Newman JJ, Bronson R, Crowley D, Yang A, McKeon F, Jacks T. 2005. Tumor predisposition in mice mutant for p63 and p73: evidence for broader tumor suppressor functions for the p53 family. *Cancer Cell* **7**: 363–73.

Flores ER, Tsai KY, Crowley D, Sengupta S, Yang A, McKeon F, Jacks T. 2002. p63 and p73 are required for p53-dependent apoptosis in response to DNA damage. *Nature* **416**: 560–4.

Friedman PN, Chen X, Bargonetti J, Prives C. 1993. The p53 protein is an unusually shaped tetramer that binds directly to DNA. *Proc Natl Acad Sci U S A* **90**: 3319–23.

Fukuda T, Daniel K, Wojtasz L, Toth A, Höög C. 2010. A novel mammalian HORMA domain-containing protein, HORMAD1, preferentially associates with unsynapsed meiotic chromosomes. *Exp Cell Res* **316**: 158–71.

Fukuda T, Pratto F, Schimenti JC, Turner JMA, Camerini-Otero RD, Höög C. 2012. Phosphorylation of chromosome core components may serve as axis marks for the status of chromosomal events during mammalian meiosis. *PLoS Genet* **8**: e1002485.

Fulco M, Costanzo A, Merlo P, Mangiacasale R, Strano S, Blandino G, Balsano C, Lavia P, Levrero M. 2003. p73 is regulated by phosphorylation at the G2/M transition. *J Biol Chem* **278**: 49196–202.

Gaiddon C, Lokshin M, Ahn J, Zhang T, Prives C. 2001. A subset of tumor-derived mutant forms of p53 down-regulate p63 and p73 through a direct interaction with the p53 core domain. *Mol Cell Biol* **21**: 1874–87.

Garcia V, Phelps SEL, Gray S, Neale MJ. 2011. Bidirectional resection of DNA double-strand breaks by Mre11 and Exo1. *Nature* **479**: 241–4.

Gersten KM, Kemp CJ. 1997. Normal meiotic recombination in p53-deficient mice. *Nat Genet* **17**: 378–9.

Getun I V, Torres B, Bois PRJ. 2011. Flow cytometry purification of mouse meiotic cells. *J Vis Exp*.

Ghafari F, Pelengaris S, Walters E, Hartshorne GM. 2009. Influence of p53 and genetic background on prenatal oogenesis and oocyte attrition in mice. *Hum Reprod* **24**: 1460–72.

Gonfloni S, Di Tella L, Caldarola S, Cannata SM, Klinger FG, Di Bartolomeo C, Mattei M, Candi E, De Felici M, Melino G, et al. 2009. Inhibition of the c-Abl-TAp63 pathway protects mouse oocytes from chemotherapy-induced death. *Nat Med* **15**: 1179–85.

Gotta M, Strahl-Bolsinger S, Renauld H, Laroche T, Kennedy BK, Grunstein M, Gasser SM. 1997. Localization of Sir2p: the nucleolus as a compartment for silent information regulators. *EMBO J* **16**: 3243–55.

Gottlieb S, Esposito RE. 1989. A new role for a yeast transcriptional silencer gene, SIR2, in regulation of recombination in ribosomal DNA. *Cell* **56**: 771–6.

Griswold MD, Oatley JM. 2013. Concise review: Defining characteristics of mammalian spermatogenic stem cells. *Stem Cells* **31**: 8–11.

Handel MA, Schimenti JC. 2010. Genetics of mammalian meiosis: regulation, dynamics and impact on fertility. *Nat Rev Genet* **11**: 124–136.

Hanson PI, Whiteheart SW. 2005. AAA+ proteins: have engine, will work. *Nat Rev Mol Cell Biol* **6**: 519–29.

Harper JW, Adami GR, Wei N, Keyomarsi K, Elledge SJ. 1993. The p21 Cdk-interacting protein Cip1 is a potent inhibitor of G1 cyclin-dependent kinases. *Cell* **75**: 805–16.

Hassold T, Hall H, Hunt P. 2007. The origin of human aneuploidy: where we have been, where we are going. *Hum Mol Genet* **16**: R203–R208.

Hillers KJ. 2004. Crossover interference. *Curr Biol* **14**: R1036–7.

Ho H-C, Burgess SM. 2011. Pch2 acts through Xrs2 and Tel1/ATM to modulate interhomolog bias and checkpoint function during meiosis. *PLoS Genet* **7**: e1002351.

Hollingsworth NM, Goetsch L, Byers B. 1990. The HOP1 gene encodes a meiosis-specific component of yeast chromosomes. *Cell* **61**: 73–84.

Hu W. 2009. The role of p53 gene family in reproduction. *Cold Spring Harb Perspect Biol* **1**: a001073.

Hu W, Feng Z, Teresky AK, Levine AJ. 2007. p53 regulates maternal reproduction through LIF. *Nature* **450**: 721–4.

Ichijima Y, Ichijima M, Lou Z, Nussenzweig A, Camerini-Otero RD, Chen J, Andreassen PR, Namekawa SH. 2011. MDC1 directs chromosome-wide silencing of the sex chromosomes in male germ cells. *Genes Dev* **25**: 959–71.

Ideue T, Adachi S, Naganuma T, Tanigawa A, Natsume T, Hirose T. 2012. U7 small nuclear ribonucleoprotein represses histone gene transcription in cell cycle-arrested cells. *Proc Natl Acad Sci U S A* **109**: 5693–8.

Inagaki A, Schoenmakers S, Baarends WM. 2010. DNA double strand break repair, chromosome synapsis and transcriptional silencing in meiosis. *Epigenetics* **5**: 255–266.

Inoue S, Tomasini R, Rufini A, Elia AJ, Agostini M, Amelio I, Cescon D, Dinsdale D, Zhou L, Harris IS, et al. 2014. TAp73 is required for spermatogenesis and the maintenance of male fertility. *Proc Natl Acad Sci U S A* **111**: 1843–8.

Inselman A, Eaker S, Handel MA. 2003. Temporal expression of cell cycle-related proteins during spermatogenesis: establishing a timeline for onset of the meiotic divisions. *Cytogenet Genome*

Res **103**: 277–84.

Jacks T, Remington L, Williams BO, Schmitt EM, Halachmi S, Bronson RT, Weinberg RA. 1994. Tumor spectrum analysis in p53-mutant mice. *Curr Biol* **4**: 1–7.

Jao CY, Salic A. 2008. Exploring RNA transcription and turnover in vivo by using click chemistry. *Proc Natl Acad Sci U S A* **105**: 15779–84.

Jaramillo-Lambert A, Harigaya Y, Vitt J, Villeneuve A, Engebrecht J. 2010. Meiotic errors activate checkpoints that improve gamete quality without triggering apoptosis in male germ cells. *Curr Biol* **20**: 2078–89.

Jin S, Antinore MJ, Lung FD, Dong X, Zhao H, Fan F, Colchagie AB, Blanck P, Roller PP, Fornace AJ, et al. 2000. The GADD45 inhibition of Cdc2 kinase correlates with GADD45-mediated growth suppression. *J Biol Chem* **275**: 16602–8.

Joerger AC, Rajagopalan S, Natan E, Veprintsev DB, Robinson C V, Fersht AR. 2009. Structural evolution of p53, p63, and p73: implication for heterotetramer formation. *Proc Natl Acad Sci U S A* **106**: 17705–10.

Joshi N, Barot A, Jamison C, Börner GV. 2009. Pch2 links chromosome axis remodeling at future crossover sites and crossover distribution during yeast meiosis. *PLoS Genet* **5**: e1000557.

Jost CA, Marin MC, Kaelin WG. 1997. p73 is a simian [correction of human] p53-related protein that can induce apoptosis. *Nature* **389**: 191–4.

Joyce EF, McKim KS. 2009. Drosophila PCH2 is required for a pachytene checkpoint that monitors double-strand-break-independent events leading to meiotic crossover formation. *Genetics* **181**: 39–51.

Joyce EF, Pedersen M, Tiong S, White-Brown SK, Paul A, Campbell SD, McKim KS. 2011. Drosophila ATM and ATR have distinct activities in the regulation of meiotic DNA damage and repair. *J Cell Biol* **195**: 359–67.

Jung MS, Yun J, Chae HD, Kim JM, Kim SC, Choi TS, Shin DY. 2001. p53 and its homologues, p63 and p73, induce a replicative senescence through inactivation of NF-Y transcription factor. *Oncogene* **20**: 5818–25.

Kalveram B, Lihoradova O, Indran S V, Head JA, Ikegami T. 2013. Using click chemistry to measure the effect of viral infection on host-cell RNA synthesis. *J Vis Exp* e50809.

Kastan MB, Lim DS. 2000. The many substrates and functions of ATM. *Nat Rev Mol Cell Biol* **1**: 179–86.

Keeney S, Giroux CN, Kleckner N. 1997. Meiosis-Specific DNA Double-Strand Breaks Are Catalyzed by Spo11, a Member of a Widely Conserved Protein Family. *Cell* **88**: 375–384.

Kerr JB, Hutt KJ, Michalak EM, Cook M, Vandenberg CJ, Liew SH, Bouillet P, Mills A, Scott CL, Findlay

JK, et al. 2012. DNA damage-induced primordial follicle oocyte apoptosis and loss of fertility require TAp63-mediated induction of Puma and Noxa. *Mol Cell* **48**: 343–52.

Khanna KK, Keating KE, Kozlov S, Scott S, Gatei M, Hobson K, Taya Y, Gabrielli B, Chan D, Lees-Miller SP, et al. 1998. ATM associates with and phosphorylates p53: mapping the region of interaction. *Nat Genet* **20**: 398–400.

Kim D-A, Suh E-K. 2014. Defying DNA double-strand break-induced death during prophase I meiosis by temporal TAp63α phosphorylation regulation in developing mouse oocytes. *Mol Cell Biol* **34**: 1460–73.

Kim S-T, Xu B, Kastan MB. 2002. Involvement of the cohesin protein, Smc1, in Atm-dependent and independent responses to DNA damage. *Genes Dev* **16**: 560–70.

Kleckner N. 1996. Meiosis: how could it work? *Proc Natl Acad Sci U S A* **93**: 8167–74.

Kneitz B, Cohen PE, Avdievich E, Zhu L, Kane MF, Hou H, Kolodner RD, Kucherlapati R, Pollard JW, Edelmann W. 2000. MutS homolog 4 localization to meiotic chromosomes is required for chromosome pairing during meiosis in male and female mice. *Genes Dev* **14**: 1085–97.

Kouznetsova A, Benavente R, Pastink A, Höög C. 2011. Meiosis in mice without a synaptonemal complex. *PLoS One* **6**: e28255.

Krogh BO, Symington LS. 2004. Recombination proteins in yeast. *Annu Rev Genet* **38**: 233–71.

Kurita T, Cunha GR, Robboy SJ, Mills AA, Medina RT. 2005. Differential expression of p63 isoforms in female reproductive organs. *Mech Dev* **122**: 1043–55.

Lam I, Keeney S. 2015. Mechanism and regulation of meiotic recombination initiation. *Cold Spring Harb Perspect Biol* **7**: a016634.

Lammers JH, Offenberg HH, van Aalderen M, Vink AC, Dietrich AJ, Heyting C. 1994. The gene encoding a major component of the lateral elements of synaptonemal complexes of the rat is related to X-linked lymphocyte-regulated genes. *Mol Cell Biol* **14**: 1137–46.

Lane DP, Crawford L V. 1979. T antigen is bound to a host protein in SY40-transformed cells. *Nature* **278**: 261–263.

Lange J, Pan J, Cole F, Thelen MP, Jasin M, Keeney S. 2011. ATM controls meiotic double-strand-break formation. *Nature* **479**: 237–40.

Lao JP, Hunter N. 2010. Trying to avoid your sister. *PLoS Biol* **8**: e1000519.

Lau CPY, Ng PKS, Li MS, Tsui SKW, Huang L, Kumta SM. 2013. p63 regulates cell proliferation and cell cycle progression-associated genes in stromal cells of giant cell tumor of the bone. *Int J Oncol* **42**: 437–443.

Lavin MF. 2007. ATM and the Mre11 complex combine to recognize and signal DNA double-strand breaks. *Oncogene* **26**: 7749–58.

Lavin MF, Kozlov S. 2007. ATM activation and DNA damage response. *Cell Cycle* **6**: 931–42.

Leu JY, Roeder GS. 1999. The pachytene checkpoint in S. cerevisiae depends on Swe1-mediated phosphorylation of the cyclin-dependent kinase Cdc28. *Mol Cell* **4**: 805–14.

Levine AJ, Tomasini R, McKeon FD, Mak TW, Melino G. 2011. The p53 family: guardians of maternal reproduction. *Nat Rev Mol Cell Biol* **12**: 259–65.

Li R, Albertini DF. 2013. The road to maturation: somatic cell interaction and self-organization of the mammalian oocyte. *Nat Rev Mol Cell Biol* **14**: 141–52.

Li XC, Li X, Schimenti JC. 2007. Mouse pachytene checkpoint 2 (trip13) is required for completing meiotic recombination but not synapsis. *PLoS Genet* **3**: e130.

Lin AW, Lowe SW. 2001. Oncogenic ras activates the ARF-p53 pathway to suppress epithelial cell transformation. *Proc Natl Acad Sci U S A* **98**: 5025–30.

Lin Y-L, Sengupta S, Gurdziel K, Bell GW, Jacks T, Flores ER. 2009. p63 and p73 transcriptionally regulate genes involved in DNA repair. *PLoS Genet* **5**: e1000680.

Linzer DI, Levine AJ. 1979. Characterization of a 54K dalton cellular SV40 tumor antigen present in SV40-transformed cells and uninfected embryonal carcinoma cells. *Cell* **17**: 43–52.

Livera G, Petre-Lazar B, Guerquin M-J, Trautmann E, Coffigny H, Habert R. 2008. p63 null mutation protects mouse oocytes from radio-induced apoptosis. *Reproduction* **135**: 3–12.

Lu W-J, Chapo J, Roig I, Abrams JM. 2010. Meiotic recombination provokes functional activation of the p53 regulatory network. *Science* **328**: 1278–81.

MacQueen AJ, Hochwagen A. 2011. Checkpoint mechanisms: The puppet masters of meiotic prophase. *Trends Cell Biol* **21**: 393–400.

Mahadevaiah SK, Bourc'his D, de Rooij DG, Bestor TH, Turner JMA, Burgoyne PS. 2008. Extensive meiotic asynapsis in mice antagonises meiotic silencing of unsynapsed chromatin and consequently disrupts meiotic sex chromosome inactivation. *J Cell Biol* **182**: 263–76.

Mahadevaiah SK, Costa Y, Turner JMA. 2009. Using RNA FISH to study gene expression during mammalian meiosis. *Methods Mol Biol* **558**: 433–44.

Mahadevaiah SK, Turner JM, Baudat F, Rogakou EP, de Boer P, Blanco-Rodríguez J, Jasin M, Keeney S, Bonner WM, Burgoyne PS. 2001. Recombinational DNA double-strand breaks in mice precede synapsis. *Nat Genet* **27**: 271–6.

Marco-Sola S, Sammeth M, Guigó R, Ribeca P. 2012. The GEM mapper: fast, accurate and versatile alignment by filtration. *Nat Methods* **9**: 1185–1188.

Margolin G, Khil PP, Kim J, Bellani MA, Camerini-Otero RD. 2014. Integrated transcriptome analysis of mouse spermatogenesis. *BMC Genomics* **15**: 39.

Martini E, Diaz RL, Hunter N, Keeney S. 2006. Crossover homeostasis in yeast meiosis. *Cell* **126**:

285–95.

Mateo A-RF, Kessler Z, Jolliffe AK, McGovern O, Yu B, Nicolucci A, Yanowitz JL, Derry WB. 2016. The p53-like Protein CEP-1 Is Required for Meiotic Fidelity in C. elegans. *Curr Biol*.

Matsuoka S, Ballif BA, Smogorzewska A, McDonald ER, Hurov KE, Luo J, Bakalarski CE, Zhao Z, Solimini N, Lerenthal Y, et al. 2007. ATM and ATR substrate analysis reveals extensive protein networks responsive to DNA damage. *Science* **316**: 1160–6.

Matsuoka S, Rotman G, Ogawa A, Shiloh Y, Tamai K, Elledge SJ. 2000. Ataxia telangiectasia-mutated phosphorylates Chk2 in vivo and in vitro. *Proc Natl Acad Sci U S A* **97**: 10389–94.

Melino G, Bernassola F, Ranalli M, Yee K, Zong WX, Corazzari M, Knight RA, Green DR, Thompson C, Vousden KH. 2004. p73 Induces apoptosis via PUMA transactivation and Bax mitochondrial translocation. *J Biol Chem* **279**: 8076–83.

Merlo P, Fulco M, Costanzo A, Mangiacasale R, Strano S, Blandino G, Taya Y, Lavia P, Levrero M. 2005. A role of p73 in mitotic exit. *J Biol Chem* **280**: 30354–60.

Miller MP, Amon A, Ünal E. 2013. Meiosis I: when chromosomes undergo extreme makeover. *Curr Opin Cell Biol* **25**: 687–96.

Mills AA, Zheng B, Wang XJ, Vogel H, Roop DR, Bradley A. 1999. p63 is a p53 homologue required for limb and epidermal morphogenesis. *Nature* **398**: 708–13.

Miyashita T, Reed JC. 1995. Tumor suppressor p53 is a direct transcriptional activator of the human bax gene. *Cell* **80**: 293–9.

Moens PB, Chen DJ, Shen Z, Kolas N, Tarsounas M, Heng HH, Spyropoulos B. 1997. Rad51 immunocytology in rat and mouse spermatocytes and oocytes. *Chromosoma* **106**: 207–15.

Momand J, Wu HH, Dasgupta G. 2000. MDM2--master regulator of the p53 tumor suppressor protein. *Gene* **242**: 15–29.

Monesi V. 1964. RIBONUCLEIC ACID SYNTHESIS DURING MITOSIS AND MEIOSIS IN THE MOUSE TESTIS. *J Cell Biol* **22**: 521–32.

Montgomery SB, Sammeth M, Gutierrez-Arcelus M, Lach RP, Ingle C, Nisbett J, Guigo R, Dermitzakis ET. 2010. Transcriptome genetics using second generation sequencing in a Caucasian population. *Nature* **464**: 773–7.

Moorhead GBG, Trinkle-Mulcahy L, Ulke-Lemée A. 2007. Emerging roles of nuclear protein phosphatases. *Nat Rev Mol Cell Biol* **8**: 234–44.

Murray-Zmijewski F, Lane DP, Bourdon J-C. 2006. p53/p63/p73 isoforms: an orchestra of isoforms to harmonise cell differentiation and response to stress. *Cell Death Differ* **13**: 962–72.

Myer VE, Young RA. 1998. RNA polymerase II holoenzymes and subcomplexes. *J Biol Chem* **273**: 27757–60.

Nakano K, Vousden KH. 2001. PUMA, a novel proapoptotic gene, is induced by p53. *Mol Cell* **7**: 683–94.

Neale MJ, Keeney S. 2006. Clarifying the mechanics of DNA strand exchange in meiotic recombination. *Nature* **442**: 153–8.

O'Donnell L. 2015. Mechanisms of spermiogenesis and spermiation and how they are disturbed. *Spermatogenesis* **4**: e979623.

Oatley JM, Brinster RL. 2012. The germline stem cell niche unit in mammalian testes. *Physiol Rev* **92**: 577–95.

Oda E, Ohki R, Murasawa H, Nemoto J, Shibue T, Yamashita T, Tokino T, Taniguchi T, Tanaka N. 2000. Noxa, a BH3-only member of the Bcl-2 family and candidate mediator of p53-induced apoptosis. *Science* **288**: 1053–8.

Ollmann M, Young LM, Di Como CJ, Karim F, Belvin M, Robertson S, Whittaker K, Demsky M, Fisher WW, Buchman A, et al. 2000. Drosophila p53 is a structural and functional homolog of the tumor suppressor p53. *Cell* **101**: 91–101.

Oren M. 1994. Relationship of p53 to the control of apoptotic cell death. *Semin Cancer Biol* **5**: 221–7.

Osada M, Ohba M, Kawahara C, Ishioka C, Kanamaru R, Katoh I, Ikawa Y, Nimura Y, Nakagawara A, Obinata M, et al. 1998. Cloning and functional analysis of human p51, which structurally and functionally resembles p53. *Nat Med* **4**: 839–43.

Pacheco S, Marcet-Ortega M, Lange J, Jasin M, Keeney S, Roig I. 2015. The ATM Signaling Cascade Promotes Recombination-Dependent Pachytene Arrest in Mouse Spermatocytes ed. M. Lichten. *PLOS Genet* **11**: e1005017.

Page J, de la Fuente R, Manterola M, Parra MT, Viera A, Berríos S, Fernández-Donoso R, Rufas JS. 2012. Inactivation or non-reactivation: what accounts better for the silence of sex chromosomes during mammalian male meiosis? *Chromosoma* **121**: 307–26.

Page J, Suja JA, Santos JL, Rufas JS. 1998. Squash procedure for protein immunolocalization in meiotic cells. *Chromosome Res* **6**: 639–42.

Page SL, Hawley RS. 2003. Chromosome choreography: the meiotic ballet. *Science* **301**: 785–9.

Page SL, Hawley RS. 2004. The genetics and molecular biology of the synaptonemal complex. *Annu Rev Cell Dev Biol* **20**: 525–58.

Panizza S, Mendoza MA, Berlinger M, Huang L, Nicolas A, Shirahige K, Klein F. 2011. Spo11-accessory proteins link double-strand break sites to the chromosome axis in early meiotic recombination. *Cell* **146**: 372–83.

Parvanov ED, Petkov PM, Paigen K. 2010. Prdm9 controls activation of mammalian recombination hotspots. *Science* **327**: 835.

Pateras IS, Apostolopoulou K, Niforou K, Kotsinas A, Gorgoulis VG. 2009. p57KIP2: “Kip”ing the cell under control. *Mol Cancer Res* **7**: 1902–19.

Paul C, Povey JE, Lawrence NJ, Selfridge J, Melton DW, Saunders PTK. 2007. Deletion of genes implicated in protecting the integrity of male germ cells has differential effects on the incidence of DNA breaks and germ cell loss. *PLoS One* **2**: e989.

Paull TT. 2015. Mechanisms of ATM Activation. *Annu Rev Biochem*.

Peng CY, Graves PR, Thoma RS, Wu Z, Shaw AS, Piwnica-Worms H. 1997. Mitotic and G2 checkpoint control: regulation of 14-3-3 protein binding by phosphorylation of Cdc25C on serine-216. *Science* **277**: 1501–5.

Perera D, Perez-Hidalgo L, Moens PB, Reini K, Lakin N, Syväoja JE, San-Segundo PA, Freire R. 2004. TopBP1 and ATR colocalization at meiotic chromosomes: role of TopBP1/Cut5 in the meiotic recombination checkpoint. *Mol Biol Cell* **15**: 1568–79.

Petitjean A, Mathe E, Kato S, Ishioka C, Tavtigian S V, Hainaut P, Olivier M. 2007. Impact of mutant p53 functional properties on TP53 mutation patterns and tumor phenotype: lessons from recent developments in the IARC TP53 database. *Hum Mutat* **28**: 622–9.

Phatnani HP, Greenleaf AL. 2006. Phosphorylation and functions of the RNA polymerase II CTD. *Genes Dev* **20**: 2922–36.

Pittman DL, Cobb J, Schimenti KJ, Wilson LA, Cooper DM, Brignull E, Handel MA, Schimenti JC. 1998. Meiotic prophase arrest with failure of chromosome synapsis in mice deficient for Dmc1, a germline-specific RecA homolog. *Mol Cell* **1**: 697–705.

Plug AW, Xu J, Reddy G, Golub EI, Ashley T. 1996. Presynaptic association of Rad51 protein with selected sites in meiotic chromatin. *Proc Natl Acad Sci U S A* **93**: 5920–4.

Qiao H, Prasada Rao HBD, Yang Y, Fong JH, Cloutier JM, Deacon DC, Nagel KE, Swartz RK, Strong E, Holloway JK, et al. 2014. Antagonistic roles of ubiquitin ligase HEI10 and SUMO ligase RNF212 regulate meiotic recombination. *Nat Genet* **46**: 194–9.

Refolio E, Cavero S, Marcon E, Freire R, San-Segundo PA. 2011. The Ddc2/ATRIP checkpoint protein monitors meiotic recombination intermediates. *J Cell Sci* **124**: 2488–500.

Reinhardt HC, Schumacher B. 2012. The p53 network: cellular and systemic DNA damage responses in aging and cancer. *Trends Genet* **28**: 128–36.

Reynolds A, Qiao H, Yang Y, Chen JK, Jackson N, Biswas K, Holloway JK, Baudat F, de Massy B, Wang J, et al. 2013. RNF212 is a dosage-sensitive regulator of crossing-over during mammalian meiosis. *Nat Genet* **45**: 269–78.

Robert T, Nore A, Brun C, Maffre C, Crimi B, Bourbon H-M, de Massy B. 2016. The TopoVIB-Like protein family is required for meiotic DNA double-strand break formation. *Science (80-)* **351**: 943–949.

Robinson MD, McCarthy DJ, Smyth GK. 2010. edgeR: a Bioconductor package for differential expression analysis of digital gene expression data. *Bioinformatics* **26**: 139–40.

Robinson MD, Oshlack A. 2010. A scaling normalization method for differential expression analysis of RNA-seq data. *Genome Biol* **11**: R25.

Roeder GS, Bailis JM. 2000. The pachytene checkpoint. *Trends Genet* **16**: 395–403.

Roig I, Dowdle JA, Toth A, de Rooij DG, Jasin M, Keeney S. 2010. Mouse TRIP13/PCH2 is required for recombination and normal higher-order chromosome structure during meiosis. *PLoS Genet* **6**.

Rolland T, Taşan M, Charloteaux B, Pevzner SJ, Zhong Q, Sahni N, Yi S, Lemmens I, Fontanillo C, Mosca R, et al. 2014. A Proteome-Scale Map of the Human Interactome Network. *Cell* **159**: 1212–1226.

Romanienko PJ, Camerini-Otero RD. 2000. The Mouse Spo11 Gene Is Required for Meiotic Chromosome Synapsis. *Mol Cell* **6**: 975–987.

Roos WP, Kaina B. 2006. DNA damage-induced cell death by apoptosis. *Trends Mol Med* **12**: 440–50.

Rotter V, Schwartz D, Almon E, Goldfinger N, Kapon A, Meshorer A, Donehower LA, Levine AJ. 1993. Mice with reduced levels of p53 protein exhibit the testicular giant-cell degenerative syndrome. *Proc Natl Acad Sci U S A* **90**: 9075–9.

Royo H, Polikiewicz G, Mahadevaiah SK, Prosser H, Mitchell M, Bradley A, de Rooij DG, Burgoyne PS, Turner JMA. 2010. Evidence that meiotic sex chromosome inactivation is essential for male fertility. *Curr Biol* **20**: 2117–23.

Royo H, Prosser H, Ruzankina Y, Mahadevaiah SK, Cloutier JM, Baumann M, Fukuda T, Höög C, Tóth A, de Rooij DG, et al. 2013. ATR acts stage specifically to regulate multiple aspects of mammalian meiotic silencing. *Genes Dev* **27**: 1484–94.

Rual J-F, Venkatesan K, Hao T, Hirozane-Kishikawa T, Dricot A, Li N, Berriz GF, Gibbons FD, Dreze M, Ayivi-Guedehoussou N, et al. 2005. Towards a proteome-scale map of the human protein-protein interaction network. *Nature* **437**: 1173–8.

Russell LD, Ettlin RA, Hikim APS, Clegg ED. 1993. Histological and Histopathological Evaluation of the Testis. *Int J Androl* **16**: 83–83.

Sah VP, Attardi LD, Mulligan GJ, Williams BO, Bronson RT, Jacks T. 1995. A subset of p53-deficient embryos exhibit exencephaly. *Nat Genet* **10**: 175–80.

Sancar A, Lindsey-Boltz LA, Unsal-Kaçmaz K, Linn S. 2004. Molecular mechanisms of mammalian DNA repair and the DNA damage checkpoints. *Annu Rev Biochem* **73**: 39–85.

Sanchez Y. 1997. Conservation of the Chk1 Checkpoint Pathway in Mammals: Linkage of DNA Damage to Cdk Regulation Through Cdc25. *Science (80-)* **277**: 1497–1501.

San-Segundo PA, Roeder GS. 1999. Pch2 links chromatin silencing to meiotic checkpoint control.

Cell **97**: 313–24.

Schwartz D, Goldfinger N, Rotter V. 1993. Expression of p53 protein in spermatogenesis is confined to the tetraploid pachytene primary spermatocytes. *Oncogene* **8**: 1487–94.

Serrentino M-E, Chaplais E, Sommermeyer V, Borde V. 2013. Differential association of the conserved SUMO ligase Zip3 with meiotic double-strand break sites reveals regional variations in the outcome of meiotic recombination. *PLoS Genet* **9**: e1003416.

Sherr CJ, Weber JD. 2000. The ARF/p53 pathway. *Curr Opin Genet Dev* **10**: 94–9.

Sjöblom T, Lähdetie J. 1996. Expression of p53 in normal and gamma-irradiated rat testis suggests a role for p53 in meiotic recombination and repair. *Oncogene* **12**: 2499–505.

Sogame N, Kim M, Abrams JM. 2003. Drosophila p53 preserves genomic stability by regulating cell death. *Proc Natl Acad Sci U S A* **100**: 4696–701.

Stevens C, Smith L, La Thangue NB. 2003. Chk2 activates E2F-1 in response to DNA damage. *Nat Cell Biol* **5**: 401–9.

Stracker TH, Roig I, Knobel PA, Marjanović M. 2013. The ATM signaling network in development and disease. *Front Genet* **4**: 37.

Su X, Paris M, Gi YJ, Tsai KY, Cho MS, Lin Y-L, Biernaskie JA, Sinha S, Prives C, Pevny LH, et al. 2009. TAp63 prevents premature aging by promoting adult stem cell maintenance. *Cell Stem Cell* **5**: 64–75.

Subramanian V V, Hochwagen A. 2014. The meiotic checkpoint network: step-by-step through meiotic prophase. *Cold Spring Harb Perspect Biol* **6**: a016675.

Suh E-K, Yang A, Kettenbach A, Bamberger C, Michaelis AH, Zhu Z, Elvin JA, Bronson RT, Crum CP, McKeon F. 2006. p63 protects the female germ line during meiotic arrest. *Nature* **444**: 624–8.

Taketo T, Naumova AK. 2013. Oocyte heterogeneity with respect to the meiotic silencing of unsynapsed X chromosomes in the XY female mouse. *Chromosoma* **122**: 337–49.

Talos F, Nemajerova A, Flores ER, Petrenko O, Moll UM. 2007. p73 suppresses polyploidy and aneuploidy in the absence of functional p53. *Mol Cell* **27**: 647–59.

Tani H, Mizutani R, Salam KA, Tano K, Ijiri K, Wakamatsu A, Isogai T, Suzuki Y, Akimitsu N. 2012. Genome-wide determination of RNA stability reveals hundreds of short-lived noncoding transcripts in mammals. *Genome Res* **22**: 947–56.

Taylor WR, Stark GR. 2001. Regulation of the G2/M transition by p53. *Oncogene* **20**: 1803–15.

Thacker D, Mohibullah N, Zhu X, Keeney S. 2014. Homologue engagement controls meiotic DNA break number and distribution. *Nature* **510**: 241–6.

Tingen C, Kim A, Woodruff TK. 2009. The primordial pool of follicles and nest breakdown in mammalian ovaries. *Mol Hum Reprod* **15**: 795–803.

Tipton AR, Wang K, Oladimeji P, Sufi S, Gu Z, Liu S-T. 2012. Identification of novel mitosis regulators through data mining with human centromere/kinetochore proteins as group queries. *BMC Cell Biol* **13**: 15.

Toh WH, Nam SY, Sabapathy K. 2010. An essential role for p73 in regulating mitotic cell death. *Cell Death Differ* **17**: 787–800.

Tomasini R, Tsuchihara K, Tsuda C, Lau SK, Wilhelm M, Ruffini A, Tsao M, Iovanna JL, Jurisicova A, Melino G, et al. 2009. TAp73 regulates the spindle assembly checkpoint by modulating BubR1 activity. *Proc Natl Acad Sci U S A* **106**: 797–802.

Tomasini R, Tsuchihara K, Wilhelm M, Fujitani M, Rufini A, Cheung CC, Khan F, Itie-Youten A, Wakeham A, Tsao M-S, et al. 2008. TAp73 knockout shows genomic instability with infertility and tumor suppressor functions. *Genes Dev* **22**: 2677–91.

Touati SA, Wassmann K. 2016. How oocytes try to get it right: spindle checkpoint control in meiosis. *Chromosoma* **125**: 321–35.

Tucker PA, Sallai L. 2007. The AAA+ superfamily--a myriad of motions. *Curr Opin Struct Biol* **17**: 641–52.

Turner JMA. 2002. Meiotic sex chromosome inactivation in male mice with targeted disruptions of Xist. *J Cell Sci* **115**: 4097–4105.

Turner JMA. 2015. Meiotic Silencing in Mammals. *Annu Rev Genet* **49**: 395–412.

Turner JMA, Aprelikova O, Xu X, Wang R, Kim S, Chandramouli GVR, Barrett JC, Burgoyne PS, Deng C-X. 2004. BRCA1, histone H2AX phosphorylation, and male meiotic sex chromosome inactivation. *Curr Biol* **14**: 2135–42.

Turner JMA, Mahadevaiah SK, Fernandez-Capetillo O, Nussenzweig A, Xu X, Deng C-X, Burgoyne PS. 2005. Silencing of unsynapsed meiotic chromosomes in the mouse. *Nat Genet* **37**: 41–7.

Vader G. 2015. Pch2(TRIP13): controlling cell division through regulation of HORMA domains. *Chromosoma* **124**: 333–9.

Vader G, Blitzblau HG, Tame MA, Falk JE, Curtin L, Hochwagen A. 2011. Protection of repetitive DNA borders from self-induced meiotic instability. *Nature* **477**: 115–9.

van den Hurk R, Zhao J. 2005. Formation of mammalian oocytes and their growth, differentiation and maturation within ovarian follicles. *Theriogenology* **63**: 1717–51.

Vernole P, Neale MH, Barcaroli D, Munarriz E, Knight RA, Tomasini R, Mak TW, Melino G, De Laurenzi V. 2009. TAp73alpha binds the kinetochore proteins Bub1 and Bub3 resulting in polyploidy. *Cell Cycle* **8**: 421–9.

Vogelstein B, Lane D, Levine AJ. 2000. Surfing the p53 network. *Nature* **408**: 307–10.

Wang K, Sturt-Gillespie B, Hittle JC, Macdonald D, Chan GK, Yen TJ, Liu S-T. 2014. Thyroid hormone

receptor interacting protein 13 (TRIP13) AAA-ATPase is a novel mitotic checkpoint-silencing protein. *J Biol Chem* **289**: 23928–37.

Wang S, Zickler D, Kleckner N, Zhang L. 2015. Meiotic crossover patterns: obligatory crossover, interference and homeostasis in a single process. *Cell Cycle* **14**: 305–14.

White-Cooper H, Bausek N. 2010. Evolution and spermatogenesis. *Philos Trans R Soc Lond B Biol Sci* **365**: 1465–80.

Wojtasz L, Cloutier JM, Baumann M, Daniel K, Varga J, Fu J, Anastassiadis K, Stewart AF, Reményi A, Turner JMA, et al. 2012. Meiotic DNA double-strand breaks and chromosome asynapsis in mice are monitored by distinct HORMAD2-independent and -dependent mechanisms. *Genes Dev* **26**: 958–73.

Wojtasz L, Daniel K, Roig I, Bolcun-Filas E, Xu H, Boonsanay V, Eckmann CR, Cooke HJ, Jasin M, Keeney S, et al. 2009. Mouse HORMAD1 and HORMAD2, two conserved meiotic chromosomal proteins, are depleted from synapsed chromosome axes with the help of TRIP13 AAA-ATPase. *PLoS Genet* **5**: e1000702.

Wu H-Y, Burgess SM. 2006. Two distinct surveillance mechanisms monitor meiotic chromosome metabolism in budding yeast. *Curr Biol* **16**: 2473–9.

Yan S, Michael WM. 2009. TopBP1 and DNA polymerase-alpha directly recruit the 9-1-1 complex to stalled DNA replication forks. *J Cell Biol* **184**: 793–804.

Yang A, Kaghad M, Caput D, McKeon F. 2002. On the shoulders of giants: p63, p73 and the rise of p53. *Trends Genet* **18**: 90–5.

Yang A, Kaghad M, Wang Y, Gillett E, Fleming MD, Dötsch V, Andrews NC, Caput D, McKeon F. 1998. p63, a p53 Homolog at 3q27–29, Encodes Multiple Products with Transactivating, Death-Inducing, and Dominant-Negative Activities. *Mol Cell* **2**: 305–316.

Yang A, Walker N, Bronson R, Kaghad M, Oosterwegel M, Bonnin J, Vagner C, Bonnet H, Dikkes P, Sharpe A, et al. 2000. p73-deficient mice have neurological, pheromonal and inflammatory defects but lack spontaneous tumours. *Nature* **404**: 99–103.

Yazdi PT, Wang Y, Zhao S, Patel N, Lee EY-HP, Qin J. 2002. SMC1 is a downstream effector in the ATM/NBS1 branch of the human S-phase checkpoint. *Genes Dev* **16**: 571–82.

Yoon M-K, Ha J-H, Lee M-S, Chi S-W. 2015. Structure and apoptotic function of p73. *BMB Rep* **48**: 81–90.

Yoshida K, Kondoh G, Matsuda Y, Habu T, Nishimune Y, Morita T. 1998. The mouse RecA-like gene Dmc1 is required for homologous chromosome synapsis during meiosis. *Mol Cell* **1**: 707–18.

Yuan L, Liu JG, Hoja MR, Lightfoot DA, Höög C. 2001. The checkpoint monitoring chromosomal pairing in male meiotic cells is p53-independent. *Cell Death Differ* **8**: 316–7.

Zakharyevich K, Ma Y, Tang S, Hwang PY-H, Boiteux S, Hunter N. 2010. Temporally and biochemically distinct activities of Exo1 during meiosis: double-strand break resection and resolution of double Holliday junctions. *Mol Cell* **40**: 1001–15.

Zanders S, Alani E. 2009. The pch2Δ Mutation in Baker's Yeast Alters Meiotic Crossover Levels and Confers a Defect in Crossover Interference ed. G.P. Copenhaver. *PLoS Genet* **5**: e1000571.

Zhu J, Jiang J, Zhou W, Chen X. 1998. The potential tumor suppressor p73 differentially regulates cellular p53 target genes. *Cancer Res* **58**: 5061–5.

Zickler D, Kleckner N. 1999. Meiotic chromosomes: integrating structure and function. *Annu Rev Genet* **33**: 603–754.

Zickler D, Kleckner N. 2015. Recombination, Pairing, and Synapsis of Homologs during Meiosis. *Cold Spring Harb Perspect Biol* **7**.

ANNEX

8. ANNEX

Table 8.1 Overexpressed genes in *Trip13* mutant

Gene name	logFC	P-Value	FDR	Chromosome	Cluster
Hoxd13	-4.3039918	3.8518E-64	2.087E-60	2	#N/A
1700080O16Rik	-2.7140702	2.1804E-38	7.0885E-35	X	E
RP23-280E8.2	-1.544953	2.3767E-32	6.4389E-29	X	#N/A
Ccnb3	-1.2059372	2.5392E-31	5.8963E-28	X	B
Gm7173	-1.9039167	5.6655E-25	6.7687E-22	X	#N/A
Zfy2	-1.4992904	5.8297E-25	6.7687E-22	Y	#N/A
Zfy1	-1.4746743	5.5148E-25	6.7687E-22	Y	#N/A
Gm5753	-3.1651237	1.248E-24	1.3525E-21	X	#N/A
Gm4911	-1.8372354	6.1093E-22	6.2067E-19	X	#N/A
Pet2	-1.1682045	1.2643E-21	1.1418E-18	X	B
Tktl1	-0.8028177	3.797E-19	2.4688E-16	X	B
Tsga8	-2.1589536	6.2277E-18	3.4908E-15	X	E
Usp9y	-0.9167251	1.2612E-17	6.6134E-15	Y	B
Alx3	-2.0922106	1.3376E-17	6.7944E-15	3	#N/A
3830403N18Rik	-1.450128	3.0591E-17	1.4625E-14	X	#N/A
Magea10	-1.1413396	5.9474E-17	2.7621E-14	X	B
Supt20-ps	-1.2733882	1.4977E-16	6.5798E-14	X	#N/A
RP23-328P19.4	-1.4648749	4.6937E-16	1.9563E-13	3	#N/A
Nxt2	-1.0146956	7.2261E-16	2.9365E-13	X	B
Prame	-1.9711242	8.9509E-16	3.5487E-13	X	#N/A
Ccdc177	-1.9438347	3.637E-15	1.3749E-12	12	#N/A
Cdkn1c	-0.8553643	5.4475E-15	1.925E-12	7	A
Gm9	-1.7899282	8.6489E-15	2.8774E-12	X	E
H2bfm	-1.4126567	1.6705E-14	5.2219E-12	X	#N/A
Rhox2d	-1.6287591	1.9693E-14	6.0398E-12	X	#N/A
Xk	-0.8162722	2.8726E-14	8.647E-12	X	B
Foxa2	-1.9692298	4.6617E-14	1.3531E-11	2	#N/A
Abcd1	-0.7286285	4.9616E-13	1.1202E-10	X	C
Otud6a	-1.2183344	6.7245E-13	1.4574E-10	X	#N/A
Pcdh8	-1.5759375	1.2834E-12	2.589E-10	X	B
1700013H16Rik	-0.8060756	1.2901E-12	2.589E-10	14	E
Mageb17-ps	-1.2225431	1.3396E-12	2.6235E-10	X	#N/A
Apob	-1.7209116	1.4465E-12	2.7635E-10	12	#N/A
Maoa	-0.7042803	1.4621E-12	2.7635E-10	X	B
Gm371	-0.8874973	2.4991E-12	4.5643E-10	X	#N/A
Gm5071	-1.8630904	3.025E-12	5.4635E-10	X	#N/A
Elavl3	-0.8847715	7.1767E-12	1.228E-09	9	C
3830417A13Rik	-1.6654976	1.4151E-11	2.3472E-09	X	E
Npr2	-0.666628	2.0982E-11	3.4451E-09	4	A
Gm773	-0.8006855	2.5085E-11	4.0775E-09	X	B
Dmrtc1c1	-0.8312288	4.5576E-11	7.1235E-09	X	#N/A
Dmrtc1c2	-0.8203094	8.8015E-11	1.2774E-08	X	#N/A
Gm650	-1.1910767	1.6456E-10	2.306E-08	X	#N/A
Abcb4	-1.7575296	3.4678E-10	4.6975E-08	5	#N/A
Usp11	-0.5654829	6.1695E-10	7.8348E-08	X	A

Fmr1	-0.4837301	7.1181E-10	8.9004E-08	X	B
Fndc3c1	-1.289788	8.38E-10	1.032E-07	X	#N/A
Taf9b	-0.5193741	1.0723E-09	1.2631E-07	X	B
Usp26	-0.470217	1.0986E-09	1.2847E-07	X	B
Ltk	-1.3474641	1.1472E-09	1.3319E-07	2	#N/A
Srgap1	-0.8440006	1.3761E-09	1.5642E-07	10	E
Pmaip1	-0.7691144	1.5749E-09	1.7656E-07	18	B
BC023829	-0.4953352	1.707E-09	1.8875E-07	X	B
5730457N03Rik	-1.6333142	2.8651E-09	3.064E-07	6	#N/A
Rhox2g	-1.5877296	3.9752E-09	4.1688E-07	X	#N/A
Slc35a2	-0.5516061	4.1389E-09	4.3127E-07	X	C
Scml1	-0.9231293	5.029E-09	5.1738E-07	X	#N/A
Scml2	-0.5199983	5.3462E-09	5.4656E-07	X	B
Tex16	-0.4573251	9.7405E-09	9.3136E-07	X	B
Rhox2f	-1.2912115	1.099E-08	1.0447E-06	X	#N/A
A830018L16Rik	-1.2487204	1.6499E-08	1.5325E-06	1	#N/A
Xlr	-0.8365351	1.9669E-08	1.7962E-06	X	#N/A
Rhox2h	-1.4185101	3.1329E-08	2.6662E-06	X	#N/A
Cyp4f17	-1.1476196	3.7502E-08	3.1205E-06	17	#N/A
Gm595	-1.0323419	3.7626E-08	3.1205E-06	X	E
Rhox13	-0.4945382	4.0315E-08	3.3097E-06	X	#N/A
Foxd2	-1.0685051	5.8906E-08	4.7168E-06	4	#N/A
Tex264	-0.4172813	8.869E-08	6.931E-06	9	D
Gm6038	-0.8319467	1.203E-07	9.138E-06	X	#N/A
Gm6207	-0.7942627	1.222E-07	9.1962E-06	X	#N/A
Piga	-0.5737855	1.2616E-07	9.4067E-06	X	A
AU022751	-0.5701061	1.2609E-07	9.4067E-06	X	B
Wdfy1	-1.0405665	1.3021E-07	9.6646E-06	1	E
Magea4	-0.9522146	1.3301E-07	9.8277E-06	X	#N/A
Irx2	-1.1680003	1.444E-07	1.0573E-05	13	#N/A
Mageb18	-0.8736122	1.4708E-07	1.0721E-05	X	#N/A
Xaf1	-1.4447872	1.6105E-07	1.1584E-05	11	#N/A
Dmrta2	-1.1768323	1.6437E-07	1.177E-05	4	#N/A
Gm6215	-0.7715882	2.252E-07	1.5577E-05	X	#N/A
Tfap2e	-1.2300774	2.5091E-07	1.7209E-05	4	#N/A
Gabrb3	-0.9214693	2.5798E-07	1.762E-05	7	#N/A
Phf2	-0.4639373	3.0069E-07	2.0281E-05	13	D
Abcg4	-0.8892219	3.035E-07	2.0386E-05	9	A
Alpk3	-1.1895536	3.0929E-07	2.069E-05	7	#N/A
Ube2a	-0.5682127	3.2313E-07	2.1527E-05	X	B
Dnajc12	-0.6882517	3.5478E-07	2.3443E-05	10	C
Esx1	-0.4531886	4.3803E-07	2.8255E-05	X	B
Slc6a8	-0.5745561	4.4849E-07	2.8815E-05	X	A
Prps1	-0.4053128	4.5212E-07	2.8934E-05	X	B
Uba1y	-0.3630229	4.566E-07	2.8992E-05	Y	#N/A
Efhc2	-0.8211616	4.6461E-07	2.9272E-05	X	E
Tbx4	-0.9780916	5.9707E-07	3.6903E-05	11	#N/A
Gm1140	-0.7259651	6.1422E-07	3.7676E-05	X	#N/A
Taf7l	-0.4324687	6.7085E-07	4.0841E-05	X	B
Gm6228	-0.7461949	7.3021E-07	4.4289E-05	X	#N/A
Mageb1	-0.9818932	8.0397E-07	4.8582E-05	X	#N/A
Gm14692	-0.7123616	8.5297E-07	5.1056E-05	X	#N/A

Mageb2	-0.9214531	8.9693E-07	5.3405E-05	X	#N/A
Magea2	-1.1231655	1.0846E-06	6.3191E-05	X	#N/A
Tfcp2l1	-0.4223449	1.4084E-06	8.1183E-05	1	B
Eif2s3y	-0.3802877	1.5513E-06	8.8792E-05	Y	B
Atp11c	-0.3739301	1.5747E-06	8.9498E-05	X	B
Tmem121	-1.1127808	1.5907E-06	9.0093E-05	12	#N/A
Vbp1	-0.4228854	2.0372E-06	0.00011187	X	B
Gm15205	-0.9310918	2.0942E-06	0.00011423	X	#N/A
Plxna3	-0.6513312	2.2423E-06	0.0001215	X	A
Slc10a3	-0.4808646	2.5291E-06	0.00013568	X	B
Nsdhl	-0.4375281	3.4424E-06	0.00017935	X	A
Gm5345	-1.0151072	4.1539E-06	0.00021367	8	#N/A
Gm16441	-0.8884913	5.2192E-06	0.00026347	X	#N/A
Fgfrl1	-0.3574525	5.7066E-06	0.00028542	5	B
Pramel3	-0.8498621	6.3696E-06	0.00031567	X	#N/A
Bcap31	-0.3699434	8.4116E-06	0.00040688	X	B
Rbmx2	-0.3755748	1.7172E-05	0.00078851	X	B
Txlng	-0.3384033	1.7517E-05	0.00079981	X	#N/A
Pcbd1	-0.9873301	1.7854E-05	0.00081068	10	#N/A
Cetn2	-0.4054205	2.0504E-05	0.00091814	X	A
Tex11	-0.2863764	2.1406E-05	0.0009533	X	B
Psd2	-0.7702852	2.6409E-05	0.00114474	18	#N/A
Dlg3	-0.4794546	3.3307E-05	0.00141729	X	C
Nyx	-1.0318834	3.5574E-05	0.00150196	X	#N/A
Magea6	-0.7768176	3.7945E-05	0.0015938	X	#N/A
Suv39h1	-0.3010231	4.2542E-05	0.0017641	X	B
Magea5	-0.6199273	4.2709E-05	0.00176532	X	#N/A
Clcf1	-0.7049515	4.3076E-05	0.00177265	19	#N/A
Faxc	-0.5305015	4.3742E-05	0.00179554	4	#N/A
Cldn34b1	-0.7469308	4.5574E-05	0.00186602	X	#N/A
Tmem56	-0.4189872	4.9167E-05	0.0019881	3	E
Fam46d	-0.4638479	5.0131E-05	0.00201701	X	#N/A
Slc7a2	-0.3462948	5.5776E-05	0.00221671	8	B
Tbc1d8b	-0.3651556	5.9994E-05	0.00236699	X	B
Ppef1	-1.0932674	6.4746E-05	0.00253603	X	E
Magea8	-0.6306112	6.564E-05	0.00255869	X	#N/A
Uty	-0.3595678	7.1105E-05	0.00276512	Y	B
Hprt	-0.3273468	7.1909E-05	0.00278969	X	B
Ikbip	-0.3911422	7.8372E-05	0.00300455	10	A
Ap1s2	-0.3440613	8.1317E-05	0.00311012	X	B
Gm2098	-0.3244258	9.0744E-05	0.00343833	Y	#N/A
Rpgr	-0.4471613	9.4062E-05	0.00355578	X	B
Pabpc1l2b-ps	-0.7805428	0.00010041	0.00376088	X	#N/A
Ribc1	-0.5710336	0.00010439	0.00389193	X	E
Gpx8	-0.4603716	0.00011184	0.00415049	13	A
BC067074	-0.5291431	0.00011897	0.00438532	13	A
Ercc6l	-0.3446594	0.00012776	0.00468791	X	A
AV320801	-0.5798586	0.00012808	0.00468907	X	#N/A
Gyg	-0.4055514	0.00014365	0.00521226	3	A
Bex1	-0.4788206	0.00015002	0.00539516	X	A
Tsc22d3	-0.2991701	0.00015398	0.00552531	X	B
Ryr2	-0.8216779	0.00015919	0.00566946	X	#N/A

Rhox1	-0.6715154	0.00015939	0.00566946	13	A
St7	-0.4327674	0.00018402	0.00641899	6	C
Tsr2	-0.3276677	0.00018945	0.00659427	X	B
Ppwd1	-0.3260237	0.00019374	0.00671477	13	B
Saraf	-0.2628638	0.00021946	0.00747855	8	#N/A
Gm4779	-0.3897684	0.00022254	0.0075521	X	#N/A
Magea3	-0.9172199	0.00023212	0.00781194	X	#N/A
Cib2	-0.5926677	0.00024229	0.00813722	9	#N/A
Gm15023	-0.5865166	0.00025502	0.00852958	X	#N/A
Hsd17b3	-0.4886306	0.0002653	0.00885507	13	A
Zfx	-0.2725226	0.00028947	0.00962246	X	B
Tro	-0.3505146	0.00029251	0.00970344	X	A
2810474O19Rik	-0.32052	0.00031086	0.01014656	6	B
Xlr4b	-0.561773	0.00035142	0.01131154	X	#N/A
Nxf2	-0.2871468	0.00038538	0.01216377	X	B
Slc30a4	-0.2706172	0.00039871	0.01253578	2	B
Rps6ka6	-0.2628589	0.00048455	0.01483292	X	B
Wdr44	-0.3104241	0.00049797	0.01515813	X	B
Tex19.1	-0.2630025	0.00050908	0.01540986	11	A
Cenpi	-0.3450912	0.00051743	0.01560446	X	B
Kdm6a	-0.2606463	0.00057694	0.01720752	X	B
Dmc1	-0.285574	0.00059623	0.01762133	15	B
2610002M06Rik	-0.3050755	0.00060521	0.01785411	X	B
Lonrf2	-0.5781186	0.0006114	0.01797175	1	B
Alg13	-0.2552809	0.00071204	0.02052171	X	B
5031439G07Rik	-0.2554673	0.00074423	0.02122352	15	E
Pbdc1	-0.2925102	0.0007837	0.02219337	X	#N/A
Atp6ap2	-0.3056242	0.00079966	0.02256689	X	B
Mageb6-ps	-0.5899011	0.00081739	0.02294773	X	#N/A
Idh3g	-0.2793907	0.00082933	0.02324275	X	B
Pabpc1l2a-ps	-0.7520981	0.00084104	0.02353017	X	#N/A
Apool	-0.3742703	0.00087059	0.0242517	X	A
Pygo1	-0.3088875	0.00090132	0.02504451	9	A
Slc25a14	-0.3792047	0.00090948	0.02522809	X	B
Cdk1	-0.3120856	0.0009549	0.02630825	10	C
Nuak1	-0.3820859	0.00098191	0.02691566	10	A
Aplp1	-0.4572333	0.00104878	0.02850811	7	D
Dynlt3	-0.302733	0.00105379	0.02854884	X	B
Nkap	-0.3415227	0.00106077	0.02869026	X	B
Map3k15	-0.3640896	0.00109811	0.02965092	X	#N/A
Gata3	-0.9841415	0.00113169	0.0304065	2	#N/A
Bex2	-0.3325256	0.00114966	0.03073632	X	A
Pbx3	-0.3006171	0.00118592	0.03149869	2	B
Ebf3	-0.29808	0.00119453	0.0316756	7	B
Gm7061	-0.5114274	0.00123372	0.03260837	X	#N/A
Lhfpl4	-0.7404996	0.00123921	0.03270026	6	#N/A
Npdc1	-0.3177252	0.00125177	0.03297821	2	A
Ppp1r3fos	-0.633562	0.00128091	0.03363688	X	#N/A
Crmp1	-0.8592735	0.00133376	0.03461134	8	B
Usp51	-0.6821221	0.00133161	0.03461134	5	C
Gm15017	-0.6725254	0.00133505	0.03461134	X	#N/A
Asah1	-0.2233611	0.00133236	0.03461134	X	#N/A

Rad21l	-0.3355452	0.00138315	0.03574419	2	#N/A
Fgf2	-0.3589929	0.00145801	0.03744828	3	#N/A
Mbtps2	-0.2697081	0.00147832	0.03778311	X	B
Rdh11	-0.3610988	0.00150435	0.03832786	12	D
Yipf6	-0.262077	0.00151522	0.03848414	X	B
A830080D01Rik	-0.2467052	0.00161471	0.04056753	X	B
Syngr2	-0.2370591	0.0016248	0.04075779	11	C
Trim52	-0.3219522	0.00171865	0.04285684	14	B
Hspa13	-0.2649786	0.0017281	0.04295145	16	#N/A
Cyp46a1	-0.5610384	0.0017572	0.04340916	12	C
Pdzd4	-0.4544886	0.00179147	0.04405495	X	A
Nkrf	-0.3078992	0.00182543	0.04468737	X	B
Ifngr1	-0.266646	0.00183996	0.04496348	10	C
Gmds	-0.2821265	0.00185318	0.04509501	13	B
Lrch2	-0.3225741	0.00187616	0.04558587	X	A
Asb1	-0.2661504	0.00194191	0.04683347	1	C
Mmgt1	-0.2948245	0.00195687	0.04705458	X	B
Xlr4c	-0.5109194	0.00197953	0.04752915	X	#N/A
Aldh1a2	-0.2079807	0.00198641	0.04753122	9	D
Cdh4	-0.7187891	0.00204228	0.0487477	2	#N/A

Table 8.2 Overexpressed genes in wild type mice

Gene name	logFC	P-Value	FDR	Chromosome	Cluster
Trip13	2.482550624	2.2675E-149	3.6858E-145	13	B
Cldn23	4.794879712	1.22786E-64	9.97944E-61	8	#N/A
Fbp1	4.391364153	1.07607E-39	4.37288E-36	13	D
Abcc12	4.058359178	5.56189E-30	1.13011E-26	8	D
1700074P13Rik	8.458032827	7.46285E-28	1.34787E-24	6	E
Hrasls5	4.77921339	2.03794E-26	3.28532E-23	19	E
RP24-456F12.1	6.307863969	2.22323E-26	3.28532E-23	5	#N/A
Rbakdn	4.354008078	6.63083E-22	6.34025E-19	5	#N/A
1700020N18Rik	5.179865789	2.48967E-21	2.12998E-18	1	#N/A
Qrich2	4.090371844	8.99567E-21	7.31123E-18	11	E
4930544G11Rik	4.982319602	1.80803E-20	1.3995E-17	6	D
Tmbim7	5.353942178	5.1229E-20	3.78513E-17	5	#N/A
4930430A15Rik	4.449146035	1.21857E-19	8.61214E-17	2	D
Gm5878	4.338650411	1.28561E-19	8.70735E-17	6	D
RP23-42M8.7	4.616710565	4.51486E-19	2.82266E-16	6	#N/A
Fam181a	4.04181841	5.79408E-19	3.48825E-16	12	#N/A
Cfap70	2.959912766	7.90518E-19	4.58924E-16	14	#N/A
Aqp9	3.421179266	1.18985E-17	6.447E-15	9	D
Ccdc144b	3.929663822	1.70052E-17	8.37636E-15	3	D
Mroh2b	3.567198475	9.39541E-17	4.24229E-14	15	#N/A
Atp8b3	2.68180001	2.63631E-16	1.12772E-13	10	E
Nnt	0.751080359	1.32367E-15	5.1229E-13	13	D
Gm1698	3.888133137	4.3659E-15	1.6129E-12	8	D
Armc3	3.999203902	5.00904E-15	1.80938E-12	2	D
Ldhc	2.995038316	6.84453E-15	2.36719E-12	7	D
Adam5	3.267147534	8.6738E-15	2.8774E-12	8	D
Erich2	2.759327522	1.0208E-14	3.31863E-12	2	E
Slc2a3	1.501483768	1.54265E-14	4.91682E-12	6	D
Prok2	1.929079704	3.18901E-14	9.42496E-12	6	D
Dnah1	1.754049418	7.53114E-14	2.1477E-11	14	#N/A
March10	2.99937373	7.86835E-14	2.20517E-11	11	E
Spink2	2.677023597	1.06336E-13	2.92963E-11	5	D
Cmtm2a	3.913899177	1.12014E-13	3.03464E-11	8	E
Cetn1	2.741583606	1.21369E-13	3.23418E-11	18	D
Pifo	3.859769875	1.241E-13	3.25362E-11	3	E
Spata31d1a	2.611341037	1.29481E-13	3.34081E-11	13	E
Piwil1	2.805538029	1.42854E-13	3.62827E-11	5	D
Poteg	3.00401665	1.49768E-13	3.74535E-11	8	#N/A
4933404O12Rik	1.596849609	1.56057E-13	3.8435E-11	5	#N/A
Dnah17	1.457732513	1.67079E-13	4.05355E-11	11	D
1700011E24Rik	4.943475754	2.79356E-13	6.67784E-11	17	D
Fam170a	3.265327253	3.79875E-13	8.9491E-11	18	D
Gk2	2.446599997	4.22576E-13	9.81281E-11	5	D
RP23-412L13.5	4.189947484	4.76168E-13	1.09016E-10	3	#N/A
Gykl1	3.067682357	5.35896E-13	1.19329E-10	18	E
Ropn1l	1.680708562	6.36417E-13	1.39797E-10	15	E

Tex40	2.340214975	1.03197E-12	2.12337E-10	15	D
Mapk15	2.369578435	1.0274E-12	2.12337E-10	18	E
Tcp11	2.537870669	1.02712E-12	2.12337E-10	17	E
Pabpc2	4.293381912	1.00286E-12	2.12337E-10	19	E
Iqub	2.789137253	1.31874E-12	2.61415E-10	6	E
RP24-297N9.13	3.167362776	1.4176E-12	2.74322E-10	5	#N/A
4922502D21Rik	2.1086999	1.8167E-12	3.39431E-10	6	D
5330417C22Rik	1.462950828	2.44452E-12	4.51542E-10	3	D
Tsnaxip1	2.457255498	3.24534E-12	5.76558E-10	1	#N/A
Daw1	3.224442048	3.2632E-12	5.76558E-10	8	D
Smpd5	2.684232601	3.3832E-12	5.91332E-10	15	#N/A
Spata16	2.243649258	5.92028E-12	1.02377E-09	3	D
Cdkl4	2.073974725	7.84395E-12	1.32816E-09	17	D
Hydin	1.758934032	1.05757E-11	1.77225E-09	8	D
E230008N13Rik	1.995760445	3.07503E-11	4.94898E-09	4	#N/A
Chst1	1.759110783	3.27861E-11	5.22488E-09	2	D
1700003M02Rik	2.375248355	4.4483E-11	7.02012E-09	4	D
Tekt1	2.740473729	5.02335E-11	7.77663E-09	11	D
Dpy19l2	2.145585382	6.34163E-11	9.72483E-09	9	#N/A
Elfn2	1.755307966	6.7065E-11	1.01882E-08	15	D
Triml2	1.518279055	6.97172E-11	1.04931E-08	8	#N/A
1700010I14Rik	1.835909994	7.20435E-11	1.07437E-08	17	D
Papolb	1.166283638	7.82486E-11	1.1563E-08	5	E
RP24-289G19.2	3.26493784	7.9271E-11	1.16086E-08	5	#N/A
4930444P10Rik	2.456337156	8.89573E-11	1.27965E-08	1	#N/A
Crisp2	1.753475148	1.32764E-10	1.89305E-08	17	D
Gm20621	1.655016179	1.34526E-10	1.90149E-08	15	#N/A
D130043K22Rik	1.744968004	2.05825E-10	2.85956E-08	13	D
Spag17	2.752631601	2.31131E-10	3.18393E-08	3	D
Odf4	3.242808095	2.39758E-10	3.27501E-08	11	D
Gm10619	4.351910241	3.55142E-10	4.77094E-08	7	D
Cfap52	2.705452459	3.59215E-10	4.7861E-08	11	D
1700006A11Rik	3.800677812	3.64925E-10	4.82264E-08	3	D
Ccdc65	2.389854744	3.76688E-10	4.93796E-08	15	D
Wdr63	2.763927895	4.4794E-10	5.77879E-08	16	#N/A
Tmem30c	2.842231445	4.45794E-10	5.77879E-08	3	D
Cct6b	1.770871543	6.00946E-10	7.69163E-08	11	D
Ms4a13	2.517089661	6.84392E-10	8.62387E-08	19	D
Mdh1b	2.310132193	7.21634E-10	8.95432E-08	1	D
Cfap46	2.424283184	9.05492E-10	1.10668E-07	7	#N/A
Cox8c	1.390187507	9.29303E-10	1.1273E-07	12	D
Cfap45	2.054482474	9.45429E-10	1.13837E-07	1	#N/A
Spata4	2.074567151	9.98897E-10	1.1939E-07	8	D
Mgat4d	2.797182225	1.03595E-09	1.22915E-07	8	D
Adam32	2.075400805	1.1659E-09	1.34409E-07	8	D
Drc1	1.912436569	1.20485E-09	1.37921E-07	5	#N/A
Cfap74	1.467593074	1.40244E-09	1.5831E-07	4	D
Dnali1	1.937116239	1.68174E-09	1.87237E-07	4	D
Cfap54	1.239467295	1.80666E-09	1.98428E-07	10	D
Wdr66	1.541490102	2.04294E-09	2.22872E-07	5	D
Drc7	2.515406402	2.60246E-09	2.8202E-07	8	D
4930463O16Rik	1.937702955	2.74982E-09	2.96016E-07	10	#N/A

Adam2	1.896465641	2.88684E-09	3.06703E-07	14	D
4930465K10Rik	1.826987173	3.91868E-09	4.13624E-07	18	D
Tdrd6	2.226286882	4.80027E-09	4.96996E-07	17	D
Trim11	0.684320316	5.69326E-09	5.74807E-07	11	C
Ypel1	0.878810691	5.65821E-09	5.74807E-07	16	D
Tcp10a	2.233788059	5.97571E-09	5.99599E-07	17	D
Spag16	1.40527158	6.70079E-09	6.68229E-07	1	D
Stambp	0.774835514	6.83598E-09	6.77554E-07	6	C
Gstt2	1.299849918	7.11577E-09	6.98476E-07	2	D
4932414N04Rik	2.358911538	7.13301E-09	6.98476E-07	10	C
Ccdc146	1.61905353	8.08372E-09	7.86832E-07	5	E
Gm27045	2.438492965	8.50431E-09	8.22842E-07	8	#N/A
Lin7a	1.970705672	9.43524E-09	9.07513E-07	10	D
Krt8	2.094520539	1.25403E-08	1.18513E-06	15	#N/A
Fabp9	1.851002139	1.26829E-08	1.19168E-06	3	D
Gm14244	3.529590904	1.31237E-08	1.22601E-06	2	#N/A
Bspry	1.031831161	1.72836E-08	1.59627E-06	4	E
Ccdc89	1.951632454	1.84738E-08	1.69656E-06	7	#N/A
Nup210l	1.065249793	2.10537E-08	1.90127E-06	16	#N/A
Cfap44	1.715357748	2.10327E-08	1.90127E-06	3	#N/A
Spag8	1.448974334	2.19538E-08	1.96077E-06	4	D
Zmynd10	1.882834103	2.18856E-08	1.96077E-06	9	D
Cers3	1.30034982	2.34746E-08	2.08513E-06	7	#N/A
Lypd4	1.581059443	2.42172E-08	2.13941E-06	7	E
Lrguk	1.393824535	2.58612E-08	2.27229E-06	6	D
Dnah7c	1.261191314	2.64843E-08	2.31453E-06	1	#N/A
Gtf2a1l	1.739071772	2.6645E-08	2.31612E-06	17	E
Dnah7b	0.887080771	2.82724E-08	2.44451E-06	1	#N/A
Fam184a	1.321167799	2.98987E-08	2.57145E-06	10	#N/A
Ptchd3	1.78186377	3.12252E-08	2.66623E-06	11	D
AY702103	2.932429882	3.29054E-08	2.78582E-06	17	#N/A
Lrrc23	2.059357516	3.36369E-08	2.83299E-06	6	D
Mroh4	2.262576313	3.40328E-08	2.85156E-06	15	#N/A
Iqcd	1.754951599	3.87532E-08	3.19763E-06	5	D
Ift172	0.729430469	4.06831E-08	3.32314E-06	5	D
Gm13814	2.33390412	4.82348E-08	3.92028E-06	2	#N/A
Dnah6	2.12010391	5.74111E-08	4.63509E-06	4	D
1700042G15Rik	4.195632488	5.76E-08	4.63509E-06	6	#N/A
Ppp3r2	1.776519636	6.11996E-08	4.87647E-06	4	D
Cuzd1	3.074000021	6.21368E-08	4.92699E-06	7	E
4931429I11Rik	1.605979807	6.80976E-08	5.37343E-06	9	D
Ttc30a2	1.252753501	8.17251E-08	6.41759E-06	2	D
Slc2a5	1.465829152	9.00705E-08	7.00524E-06	4	E
M5C1000I18Rik	1.627703667	9.37462E-08	7.2564E-06	9	#N/A
Slc9c1	1.88864348	9.9909E-08	7.69678E-06	16	#N/A
Ttc25	1.245851275	1.15641E-07	8.86671E-06	11	E
Fhad1	1.344813614	1.18401E-07	9.03571E-06	4	E
Chgb	1.37020938	1.2159E-07	9.19275E-06	2	D
1700008K24Rik	1.542124336	1.3996E-07	1.02944E-05	17	#N/A
Lrriq1	1.516796747	1.54269E-07	1.11948E-05	10	D
Agbl2	1.322376684	1.57684E-07	1.13918E-05	2	D
Slco2a1	1.187447254	1.75124E-07	1.24853E-05	9	A

Ak8	1.361503018	1.89179E-07	1.34284E-05	2	E
Dnah2	0.867293955	1.94334E-07	1.37344E-05	11	D
Acrbp	1.083180922	1.96195E-07	1.38058E-05	6	E
Nsun7	1.133930841	2.04225E-07	1.43003E-05	17	D
Ldhal6b	1.364076994	2.04981E-07	1.43003E-05	5	E
Krt18	2.052018459	2.09341E-07	1.4542E-05	15	A
1700102P08Rik	1.131973389	2.37986E-07	1.63918E-05	9	C
Spats1	1.700997077	2.67762E-07	1.82112E-05	17	D
Fam229b	1.162994028	2.94133E-07	1.99214E-05	10	E
Ccdc108	2.072683841	3.40369E-07	2.25824E-05	1	D
Gramd1c	0.998019688	3.56854E-07	2.34845E-05	16	D
Dnajb13	2.127405467	3.62658E-07	2.37702E-05	7	E
Gm29050	1.328938267	3.75169E-07	2.44914E-05	17	#N/A
Acr	2.782723459	4.10756E-07	2.67073E-05	15	E
Tmprss12	1.387526574	4.21582E-07	2.7302E-05	15	D
Lrrc6	1.425921293	4.55661E-07	2.89924E-05	15	D
1700040L02Rik	1.162099098	4.62706E-07	2.92657E-05	10	D
Pom121l2	1.65747905	5.14903E-07	3.23156E-05	13	#N/A
Ankrd36	1.530595705	5.19324E-07	3.24677E-05	11	D
Lca5l	0.944196943	5.35698E-07	3.33631E-05	16	D
Dynlrb2	2.186086633	5.87225E-07	3.64326E-05	8	D
Mroh8	1.204019954	6.05331E-07	3.72714E-05	2	#N/A
Prom1	2.094028354	6.24596E-07	3.81685E-05	5	E
Tkfc	0.644243147	8.24505E-07	4.96382E-05	19	D
Cpn1	1.200131667	8.54329E-07	5.10556E-05	19	D
1700018B08Rik	1.502276501	9.33827E-07	5.53991E-05	8	E
Tdrd5	0.740206727	9.77417E-07	5.77742E-05	1	C
Ybx2	0.805501381	9.95806E-07	5.84362E-05	1	D
Ankar	1.928915959	9.93898E-07	5.84362E-05	11	D
Ccdc40	0.865332629	1.07874E-06	6.30751E-05	11	D
Pdcl2	1.316460974	1.10375E-06	6.40765E-05	5	D
6430531B16Rik	1.320969604	1.14545E-06	6.62606E-05	7	D
Abo	1.439918286	1.48314E-06	8.51886E-05	2	D
Dkkl1	1.55335047	1.5576E-06	8.88379E-05	7	E
Dnah14	1.330419641	1.60966E-06	9.08508E-05	1	D
Axdnd1	1.200612425	1.62124E-06	9.11876E-05	1	#N/A
4933411G11Rik	1.380993168	1.7888E-06	0.000100265	5	D
Dnhd1	0.818459322	1.80433E-06	0.000100788	7	#N/A
4933415F23Rik	1.181540944	1.83828E-06	0.000102333	1	D
Lrrc61	0.837912993	1.86424E-06	0.000103424	6	D
Ttc29	1.401838039	2.00064E-06	0.000110614	8	D
Gpx3	1.107874998	2.02602E-06	0.000111637	11	C
Mif4gd	0.584883679	2.09151E-06	0.000114231	11	C
Fam186b	1.696150421	2.21065E-06	0.000120181	15	D
Mag	1.451479732	2.28805E-06	0.000123562	7	D
Smim24	1.292156833	2.52009E-06	0.000135643	10	D
Psma8	0.88555175	2.6466E-06	0.000141515	18	C
Rfx4	2.165011461	2.75037E-06	0.000146581	10	D
Ccdc39	1.062458919	2.85196E-06	0.000151499	3	C
Gm11992	1.006863517	2.92302E-06	0.000154768	11	D
Dnah8	1.205982318	3.01865E-06	0.000159312	17	D
Cfap57	1.346087185	3.07819E-06	0.000161929	4	#N/A

Pxt1	1.089615572	3.2409E-06	0.000169938	17	D
4933408B17Rik	0.969567328	3.40556E-06	0.000177998	18	C
4933412E24Rik	1.434011205	3.78714E-06	0.000196677	15	#N/A
Ptpn20	1.025051983	3.82583E-06	0.000198054	14	D
Pnpla7	0.395205561	4.02791E-06	0.000207853	2	D
Samd7	1.6736769	4.27324E-06	0.000219122	3	D
Ttll9	1.070638922	4.61056E-06	0.000235675	2	E
Xrra1	0.922384603	4.8172E-06	0.000245466	7	E
Ccdc13	1.163019319	4.85734E-06	0.000246738	9	D
AI429214	0.906600912	5.06218E-06	0.000256342	8	D
Gm7068	3.262296944	5.42933E-06	0.000273231	1	#N/A
Usp2	0.71012989	5.68246E-06	0.000285088	9	E
March11	2.016068232	6.22616E-06	0.000310449	15	E
Ddx25	0.525819476	6.31481E-06	0.000313906	9	D
Lrrc27	0.748124218	6.59308E-06	0.000325746	7	E
Agbl5	0.592861991	7.05004E-06	0.000347268	5	D
Ttll13	0.810335961	7.78943E-06	0.000382529	7	E
Ccdc60	1.72100552	7.87817E-06	0.000385722	5	E
Defb42	2.86604846	8.31872E-06	0.000406069	14	#N/A
Als2cr12	1.043225783	8.37024E-06	0.000406878	16	#N/A
Ppp1r36	1.229987704	8.43544E-06	0.000406878	1	D
Sept12	1.242742678	8.41668E-06	0.000406878	12	#N/A
Tdrd1	0.656438479	8.5548E-06	0.000411415	19	C
Mgll	0.49030644	8.62758E-06	0.000413691	6	D
Cul9	0.443533215	8.96619E-06	0.000428663	17	#N/A
4933440M02Rik	2.028681134	9.04612E-06	0.000431216	7	#N/A
Atp8b5	0.918045008	9.14721E-06	0.00043476	4	D
Lrrc29	1.498554885	9.56929E-06	0.000453495	8	C
Spag6	1.646044605	1.06492E-05	0.000503205	2	D
Pgam2	1.694487731	1.08238E-05	0.000509976	11	E
Gm5134	1.126623493	1.16142E-05	0.000545632	10	#N/A
D130017N08Rik	1.10856294	1.18695E-05	0.000556021	5	#N/A
Eno3	0.653303399	1.26025E-05	0.000588661	11	C
5033403F01Rik	1.181918556	1.34518E-05	0.000626528	13	#N/A
Armt1	0.617340592	1.44078E-05	0.000669141	10	C
Rnf182	0.931597535	1.48657E-05	0.000688436	13	#N/A
Zfp820	0.760513504	1.49828E-05	0.000691892	17	C
Prr7	0.793780515	1.70222E-05	0.000783839	13	C
Fbf1	0.503103642	1.72449E-05	0.000789623	11	C
Insl6	1.217692112	1.76072E-05	0.000801693	19	D
Dnaaf1	0.729134441	1.81192E-05	0.000820413	8	E
Ddx4	0.515371541	1.84409E-05	0.000832659	13	C
Dlec1	0.981749829	1.91727E-05	0.000863303	9	#N/A
Tmem232	1.139657381	1.92329E-05	0.00086362	17	E
Fam50b	1.705130027	2.08834E-05	0.000932584	13	E
Trp53	0.502567401	2.1738E-05	0.000965439	11	C
Morn5	0.967392316	2.19873E-05	0.000973854	2	D
Prps1l1	1.648056925	2.42502E-05	0.001071162	12	E
Mtl5	0.572979466	2.45817E-05	0.001079935	3	#N/A
Gm33589	1.15816424	2.45747E-05	0.001079935	19	C
Ttc16	0.846788693	2.52928E-05	0.00110584	2	E
AC133459.1	1.654531066	2.53074E-05	0.00110584	2	D

Wdr93	0.927286874	2.59586E-05	0.001131251	7	D
Ptpdc1	0.487198318	2.6132E-05	0.001135766	13	D
Ube2d2b	1.197170176	2.67388E-05	0.001155956	5	#N/A
Eps8l3	0.981451228	2.7538E-05	0.001187347	3	D
Rnf32	0.839218057	2.89241E-05	0.001242221	7	D
Fank1	1.036947417	2.89635E-05	0.001242221	5	D
Ces1d	1.040632333	2.99333E-05	0.001280435	8	E
Clgn	1.031179963	3.14294E-05	0.001340903	8	D
Ankef1	0.960777346	3.47572E-05	0.001474931	2	E
Susd5	1.05455107	3.4843E-05	0.001474931	9	#N/A
AI464131	0.954572523	3.67529E-05	0.001547715	4	D
C2cd4b	1.350429832	3.91982E-05	0.001642181	9	#N/A
Efhc1	0.843962631	4.13406E-05	0.001727483	1	D
Gm37389	1.591890818	4.17279E-05	0.001739196	3	#N/A
Rsph9	0.841652143	4.22915E-05	0.00175818	17	E
Morc2b	1.78606934	4.27891E-05	0.001765322	17	D
Mok	0.611319651	4.65099E-05	0.001894783	4	C
Fgr	1.076476767	4.64014E-05	0.001894783	12	E
Csl	1.074367777	4.74021E-05	0.001926302	10	E
Ttll6	1.358653004	4.83576E-05	0.001960233	11	E
Cfap43	0.746468081	4.95245E-05	0.001997571	19	E
Gm15881	1.367449215	5.17171E-05	0.002075709	8	#N/A
Arsk	0.475162252	5.38597E-05	0.002156379	13	B
Ubxn11	0.678260458	5.43017E-05	0.002168734	4	#N/A
Lrrc36	0.998744487	5.5124E-05	0.002196179	8	E
Crem	0.681284266	5.68341E-05	0.002253265	18	E
Ift140	0.397076608	5.99585E-05	0.002366989	17	D
Kif6	0.677325362	6.21098E-05	0.00244454	17	D
Cyct	0.645729477	6.29907E-05	0.002473223	2	C
Ccdc87	0.982955419	6.54533E-05	0.002557555	19	D
Ccdc113	1.409129624	7.35743E-05	0.0028475	8	D
Crtam	1.412619127	7.57312E-05	0.002924016	9	D
Trp63	0.784285985	7.62707E-05	0.002937868	16	#N/A
Spef2	1.169331364	7.82473E-05	0.003004553	15	D
1700009C05Rik	2.067663118	8.46885E-05	0.003231482	6	#N/A
Adamts6	0.643114044	8.64808E-05	0.003292144	13	A
1700029M20Rik	0.901226627	8.74261E-05	0.003320353	4	#N/A
Cdc42ep3	0.728446738	9.54042E-05	0.003598132	17	D
Tcte2	0.88456668	9.64312E-05	0.003628446	17	D
Rnls	0.615951773	0.000100274	0.003760881	19	#N/A
Pex11g	0.720414045	0.000103375	0.003862902	8	D
Ccdc136	0.605850217	0.000108844	0.004048662	6	E
Atp11a	0.361384368	0.000116454	0.004311999	8	C
Mum1	0.399482254	0.000118931	0.004385322	10	D
Shcbp1l	0.603686881	0.000121515	0.004468829	1	D
Cchcr1	0.516531404	0.000129969	0.004738965	17	D
Phf7	0.579727768	0.000130026	0.004738965	14	D
Wdfy4	0.645408217	0.000135103	0.004912976	14	D
Pnmal1	1.186308553	0.000145044	0.005250968	7	D
Ptprq	0.966690699	0.000147443	0.005325973	10	D
Ggnbp1	0.482754614	0.000147791	0.0053267	17	E
Ankrd45	0.6661053	0.000154461	0.005530299	1	C

1700016K19Rik	0.90654787	0.000159188	0.00566946	11	E
Dynlt1-ps1	0.413167948	0.000161089	0.00571727	6	#N/A
C530008M17Rik	0.651316705	0.000164356	0.005820488	5	E
9230110C19Rik	0.459371624	0.000169923	0.005991532	9	C
Hsf5	0.737410855	0.000169873	0.005991532	11	D
Dnah7a	1.021656687	0.000170432	0.005996471	1	D
8430419L09Rik	0.530428288	0.000177763	0.006240898	6	D
Ptgs1	1.481932672	0.000180186	0.006312322	2	#N/A
Cd74	0.742888134	0.000183726	0.006418988	18	C
Krt19	1.374871356	0.000190568	0.006618982	11	#N/A
Zfa-ps	0.792943085	0.000194859	0.006739222	10	#N/A
Fam174b	0.683725457	0.000196423	0.006778903	7	#N/A
Mlph	1.055960943	0.000198253	0.006827533	1	#N/A
Meig1	0.823292033	0.000204254	0.007019343	2	D
Cep128	0.608086232	0.000205727	0.007055055	12	#N/A
Sdr39u1	0.482052302	0.000206839	0.007078253	14	C
Fam217a	1.104732313	0.00020857	0.0071225	13	#N/A
Rgs22	0.582395953	0.000219996	0.007481243	15	#N/A
Muc3	0.91060983	0.000227898	0.007717683	5	D
Cpt1b	1.052155604	0.000229435	0.007753563	15	D
Ak9	1.102141583	0.000231203	0.007797118	10	#N/A
Klhdc9	0.77781896	0.00024914	0.008350052	1	D
Pou6f1	0.597297973	0.000272431	0.009074534	15	C
Phf1	0.493859106	0.000294634	0.009754136	17	D
Rapgef1	0.318484892	0.000295291	0.009755994	2	C
Wdr20rt	0.838525133	0.000298633	0.009846394	12	D
Fhl4	0.591464425	0.000305975	0.01006807	10	E
Spata33	0.712146553	0.000308727	0.01013811	8	E
Ankmy1	0.983406052	0.000309367	0.010138644	1	D
Lrat	0.810904517	0.000310084	0.01014169	3	C
Asrgl1	0.500140968	0.000317996	0.010358781	19	D
Tcam1	0.842379432	0.000319388	0.010383319	11	D
Glipr1l2	0.745807297	0.000323511	0.010496337	10	C
Cds1	0.55799829	0.000338582	0.010963433	5	D
Gm128	0.863406194	0.000343125	0.01108846	3	E
4921506M07Rik	0.892399604	0.000349375	0.011268048	12	E
Rfx8	1.222596485	0.000352375	0.011319876	1	#N/A
Sv2c	0.895152459	0.000354298	0.011359201	13	E
Tdrd9	0.45058348	0.000358927	0.011484968	12	C
Gm973	0.740802298	0.000363019	0.011593062	1	E
Dnaaf3	0.674293195	0.000366485	0.011680808	7	E
Fam178b	0.484414076	0.000373043	0.011866566	1	#N/A
Fam13c	0.522991395	0.000378239	0.011991381	10	#N/A
Oscp1	0.631491143	0.000378442	0.011991381	4	D
1700006J14Rik	1.212966644	0.000383886	0.012140211	10	D
Gm15676	1.175169503	0.000396064	0.012476779	-	#N/A
Sphkap	1.449991317	0.000410709	0.012888184	1	#N/A
Iglon5	1.013563445	0.000433428	0.013574892	7	#N/A
Rimbp3	0.865770121	0.00043984	0.013749233	16	#N/A
Khdrbs3	0.516498132	0.000441217	0.013765797	15	C
Pla2g2c	0.831124677	0.000447074	0.013917476	18	#N/A
Cfap53	0.962074986	0.000447791	0.013917476	4	D

Cldn3	0.981271364	0.000452133	0.014025616	5	E
Neat1	0.483567861	0.000457154	0.014154351	19	D
Abhd8	0.451135995	0.000460361	0.014226553	8	D
Slx4	0.321624748	0.000469637	0.014485683	16	#N/A
Pou2f2	0.751926149	0.000474954	0.014621915	7	D
Crat	0.426740495	0.000480102	0.014724623	12	#N/A
Ccdc175	1.033568951	0.000479779	0.014724623	2	D
Ttc12	0.704118608	0.000494396	0.015082155	3	D
Lrrc34	1.170362836	0.000494543	0.015082155	9	D
Gm904	0.921357819	0.00050313	0.015286698	13	#N/A
Ccdc62	0.605840162	0.000504643	0.015304046	5	#N/A
Ccdc74a	0.918650283	0.000514262	0.015537794	16	#N/A
Gm4763	1.209325217	0.00052031	0.015662291	7	D
Pkmyt1	0.623472465	0.000539087	0.016197519	17	C
Dnajc5g	0.745857933	0.000546535	0.016391008	5	D
Tex101	0.469025091	0.000568907	0.017030527	7	C
Fcgr3	0.63622513	0.000573264	0.017129427	1	E
Sh3gl3	0.289638267	0.000583126	0.017360279	7	C
Ppp1r13l	0.539924525	0.000586555	0.017430452	7	D
Mlh3	0.373090593	0.000593006	0.017589972	12	C
Ift122	0.381724408	0.000594397	0.017599131	6	C
Cdh16	1.784856558	0.00061121	0.017971753	8	A
Ribc2	0.697253238	0.000617682	0.018123514	15	E
Cage1	0.712930535	0.00066484	0.019472031	13	D
Myd88	0.433881612	0.000668712	0.019550198	9	D
1700003E16Rik	0.856367382	0.000673503	0.01965491	6	E
Smg9	0.404368315	0.000676561	0.019702259	1	E
Adcy10	0.792890265	0.000677549	0.019702259	7	D
Prss45	1.076639446	0.000685416	0.019895435	9	D
Iqce	0.379875721	0.000692282	0.020005808	5	E
Sptb	0.419861025	0.000692911	0.020005808	18	D
Katnal2	0.596165696	0.000692796	0.020005808	12	A
Catsperg2	0.923488248	0.000714458	0.020554892	7	#N/A
Syngr4	0.554002137	0.000721589	0.020686815	11	D
Lrrc46	0.801592367	0.000720929	0.020686815	7	D
Brd9	0.281008635	0.000725609	0.020765442	13	D
Caps2	1.160043836	0.000738872	0.021107856	10	D
Efcab6	1.03618822	0.000755586	0.021509714	15	E
Catsperg1	0.702221819	0.000768805	0.021847771	7	#N/A
Fam188b	0.629815327	0.000779306	0.022107531	6	D
Rtn1	0.635286852	0.000789341	0.022314326	12	E
Cep72	0.438123521	0.000810744	0.022839939	13	D
Il4i1	0.65536577	0.000813765	0.022885374	7	E
Skiv2l	0.295655027	0.000843855	0.02356848	17	C
Ppil6	0.809049061	0.000871301	0.024251699	10	#N/A
Il9r	0.851537638	0.000912378	0.025265259	11	#N/A
Dnajb3	0.596712673	0.000931646	0.025754943	1	E
Gstm5	0.348154616	0.00095109	0.026247831	3	E
Rab36	0.368634052	0.000976551	0.026859279	10	D
Vwa3b	0.83292473	0.000981225	0.026915661	1	E
Tex9	0.354834165	0.001015398	0.027786702	9	C
Ccdc103	0.617322308	0.001022239	0.027926889	11	E

Ralgps1	0.31914416	0.001031219	0.02812495	2	D
Art3	0.268657043	0.001040254	0.028323843	5	C
Mroh1	0.27613328	0.00105345	0.02854884	15	#N/A
Gm11837	0.531886569	0.001125171	0.03033109	4	#N/A
Skiv2l2	0.230970406	0.001131985	0.030406501	13	C
Sprtn	0.419474178	0.00113358	0.030406501	8	#N/A
Rhpn1	0.57866333	0.001141261	0.030562095	15	C
Ubxn10	0.537428554	0.001163599	0.03100706	8	D
BC048644	0.835413803	0.001162254	0.03100706	4	#N/A
Gria4	1.168750449	0.001180263	0.031399642	9	#N/A
Enkur	0.755101642	0.00120597	0.031926777	2	D
Syt11	0.354183566	0.001269142	0.033381712	3	C
Ndufaf3	0.480931495	0.001288837	0.033735989	19	#N/A
Eno4	0.606878074	0.001287319	0.033735989	9	D
Tcte1	0.99739351	0.001296411	0.033879691	17	E
Pgbd1	0.604867501	0.001314802	0.034305143	13	#N/A
Lrwd1	0.275232098	0.001378956	0.035692568	5	#N/A
Tuba3b	0.377045321	0.001406238	0.036225673	7	#N/A
Slc6a16	0.93160912	0.00140482	0.036225673	6	D
Nme5	0.871458267	0.001458306	0.037448285	18	E
Ppp4r1l-ps	0.345970276	0.001461004	0.037458391	2	#N/A
Rnf123	0.29093378	0.001464481	0.03748842	9	C
4930509G22Rik	0.655587927	0.001487717	0.037963635	16	#N/A
Sgpp2	0.585180487	0.001510947	0.038435756	1	D
1700088E04Rik	0.415992717	0.0015304	0.038809137	15	D
Tctex1d2	0.486364042	0.001557563	0.039313943	13	D
Gm17167	0.835334927	0.001556523	0.039313943	4	#N/A
Dcdc2a	0.857255731	0.001554959	0.039313943	16	C
4930524O08Rik	1.021697765	0.001570849	0.039587839	9	#N/A
1700012B07Rik	0.912997593	0.001600781	0.040279703	11	E
Syt5	0.657580558	0.001629312	0.040808109	7	D
Ptges	0.646771337	0.001645796	0.041157566	2	A
Nkapl	0.675188399	0.001719019	0.042856837	13	D
Mlc1	0.434202912	0.001726401	0.042951455	15	C
4930550C14Rik	0.899766174	0.001733765	0.04302649	9	D
Hemt1	0.626174229	0.001747269	0.043295521	15	C
Trafd1	0.400647424	0.001753233	0.043377185	5	D
Fbxo43	0.681413021	0.001767996	0.043609669	15	D
Acox3	0.363996001	0.001784273	0.04394449	5	D
Krba1	0.24217427	0.001799916	0.044195818	6	D
Dis3l	0.499281125	0.001821486	0.044658011	9	D
Dmrtc2	0.497237833	0.001842244	0.044963479	7	C
Kndc1	0.49645147	0.001845462	0.044974485	7	C
BC051142	0.511562673	0.001881062	0.04563681	17	D
Stkld1	1.045126355	0.001885883	0.04568558	2	D
Gstt3	0.538928455	0.001925959	0.04658699	10	D
Wdr35	0.378222317	0.001937726	0.046801981	12	C
4930504O13Rik	0.971843485	0.00194862	0.046925652	11	D
Wwc2	0.260001265	0.001985312	0.04753122	8	C
Zfand4	0.46586908	0.001988387	0.04753122	6	#N/A
Ccdc176	0.636779522	0.002062851	0.049166642	12	#N/A
Col15a1	0.318676431	0.002069264	0.049247276	4	A